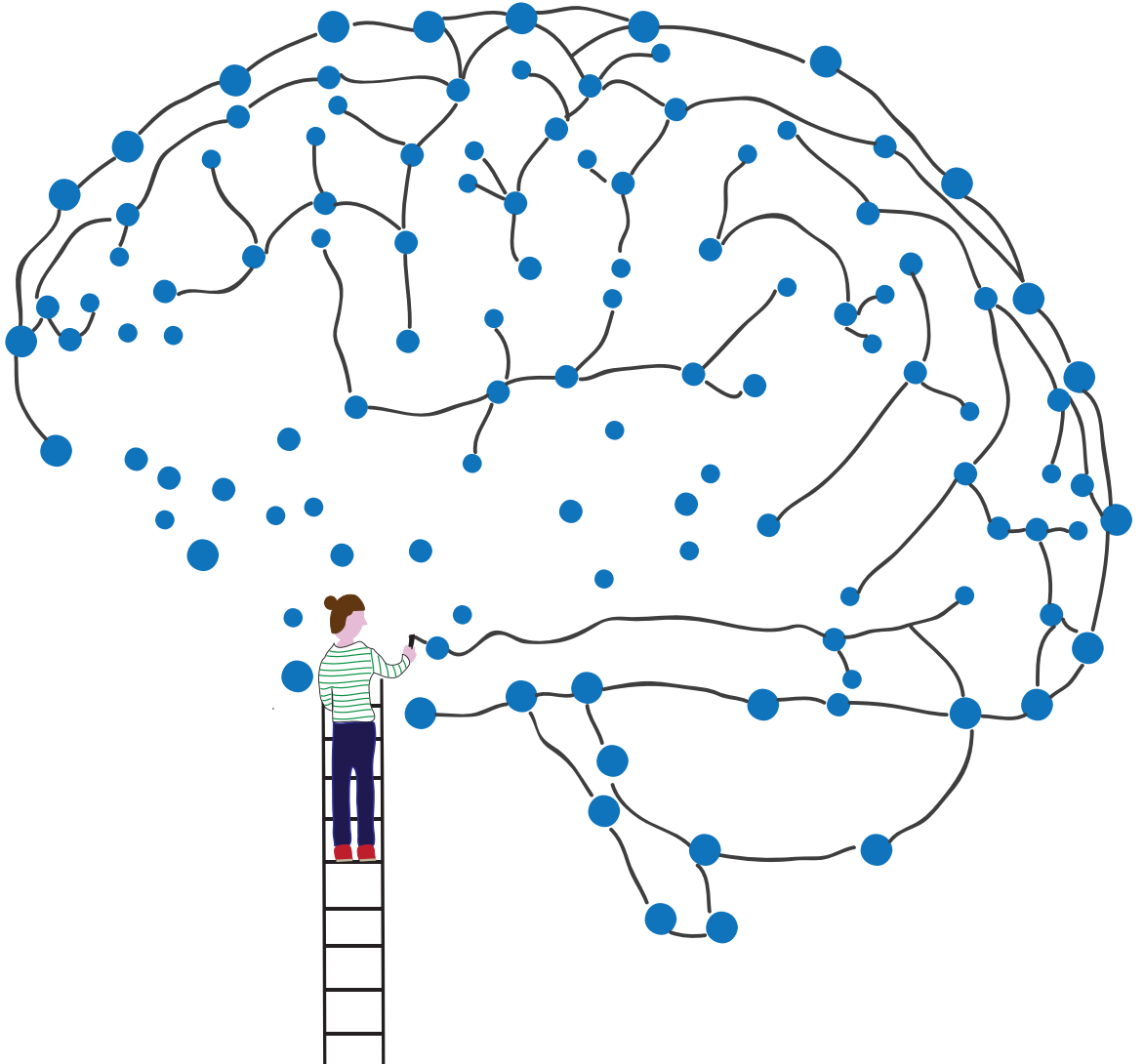


Connecting the dots: Structural and functional connections in healthy and diseased brain



Connecting the dots: Structural and functional connections in healthy and diseased brain

Milou Straathof

Cover	Milou Straathof
Layout	Milou Straathof
Printing	ProefschriftMaken, de Bilt
ISBN	978-94-6423-484-8

Copyright © Milou Straathof, 2021

All rights reserved. No part of this thesis may be reproduced, stored in a retrieval system, or transmitted in any form or by any means, without prior permission of the holder of the copyright.

Connecting the dots: Structural and functional connections in healthy and diseased brain

Verbinding van punten: Structurele en functionele verbindingen in gezonde en zieke hersenen

(met een samenvatting in het Nederlands)

Proefschrift

ter verkrijging van de graad van doctor aan de
Universiteit Utrecht op gezag van de rector magnificus,
prof.dr. H.R.B.M. Kummeling, ingevolge het besluit van het
college voor promoties in het openbaar te verdedigen op
dinsdag 14 december 2021 des middags te 12.15 uur

door

Milou Straathof

geboren op 18 mei 1992
te Haarlem

Promotor:

Prof. dr. R.M. Dijkhuizen

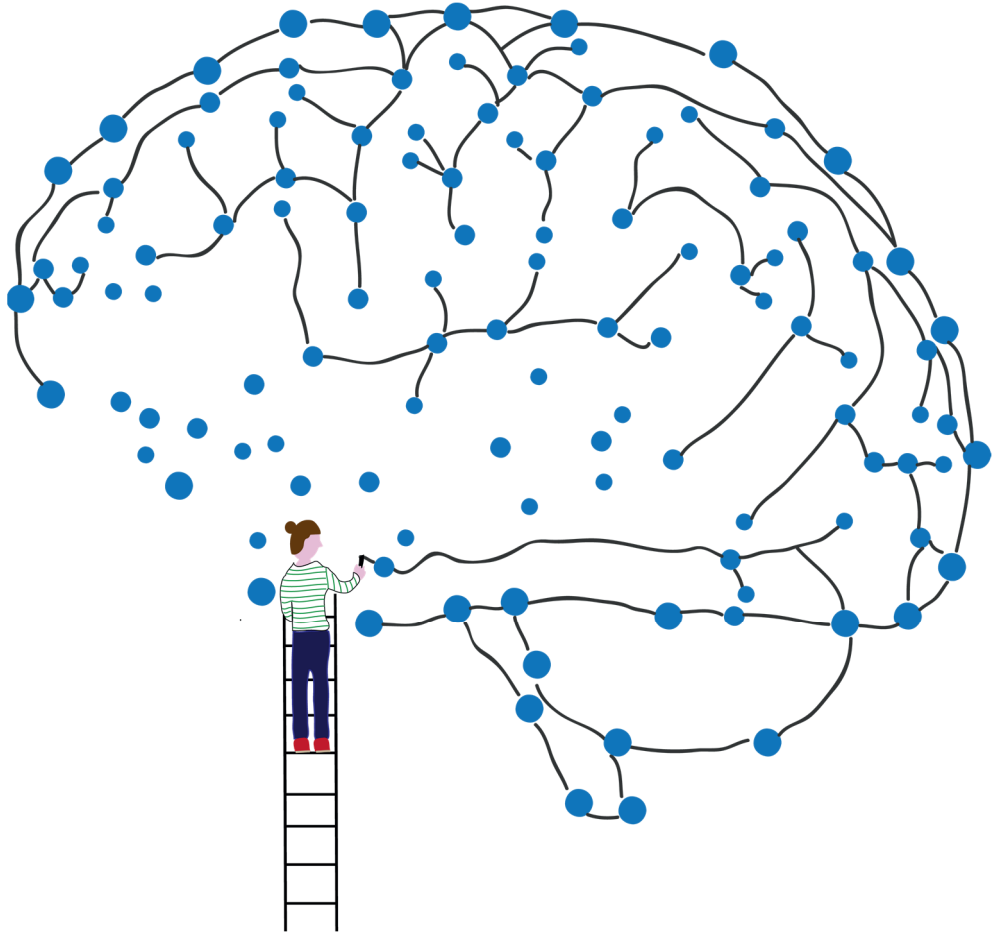
Copromotor:

Dr. W.M. Otte

The work was financially supported by funding from the Netherlands Organization for Scientific Research (NWO-VICI 016.130.662, NWO-VENI 016.168.038), the Dutch Brain Foundation [F2014(1)-06] and the European Union Seventh Framework Program (FP/2007-2013 under grant agreement number 278948 [TACTICS]).

Contents

Chapter 1	General Introduction	7
Chapter 2	Distinct structure-function relationships across cortical regions and connectivity scales in the rat brain.	23
Chapter 3	Non-linear relationships between structural and functional connectivity in the human and rat brain.	53
Chapter 4	Structural and functional MRI of altered brain development in a novel adolescent rat model of quinpirole-induced compulsive checking behavior.	79
Chapter 5	Memantine treatment does not affect compulsive behavior or frontostriatal connectivity in an adolescent rat model for quinpirole-induced compulsive checking behavior.	103
Chapter 6	Differences in structural and functional networks between young adult and aged rat brains before and after stroke lesion simulations.	131
Chapter 7	General Discussion	165
	Summary	177
	Samenvatting (Summary in Dutch)	183
	Dankwoord	189
	About the author	195



1

General introduction

The brain is one of the most intriguing organs of the body. It consists of billions of nerve cells (called neurons), which are communicating through trillions of synaptic connections. The communication between neurons and brain regions via their connections is essential for all our daily life functions, including reading this thesis. Understanding the organization and functioning of the brain has been one of the fundamental questions in Neuroscience and forms the basis of this thesis. In this thesis, we aim to “connect the dots”. On the smallest level, we connected dots in the brain, by looking at the connectivity between different brain regions that are often visualized as circles (or dots). In addition, we aimed to connect dots in a more figurative way, by identifying how larger phenomena, like aging across the life span or disease processes, affect brain network organization.

The brain as a network

In the 18th century, Franz Joseph Gall introduced the idea of brain localization, by stating that specific functions of the brain could be ascribed to specific brain regions (Zola-Morgan, 1995). This idea of localized brain functions was later supported by Paul Broca, who identified an area in the brain specialized in speech (Broca, 1861; Finger, 2004). The connection between cerebral localization and brain organization implies that different regions in the brain have specific functions and may therefore be responsible for specific behavior. Another famous example of cerebral localization is the case study of Phineas Gage, also known as the “American Crowbar Case”, from 1848. Phineas Gage survived an accident in which a large iron rod was driven through his left frontal cortex (Barker, 1995; Bigelow, 1850). Surprisingly, he recovered without any motor and sensory deficits, but his personality changed, suggesting that certain parts of the frontal cortex are important for specific mental and higher cognitive functions.

More recently, a novel view on how complex systems, such as the brain, are organized has emerged as network science (Borner et al., 2007). According to network science, the connections and interactions between individual components should be considered to fully understand the organization and behavior of complex systems. In line with this view, researchers have shown that many functions of the brain require distributed brain areas, showing the importance of connections and communication between brain regions (Tononi et al., 1998). Within network neuroscience, the brain is seen as a network of interacting brain regions at the micro-, meso- and macroscopic level. To study these multilevel brain networks, the brain is conceptually divided into brain regions (i.e. nodes or dots) and connections (i.e. edges) (Bassett and Sporns, 2017). You can look at these connections in two ways. First, there are functional connections between brain regions, which

are assumed to reflect information transfer between regions (i.e., signals sent from one brain region to another). Second, there are structural connections, which are the physical connections between brain regions or neurons. The concept of structural and functional connectivity is also found elsewhere. For example, in the behavior of a railway network. In this example, a structural connection is the railway between two stations, whereas the number of trains that is using this railway is the functional connection.

Many studies have characterized features of structural and functional brain connectivity in isolation, but there is limited knowledge about the mutual relationship between them. Whether and how structural connections constrain, maintain, and restrict functional connections in the brain is a fundamental question in Neuroscience. Especially also because many disorders have been associated with disturbances in structural and functional brain networks (Fornito et al., 2015; van den Heuvel and Sporns, 2019; Van Essen and Barch, 2015). Ideally, the network organization of structural and functional brain connections is studied non-invasively *in vivo* using magnetic resonance imaging (MRI).

Structural and functional connectivity in the brain measured with MRI

MRI offers powerful techniques to study the organization and functioning of the brain and connections between brain regions *in vivo*. The two techniques that are often used to study brain connectivity are resting-state functional MRI to study functional connectivity and diffusion-weighted MRI to study structural connectivity.

Functional connectivity

Functional MRI (fMRI) can be used to map the activity of the brain in response to specific stimuli, pharmacological compounds, or tasks. Brain activity measured with fMRI is based on the local level of blood oxygenation (BOLD) (Nikos K. Logothetis, 2008; Ogawa et al., 1990). Resting-state fMRI, which is an fMRI scan without a task or a stimulus, has been used to study the organization of the brain during rest. During rest, brain regions exhibit spontaneous low frequency fluctuations in their BOLD signal. We know from primate, rodent and human studies that these spontaneous BOLD fluctuations match with specific patterns of neuronal activity (He et al., 2008; Magri et al., 2012; Pan et al., 2011; Shmuel and Leopold, 2008). Hereby, resting-state BOLD fMRI offers a non-invasive way to measure resting brain activity non-invasively *in vivo*. Two brain regions that are involved in similar functions, such as the motor cortex in the left and right hemisphere, appear to have correlated BOLD signal fluctuations during rest (B. B. Biswal et al., 1995; M D Fox and Raichle, 2007). The degree of correlation between spontaneously fluctuating BOLD signal time series in two

brain regions is considered as resting-state functional connectivity. Based on functional connectivity, several resting-state networks, including the default mode network and the sensorimotor network, have been identified in the brain (Damoiseaux et al., 2006; Fox et al., 2005).

Often, functional connectivity is determined statically, i.e., the time series of the entire resting-state fMRI scan is used to calculate functional connectivity. Recently, functional connectivity is demonstrated to fluctuate during a resting-state fMRI scan (Chang and Glover, 2010) and dynamic analyses approaches have been developed, such as a sliding window approach. With this approach, you take a smaller part of the time series (e.g., 100 seconds), which is called a window, you move this window along the time series with a specific step size and you quantify functional connectivity between brain regions for each window separately. The dynamic fluctuations in functional connectivity are assumed to be of neuronal origin, and potentially reflective of ongoing mental activity, consciousness or daydreaming (Barttfeld et al., 2015; Hutchison et al., 2013; Matsui et al., 2019).

Structural connectivity

Diffusion-weighted MRI can be used to map the anatomical connections, or white matter fiber bundles, between different brain regions. Diffusion-weighted MRI is sensitive to the random diffusion of water molecules (Basser et al., 1994; Le Bihan, 2003). A diffusion-weighted MRI scan typically includes scans sensitive to different diffusion directions. Based on the variation of diffusion along these different directions, you can calculate the fractional anisotropy (FA), a scalar value for the degree of directionality-dependent diffusion. The FA value is suggested to be reflective of the integrity of the white matter fiber bundle, with a high FA value reflecting a better integrity. However, these claims are not yet definitive (Alexander et al., 2007).

The diffusion is restricted (or anisotropic) in areas of the brain with strong natural boundaries, such as in white matter fiber bundles. In these areas, water diffusion is higher along white matter bundles, compared to perpendicular to white matter bundles. Therefore, we consider the main direction of water diffusion in a voxel as the main direction of white matter fiber bundles. To map the anatomical connectivity between brain regions, diffusion-based tractography algorithms follow this main diffusion direction in each voxel of the brain to reconstruct streamlines reflecting large white matter fiber bundles (Basser et al., 2000; Mori and Van Zijl, 2002). The (number of) reconstructed streamlines, or values of white matter integrity such as FA, between brain regions can subsequently be considered as diffusion-based structural connectivity.

Structure-function correlation

Because functional connectivity is found between brain areas that are close together but also further apart from each other, structural connections seem essential. Indeed, functional connections are shaped by the presence of underlying structural connections, but functional connectivity also exists between regions without direct structural connections (Damoiseaux and Greicius, 2009; Honey et al., 2009; O'Reilly et al., 2013; van den Heuvel et al., 2009). In addition, in a systematic review, we showed that the stronger a structural connection, in general also the stronger the functional connection (Straathof et al., 2019). However, the structure-function relationship in the brain varied considerably between studies, indicating that the exact structure-function relationship still needs to be elucidated. In addition, different network resolutions, brain subsystems and connectivity measures may expose distinct structure-function relationships, which emphasizes the need to assess functional and structural connectivity at multiple scales. Lastly, how a relatively stable structural network supports dynamic functional connectivity remains an unanswered question (Cabral et al., 2017).

Graph theory analysis

Structural and functional connectivity between brain regions can be used to quantify network organization and topology with graph theory analyses (Bullmore and Sporns, 2009a). This includes measurements of segregation (specialized brain regions, local connections) and integration (long, global connections), as well as the optimal balance between those two (small-worldness) (Bullmore and Sporns, 2009b). Both structural and functional networks are organized as small-world networks, with many local connections for segregation and a few global long distance connections for integration (Bullmore and Sporns, 2009a). This balance between segregation and integration seems essential for healthy brain functioning (Sporns, 2013; Tononi et al., 1994), it changes during development and aging and many disorders are assumed to be caused by a shift in this balance (van den Heuvel and Sporns, 2019).

Changes in structural and functional brain networks during maturation and aging

The brain develops and ages and structural and functional connections between brain regions change over the lifespan. Both resting-state fMRI and diffusion-weighted MRI have been successfully used to study these changes in the brain during different age periods, such as maturation and aging. The structural and functional changes in these age periods may explain

the risk of developing neurodevelopmental or neurodegenerative disorders during these periods.

Maturation

Functional networks change during the development from childhood, through adolescence to adulthood (Grayson and Fair, 2017), although resting-state networks may already be present in children (Thomason et al., 2013). Functional connectivity between brain regions both decreases and increases during maturation (Wang et al., 2012), mainly characterized by decreases in short-distance functional connectivity (less segregation) and increases in long-distance functional connectivity (more integration) (Dosenbach et al., 2010; Fair et al., 2009; Power et al., 2010; Supekar et al., 2009). Most of the structural connections are already present at the beginning of this developmental period. However, these structural pathways get refined during maturation, by increasing or decreasing myelination and/or axonal density, which change white matter integrity values, resulting in increases in FA (Brouwer et al., 2012; Hagmann et al., 2010). During late childhood, structural networks become less local but more globally efficient, with sensorimotor regions maturing first (Khundrakpam et al., 2013). Similar to functional networks, during adolescence, there is an increase in structural network integration (Dennis et al., 2013). Finally, the relationship between structural and functional connectivity significantly increases with age from 18 months to 18 years old (Hagmann et al., 2010).

Because structural and functional networks mature during the development from childhood through adolescence, this period is also sensitive to disturbances in the maturation of connections, which can result in neurodevelopmental disorders, such as obsessive-compulsive disorder (OCD). Children and adolescents with OCD are indeed characterized by abnormalities in structural and functional networks. For example, children and adolescents with OCD have increased fractional anisotropy (i.e. more diffusion along white matter fiber bundles) in large white matter tracts (Gruner et al., 2012; Zarei et al., 2011). This may be reflective of premature myelination of white matter tracts (Zarei et al., 2011). In addition, both decreased and increased functional connectivity in resting-state networks have been identified in children and adolescents with OCD (Bernstein et al., 2016; Fitzgerald et al., 2011a; Weber et al., 2014). Although abnormalities in the structural and functional maturation of brain regions and connections that form the frontostriatal system in the brain have been associated with OCD, the exact pathophysiological mechanisms remain incompletely understood.

Aging

Similar as during maturation, structural and functional connections change during healthy aging. In general, studies report lower functional connectivity values within the default mode network with aging (Damoiseaux et al., 2008; Ferreira and Busatto, 2013). In addition, decreases in FA values, reflective of reduced white matter integrity, have been shown in older adults (Burzynska et al., 2010; Damoiseaux et al., 2009). In addition, the network topology of both structural and functional connectivity reorganizes during aging (Betzel et al., 2014; Meier et al., 2012; Otte et al., 2015a). Functional networks in aged individuals are characterized by decreased within-network connectivity, increased between-network connectivity and lower segregation (Damoiseaux, 2017; Ferreira et al., 2016; Spreng and Schacter, 2012). In addition, functional network efficiency decreases when individuals get older (Achard and Bullmore, 2007; Cao et al., 2014). Similar to functional networks, structural networks show decreased connectivity, lower efficiency and a more localized organization (Gong et al., 2009a; Wu et al., 2012; Zhu et al., 2012). Studies investigating both structural and functional networks have demonstrated that both networks change with aging, and that changes in structural and functional network during aging may be related (Betzel et al., 2014; Fjell et al., 2016; Zimmermann et al., 2016).

These aging-induced changes in structural and functional connectivity may contribute to the vulnerability or resilience to brain disorders and may influence disease outcome and response to therapies (Herson and Traystman, 2014; Liang et al., 2016; Liu et al., 2009). With aging, the risk of several diseases, including stroke, increases. During ischemic stroke, there is a sudden disruption in blood flow to specific areas of the brain. However, not only regions close to the stroke lesion site, but also connected brain areas get affected (Carter et al., 2012; Grefkes and Fink, 2011; Silasi and Murphy, 2014), suggesting that structural and functional connectivity are interesting markers to probe stroke pathology and recovery. Experimental studies on how age-induced changes in structural and functional connectivity contribute to the vulnerability to brain disorders such as stroke are complicated, and lesion simulation studies may provide an alternative valuable strategy.

The above-described studies on (ab)normal changes in structural and functional connectivity across maturation and aging in humans are mostly cross-sectional in design and longitudinal MRI studies are scarce, due to the obvious time and money investment. Longitudinal studies in animal models of healthy development and aging, or diseases

associated with these time periods, may be used to answer important remaining questions about structural and functional connectivity in the brain.

Animal models

MRI is equally suitable to study brain function and pathology in animals as it is in humans (Dijkhuizen and Nicolay, 2003). Structural and functional connectivity measured with MRI in rats provide several unique opportunities to overcome some of the limitations researchers face in human research.

First of all, rats go through similar developmental and aging phases as humans (Semple et al., 2013; Sengupta, 2013), making them suitable for longitudinal studies of functional and structural brain connectivity. An additional practical advantage is that rats age relatively fast (their lifespan is around 3 years (Quinn, 2005; Sengupta, 2013)), making longitudinal study designs during maturation or healthy aging easier in rats than in humans.

Second, heterogeneity in human patient populations with regards to comorbidities, symptoms, and exposure to treatments complicate drawing conclusions about specific causes of abnormal structural and functional connectivity. In comparison, animal experiments are often well-controlled with less variability between different individuals (such as age or genetics). Animal experiments are therefore suited to test abnormalities in specific developmental or aging trajectories or to test the efficacy of novel therapeutic treatments.

Thirdly, rodents offer an additional measure of structural brain connectivity, called neuronal tract tracers, which are considered to be the golden standard to measure axonal connectivity (Heimer and Robards, 1981). Neuronal tract tracers are transported by the transport mechanisms within a cell and can thereby visualize individual axonal projections between brain regions (Gerfen and Sawchenko, 1984; Lavail and Lavail, 1972). Combining structural connectivity measures on different levels (diffusion-weighted MRI at the level of large fiber bundles and neuronal tracers at individual axonal projections) may provide additional insights into structural connections and their relationship with functional connectivity in the brain.

Although animal models are well-suited to investigate underlying disease mechanisms or to investigate novel therapeutic treatments, they do not always accurately reflect the clinical population. For example, many animal models of OCD are performed in adult rats, whereas the majority of OCD patients experience their first symptoms during childhood or adolescence (Taylor, 2011). As a contrast, stroke in experimental models is often induced in young adult or adult animals, whereas the clinical incidence of stroke increases

with older age. These age discrepancies between clinical and preclinical populations has been suggested to potentially explain why therapeutic drugs that seem promising in animal studies fail in the clinical human population (Dirnagl, 2016). To further understand structural and functional brain organization in health and disease, rodent animal models should be well-reflective of the clinical population by means of age and developmental stages.

Aim of the thesis: Connecting the dots

The aim of this thesis is to characterize structural and functional connectivity in the healthy and diseased brain. We literally connected dots (i.e., regions) in the brain by characterizing MRI-based structural and functional brain organization. In addition, we aimed to identify how biological phenomena, including functional connectivity, structural connectivity, maturation, OCD, aging and stroke, connect to each other (Figure 1). We characterized the relationship between structural and functional connectivity in the healthy brain in **Chapter 2 and 3**. In **Chapter 4 and 5** we linked structural and functional connectivity to maturation and compulsive behavior associated with OCD. Lastly, in **Chapter 6** we investigated how structural and functional connectivity changes associated with aging affect the impact of stroke lesions on brain networks.

Outline of the thesis

The aim of **Chapter 2** was to identify to what extent structural and functional connectivity strength are linearly correlated across the rat brain. To this aim, we combined high-field resting-state fMRI-based functional connectivity with diffusion- as well as neuronal tracer-based structural connectivity in the rat brain. We investigated local variations in the structure-function relationship, which may explain differences in the functional significance of connections and their contribution to network dysfunction in brain disorders.

Although linear correlation analyses offer a clear and easily interpretable way to determine structure-function relationships, it may not completely cover its complex nature. Therefore, in **Chapter 3**, we mapped the relationship between MRI-based structural and functional connectivity in the brain by taking non-linearity into account. To that aim, we used a generalized additive model to compare the non-linearity of the structure-function relationship in the rat and human brain.

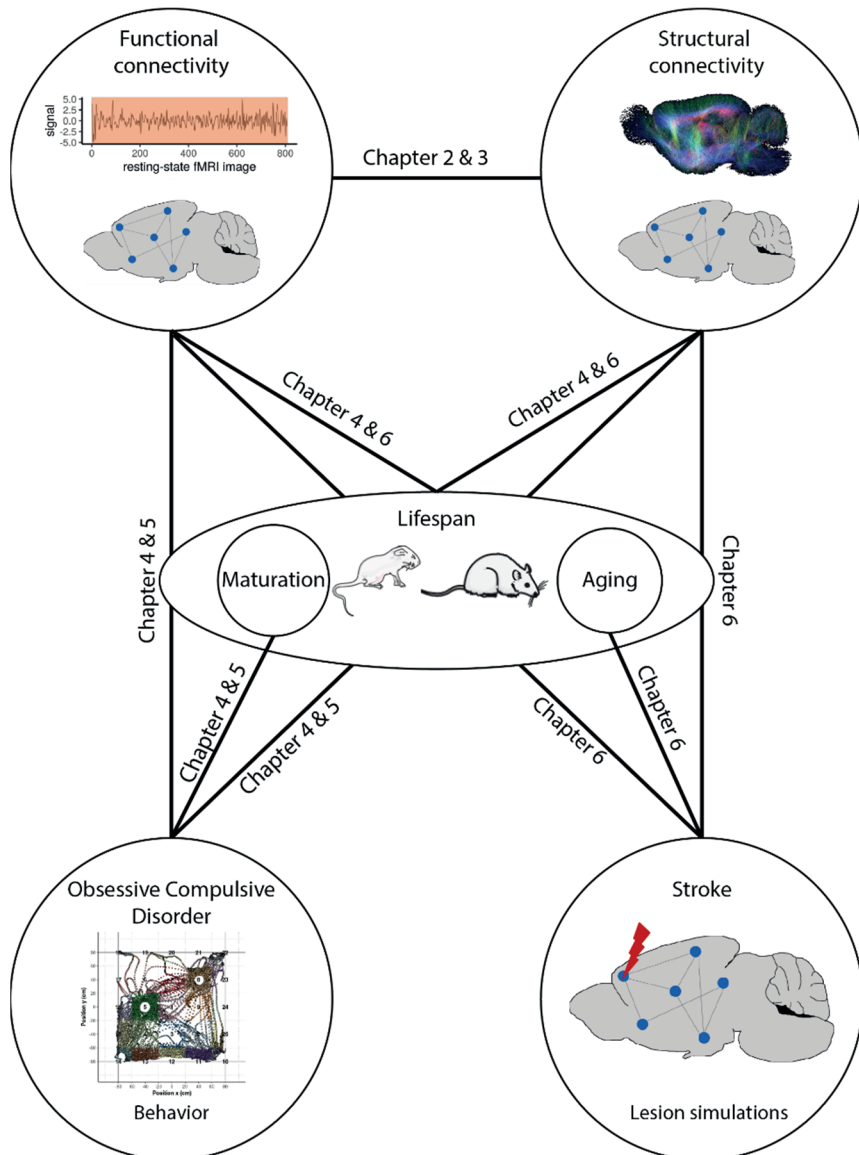


Figure 1: Overview of the connected dots in this thesis. Literally, connecting the dots in this thesis refers to the view of Network Neuroscience, in which the brain is divided into nodes (circles, “dots”) which are connected. In addition, we aimed to connect larger phenomena, here represented as circles or dots. First, in chapter 2 and 3, we connected structural and functional connectivity in the healthy brain. Second, in chapter 4 till 6, we investigated changes in structural and functional connectivity across the lifespan, and how these changes relate to brain disorders associated with these life periods. Therefore, we investigated structural and functional connectivity changes associated with maturation and compulsive behavior associated with obsessive-compulsive disorder in Chapter 4

and 5. Lastly, in Chapter 6 we investigated whether age and associated structural and functional connectivity patterns influence the impact of stroke lesion simulations on brain networks.

In **Chapter 4**, we characterized normal and abnormal developmental changes in structural and functional connections of the frontostriatal system in an adolescent rat model of compulsive checking behavior. To this aim, we adapted the adult quinpirole-induced compulsive checking behavior model, to induce compulsive checking behavior during brain maturation and applied serial structural and functional MRI of the brain. In addition, we correlated (ab)normal changes in structural and functional connectivity to compulsive behavioral measures.

In **Chapter 5**, we used the above-described adolescent rat model of compulsive checking behavior to determine the therapeutic efficacy of memantine to reduce compulsive behavior. In addition, we investigated its possible mode of action on the development of structural and functional connectivity, and functional activation within the frontostriatal system. Therefore, we applied diffusion-weighted MRI, resting-state fMRI, and pharmacological MRI before and after memantine treatment.

The aim of **Chapter 6** was to characterize differences in structural and functional brain networks between young adult and aged rats as well as their susceptibility and resilience to stroke lesions. Resting-state functional MRI and diffusion MRI were measured longitudinally, and lesions were simulated in brain areas that are typically affected in different stroke animal models.

In **Chapter 7** the implications of the findings from chapters 2-6 are discussed. Limitations and future perspectives are outlined as well.

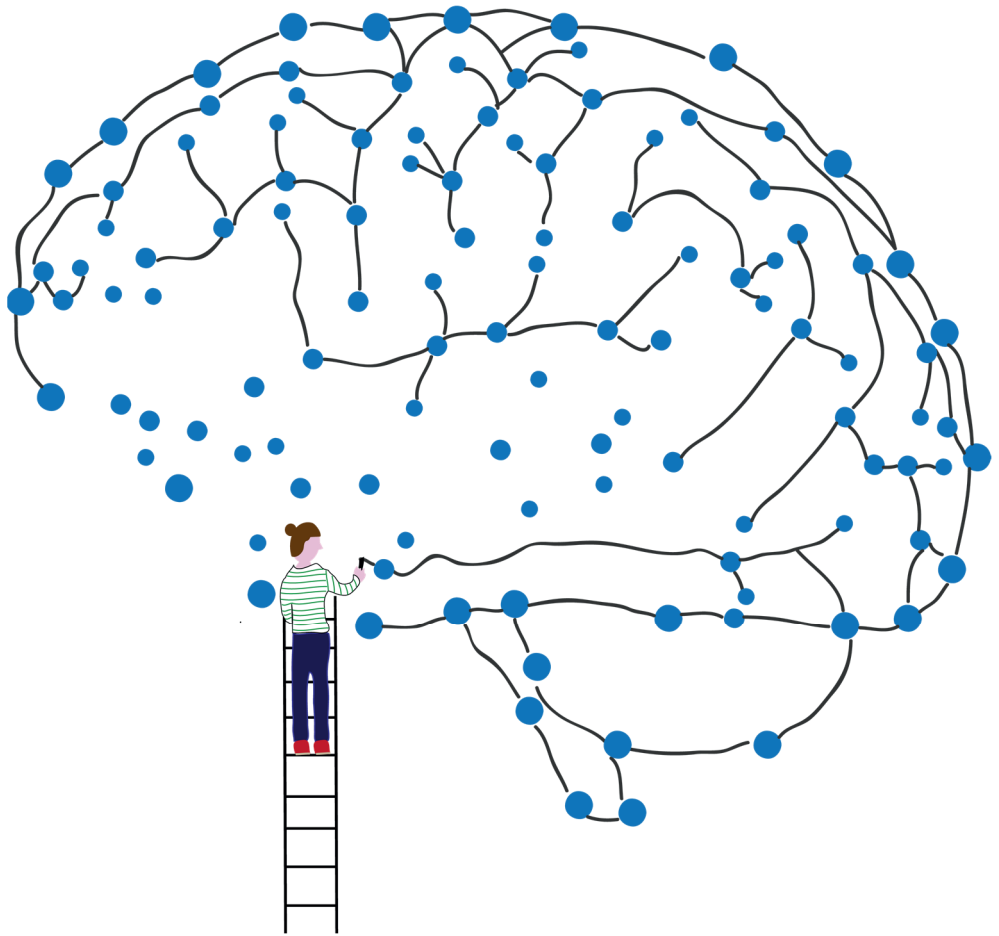
References

- Achard, S., Bullmore, E., 2007. Efficiency and cost of economical brain functional networks. *PLoS Comput. Biol.* 3, 0174–0183. <https://doi.org/10.1371/journal.pcbi.0030017>
- Alexander, A.L., Lee, J.E., Lazar, M., Field, A.S., 2007. Diffusion Tensor Imaging of the Brain. *Neurotherapeutics* 4, 316–329. <https://doi.org/10.1016/j.jalz.2013.05.815>
- Barker, F.G., 1995. Phineas among the phrenologists: the American crowbar case and nineteenth-century theories of cerebral localization. *J. Neurosurg.* 82, 672–682.
- Barttfeld, P., Uhrig, L., Sitt, J.D., Sigman, M., Jarraya, B., Dehaene, S., 2015. Signature of consciousness in the dynamics of resting-state brain activity. *Proc. Natl. Acad. Sci. U. S. A.* 112, 887–892. <https://doi.org/10.1073/pnas.1515029112>
- Basser, P.J., Mattiello, J., LeBihan, D., 1994. MR Diffusion Tensor Spectroscopy and Imaging. *Biophys. J.* 66, 259–267. [https://doi.org/10.1016/S0006-3495\(94\)80775-1](https://doi.org/10.1016/S0006-3495(94)80775-1)
- Basser, P.J., Pajevic, S., Pierpaoli, C., Duda, J., Aldroubi, A., 2000. In Vivo Fiber Tractography Using DT-MRI Data. *Magn. Reson. Med.* 44, 625–632. [https://doi.org/10.1002/1522-2594\(200010\)44:4<625::AID-MRM17>3.0.CO;2-O](https://doi.org/10.1002/1522-2594(200010)44:4<625::AID-MRM17>3.0.CO;2-O)
- Bassett, D.S., Sporns, O., 2017. Network neuroscience. *Nat. Neurosci.* 20, 353–364. <https://doi.org/10.1038/nn.4502>
- Bernstein, G.A., Mueller, B.A., Westlund Schreiner, M., Campbell, S.M., Regan, E.K., Nelson, P.M., Hour, A.K., Lee, S.S., Zagoloff, A.D., Lim, K.O., Yacoub, E.S., Cullen, K.R., 2016. Abnormal striatal resting-state functional connectivity in adolescents with obsessive-compulsive disorder. *Psychiatry Res. Neuroimaging* 247, 49–56. <https://doi.org/10.1016/j.pscychresns.2015.11.002>
- Betz, R.F., Byrge, L., He, Y., Goni, J., Zuo, X.N., Sporns, O., 2014. Changes in structural and functional connectivity among resting-state networks across the human lifespan. *Neuroimage* 102, 345–357. <https://doi.org/10.1016/j.neuroimage.2014.07.067>
- Bigelow, H.J., 1850. Dr. Harlow’s Case of Recovery from the Passage of an Iron Bar through the Head. *Am. J. Med. Sci.*
- Biswal, B.B., Yetkin, F.Z., Haughton, V.M., Hyde, J.S., 1995. Functional connectivity in the motor cortex of resting human brain using Echo-Planar MRI. *Magn. Reson. Med.* 34, 537–541. <https://doi.org/10.1002/mrm.1910340409>
- Borner, K., Sanyal, S., Vespignani, A., 2007. Network Science. *Annu. Rev. Inf. Sci. Technol.* 41, 537–607. <https://doi.org/10.1002/aris.2007.1440410119>
- Broca, P., 1861. Remarques sur le siège de la faculté du langage articulé suivies d’une observation d’aphémie. *Bull. la Société Anat.* 6, 330–357.
- Brouwer, R.M., Mandl, R.C.W., Schnack, H.G., Soelen, I.L.C. van, Baal, G.C. van, Peper, J.S., Kahn, R.S., Boomsma, D.I., Pol, H.E.H., 2012. White matter development in early puberty: A longitudinal volumetric and diffusion tensor imaging twin study. *PLoS One* 7, 1–10. <https://doi.org/10.1371/journal.pone.0032316>
- Bullmore, E., Sporns, O., 2009a. Complex brain networks: Graph theoretical analysis of structural and functional systems. *Nat. Rev. Neurosci.* 10, 186–198. <https://doi.org/10.1038/nrn2575>
- Bullmore, E., Sporns, O., 2009b. Complex brain networks: Graph theoretical analysis of structural and functional systems. *Nat. Rev. Neurosci.* 10, 186–198. <https://doi.org/10.1038/nrn2575>
- Burzynska, A.Z., Preuschhof, C., Bäckman, L., Nyberg, L., Li, S.-C., Lindenberger, U., Heekeren, H.R., 2010. Age-related differences in white matter microstructure: Region-specific patterns of diffusivity. *Neuroimage* 49, 2104–2112. <https://doi.org/10.1016/j.neuroimage.2009.09.041>
- Cabral, J., Kringelbach, M.L., Deco, G., 2017. Functional connectivity dynamically evolves on multiple time-scales over a static structural connectome: Models and mechanisms. *Neuroimage* 160, 84–96. <https://doi.org/10.1016/j.neuroimage.2017.03.045>
- Cao, M., Wang, J.H., Dai, Z.J., Cao, X.Y., Jiang, L.-L., Fan, F.-M., Song, X.-W., Xia, M.-R., Shu, N., Dong, Q., Milham, M.P., Castellanos, F.X., Zuo, X.-N., He, Y., 2014. Topological organization of the human brain functional connectome across the lifespan. *Dev. Cogn. Neurosci.* 7, 76–93. <https://doi.org/10.1016/j.dcn.2013.11.004>
- Chang, C., Glover, G.H., 2010. Time-frequency dynamics of resting-state brain connectivity measured with fMRI. *Neuroimage* 50, 81–98. <https://doi.org/10.1016/j.neuroimage.2009.12.011>
- Damoiseaux, J.S., 2017. Effects of Aging on Functional and Structural Brain Connectivity. *Neuroimage* 160, 32–40. <https://doi.org/10.1016/j.neuroimage.2017.01.077>
- Damoiseaux, J.S., Beckmann, C.F., Arigita, E.J.S., Barkhof, F., Scheltens, P., Stam, C.J., Smith, S.M., Rombouts, S.A.R.B., 2008. Reduced resting-state brain activity in the “default network” in normal aging. *Cereb. Cortex* 18, 1856–1864. <https://doi.org/10.1093/cercor/bhm207>
- Damoiseaux, J.S., Greicius, M.D., 2009. Greater than the sum of its parts : a review of studies combining structural connectivity and resting-state functional connectivity. *Brain Struct. Funct.* 213, 525–533. <https://doi.org/10.1007/s00429-009-0208-6>
- Damoiseaux, J.S., Rombouts, S.A.R.B., Barkhof, F., Scheltens, P., Stam, C.J., Smith, S.M., Beckmann, C.F., 2006. Consistent resting-state networks across healthy subjects. *Proc. Natl. Acad. Sci. U. S. A.* 103, 13848–13853.

- <https://doi.org/10.1073/pnas.0601417103>
- Damoiseaux, J.S., Smith, S.M., Witter, M.P., Sanz-Arigitia, E.J., Barkhof, F., Scheltens, P., Stam, C.J., Zarei, M., Rombouts, S.A.R.B., 2009. White matter tract integrity in aging and alzheimer's disease. *Hum. Brain Mapp.* 30, 1051–1059. <https://doi.org/10.1002/hbm.20563>
- Dennis, E.L., Jahanshad, N., McMahon, K.L., de Zubicaray, G.I., Martin, N.G., Hickie, I.B., Toga, A.W., Wright, M.J., Thompson, P.M., 2013. Development of brain structural connectivity between ages 12 and 30: A 4-Tesla diffusion imaging study in 439 adolescents and adults. *Neuroimage* 64, 671–684. <https://doi.org/10.1016/j.neuroimage.2012.09.004>
- Dijkhuizen, R.M., Nicolay, K., 2003. Magnetic Resonance Imaging in experimental models of brain disorders. *J. Cereb. Blood Flow Metab.* 23, 1383–1402. <https://doi.org/10.1097/01.WCB.0000100341.78607.EB>
- Dirnagl, U., 2016. Thomas Willis lecture: Is translational stroke research broken, and if so, how can we fix it? *Stroke* 47, 2148–2153. <https://doi.org/10.1161/STROKEAHA.116.013244>
- Dosenbach, N.U.F., Nardos, B., Cohen, A.L., Fair, D.A., Power, J.D., Church, J.A., Nelson, S.M., Wig, G.S., Vogel, A.C., Lessov-Schlaggar, C.N., Barnes, K.A., Dubis, J.W., Feczko, E., Coalson, R.S., Pruett, J.R., Barch, D.M., Petersen, S.E., Schlaggar, B.L., 2010. Prediction of individual brain maturity using fMRI. *Science* (80-.). 329, 1358–1361. <https://doi.org/10.1126/science.1194144>
- Fair, D.A., Cohen, A.L., Power, J.D., Dosenbach, N.U.F., Church, J.A., Miezin, F.M., Schlaggar, B.L., Petersen, S.E., 2009. Functional brain networks develop from a “local to distributed” organization. *PLoS Comput. Biol.* 5, 14–23. <https://doi.org/10.1371/journal.pcbi.1000381>
- Ferreira, L.K., Busatto, G.F., 2013. Resting-state functional connectivity in normal brain aging. *Neurosci. Biobehav. Rev.* 37, 384–400. <https://doi.org/10.1016/j.neubiorev.2013.01.017>
- Ferreira, L.K., Regina, A.C.B., Kovacevic, N., Martin, M.D.G.M., Santos, P.P., Carneiro, C.D.G., Kerr, D.S., Amaro, E., McIntosh, A.R., Busatto, G.F., 2016. Aging effects on whole-brain functional connectivity in adults free of cognitive and psychiatric disorders. *Cereb. Cortex* 26, 3851–3865. <https://doi.org/10.1093/cercor/bhv190>
- Finger, S., 2004. Paul Broca: 1824–1880. *J. Neurol.* 251, 769–770. <https://doi.org/10.1007/s00415-004-0456-6>
- Fitzgerald, K.D., Welsh, R.C., Stern, E.R., Angstadt, M., Hanna, G.L., Abelson, J.L., Taylor, S.F., 2011. Developmental alterations of frontal-striatal-thalamic connectivity in obsessive-compulsive disorder. *J. Am. Acad. Child Adolesc. Psychiatry* 50, 938–948. <https://doi.org/10.1016/j.jaac.2011.06.011>
- Fjell, A.M., Sneve, M.H., Grydeland, H., Storsve, A.B., Amlien, I.K., Yendiki, A., Walhovd, K.B., 2016. Relationship between structural and functional connectivity change across the adult lifespan: A longitudinal investigation. *Hum. Brain Mapp.* 573, 561–573. <https://doi.org/10.1002/hbm.23403>
- Fornito, A., Zalesky, A., Breakspear, M., 2015. The connectomics of brain disorders. *Nat. Rev. Neurosci.* 16, 159–172. <https://doi.org/10.1038/nrn3901>
- Fox, M.D., Raichle, M.E., 2007. Spontaneous fluctuations in brain activity observed with functional magnetic resonance imaging. *Nat Rev Neurosci* 8, 700–711. <https://doi.org/10.1038/nrn2201>
- Fox, M.D., Snyder, A.Z., Vincent, J.L., Corbetta, M., Van Essen, D.C., Raichle, M.E., 2005. The human brain is intrinsically organized into dynamic, anticorrelated functional networks. *Proc. Natl. Acad. Sci. U. S. A.* 102, 9673–9678. <https://doi.org/10.1073/pnas.0504136102>
- Gerfen, C.R., Sawchenko, P.E., 1984. An anterograde neuroanatomical tracing method that shows the detailed morphology of neurons, their axons and terminals: Immunohistochemical localization of an axonally transported plant lectin, Phaseolus vulgaris-leucoagglutinin (PHA-L). *Brain Res.* 290, 219–238.
- Gong, G., Rosa-neto, P., Carbonell, F., Chen, Z.J., He, Y., Evans, A.C., 2009. Age- and gender-related differences in the cortical anatomical network. *J. Neurosci.* 29, 15684–15693. <https://doi.org/10.1523/JNEUROSCI.2308-09.2009>
- Grayson, D.S., Fair, D.A., 2017. Development of large-scale functional networks from birth to adulthood: A guide to the neuroimaging literature. *NeuroImage*. <https://doi.org/10.1016/j.neuroimage.2017.01.079>
- Gruner, P., Vo, A., Ikuta, T., Mahon, K., Peters, B.D., Malhotra, A.K., Uluğ, A.M., Szeszko, P.R., 2012. White matter abnormalities in pediatric obsessive-compulsive disorder. *Neuropsychopharmacology* 37, 2730–2739. <https://doi.org/10.1038/npp.2012.138>
- Hagmann, P., Sporns, O., Madan, N., Cammoun, L., Pienaar, R., Wedeen, V.J., Meuli, R., Thiran, J.-P., Grant, P.E., 2010. White matter maturation reshapes structural connectivity in the late developing human brain. *Proc. Natl. Acad. Sci. U. S. A.* 107, 19067–19072. <https://doi.org/10.1073/pnas.1009073107>
- He, B.J., Snyder, A.Z., Zempel, J.M., Smyth, M.D., Raichle, M.E., 2008. Electrophysiological correlates of the brain's intrinsic large-scale functional architecture. *Proc. Natl. Acad. Sci. U. S. A.* 105, 16039–16044. <https://doi.org/10.1073/pnas.0807010105>
- Heimer, L., Robards, M.J. (Eds.), 1981. *Neuroanatomical Tract-Tracing Methods*. Plenum Press, New York and London. <https://doi.org/10.1007/978-1-4613-3189-6>
- Herson, P.S., Traystman, R.J., 2014. Animal models of stroke: translational potential at present and in 2050. *Future Neurol.* 9, 541–551. <https://doi.org/10.2217/fnl.14.44>

- Honey, C.J., Sporns, O., Cammoun, L., Gigandet, X., Thiran, J.P., Meuli, R., Hagmann, P., 2009. Predicting human resting-state functional connectivity from structural connectivity. *Proc. Natl. Acad. Sci. U. S. A.* 106, 2035–2040. <https://doi.org/10.1073/pnas.0811168106>
- Hutchison, R.M., Womelsdorf, T., Allen, E.A., Bandettini, P.A., Calhoun, V.D., Corbetta, M., Della Penna, S., Duyn, J.H., Glover, G.H., Gonzalez-Castillo, J., Handwerker, D.A., Keilholz, S., Kiviniemi, V., Leopold, D.A., de Pasquale, F., Sporns, O., Walter, M., Chang, C., 2013. Dynamic functional connectivity: Promise, issues, and interpretations. *Neuroimage* 80, 360–78. <https://doi.org/10.1016/j.neuroimage.2013.05.079>
- Khundrakam, B.S., Reid, A., Brauer, J., Carbonell, F., Lewis, J., Ameis, S., Karama, S., Lee, J., Chen, Z., Das, S., Evans, A.C., 2013. Developmental changes in organization of structural brain networks. *Cereb. Cortex* 23, 2072–2085. <https://doi.org/10.1093/cercor/bhs187>
- Lavaill, J.H., Lavaill, M.M., 1972. Retrograde Axonal Transport in the Central Nervous System. *Science* (80-). 176, 1416–1417.
- Le Bihan, D., 2003. Looking into the functional architecture of the brain with diffusion MRI. *Nat. Rev. Neurosci.* 4, 469–480. <https://doi.org/10.1038/nrn1119>
- Liang, A.C., Mandeville, E.T., Maki, T., Shindo, A., Som, A.T., Egawa, N., Itoh, K., Chuang, T.T., McNeish, J.D., Holder, J.C., Lok, J., Lo, E.H., Arai, K., 2016. Effects of aging on neural stem/progenitor cells and oligodendrocyte precursor cells after focal cerebral ischemia in spontaneously hypertensive rats. *Cell Transplant.* 25, 705–714. <https://doi.org/10.3727/096368916X690557>
- Liu, F., Yuan, R., Benashski, S.E., McCullough, L.D., 2009. Changes in experimental stroke outcome across the lifespan. *J. Cereb. Blood Flow Metab.* 29, 792–802. <https://doi.org/10.1038/jcbfm.2009.5>
- Logothetis, N.K., 2008. What we can do and what we cannot do with fMRI. *Nature* 453, 869–878. <https://doi.org/10.1038/nature06976>
- Magri, C., Schridde, U., Murayama, Y., Panzeri, S., Logothetis, N.K., 2012. The amplitude and timing of the BOLD signal reflects the relationship between local field potential power at different frequencies. *J. Neurosci.* 32, 1395–1407. <https://doi.org/10.1523/JNEUROSCI.3985-11.2012>
- Matsui, T., Murakami, T., Ohki, K., 2019. Neuronal Origin of the Temporal Dynamics of Spontaneous BOLD Activity Correlation. *Cereb. Cortex* 29, 1496–1508. <https://doi.org/10.1093/cercor/bhy045>
- Meier, T.B., Desphande, A.S., Vergun, S., Nair, V. a., Song, J., Biswal, B.B., Meyerand, M.E., Birn, R.M., Prabhakaran, V., 2012. Support vector machine classification and characterization of age-related reorganization of functional brain networks. *Neuroimage* 60, 601–613. <https://doi.org/10.1016/j.neuroimage.2011.12.052>
- Mori, S., Van Zijl, P.C.M., 2002. Fiber tracking: Principles and strategies - A technical review. *NMR Biomed.* 15, 468–480. <https://doi.org/10.1002/nbm.781>
- O'Reilly, J.X., Crosson, P.L., Jbabdi, S., Sallet, J., Noonan, M.P., Mars, R.B., Browning, P.G.F., Wilson, C.R.E., Mitchell, A.S., Miller, K.L., Rushworth, M.F.S., Baxter, M.G., 2013. Causal effect of disconnection lesions on interhemispheric functional connectivity in rhesus monkeys. *Proc. Natl. Acad. Sci. U. S. A.* 110, 13982–13987. <https://doi.org/10.1073/pnas.1305062110>
- Ogawa, S., Lee, T.M., Kay, A.R., Tank, D.W., 1990. Brain magnetic resonance imaging with contrast dependent on blood oxygenation. *Proc Natl Acad Sci U S A* 87, 9868–9872. <https://doi.org/10.7556/JPSJ.84.064704>
- Otte, W.M., van Diessen, E., Paul, S., Ramaswamy, R., Subramanyam Rallabandi, V.P., Stam, C.J., Roy, P.K., 2015. Aging alterations in whole-brain networks during adulthood mapped with the minimum spanning tree indices: The interplay of density, connectivity cost and life-time trajectory. *Neuroimage* 109, 171–189. <https://doi.org/10.1016/j.neuroimage.2015.01.011>
- Pan, W.-J., Thompson, G., Magnuson, M., Majeed, W., Jaeger, D., Keilholz, S., 2011. Broadband local field potentials correlate with spontaneous fluctuations in functional Magnetic Resonance Imaging signals in the rat somatosensory cortex under isoflurane anesthesia. *Brain Connect.* 1, 119–131. <https://doi.org/10.1089/brain.2011.0014>
- Power, J.D., Fair, D.A., Schlaggar, B.L., Petersen, S.E., 2010. The development of Human Functional Brain Networks. *Neuron* 67, 735–748. <https://doi.org/10.1016/j.neuron.2010.08.017>
- Quinn, R., 2005. Comparing rat's to human's age: How old is my rat in people years? *Nutrition* 21, 775–777. <https://doi.org/10.1016/j.nut.2005.04.002>
- Semple, B.D., Blomgren, K., Gimlin, K., Ferriero, D.M., Noble-Haeusslein, L.J., 2013. Brain development in rodents and humans: Identifying benchmarks of maturation and vulnerability to injury across species. *Prog. Neurobiol.* 106–107, 1–16. <https://doi.org/10.1016/j.pneurobio.2013.04.001>
- Sengupta, P., 2013. The Laboratory Rat: Relating Its Age With Human's. *Int. J. Prev. Med.* 4, 624–630.
- Shmuel, A., Leopold, D.A., 2008. Neuronal correlates of spontaneous fluctuations in fMRI signals in monkey visual cortex: Implications for functional connectivity at rest. *Hum. Brain Mapp.* 29, 751–761. <https://doi.org/10.1002/hbm.20580>
- Sporns, O., 2013. Network attributes for segregation and integration in the human brain. *Curr. Opin. Neurobiol.* 23, 162–171. <https://doi.org/10.1016/j.conb.2012.11.015>
- Spreng, N.R., Schacter, D.L., 2012. Default network modulation and large-scale network interactivity in healthy young and old adults. *Cereb. Cortex* 22, 2610–2621. <https://doi.org/10.1093/cercor/bhr339>

- Straathof, M., Sinke, M.R., Dijkhuizen, R.M., Otte, W.M., on behalf of the TACTICS consortium, 2019. A systematic review on the quantitative relationship between structural and functional network connectivity strength in mammalian brains. *J. Cereb. Blood Flow Metab.* 39, 189–209. <https://doi.org/10.1177/0271678X18809547>
- Supekar, K., Musen, M., Menon, V., 2009. Development of large-scale functional brain networks in children. *PLoS Biol.* 7. <https://doi.org/10.1371/journal.pbio.1000157>
- Taylor, S., 2011. Early versus late onset obsessive-compulsive disorder: evidence for distinct subtypes. *Clin. Psychol. Rev.* 31, 1083–1100. <https://doi.org/10.1016/j.cpr.2011.06.007>
- Thomason, M.E., Dassanayake, M.T., Shen, S., Katkuri, Y., Alexis, M., Anderson, A.L., Yeo, L., Mody, S., Hernandez-Andrade, E., Hassan, S.S., Studholme, C., Jeong, J.W., Romero, R., 2013. Cross-hemispheric functional connectivity in the human fetal brain. *Sci. Transl. Med.* 5, 173ra24. <https://doi.org/doi:10.1126/scitranslmed.3004978>
- Tononi, G., Edelman, G.M., Sporns, O., 1998. Complexity and coherency: Integrating information in the brain. *Trends Cogn. Sci.* 2, 474–484. [https://doi.org/10.1016/S1364-6613\(98\)01259-5](https://doi.org/10.1016/S1364-6613(98)01259-5)
- Tononi, G., Sporns, O., Edelman, G.M., 1994. A measure for brain complexity: Relating functional segregation and integration in the nervous system. *Proc. Natl. Acad. Sci. U. S. A.* 91, 5033–5037.
- van den Heuvel, M.P., Mandl, R.C.W., Kahn, R.S., Hulshoff Pol, H.E., 2009. Functionally Linked Resting-State Networks Reflect the Underlying Structural Connectivity Architecture of the Human Brain. *Hum. Brain Mapp.* 30, 3127–3141. <https://doi.org/10.1002/hbm.20737>
- van den Heuvel, M.P., Sporns, O., 2019. A cross-disorder connectome landscape of brain dysconnectivity. *Nat. Rev. Neurosci.* 20, 435–446. <https://doi.org/10.1038/s41583-019-0177-6>
- Van Essen, D.C., Barch, D.M., 2015. The human connectome in health and psychopathology. *World Psychiatry* 14, 154–157. <https://doi.org/10.1002/wps.20228>
- Wang, L., Su, L., Shen, H., Hu, D., 2012. Decoding lifespan changes of the human brain using resting-state functional connectivity MRI. *PLoS One* 7, e44530. <https://doi.org/10.1371/journal.pone.0044530>
- Weber, A.M., Soreni, N., Noseworthy, M.D., 2014. A preliminary study of functional connectivity of medication naïve children with obsessive-compulsive disorder. *Prog. Neuropsychopharmacol. Biol. Psychiatry* 53, 129–136. <https://doi.org/10.1016/j.pnpbp.2014.04.001>
- Wu, K., Taki, Y., Sato, K., Kinomura, S., Goto, R., Okada, K., Kawashima, R., He, Y., Evans, A.C., Fukuda, H., 2012. Age-related changes in topological organization of structural brain networks in healthy individuals. *Hum. Brain Mapp.* 33, 552–568. <https://doi.org/10.1002/hbm.21232>
- Zarei, M., Mataix-Cols, D., Heyman, I., Hough, M., Doherty, J., Burge, L., Winnill, L., Nijhawan, S., Matthews, P.M., James, A., 2011. Changes in gray matter volume and white matter microstructure in adolescents with obsessive-compulsive disorder. *Biol. Psychiatry* 70, 1083–1090. <https://doi.org/10.1016/j.biopsych.2011.06.032>
- Zhu, W., Wen, W., He, Y., Xia, A., Anstey, K.J., Sachdev, P., 2012. Changing topological patterns in normal aging using large-scale structural networks. *Neurobiol. Aging* 33, 899–913. <https://doi.org/10.1016/j.neurobiolaging.2010.06.022>
- Zimmermann, J., Ritter, P., Shen, K., Rothmeier, S., Schirner, M., McIntosh, A.R., 2016. Structural architecture supports functional organization in the human aging brain at a regionwise and network Level. *Hum. Brain Mapp.* 37, 2645–2661. <https://doi.org/10.1002/hbm.23200>
- Zola-Morgan, S., 1995. Localization of Brain Function: The Legacy of Franz Joseph Gall (1758–1828). *Annu. Rev. Neurosci.* 18, 359–383. <https://doi.org/10.1146/annurev.neuro.18.1.359>



Distinct structure-function relationships across cortical regions and connectivity scales in the rat brain

Milou Straathof¹, Michel R.T. Sinke¹, Theresia J.M. Roelofs^{1,2}, Erwin L.A. Blezer¹, R. Angela Sarabdjitsingh², Annette van der Toorn¹, Oliver Schmitt³, Willem M. Otte^{1,4} & Rick M. Dijkhuizen¹

¹ *Biomedical MR Imaging and Spectroscopy Group, Center for Image Sciences, University Medical Center Utrecht and Utrecht University, Utrecht, The Netherlands.*

² *Department of Translational Neuroscience, UMC Utrecht Brain Center, University Medical Center Utrecht and Utrecht University, Utrecht, the Netherlands.*

³ *Department of Anatomy, University of Rostock, Rostock, Germany.*

⁴ *Department of Pediatric Neurology, UMC Utrecht Brain Center, University Medical Center Utrecht and Utrecht University, Utrecht, the Netherlands.*

Scientific Reports 2020; 10(1); 56.

Supplementary material is available at Scientific Reports online.

Abstract

An improved understanding of the structure-function relationship in the brain is necessary to know to what degree structural connectivity underpins abnormal functional connectivity seen in disorders. We integrated high-field resting-state fMRI-based functional connectivity with high-resolution macro-scale diffusion-based and meso-scale neuronal tracer-based structural connectivity, to obtain an accurate depiction of the structure-function relationship in the rat brain. Our main goal was to identify to what extent structural and functional connectivity strengths are correlated, macro- and meso-scopically, across the cortex. Correlation analyses revealed a positive correspondence between functional and macro-scale diffusion-based structural connectivity, but no significant correlation between functional connectivity and meso-scale neuronal tracer-based structural connectivity. Zooming in on individual connections, we found strong functional connectivity in two well-known resting-state networks: the sensorimotor and default mode network. Strong functional connectivity within these networks coincided with strong short-range intrahemispheric structural connectivity, but with weak heterotopic interhemispheric and long-range intrahemispheric structural connectivity. Our study indicates the importance of combining measures of connectivity at distinct hierarchical levels to accurately determine connectivity across networks in the healthy and diseased brain. Although characteristics of the applied techniques may affect where structural and functional networks (dis)agree, distinct structure-function relationships across the brain could also have a biological basis.

Introduction

The brain is a complex organ that can be regarded as a structural and functional network of interacting regions at the micro-, meso- and macroscopic level. At the macro-scale, whole-brain functional networks can be non-invasively mapped with resting-state functional MRI (resting-state fMRI). In resting-state fMRI data the inter-regional temporal correlations of spontaneous low-frequency blood oxygenation level-dependent (BOLD) fluctuations reflect functional connectivity (B. Biswal et al., 1995; Michael D. Fox and Raichle, 2007). Based on clusters of functionally connected regions, various resting-state networks have been identified, such as the default mode network (Greicius et al., 2003). These networks have been related to behavioral functioning in health and disease, and abnormalities partially explain pathophysiological processes and disease progression (Raichle, 2015; van den Heuvel and Hulshoff Pol, 2010; Zhang and Raichle, 2010).

The exact nature of functional connectivity is nonetheless not yet fully established. Since functional connectivity measured with resting-state fMRI relies on synchronous BOLD signals, understanding functional connectivity starts with understanding the origin of BOLD signals. The BOLD signal captures hemodynamic changes, such as blood flow, in response to neural activity. Although it is clear that BOLD signals reflect aspects of neural responses, it is still unclear which processes are the main contributors, i.e. excitation or inhibition, local field potentials, action potentials or multi-unit activity (Logothetis et al., 2001; Nikos K Logothetis, 2008; Logothetis and Wandell, 2004). We know from primate and rodent studies that spontaneous BOLD fluctuations match with slow fluctuations in neuronal activity (Magri et al., 2012; Pan et al., 2011; Shmuel and Leopold, 2008). Moreover, in humans, BOLD signal fluctuations are related to slow cortical potentials and gamma band-limited power (He et al., 2008). Still, the underlying structure of functional connectivity remains largely unknown. Since functional connectivity is found between adjacent and remote brain areas, short- and long-distance structural connections seem essential. Structural connectivity can be measured non-invasively with diffusion MRI and invasively with neuronal tracers. Diffusion-based tractography enables reconstruction of whole-brain macro-scale structural networks, by indirectly inferring the direction and strength of large white matter tracts from the diffusion of water (Basser et al., 1994; Turner et al., 1990). In contrast, neuronal tracers use the transport mechanisms of cells to label existing mono- or polysynaptic connections. Tracers thus provide a direct and accurate measure of the directionality and strength at the meso-scale of individual axonal projections (Heimer and Robards, 1981).

Functional connectivity strength correlates with both diffusion- and neuronal tracer-based structural connectivity strength at the whole-brain level (Honey et al., 2009; Miranda-Dominguez et al., 2014); for an overview see (Straathof et al., 2019). However, different regions and connections display different structure-function relationships (Grandjean et al., 2017; Wang et al., 2012; Zimmermann et al., 2016). Identifying where and to what extent structural and functional connectivity strengths correlate will help to understand how brain networks are organized, and why functional abnormalities in brain disorders are related to characteristic patterns of disconnection or reorganization. So far, most studies have compared functional connectivity with structural connectivity measured at either the macro-scale or meso-scale, and thereby did not capture all aspects of structural connectivity. In addition, studies that applied diffusion MRI are hampered by the fact that a diffusion-based structural network is a suboptimal reconstruction of macro-scale axonal projections (Maier-Hein et al., 2017; Schilling et al., 2019; Sinke et al., 2018; Thomas et al., 2014). More accurate assessment of the structure-function relationships requires integration of functional connectivity with both macro-scale diffusion- and meso-scale neuronal tracer-based structural measures. Distinct structure-function relationships may be present at these different hierarchical levels (Reid et al., 2016). Rodents are excellent species to study these relationships as resting-state fMRI and diffusion MRI-based tractography are feasible in rodents (Dijkhuizen and Nicolay, 2003) and comprehensive rodent databases of neuronal tracer-based structural connectivity are available as well (Noori et al., 2017; Schmitt and Eipert, 2012).

In this study we combined high-field resting-state fMRI-based functional connectivity measurements and diffusion- as well as neuronal tracer-based structural connectivity measurements from the rat brain to spatially map the structure-function relationship at the macro- and meso-scale. Our main goal was to identify to what extent structural and functional connectivity strength are correlated, macro- and meso-scopically, across the rat brain, which could explain differences in the functional significance of connections and their contribution to network dysfunction in brain disorders. We distinguished interhemispheric and intrahemispheric connections, as well as specific functional networks (sensorimotor or default mode network).

Methods

Ethics statement

All experiments were approved by the Committee for Animal Experiments of the University Medical Center Utrecht, The Netherlands, and were conducted in agreement with European regulations (Guideline 86/609/EEC) and Dutch laws ('Wet op de Dierproeven', 1996).

Animals

In vivo resting-state functional connectivity

Resting-state functional connectivity was measured in twelve healthy adult male Wistar rats with a weight of 479 ± 44 g (mean \pm standard deviation (SD)), which were group-housed and used for an earlier described study (Roelofs et al., 2017). All animals had *ad libitum* access to food and water and were housed under the same environmental conditions (temperature 22-24° and 12 h light/dark cycle with lights on at 7:00 AM).

Post-mortem diffusion-based structural connectivity

Diffusion-based structural connectivity was measured in ten healthy adult male Wistar rats with an age of around twelve weeks. These animals were previously used in another study (Sarabdjitsingh et al., 2017) and group-housed under standard environmental conditions (12h light/dark cycle with lights on at 7:00 AM). Animals were sacrificed by an intraperitoneal pentobarbital injection followed by transcardial perfusion-fixation with 4% paraformaldehyde in phosphate-buffered saline, as previously described (Sarabdjitsingh et al., 2017). We extracted the brains by removing all extracranial tissue, while leaving them inside the skull, and placed these in a proton-free oil (Fomblin*) prior to MR imaging to minimize susceptibility artefacts.

MRI acquisition

All MRI experiments were conducted on a 9.4T horizontal bore Varian MR system (Palo Alto, CA, USA), equipped with a 400 mT/m gradient coil (Agilent).

In vivo resting-state functional connectivity

Before MRI, the animals were anesthetized (with 4% of isoflurane in air for induction). Endotracheal intubation was performed to mechanically ventilate the rats with 1.5% of isoflurane in a mixture of air and O₂ (4:1). End-tidal CO₂ was continuously monitored with a capnograph (Microcap, Oridion Medical 1987 Ltd., Jerusalem, Israel). The animals were

placed in an animal cradle and immobilized in a specially designed stereotactic holder. During MRI, a feed-back controlled heating pad ensured that the body temperature of the rats was maintained at 37.0 ± 1.0 °C. Blood oxygen saturation and heart rate were monitored with a pulse-oximeter from signals recorded with an infrared sensor attached to the hind paw of the animal.

We used a home-built 90 mm diameter Helmholtz volume coil for radiofrequency transmission, and an inductively coupled 25 mm diameter surface coil for signal detection. Prior to resting-state fMRI acquisition we acquired an anatomical image for registration purposes using 3D balanced steady-state free precession (bSSFP) imaging with four phase-cycling angles (0°, 90°, 180°, 270°). The acquisition parameters were as follows: repetition time (TR) / echo time (TE) = 5/2.5 ms; flip angle = 20°; field-of-view (FOV) = $40 \times 32 \times 24$ mm³; acquisition matrix = $160 \times 128 \times 96$; image resolution = 250 μm isotropic. Total acquisition time = 12.5 min. Resting-state fMRI images were acquired with T₂'-weighted blood oxygenation level-dependent (BOLD) single shot 3D gradient-echo Echo Planar Imaging (EPI). The acquisition parameters were as follows: TR/TE = 26.1/15 ms; flip angle = 13°; FOV = $32.4 \times 32.4 \times 16.8$ mm³, Acquisition matrix = $54 \times 54 \times 28$; Spatial Resolution = 600 μm isotropic. The acquisition time was 730.8 ms per volume, with a total of 800 volumes, resulting in a scan time of 9 minutes and 45 seconds.

Post-mortem diffusion-based structural connectivity

For diffusion MRI we used a custom-made solenoid coil with an internal diameter of 26 mm. High spatial and angular resolution diffusion imaging (HARDI) was performed with an 8-shot 3D EPI sequence. The acquisition parameters were as follows: TR/TE = 500/32.4 ms, Δ/δ = 15/4 ms; b-value = 3842 s/mm²; FOV = $19.2 \times 16.2 \times 33$ mm³; Acquisition matrix = $128 \times 108 \times 220$; spatial resolution: $150 \times 150 \times 150$ μm³. Diffusion-weighting was executed in 60 non-collinear directions on a half sphere and included five b₀ non-diffusion-weighted images, with a total scan time of 8 hours.

MRI processing

All MRI analyses were performed using FMRIB's Software Library (FSL) v5.0, unless otherwise stated.

Regions of interest

To enable the selection of regions of interest, the mean resting-state fMRI image of each dataset was first linearly registered (*FLIRT* (Jenkinson et al., 2002; Jenkinson and Smith,

2001)) to the anatomical image of the same animal, followed by non-linear registration (*FNIRT* (Andersson et al., 2007a)) to a custom-built 3D model of the Paxinos and Watson rat brain atlas (Majka et al., 2012; G. Paxinos and Watson, 2005). For diffusion MRI, the average of the non-diffusion-weighted images of each individual rat was non-linearly registered to this rat brain atlas. These registrations were used to transform 106 cortical bilateral regions into individual diffusion MRI and resting-state fMRI spaces. We only included regions of interest with sufficient assurance of spatial alignment, i.e., regions consisting of at least 8 voxels in individual resting-state fMRI space. This resulted in 82 bilateral cortical regions (Supplementary Table S1).

In vivo resting-state functional connectivity

The first twenty images of the resting-state fMRI scan were removed to ensure a steady state and the remaining images were motion-corrected to the mean volume with *MCFLIRT* (Jenkinson et al., 2002) and brain-extracted with *BET* (Smith, 2002). The six motion correction parameters were used as regressors for the resting-state fMRI signal. No global signal regression was performed. Low-frequency BOLD fluctuations were obtained by band-pass filtering between 0.01 and 0.1 Hz in *AFNI* (Cox, 1996). We performed an independent component analysis (Beckmann and Smith, 2004) with 20 components to identify resting-state networks in the rat brain (Supplementary Figure S1). To determine functional connectivity between brain regions, we calculated Fisher's Z-transformed full correlation coefficients between the time-series for all pairs of regions of interest. These Fisher's Z-transformed correlation coefficients were averaged over all rats to obtain a group-level measurement of functional connectivity strength between our regions of interest.

Post-mortem diffusion-based structural connectivity

We used single shell constrained spherical deconvolution (CSD) to construct a fiber orientation distribution (FOD) map for every rat. Next, CSD-based tractography, using the iFOD2 algorithm, was performed in MRtrix3[®] (<http://www.mrtrix.org/>) (Tournier et al., 2010; J. D. Tournier et al., 2012). The iFOD2 algorithm uses 2nd order integration over adjacent orientation distributions (Tournier et al., 2010). Whole brain tractography was done in individual subject space using dynamic seeding, thereby generating 2.5 million streamlines with a step size of 75 μm , an angle threshold of 40° and a FOD threshold of 0.2. The generated tractograms were filtered by *Spherical deconvolution Informed Filtering of Tracts* (SIFT) (Smith et al., 2015, 2013). Subsequently, the connectomes were constructed by matching the whole-brain filtered tractograms with the regions of interest in subject space, by applying the

registration procedure described above. Regions of interest were structurally connected if one or multiple streamlines had their endpoints in both regions, where the filtered number of inter-regional streamlines was indicative of structural connectivity strength. Finally, we calculated an average weighted connectome, in which the edge values represent structural connectivity strengths, to obtain a group-level measurement of diffusion-based structural connectivity strength between our regions of interest.

Neuronal tracer-based structural connectivity

Neuronal tracer-based structural connectivity data was extracted from the NeuroVIISAS database (Schmitt and Eipert, 2012). This database contains rat nervous system data from over 7860 published tract-tracing studies, describing in total 591,435 ipsi- and contralateral connections. Many of these connections are described in multiple studies, affirming the robustness of the dataset. Studies with anterograde as well as retrograde monosynaptic tracers have been included, giving directionality information about the structural connections.

We used the same regions of interest as described for the functional connectivity and diffusion-based structural connectivity analyses to extract neuronal tracer-based structural connectivity for all pairs of regions (Supplementary Table S1). The weights of the directed connections are assigned in the NeuroVIISAS database as follows: 0: no connection or no information available; 1: light/sparse connection; 2: moderate/dense connection; 3: strong connection and 4: very strong connection. We averaged these connection weights over all studies investigating the same connection, resulting in a scale for neuronal tracer-based structural connectivity between 0 and 4.

Experimental design and statistical analysis

The analysis pipeline is illustrated in Figure 1. All statistical and descriptive analyses were performed in R (version 3.2.3) (R Core Team, 2014).

The network of 82 regions consisted of 6,724 directed connections, of which we removed the self-connections, resulting in a total of 6,642 unique connections. For the resting-state functional connectivity and diffusion-based structural connectivity networks, which did not contain directionality information, the network consisted of 3,321 unique connections. Only connections that existed in both the macro- and mesoscale structural connectivity datasets, meaning that they had a structural connectivity strength higher than zero in both datasets, were included for the analysis. In this way, we excluded connections with no information available in the neuronal tracer database, and minimized the amount of

false-positives often present in diffusion-based tractography networks (Maier-Hein et al., 2017).

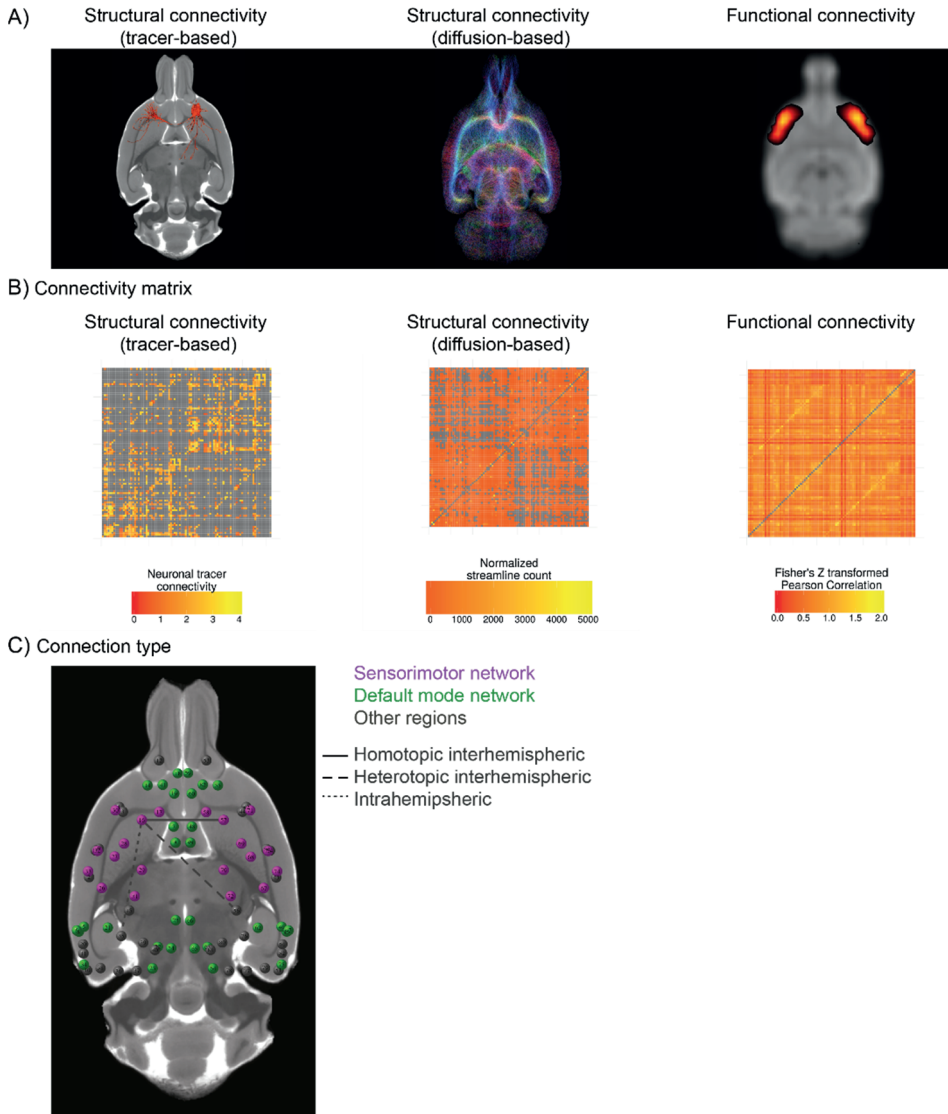


Figure 1: Overview of the analysis pipeline. Rat brain images are shown as axial views. Different measures of connectivity in the rat brain were assessed (a): meso-scale neuronal tracer-based structural connectivity (left), macro-scale diffusion-based structural connectivity (middle) and macro-scale resting-state functional connectivity (right). For each measure, we determined the connectivity matrix between 82 cortical regions of interest, with exclusion of the self-connections (central diagonal line) (b). We combined all connectivity matrices to determine the structure-function connectome of the rat brain (c) (circles representing nodes). The connectomes were reconstructed in 3D but are visualized in 2D. The colors in (c) represent two well-described functional resting-state

networks in the rat brain: the sensorimotor network (purple) and the default mode network (green). Regions not belonging to these networks are shown in gray. The lines represent different regional types of connections: homotopic interhemispheric connection (solid line), heterotopic interhemispheric connection (dashed line) or intrahemispheric connection (dotted line) (see Methods section for an explanation of these connection types).

Relationship between structural and functional connectivity strength at whole-brain level

To map the structure-function relationship globally, we performed correlation analyses between functional connectivity strength and macro-scale diffusion-based or meso-scale neuronal tracer-based structural connectivity separately. We applied a natural logarithmic transformation to both structural connectivity weights because they were skewed towards smaller connectivity weight values. Since the functional connectivity dataset and logarithmically transformed diffusion-based and neuronal tracer-based structural connectivity datasets were not normally distributed, we calculated a two-tailed Spearman rank correlation coefficient (ρ) between functional connectivity strength and logarithmically transformed macro-scale diffusion-based or meso-scale neuronal tracer-based structural connectivity strength. In addition, we calculated the correlation between functional and diffusion-based and neuronal tracer-based structural connectivity for interhemispheric and intrahemispheric connections separately. We determined the 95% confidence intervals of all Spearman rank correlation coefficients by means of bootstrapping with 5000 replicates. In addition, we determined whether functional connectivity strength was different between intrahemispheric and interhemispheric connections with a Wilcoxon rank sum test.

Relationship between structural and functional connectivity strength at connection level

To map the level of agreement between structural and functional connectivity at connection level, we selected the strongest and weakest structural connections at both the macro- and meso-scale. The strongest structural network was defined by connections that belonged to the 25% strongest diffusion-based and 25% strongest neuronal tracer-based structural connections. The weakest structural network was defined by connections that belonged to the 25% weakest diffusion-based and 25% weakest neuronal tracer-based structural connections. By combining macro- and meso-scale structural connectivity strengths, we selected the structural networks that were strong or weak at the level of individual axonal projections as well as at the level of large white matter bundles. This heightened the reliability of our assessment of the strength of structural connections and reduced the influence of methodological bias for specific connections. We compared functional connectivity strength between the strongest and weakest structural networks with a Wilcoxon rank sum test.

For both the strongest and weakest structural network, we determined the 25% strongest and 25% weakest functional connections, resulting in four sub-groups of connections. Two of these sub-groups represent connections where structural and functional connectivity strength agree: strong structural and functional connectivity or weak structural and functional connectivity. The other two subgroups are connections where structural and functional connectivity strength disagree: strong structural connectivity but weak functional connectivity or weak structural connectivity but strong functional connectivity.

To determine whether these subgroups of connections share common characteristics, we determined the Euclidian distance and type of connections and regions for all connections.

Between each pair of regions, we calculated the Euclidian distance, which is the shortest distance between two points in space (i.e., in a straight line). We determined the Euclidian distance for each pair of brain regions, because both structural and functional connectivity depend on distance, with in general lower connectivity for longer distances (Ercsey-Ravasz et al., 2013; Reveley et al., 2015; Salvador et al., 2005). Therefore, we determined the x, y, and z coordinate in mm of the center of gravity of each region in atlas space. Subsequently, we calculated the Euclidean distance, between each pair of regions i and j , with the following formula:

$$d(i, j) = \sqrt{(x_i - x_j)^2 + (y_i - y_j)^2 + (z_i - z_j)^2}$$

We divided the included connections and regions in sub-groups based on two different criteria. First, for each connection, we identified whether it was an intrahemispheric connection, which runs between two regions in the same hemisphere, or an interhemispheric connection, which runs between two regions in different hemispheres. In addition, we subdivided the interhemispheric connections into homotopic interhemispheric connections, which run between two homologous areas in different hemispheres and heterotopic interhemispheric connections, which run between two dissimilar areas in different hemispheres (Figure 1C). Second, for each region of interest, we assessed whether it belonged to one of two well-described functional networks in the rat brain, which were identified as the two networks explaining most of the variance in the independent component analysis of the functional connectivity dataset (Supplementary Figure S1): the sensorimotor network or the default mode network (Figure 1C). The sensorimotor network was defined as consisting of the left and right primary and secondary motor cortex (M1 and M2), subdivisions of the primary somatosensory cortex (S1BF, S1DZ, S1FL, S1HL, S1J, S1Tr, S1ULp) and the

secondary somatosensory cortex (S2) (Sierakowiak et al., 2015). The default mode network was defined as consisting of the left and right medial prefrontal cortex (mPFC), the cingulate cortex (Cg1 and Cg2), the orbital cortex (VO, MO and LO), the auditory/temporal association cortex (Au1, AuD, AuV and TeA), the posterior parietal cortex (ParPD) and the retrosplenial cortex (RSd, RSGb, RSGc) (Lu et al., 2012). For each connection, we determined whether the connection was within one of these functional networks, or whether it was connecting one of these functional networks with another functional network.

Results

Of all the possible 6,642 connections between the 82 selected regions of the cortical network, 1,175 connections (17.7% of the possible 6,642 connections) displayed structural connectivity in both the diffusion MRI and the neuronal tracer dataset. The average Euclidean distance for all the included connections in this network was 6.08 ± 3.35 mm (mean \pm standard deviation (SD)).

Global correlation between structural and functional connectivity depends on method and scale

Functional connectivity strength was positively correlated with diffusion-based structural connectivity strength in cortical connections ($\rho=0.41$; $p<0.0001$; 95% confidence interval: 0.36 – 0.46; Figure 2a). For the same cortical connections, functional connectivity strength did not significantly correlate with neuronal tracer-based structural connectivity strength ($\rho=0.04$, $p=0.14$; 95% confidence interval: -0.01 – 0.10; Figure 2b). In addition, we determined the structure-function correlation for interhemispheric and intrahemispheric connections separately. For interhemispheric connections, functional connectivity was significantly positively correlated with diffusion-based structural connectivity ($\rho=0.41$; $p<0.0001$; 95% confidence interval: 0.30 – 0.51) and with neuronal tracer-based structural connectivity ($\rho=0.25$; $p<0.0001$; 95% confidence interval: 0.14 – 0.35). In intrahemispheric connections, functional connectivity was significantly positively correlated with diffusion-based structural connectivity ($\rho=0.51$; $p<0.0001$; 95% confidence interval: 0.46 – 0.57), but not with neuronal tracer-based structural connectivity ($\rho=-0.02$; $p=0.64$; 95% confidence interval: -0.08 – 0.05). In addition, functional connectivity was slightly higher in interhemispheric compared to intrahemispheric connections, although the distribution of functional connectivity values in

these structural categories almost completely overlapped (interhemispheric connections: Fisher's $Z = 0.85 \pm 0.28$ (mean \pm standard deviation); intrahemispheric connections: Fisher's $Z = 0.77 \pm 0.25$ $p=0.0002$) (Supplementary Figure S2).

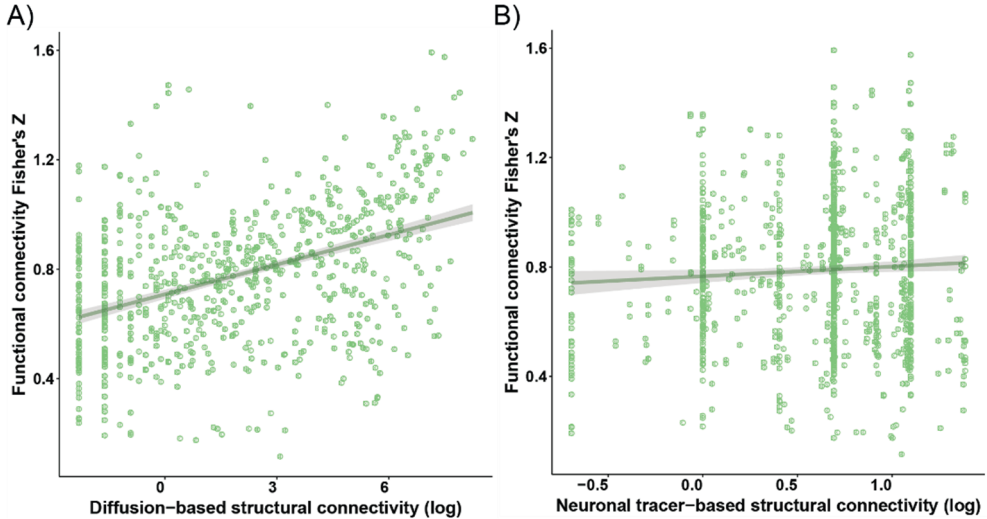


Figure 2: Whole-brain structure-function relationships at the structural macro-scale (diffusion-based structural connectivity) and meso-scale (neuronal tracer-based structural connectivity). Functional connectivity strength is plotted as the Fisher's Z-transformed correlation coefficient versus the natural logarithmically transformed diffusion-based (a) or neuronal tracer-based structural connectivity strength (b). Individual connections are plotted as green circles. The structure-function relationship is shown as a linear fit, with shading representing the 95% confidence intervals of the fit.

Different pathways and brain circuits display distinct structure-function relationships

The strongest structural network at the macro- and meso-scale consisted of 107 cortical connections. These strongest structural connections were mainly intrahemispheric (93% of strongest structural network; left: 47%, right: 46 %) with an average Euclidean distance of 2.54 ± 1.71 mm (see Figure 3). The weakest structural network at the macro- and meso-scale consisted of 93 connections. Of these weakest structural connections 31% was interhemispheric and 69% was intrahemispheric (left: 32%, right: 37%), with an average distance of 9.55 ± 2.42 mm (see Figure 3). Functional connectivity was higher in the strongest structural network compared to the weakest structural network (Strong: Fisher's $Z = 0.94 \pm 0.26$; Weak: Fisher's $Z = 0.65 \pm 0.21$; $p < 0.0001$) (Supplementary Figure S3).

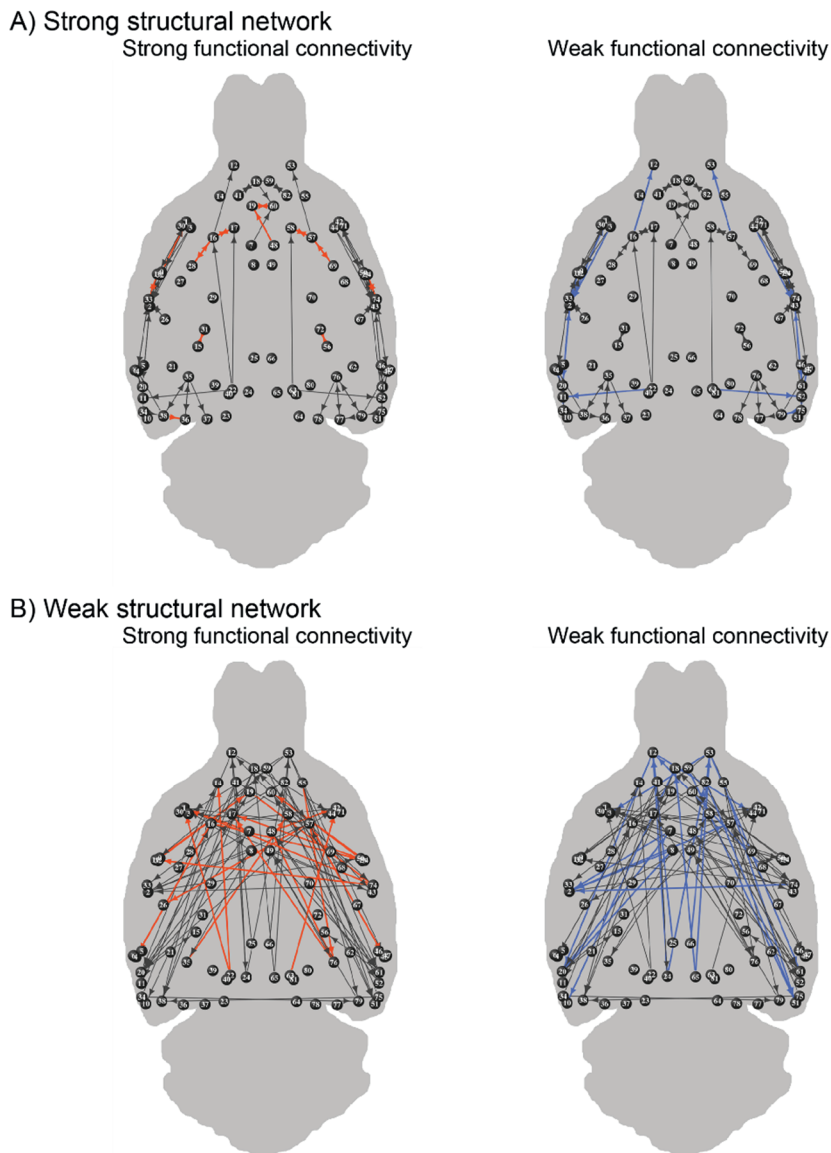


Figure 3: Strongest and weakest functional connections within the strongest and weakest structural networks. The strongest structural network consists of the connections that belong to both the 25% strongest structural connections at the macro-scale and the 25% strongest connections at the meso-scale (a), and the weakest structural network consists of the connections belonging to the 25% weakest at both hierarchical scales (b). Functional connectivity is orange colored for the 25% strongest (left) and blue colored for the 25% weakest functional connections (right). Circles represent the nodes (regions of interest), with numbers representing the regions listed in Table 1, and lines represent the edges (connections). The connectomes were reconstructed in 3D but are visualized in 2D. The arrowheads reflect directionality information determined from the neuronal tracer-based structural connectivity dataset.

Within both the strongest and weakest cortical structural networks, we determined the 25% strongest and 25% weakest functional connections. These strongest and weakest functional connections are depicted in Figure 3. The characteristics of these subcategories of connections are summarized in Figure 4 and described below.

	Strong structural connectivity (macro- and meso-scale)	Weak structural connectivity (macro- and meso-scale)	
Strong functional connectivity	<ul style="list-style-type: none"> * Intrahemispheric connections * Sensorimotor network / within default mode network * Short distance 	<ul style="list-style-type: none"> * Heterotopic interhemispheric/ intrahemispheric connections * Sensorimotor network / Default mode network * Long distance 	<i>Cortical connections within or between the sensorimotor network and default mode network</i>
Weak functional connectivity	<ul style="list-style-type: none"> * Intrahemispheric connections * Parahippocampal areas, insular, auditory cortex * Outside of functional networks * Short/Intermediate distance 	<ul style="list-style-type: none"> * Heterotopic interhemispheric/ intrahemispheric connections * Frontal cortices, parahippocampal areas, retrosplenial cortex * Default mode network to other network * Long distance 	<i>Cortical connections outside of included functional networks or between the default mode network and another functional network</i>
	<i>Short distance intrahemispheric cortical connections</i>	<i>Long distance interhemispheric or intrahemispheric cortical connections</i>	

Figure 4: Characteristics of connections per subcategory of structural and functional connectivity. Structural connectivity is depicted in columns, whereas functional connectivity is depicted in rows. Strong connections belong to the 25% strongest connections; structurally based on diffusion MRI and neuronal tracing (i.e., at both the macro- and meso-scale) and functionally based on resting-state fMRI. Similarly, weak structural connections belong to the 25% weakest connections.

Connections with strong structural and functional connectivity are shown in Table 1. The average length of the connections was 1.34 ± 0.69 mm. Eighty-eight percent of these strongest connections was intrahemispheric (left: 50%; right: 38%). Sixty-two percent of the connections was part of the sensorimotor network. The homotopic connection between the left and right medial prefrontal cortex, which is part of the default mode network, was also one of the identified strongest connections.

Table 2 shows the connections that we identified as belonging to the 25% weakest structural and functional connections. The average length of the weakest structural and functional connections was 10.84 ± 2.09 mm. The identified connections included 30% heterotopic interhemispheric and 70% intrahemispheric (left: 44%, right: 26 %) connections,

and were mainly between frontal cortices, parahippocampal areas and the retrosplenial cortex. Sixty-one percent of the connections connected the default mode network with another functional network.

Table 3 shows connections with strong structural but weak functional connectivity. All these connections were intrahemispheric (50% right; 50% left), of which the average Euclidean distance between regions was 3.23 ± 1.64 mm. Many of these connections were between parahippocampal areas and the insular cortex or auditory cortex, and within the insular cortex.

The connections belonging to 25% strongest functional but 25% weakest structural connections are shown in Table 4. The average Euclidean length of the connections was 8.67 ± 1.78 mm and 35% were heterotopic interhemispheric, all of which were part of the sensorimotor network. Fifty-two percent of the connections resided within the sensorimotor network or between the sensorimotor network and another network, of which 42% connected the sensorimotor with the default mode network. Forty-three percent of the connections was between the default mode network and another functional network.

Discussion

Our study on the rat brain shows that cortical brain networks are characterized by functional connectivity strengths, as measured with resting-state fMRI, that partly associate with macro-scale diffusion-based structural connectivity strength but not significantly associate with meso-scale neuronal tracer-based structural connectivity strength. When examining brain areas where structural and functional connectivity agreed or disagreed, we found that strong functional connectivity in the sensorimotor and default mode network matched with strong structural connectivity of intrahemispheric connections but was accompanied by weak structural connectivity of interhemispheric and long-range intrahemispheric connections.

Distinct global structure-function relationships across different hierarchical levels of structural connectivity

The partial positive correspondence between functional connectivity and diffusion-based structural connectivity strength in the rat brain is in line with structure-function relationships found in humans (Straathof et al., 2019). However, we did not find a significant correlation between functional connectivity and meso-scale neuronal tracer-based structural

connectivity strength. One previous study investigated this relationship at the meso-scale in rats and reported a positive structure-function correlation ($r=0.48$) (Díaz-Parra et al., 2017). However, this study did not include essential interhemispheric connections. Interhemispheric connections are known to have lower structure-function relationships (Shen et al., 2012), which may be explained by long inter-regional distances, sparser interhemispheric connectivity or involvement of polysynaptic or indirect connections (O'Reilly et al., 2013). Distinct structure-function relationships at the structural macro- and meso-scale have already been demonstrated in a study combining datasets in humans (functional and diffusion-based structural connectivity) and macaques (neuronal tracer-based structural connectivity) (Reid et al., 2016). However, the authors could not disentangle whether these distinct relationships were due to species differences or due to different measures of structural connectivity. Since we compared all three measures in the same species, (dis)agreement between structural and functional connectivity most likely reflects topological differences in the structure-function relationship across different hierarchical levels.

Besides being measurements at different hierarchical levels, another important difference between macro-scale diffusion-based and meso-scale neuronal tracer-based structural connectivity is the directionality information available in the data. Whereas diffusion-based structural connectivity does not provide directionality information, meaning that all connections are considered to be fully reciprocal, neuronal tracer-based structural connectivity does provide this directionality information. Since resting-state functional connectivity is also directionless, the correlation of functional connectivity with diffusion-based structural connectivity may be higher than with neuronal tracer-based structural connectivity. In addition, the correlation between functional connectivity and diffusion-based structural connectivity may also be explained by the fact that both connectivity measures are determined with the same measurement tool, i.e., MRI.

Strong functional connectivity in robust resting-state networks is supported by strong short-range intrahemispheric connections

The sensorimotor and default mode network are robustly established resting-state networks in the rodent brain (Pawela et al., 2008; Sierakowiak et al., 2015), which was corroborated by our finding of strong functional connectivity in or between these networks. We also observed strong short-range intrahemispheric structural connections at meso- and macro-scale in these networks. Strong reciprocal structural connections have previously been shown

between ipsilateral sensorimotor cortices, measured with neuronal tracers (Hoffer et al., 2003; Miyashita et al., 1994; Rocco-Donovan et al., 2011), and between default mode network regions, measured with diffusion MRI (Greicius et al., 2009; Horn et al., 2014). In comparison, in the current study we found that heterotopic interhemispheric structural connections in the sensorimotor network and long-range intrahemispheric structural connections between the default mode network and other functional networks were weak at both the macro- and the meso-scale. Since both connection types were between areas located far apart from each other, this observation may reflect the difficulties of diffusion-based tractography to reconstruct long-distance connections (Reveley et al., 2015), and the distance-dependence of neuronal tracer-based structural connectivity strength (Ercsey-Ravasz et al., 2013). Hereby, our data point out that the distance-dependence of structural connectivity strength, as determined from diffusion MRI or neuronal tracing, influences measurements of structure-function relationships. This should be taken into account in studies on the relation between structural and functional connectivity. However, weak heterotopic interhemispheric connectivity may also reflect the smaller role these connections play in functional brain organization as compared to homotopic interhemispheric connections (Deco et al., 2014; Messé et al., 2014). Interestingly, strong functional connectivity in homotopic interhemispheric connections within the sensorimotor network was not accompanied by strong structural connectivity, despite the presence of a large bundle of neuronal fibers, i.e., the corpus callosum, connecting the two hemispheres. This may be a result of our approach of only including connections that exhibit macro- and meso-scale structural connectivity. Homotopic interhemispheric connections in the sensorimotor network were included in the 25% strongest meso-scale neuronal tracer-based structural network, but not in the 25% strongest macro-scale diffusion-based structural network. Therefore, we limit our conclusions to connections with matching macro- and meso-scale structural connectivity, while other structure-function relationships may exist in connections where macro-, and meso-scale structural connectivity do not match.

Implications of different structure-function relationships across the brain in health and disease

We have shown that distinct structure-function relationships exist in different cortical connections of the rat brain, in line with a previous study reporting that 25% of valid structural connections are very weak functional connections (Lee and Xue, 2018). Different structure-function relationships can have implications for brain functioning and behavior.

Healthy brain functioning relies on a balance between segregation and integration of neuronal communications (Fox and Friston, 2012; Tononi et al., 1994). Structure-function relationships have been shown to be stronger when functional networks are in an integrated state, compared to a segregated state (Fukushima et al., 2018). In another study, white matter integrity was associated with BOLD signal complexity in local connections (structure-function agreement) but not in distributed connections (structure-function disagreement) (McDonough and Siegel, 2018). This suggests that information integration relies on a strong structure-function relationship, whereas weak structure-function relationships are implied in segregation.

Next to the implication of structure-function relationships on healthy brain functioning, structure-function relationships may (partly) determine the functional effects of structural damage to the brain. Intuitively, it may be deduced that structural damage to connections with strong structure-function relationships will have severer functional consequences than structural damage to connections with weak structure-function relationships. Novel algorithms may enable us to predict the functional effects of specific structural damage (Meier et al., 2016). Alterations and preservations of structural and functional connectivity in human patients, and in animal models of neurological and psychiatric diseases, can provide insights into the impact of structure-function couplings on outcome. For example, after stroke significant changes in structural and functional connectivity have been measured in the remaining intact sensorimotor network in rodents (Schmitt et al., 2017; van Meer et al., 2010a, 2012) and humans (Carter et al., 2010; Grefkes and Fink, 2014; Radlinska et al., 2012). Chronically after experimental stroke in rats, structural and functional connectivity changes were related intrahemispherically –on the side of the stroke lesion– while this was not evident for interhemispheric connections (van Meer et al., 2010a). This may be explained by a stronger structure-function agreement in intrahemispheric sensorimotor connections as compared to interhemispheric sensorimotor connections, as we found in the current study.

A strength of the current study is the inclusion of three different measures of connectivity within a single species. Comparing functional connectivity against macro-scale diffusion-based as well as meso-scale neuronal tracer-based structural connectivity in rats enabled the investigation of structure-function relationships across hierarchical levels. In addition, by including both diffusion- and neuronal tracer-based structural connectivity measures, we could avoid inclusion of false positives that are often present in diffusion-based structural networks (Evan Calabrese et al., 2015; Chen et al., 2015; Maier-Hein et al., 2017;

Sinke et al., 2018). A reliable structural network of the rat brain was created by only selecting connections present in both diffusion- and neuronal tracer-based structural networks. The relationship between diffusion-based structural connectivity and resting-state functional connectivity may have been higher when both measures would have been acquired in the same rat. However, neuronal tracer-based structural connectivity was acquired from many different groups of rats. Therefore, we also measured diffusion-based structural connectivity in a separate group of rats, to prevent inappropriate comparison with potentially higher within-subject correlations. A limitation could be the restriction of our assessments to monosynaptic connections. In addition, resting-state functional connectivity was determined under anesthesia, which influences functional connectivity measures (Paasonen et al., 2018) and possibly affects the structure-function relationship.

In conclusion, we demonstrated a correlation between functional connectivity and diffusion-based structural connectivity, but no significant correlation between functional connectivity and neuronal tracer-based structural connectivity in the rat cortex. These distinct structure-function relationships may be due to different hierarchical levels of measurement or directionality information available in the data. In addition, the structure-function relationship varies across cortical regions in the rat brain. Characteristics of the used techniques, such as distance-dependency, affect where structural and functional networks (dis)agree. Conclusions about connectivity based on a single technique may therefore be biased. This shows the importance of combining different complementary measures of connectivity at distinct hierarchical levels to accurately determine connectivity across networks in the healthy and diseased brain.

References

- Andersson, J.L.R., Jenkinson, M., Smith, S., 2007. Non-linear registration aka Spatial normalisation. FMRIB Tech. Rep. TR07JA2.
- Basser, P.J., Mattiello, J., LeBihan, D., 1994. MR Diffusion Tensor Spectroscopy and Imaging. *Biophys. J.* 66, 259–267. [https://doi.org/10.1016/S0006-3495\(94\)80775-1](https://doi.org/10.1016/S0006-3495(94)80775-1)
- Beckmann, C.F., Smith, S.M., 2004. Probabilistic independent component analysis for functional magnetic resonance imaging. *IEEE Trans. Med. Imaging* 23, 137–152. <https://doi.org/10.1109/TMI.2003.822821>
- Biswal, B., Yetkin, F., Haughton, V., Hyde, J., 1995. Functional connectivity in the motor cortex of resting human brain using echoplanar MRI. *Magn. Reson. Med.* 34, 537–541. <https://doi.org/10.1002/mrm.1910340409>
- Calabrese, E., Badea, A., Cofer, G., Qi, Y., Allan Johnson, G., 2015. A diffusion MRI tractography connectome of the mouse brain and comparison with neuronal tracer data. *Cereb. Cortex* 25, 4628–4637. <https://doi.org/10.1093/cercor/bhv121>
- Carter, A.R., Astafiev, S. V., Lang, C.E., Connor, L.T., Rengachary, J., Strube, M.J., Pope, D.L.W., Shulman, G.L., Corbetta, M., 2010. Resting inter-hemispheric fMRI connectivity predicts performance after stroke. *Ann. Neurol.* 67, 365–375. <https://doi.org/10.1002/ana.21905>

- Chen, H., Liu, Tao, Zhao, Y., Zhang, T., Li, Y., Li, M., Zhang, H., Kuang, H., Guo, L., Tsien, J.Z., Liu, Tianming, 2015. Optimization of large-scale mouse brain connectome via joint evaluation of DTI and neuron tracing data. *Neuroimage* 115, 202–213. <https://doi.org/10.1016/j.neuroimage.2015.04.050>
- Cox, R.W., 1996. AFNI: Software for Analysis and Visualization of Functional Magnetic Resonance Neuroimages. *Comput. Biomed Res.* 29, 162–173.
- Deco, G., McIntosh, A.R., Shen, K., Hutchison, R.M., Menon, R.S., Everling, S., Hagmann, P., Jirsa, V.K., 2014. Identification of optimal structural connectivity using functional connectivity and neural modeling. *J. Neurosci.* 34, 7910–7916. <https://doi.org/10.1523/JNEUROSCI.4423-13.2014>
- Díaz-Parra, A., Osborn, Z., Canals, S., Moratal, D., Sporns, O., 2017. Structural and functional, empirical and modeled connectivity in the cerebral cortex of the rat. *Neuroimage* 159, 170–184. <https://doi.org/10.1016/j.neuroimage.2017.07.046>
- Dijkhuizen, R.M., Nicolay, K., 2003. Magnetic Resonance Imaging in experimental models of brain disorders. *J. Cereb. Blood Flow Metab.* 23, 1383–1402. <https://doi.org/10.1097/01.WCB.0000100341.78607.EB>
- Ercsey-Ravasz, M., Markov, N.T., Lamy, C., Van Essen, D.C., Knoblauch, K., Toroczkai, Z., Kennedy, H., 2013. A predictive network model of cerebral cortical connectivity based on a distance rule. *Neuron* 80, 184–97. <https://doi.org/10.1016/j.neuron.2013.07.036>
- Fox, M.D., Raichle, M.E., 2007. Spontaneous fluctuations in brain activity observed with functional magnetic resonance imaging. *Nat. Rev. Neurosci.* 8, 700–711. <https://doi.org/10.1038/nrn2201>
- Fox, P.T., Friston, K.J., 2012. Distributed processing; distributed functions? *Neuroimage* 61, 407–426. <https://doi.org/10.1016/j.neuroimage.2011.12.051>
- Fukushima, M., Betzel, R.F., He, Y., Heuvel, M.P. Van Den, Zuo, X.-N., Sporns, O., 2018. Structure – function relationships during segregated and integrated network states of human brain functional connectivity. *Brain Struct. Funct.* 223, 1091–1106. <https://doi.org/10.1007/s00429-017-1539-3>
- Grandjean, J., Zerbi, V., Balsters, J.H., Wenderoth, N., Rudin, M., 2017. Structural basis of large-scale functional connectivity in the mouse. *J. Neurosci.* 37, 8092–8101. <https://doi.org/10.1523/JNEUROSCI.0438-17.2017>
- Grefkes, C., Fink, G.R., 2014. Connectivity-based approaches in stroke and recovery of function. *Lancet Neurol.* 13, 206–216. [https://doi.org/10.1016/S1474-4422\(13\)70264-3](https://doi.org/10.1016/S1474-4422(13)70264-3)
- Greicius, M.D., Krasnow, B., Reiss, A.L., Menon, V., 2003. Functional connectivity in the resting brain: A network analysis of the default mode hypothesis. *Proc. Natl. Acad. Sci. U. S. A.* 100, 253–258. <https://doi.org/10.1073/pnas.0135058100>
- Greicius, M.D., Supekar, K., Menon, V., Dougherty, R.F., 2009. Resting-state functional connectivity reflects structural connectivity in the default mode network. *Cereb. Cortex* 19, 72–78. <https://doi.org/10.1093/cercor/bhn059>
- He, B.J., Snyder, A.Z., Zempel, J.M., Smyth, M.D., Raichle, M.E., 2008. Electrophysiological correlates of the brain's intrinsic large-scale functional architecture. *Proc. Natl. Acad. Sci. U. S. A.* 105, 16039–16044. <https://doi.org/10.1073/pnas.0807010105>
- Heimer, L., Robards, M.J. (Eds.), 1981. *Neuroanatomical Tract-Tracing Methods*. Plenum Press, New York and London. <https://doi.org/10.1007/978-1-4613-3189-6>
- Hoffer, Z.S., Hoover, J.E., Alloway, K.D., 2003. Sensorimotor Corticocortical Projections from Rat Barrel Cortex Have an Anisotropic Organization That Facilitates Integration of Inputs from Whiskers in the Same Row. *J. Comp. Neurol.* 466, 525–544. <https://doi.org/10.1002/cne.10895>
- Honey, C.J., Sporns, O., Cammoun, L., Gigandet, X., Thiran, J.P., Meuli, R., Hagmann, P., 2009. Predicting human resting-state functional connectivity from structural connectivity. *Proc. Natl. Acad. Sci. U. S. A.* 106, 2035–2040. <https://doi.org/10.1073/pnas.0811168106>
- Horn, A., Ostwald, D., Reiser, M., Blankenburg, F., 2014. The structural-functional connectome and the default mode network of the human brain. *Neuroimage* 102, 142–151. <https://doi.org/10.1016/j.neuroimage.2013.09.069>
- Jenkinson, M., Bannister, P., Brady, M., Smith, S., 2002. Improved optimization for the robust and accurate linear registration and motion correction of brain images. *Neuroimage* 17, 825–841. <https://doi.org/10.1006/nimg.2002.1132>
- Jenkinson, M., Smith, S., 2001. A global optimisation method for robust affine registration of brain images. *Med. Image Anal.* 5, 143–156. [https://doi.org/10.1016/S1361-8415\(01\)00036-6](https://doi.org/10.1016/S1361-8415(01)00036-6)
- Lee, T., Xue, S., 2018. Revisiting the functional and structural connectivity of large-scale cortical networks. *Brain Connect.* 8, 129–138. <https://doi.org/10.1089/brain.2017.0536>
- Logothetis, N.K., 2008. What we can do and what we cannot do with fMRI. *Nature* 453, 869–878. <https://doi.org/10.1038/nature06976>
- Logothetis, N.K., Pauls, J., Augath, M., Trinath, T., Oeltermann, A., 2001. Neurophysiological investigation of the basis of the fMRI signal. *Nature* 412, 150–157.
- Logothetis, N.K., Wandell, B.A., 2004. Interpreting the BOLD signal. *Annu. Rev. Physiol.* 66, 735–769. <https://doi.org/10.1146/annurev.physiol.66.082602.092845>
- Lu, H., Zou, Q., Gu, H., Raichle, M.E., Stein, E.A., Yang, Y., 2012. Rat brains also have a default mode network. *Proc. Natl. Acad. Sci. U. S. A.* 109, 3979–3984. <https://doi.org/10.1073/pnas.1200506109>

- Magri, C., Schridde, U., Murayama, Y., Panzeri, S., Logothetis, N.K., 2012. The amplitude and timing of the BOLD signal reflects the relationship between local field potential power at different frequencies. *J. Neurosci.* 32, 1395–1407. <https://doi.org/10.1523/JNEUROSCI.3985-11.2012>
- Maier-Hein, K.H., Neher, P.F., Houde, J.-C., Coté, M.-A., Garyfallidis, E., Zhong, J., Chamberland, M., Yeh, F.-C., Lin, Y.-C., Ji, Q., Reddick, W.E., Glass, J.O., Chen, D.Q., Feng, Y., Gao, C., Wu, Y., Ma, J., Renhjie, H., Li, Q., Westin, C.-F., Deslauriers-Gauthier, S., Omar Ocegueda González, J., Paquette, M., St-Jean, S., Girard, G., Rheault, F., Sidhu, J., Tax, C.M.W., Guo, F., Mesri, H.Y., Szabolcs, D., Froeling, M., Heemskerk, A.M., Leemans, A., Boré, A., Pinsard, B., Bedetti, C., Desrosiers, M., Brambati, S., Doyon, J., Sarica, A., Vasta, R., Cerasa, A., Quattrone, A., Yeatman, J., Khan, A.R., Hodges, W., Alexander, S., Romascano, D., Barakovic, M., Auria, A., Esteban, O., Lemkaddem, A., Thiran, J.-P., Ertan Cetingul, H., Odry, B.L., Mailhe, B., Nadar, M.S., Pizzagalli, F., Prasad, G., Villalon-Reina, J.E., Galvis, J., Thompson, P.M., De Santiago Requejo, F., Luque Laguna, P., Lacerda, L.M., Barrett, R., Dell'Acqua, F., Catani, M., Petit, L., Caruyer, E., Daducci, A., Dyrby, T.B., Holland-Letz, T., Hilgetag, C.C., Stieltjes, B., Descoteaux, M., 2017. The challenge of mapping the human connectome based on diffusion tractography. *Nat. Commun.* 8, 1349. <https://doi.org/10.1038/s41467-017-01285-x>
- Majka, P., Kublik, E., Wurga, G., Wójcik, D.K., 2012. Common atlas format and 3D brain atlas reconstructor: Infrastructure for constructing 3D brain atlases. *Neuroinformatics* 10, 181–197. <https://doi.org/10.1007/s12021-011-9138-6>
- Mcdonough, I.M., Siegel, J.T., 2018. The Relation between white matter microstructure and network complexity: implications for processing efficiency. *Front. Integr. Neurosci.* 12, 43. <https://doi.org/10.3389/fnint.2018.00043>
- Meier, J., Tewarie, P., Hillebrand, A., Douw, L., van Dijk, B.W., Stufflebeam, S.M., van Mieghem, P., 2016. A mapping between structural and functional brain networks. *Brain Connect.* 6, 298–311. <https://doi.org/10.1089/brain.2015.0408>
- Messé, A., Rudrauf, D., Benali, H., Marrelec, G., 2014. Relating structure and function in the human brain: relative contributions of anatomy, stationary dynamics, and non-stationarities. *PLoS Comput. Biol.* 10, e1003530. <https://doi.org/10.1371/journal.pcbi.1003530>
- Miranda-Dominguez, O., Mills, B.D., Grayson, D., Woodall, A., Grant, K.A., Kroenke, C.D., Fair, D.A., 2014. Bridging the gap between the human and macaque connectome: A quantitative comparison of global interspecies structure-function relationships and network topology. *J. Neurosci.* 34, 5552–5563. <https://doi.org/10.1523/JNEUROSCI.4229-13.2014>
- Miyashita, E., Keller, A., Asanuma, H., 1994. Input-output organization of the rat vibrissal motor cortex. *Exp. Brain Res.* 99, 223–232. <https://doi.org/10.1007/BF00239589>
- Noori, H.R., Schöttler, J., Ercey-Ravasz, M., Cosa-linan, A., Varga, M., Toroczka, Z., Spanagel, R., 2017. A multiscale cerebral neurochemical connectome of the rat brain. *PLoS Biol.* 15, e2002612. <https://doi.org/https://doi.org/10.1371/journal.pbio.2002612>
- O'Reilly, J.X., Croxson, P.L., Jbabdi, S., Sallet, J., Noonan, M.P., Mars, R.B., Browning, P.G.F., Wilson, C.R.E., Mitchell, A.S., Miller, K.L., Rushworth, M.F.S., Baxter, M.G., 2013. Causal effect of disconnection lesions on interhemispheric functional connectivity in rhesus monkeys. *Proc. Natl. Acad. Sci. U. S. A.* 110, 13982–13987. <https://doi.org/10.1073/pnas.1305062110>
- Paasonen, J., Stenroos, P., Salo, R.A., Kiviniemi, V., Gröhn, O., 2018. Functional connectivity under six anesthesia protocols and the awake condition in rat brain. *Neuroimage* 172, 9–20. <https://doi.org/10.1016/j.neuroimage.2018.01.014>
- Pan, W.-J., Thompson, G., Magnuson, M., Majeed, W., Jaeger, D., Keilholz, S., 2011. Broadband local field potentials correlate with spontaneous fluctuations in functional Magnetic Resonance Imaging signals in the rat somatosensory cortex under isoflurane anesthesia. *Brain Connect.* 1, 119–131. <https://doi.org/10.1089/brain.2011.0014>
- Pawela, C.P., Biswal, B.B., Cho, Y.R., Kao, D.S., Li, R., Jones, S.R., Schulte, M.L., Matloub, H.S., Hudetz, A.G., Hyde, J.S., 2008. Resting-state functional connectivity of the rat brain. *Magn. Reson. Med.* 59, 1021–1029. <https://doi.org/10.1002/mrm.21524>
- Paxinos, G., Watson, W., 2005. *The rat brain in stereotaxic coordinates 5th edition.* Elsevier Academic Press, Amsterdam.
- R Core Team, 2014. *R: A language and environment for statistical computing.*
- Radlinska, B.A., Blunk, Y., Leppert, I.R., Minuk, J., Bruce Pike, G., Thiel, A., 2012. Changes in callosal motor fiber integrity after subcortical stroke of the pyramidal tract. *J. Cereb. Blood Flow Metab.* 32, 1515–1524. <https://doi.org/10.1038/jcbfm.2012.37>
- Raichle, M.E., 2015. The restless brain: how intrinsic activity organizes brain function. *Philosophical Trans. R. Soc. B* 370, 20140172. <https://doi.org/dx.doi.org/10.1098/rstb.2014.0172>
- Reid, A.T., Lewis, J., Bezgin, G., Khundrakpam, B., Eickhoff, S.B., McIntosh, A.R., Bellec, P., Evans, A.C., 2016. A cross-modal, cross-species comparison of connectivity measures in the primate brain. *Neuroimage* 125, 311–331. <https://doi.org/10.1016/j.neuroimage.2015.10.057>
- Reveley, C., Seth, A.K., Pierpaoli, C., Silva, A.C., Yu, D., Saunders, R.C., Leopold, D.A., Ye, F.Q., 2015. Superficial white matter fiber systems impede detection of long-range cortical connections in diffusion MR tractography. *Proc. Natl. Acad. Sci. U. S. A.* 112, E2820–E2828. <https://doi.org/10.1073/pnas.1418198112>
- Rocco-Donovan, M., Ramos, R.L., Giraldo, S., Brumberg, J.C., 2011. Characteristics of synaptic connections between rodent primary somatosensory and motor cortices. *Somatosens. Mot. Res.* 28, 63–72. <https://doi.org/10.3109/08990220.2011.606660>
- Roelofs, T.J.M., Verharen, J.P.H., van Tilborg, G.A.F., Boekhoudt, L., van der Toorn, A., de Jong, J.W., Luijendijk, M.C.M., Otte, W.M., Adan, R.A.H., Dijkhuizen, R.M., 2017. A novel approach to map induced activation of neuronal networks using

- chemogenetics and functional neuroimaging in rats: A proof-of-concept study on the mesocorticolimbic system. *Neuroimage* 156, 109–118. <https://doi.org/10.1016/j.neuroimage.2017.05.021>
- Salvador, R., Suckling, J., Coleman, M.R., Pickard, J.D., Menon, D., Bullmore, E., 2005. Neurophysiological architecture of functional magnetic resonance images of human brain. *Cereb. Cortex* 15, 1332–1342. <https://doi.org/10.1093/cercor/bhi016>
- Sarabdjitsingh, R.A., Loi, M., Joels, M., Dijkhuizen, R.M., van der Toorn, A., 2017. Early life stress-induced alterations in rat brain structures measured with high resolution MRI. *PLoS One* 12, e0185061. <https://doi.org/10.1371/journal.pone.0185061>
- Schilling, K.G., Nath, V., Hansen, C., Parvathaneni, P., Blaber, J., Gao, Y., Neher, P., Aydogan, D.B., Shi, Y., Ocampo-pineda, M., Schiavi, S., Daducci, A., Girard, G., Barakovic, M., Rafael-Patino, J., Romascano, D., Rensonnet, G., Pizzolato, M., Bates, A., Fischl, E., Thiran, J., Canales-Rodriguez, E.J., Huang, C., Zhu, H., Zhong, L., Cabeen, R., Toga, A.W., Rheault, F., Theaud, G., Houde, J.-C., Sidhu, J., Chamberland, M., Westin, C.-F., Dyrby, T.B., Verma, R., Rathi, Y., Irfanoglu, M.O., Thomas, C., Pierpaoli, C., Descoteaux, M., Anderson, A.W., Landman, B.A., 2019. Limits to anatomical accuracy of diffusion tractography using modern approaches. *Neuroimage* 185, 1–11. <https://doi.org/10.1016/j.neuroimage.2018.10.029>
- Schmitt, O., Badurek, S., Liu, W., Wang, Y., Rabiller, G., Kanoke, A., Eipert, P., Liu, J., 2017. Prediction of regional functional impairment following experimental stroke via connectome analysis. *Sci. Rep.* 7, 46316. <https://doi.org/10.1038/srep46316>
- Schmitt, O., Eipert, P., 2012. neuroVIISAS: Approaching multiscale simulation of the rat connectome. *Neuroinformatics* 10, 243–267. <https://doi.org/10.1007/s12021-012-9141-6>
- Shen, K., Bezgin, G., Hutchison, R.M., Gati, J.S., Menon, R.S., Everling, S., McIntosh, A.R., 2012. Information processing architecture of functionally defined clusters in the macaque cortex. *J. Neurosci.* 32, 17465–17476. <https://doi.org/10.1523/JNEUROSCI.2709-12.2012>
- Shmuel, A., Leopold, D.A., 2008. Neuronal correlates of spontaneous fluctuations in fMRI signals in monkey visual cortex: Implications for functional connectivity at rest. *Hum. Brain Mapp.* 29, 751–761. <https://doi.org/10.1002/hbm.20580>
- Sierakowiak, A., Monnot, C., Aski, S.N., Uppman, M., Li, T.Q., Damberg, P., Brené, S., 2015. Default mode network, motor network, dorsal and ventral basal ganglia networks in the rat brain: Comparison to human networks using resting state-fMRI. *PLoS One* 10, e0120345. <https://doi.org/10.1371/journal.pone.0120345>
- Sinke, M.R.T., Otte, W.M., Christiaens, D., Schmitt, O., Leemans, A., van der Toorn, A., Sarabdjitsingh, R.A., Joëls, M., Dijkhuizen, R.M., 2018. Diffusion MRI-based cortical connectome reconstruction: dependency on tractography procedures and neuroanatomical characteristics. *Brain Struct. Funct.* 223, 2269–2285. <https://doi.org/10.1007/s00429-018-1628-y>
- Smith, R.E., Tournier, J.D., Calamante, F., Connelly, A., 2015. The effects of SIFT on the reproducibility and biological accuracy of the structural connectome. *Neuroimage* 104, 253–265. <https://doi.org/10.1016/j.neuroimage.2014.10.004>
- Smith, R.E., Tournier, J.D., Calamante, F., Connelly, A., 2013. SIFT: Spherical-deconvolution informed filtering of tractograms. *Neuroimage* 67, 298–312. <https://doi.org/10.1016/j.neuroimage.2012.11.049>
- Smith, S.M., 2002. Fast robust automated brain extraction. *Hum. Brain Mapp.* 17, 143–155. <https://doi.org/10.1002/hbm.10062>
- Straathof, M., Sinke, M.R., Dijkhuizen, R.M., Otte, W.M., on behalf of the TACTICS consortium, 2019. A systematic review on the quantitative relationship between structural and functional network connectivity strength in mammalian brains. *J. Cereb. Blood Flow Metab.* 39, 189–209. <https://doi.org/10.1177/0271678X18809547>
- Thomas, C., Ye, F.Q., Irfanoglu, M.O., Modi, P., Saleem, K.S., Leopold, D.A., Pierpaoli, C., 2014. Anatomical accuracy of brain connections derived from diffusion MRI tractography is inherently limited. *Proc. Natl. Acad. Sci. U. S. A.* 111, 16574–16579. <https://doi.org/10.1073/pnas.1405672111>
- Tononi, G., Sporns, O., Edelman, G.M., 1994. A measure for brain complexity: Relating functional segregation and integration in the nervous system. *Proc. Natl. Acad. Sci. U. S. A.* 91, 5033–5037.
- Tournier, J.D., Calamante, F., Connelly, A., 2012. MRtrix: Diffusion tractography in crossing fiber regions. *Int. J. Imaging Syst. Technol.* 22, 53–66. <https://doi.org/10.1002/ima.22005>
- Tournier, J.D., Calamante, F., Connelly, A., 2010. Improved probabilistic streamlines tractography by 2nd order integration over fibre orientation distributions. *Proc. Int. Soc. Magn. Reson. Med.* 1670.
- Turner, R., Le Bihan, D., Maier, J., Vavrek, R., Hedges, L.K., Pekar, J., 1990. Echo-Planar Imaging of intravoxel incoherent motion. *Radiology* 177, 407–414. <https://doi.org/10.1148/radiology.177.2.2217777>
- van den Heuvel, M.P., Hulshoff Pol, H.E., 2010. Exploring the brain network: A review on resting-state fMRI functional connectivity. *Eur. Neuropsychopharmacol.* 20, 519–534. <https://doi.org/10.1016/j.euroneuro.2010.03.008>
- van Meer, M.P.A., Otte, W.M., van der Marel, K., Nijboer, C.H., Kavelaars, A., Berkelbach van der Sprenkel, J.W., Vieregger, M.A., Dijkhuizen, R.M., 2012. Extent of bilateral neuronal network reorganization and functional recovery in relation to stroke severity. *J. Neurosci.* 32, 4495–4507. <https://doi.org/10.1523/JNEUROSCI.3662-11.2012>
- van Meer, M.P.A., van der Marel, K., Otte, W.M., Berkelbach van der Sprenkel, J.W., Dijkhuizen, R.M., 2010. Correspondence between altered functional and structural connectivity in the contralesional sensorimotor cortex after unilateral stroke in rats: a combined resting-state functional MRI and manganese-enhanced MRI study. *J. Cereb. Blood Flow Metab.* 30, 1707–11. <https://doi.org/10.1038/jcbfm.2010.124>
- Wang, L., Su, L., Shen, H., Hu, D., 2012. Decoding lifespan changes of the human brain using resting-state functional connectivity

MRI. PLoS One 7, e44530. <https://doi.org/10.1371/journal.pone.0044530>

Zhang, D., Raichle, M.E., 2010. Disease and the brain's dark energy. *Nat. Rev. Neurol.* 6, 15–28. <https://doi.org/10.1038/nrneuro.2009.198>

Zimmermann, J., Ritter, P., Shen, K., Rothmeier, S., Schirner, M., McIntosh, A.R., 2016. Structural architecture supports functional organization in the human aging brain at a regionwise and network Level. *Hum. Brain Mapp.* 37, 2645–2661. <https://doi.org/10.1002/hbm.23200>

Tables

Table 1: Characteristics of cortical connections in the rat brain with strong meso- and macro-scale structural connectivity and strong functional connectivity.

Seed	Target	Neuronal tracer-based structural connectivity strength	Diffusion-based structural connectivity strength	Functional connectivity strength (Z')	Euclidean distance (mm)	Connection type (network)	Connection type (regional)
Left mPFC	Right mPFC	3.00	1790.10	1.58	1.18	Within default mode network	Homotopic interhemispheric
Right mPFC	Left mPFC	3.00	1790.10	1.58	1.18	Within default mode network	Homotopic interhemispheric
Left DI	Left GI	2.96	1046.70	1.30	0.31	No	Intrahemispheric left
Left GI	Left DI	2.89	1046.70	1.30	0.31	No	Intrahemispheric left
Left LPtA	Left S1Tr	3.00	629.20	1.28	0.97	Sensorimotor network to another network	Intrahemispheric left
Left S1Tr	Left LPtA	3.00	629.20	1.28	0.97	Sensorimotor network to another network	Intrahemispheric left
Left V2L	Left V1B	3.00	1474.60	1.28	1.43	No	Intrahemispheric left
Left M1	Left M2	2.96	3787.60	1.28	1.27	Within sensorimotor network	Intrahemispheric left
Left M2	Left M1	3.76	3787.60	1.28	1.27	Within sensorimotor network	Intrahemispheric left
Right LPtA	Right S1Tr	3.00	533.70	1.27	0.98	Sensorimotor network to another network	Intrahemispheric right
Right S1Tr	Right LPtA	3.00	533.70	1.27	0.98	Sensorimotor network to another network	Intrahemispheric right
Left GI	Left S2	3.72	1075.40	1.25	1.64	Sensorimotor network to another network	Intrahemispheric left
Left S2	Left GI	3.62	1075.40	1.25	1.64	Sensorimotor network to another network	Intrahemispheric left
Right M1	Right M2	2.96	2958.90	1.22	1.27	Within sensorimotor network	Intrahemispheric right
Right M2	Right M1	3.76	2958.90	1.22	1.27	Within sensorimotor network	Intrahemispheric right
Right GI	Right S2	3.72	1261.10	1.22	1.63	Sensorimotor network to another network	Intrahemispheric right
Right S2	Right GI	3.62	1261.10	1.22	1.63	Sensorimotor network to another network	Intrahemispheric right
Right DI	Right GI	2.96	1200.00	1.21	0.31	No	Intrahemispheric right
Right GI	Right DI	2.89	1200.00	1.21	0.31	No	Intrahemispheric right
Left M1	Left S1FL	2.88	1189.60	1.20	1.90	Within sensorimotor network	Intrahemispheric left

Left S1FL	Left M1	2.86	1189.60	1.20	1.90	Within sensorimotor network	Intrahemispheric left
Right M1	Right S1FL	2.88	1077.70	1.20	1.91	Within sensorimotor network	Intrahemispheric right
Right S1FL	Right M1	2.86	1077.70	1.20	1.91	Within sensorimotor network	Intrahemispheric right
Left AuD	Left Au1	3.00	1098.90	1.18	0.78	Within default mode network	Intrahemispheric left
Right Cg1	Left mPFC	3.00	260.00	1.18	2.87	Within default mode network	Heterotopic interhemispheric
Left DI	Left AID	3.00	851.00	1.16	3.05	No	Intrahemispheric left

Seed and target regions were determined from the NeuroVIASAS tracer database. AID: agranular insular cortex dorsal part; Au1: primary auditory cortex; AuD: secondary auditory cortex dorsal area; Cg1: cingulate cortex area 1; DI: dysgranular insular cortex; GI: granular insular cortex; LPtA: lateral parietal association cortex; M1: primary motor cortex; M2: secondary motor cortex; mPFC: medial prefrontal cortex; S1FL: primary somatosensory cortex forelimb region; S1Tr: primary somatosensory cortex trunk region; S2: secondary somatosensory cortex; V1B: primary visual cortex binocular area; V2L: secondary visual cortex lateral area.

Table 2: Characteristics of cortical connections in the rat brain with weak meso- and macro-scale structural connectivity and weak functional connectivity.

Seed	Target	Neuronal tracer-based structural connectivity strength	Diffusion-based structural connectivity strength	Functional connectivity strength (Z')	Euclidean distance (mm)	Connection type (network)	Connection type (regional)
Right LO	Right DLEnt	0.50	0.20	0.19	12.49	Default mode network to another network	Intrahemispheric right
Right VO	Right DLEnt	0.90	0.30	0.23	12.85	Default mode network to another network	Intrahemispheric right
Left MO	Left DLEnt	1.00	0.20	0.25	13.99	Default mode network to another network	Intrahemispheric left
Right MO	Right DLEnt	1.00	0.10	0.26	14.00	Default mode network to another network	Intrahemispheric right
Left FrA	Left PRh	1.05	0.20	0.28	13.11	No	Intrahemispheric left
Right RSGb	Right FrA	0.50	0.20	0.33	11.97	Default mode network to another network	Intrahemispheric right
Right FrA	Right PRh	1.05	0.20	0.37	13.10	No	Intrahemispheric right
Left RSGb	Left FrA	0.50	0.50	0.39	11.95	Default mode network to another network	Intrahemispheric left
Right RSGc	Right FrA	0.50	0.40	0.40	10.26	Default mode network to another network	Intrahemispheric right
Left Cg2	Left AIP	0.50	0.30	0.41	7.61	Default mode network to another network	Intrahemispheric left
Left Cg1	Left AIP	0.50	0.10	0.43	8.50	Default mode network to another network	Intrahemispheric left
Left Cg2	Left PRh	1.00	0.20	0.44	9.54	Default mode network to another network	Intrahemispheric left
Left PRh	Left Cg2	1.00	0.20	0.44	9.54	Default mode network to another network	Intrahemispheric left
Right S1DZ	Left FrA	1.00	0.10	0.45	8.66	Sensorimotor network to another network	Heterotopic interhemispheric
Right FrA	Left AIV	1.13	0.30	0.45	7.12	No	Heterotopic interhemispheric
Left AIP	Right M1	0.74	0.20	0.45	11.15	Sensorimotor network to another network	Heterotopic interhemispheric

Left RSGc	Left FrA	0.50	0.40	0.46	10.24	Default mode network to another network	Intrahemispheric left
Left FrA	Right AIV	1.13	0.10	0.46	7.11	No	Heterotopic interhemispheric
Left Cg1	Left PRh	1.00	0.20	0.46	10.58	Default mode network to another network	Intrahemispheric left
Left PRh	Left Cg1	0.75	0.20	0.46	10.58	Default mode network to another network	Intrahemispheric left
Right S2	Left AIP	0.75	0.10	0.47	12.64	Sensorimotor network to another network	Heterotopic interhemispheric
Right RSGb	Left MO	0.50	0.10	0.47	11.36	Within default mode network	Heterotopic interhemispheric
Left RSGb	Right VO	0.50	0.10	0.47	10.90	Within default mode network	Heterotopic interhemispheric

Seed and target regions were determined from the NeuroVIISAS tracer database. AIP: agranular insular cortex posterior part; AIV: agranular insular cortex ventral part; Cg1: cingulate cortex area 1; Cg2: cingulate cortex area 2; DLEnt: dorsolateral entorhinal cortex; FrA: frontal association cortex; LO: lateral orbital cortex; M1: Primary motor cortex; MO: medial orbital cortex; Prh: perirhinal cortex; RSGb: retrosplenial granular cortex b region; RSGc: retrosplenial granular cortex c region; SIDZ: primary somatosensory cortex dysgranular region; S2: Secondary somatosensory cortex; VO: ventral orbital cortex.

Table 3: Characteristics of cortical connections in the rat brain with strong meso- and macro-scale structural connectivity and weak functional connectivity.

Seed	Target	Neuronal tracer-based structural connectivity strength	Diffusion-based structural connectivity strength	Functional connectivity strength (Z')	Euclidean distance (mm)	Connection type (network)	Connection type (regional)
Left AIP	Left PRh	3.66	317.50	0.42	4.37	No	Intrahemispheric left
Left PRh	Left AIP	4.00	317.50	0.42	4.37	No	Intrahemispheric left
Right TeA	Right PRh	2.94	250.70	0.46	2.38	Default mode network to another network	Intrahemispheric right
Left AuV	Left PRh	2.75	141.30	0.48	1.49	Default mode network to another network	Intrahemispheric left
Left TeA	Left PRh	2.94	466.60	0.51	2.38	Default mode network to another network	Intrahemispheric left
Right M1	Right FrA	2.93	154.80	0.52	4.17	Sensorimotor network to another network	Intrahemispheric right
Right AIP	Right PRh	3.66	316.30	0.53	4.35	No	Intrahemispheric right
Right PRh	Right AIP	4.00	316.30	0.53	4.35	No	Intrahemispheric right
Left Ect	Left PRh	3.90	1523.80	0.56	1.14	No	Intrahemispheric left
Left PRh	Left Ect	3.83	1523.80	0.56	1.14	No	Intrahemispheric left
Right S2	Right AIP	3.00	125.00	0.56	2.22	Sensorimotor network to another network	Intrahemispheric right
Left AIV	Left AIP	3.00	301.10	0.59	4.86	No	Intrahemispheric left
Left M1	Left FrA	2.93	181.70	0.59	4.18	Sensorimotor network to another network	Intrahemispheric left
Right Ect	Right PRh	3.90	1215.60	0.61	1.12	No	Intrahemispheric right
Right PRh	Right Ect	3.83	1215.60	0.61	1.12	No	Intrahemispheric right

Right RSd	Right Ect	3.00	226.80	0.62	6.12	Default mode network to another network	Intrahemispheric right
Left AID	Left AIP	3.00	145.90	0.63	5.20	No	Intrahemispheric left
Left AIP	Left AID	2.90	145.90	0.63	5.20	No	Intrahemispheric left
Right AIV	Right AIP	3.00	277.30	0.66	4.88	No	Intrahemispheric right
Right Ect	Right Au1	3.00	217.30	0.67	1.81	Default mode network to another network	Intrahemispheric right
Left AIP	Left GI	3.69	249.30	0.68	2.21	No	Intrahemispheric left
Left GI	Left AIP	2.91	249.30	0.68	2.21	No	Intrahemispheric left
Left RSd	Left Ect	3.00	152.40	0.71	6.12	Default mode network to another network	Intrahemispheric left
Right TeA	Right V2L	2.86	1078.80	0.71	2.17	Default mode network to another network	Intrahemispheric right
Right AIP	Right GI	3.69	354.00	0.72	2.20	No	Intrahemispheric right
Right GI	Right AIP	2.91	354.00	0.72	2.20	No	Intrahemispheric right

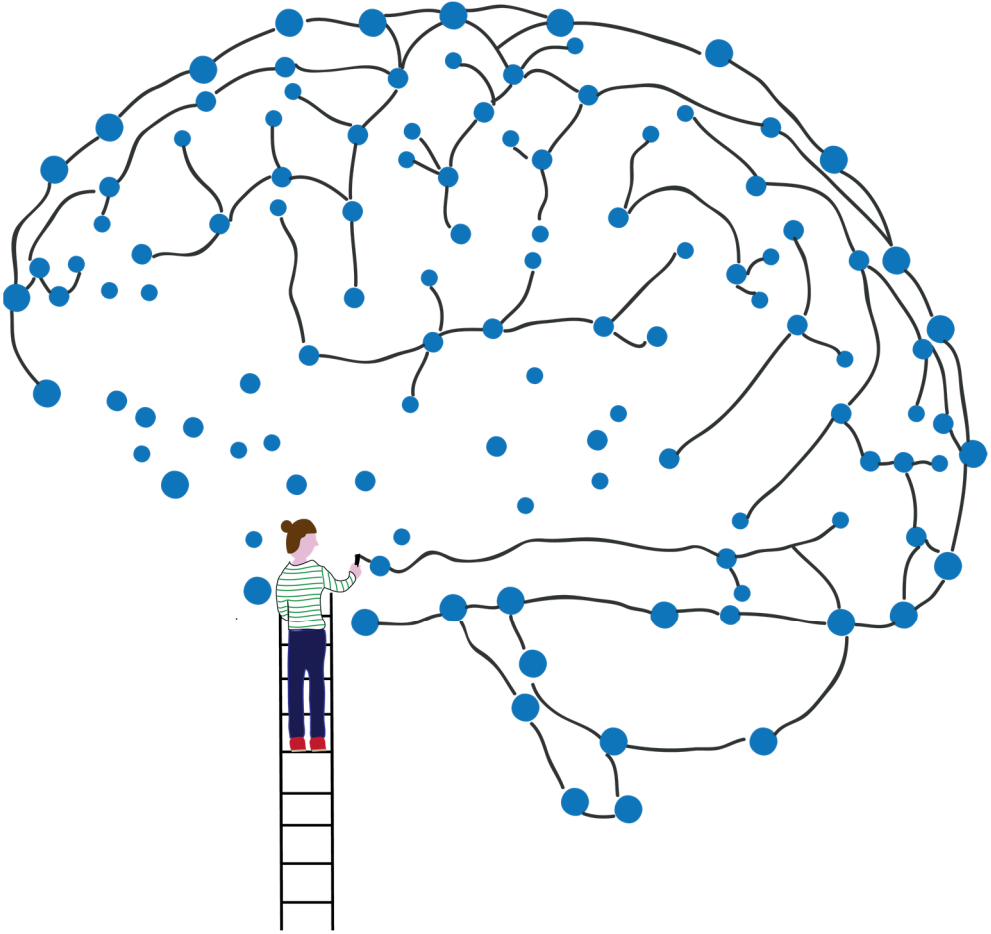
Seed and target regions were determined from the NeuroVIISAS tracer database. AID: agranular insular cortex dorsal part; AIP: agranular insular cortex posterior part; AIV: agranular insular cortex ventral part; Au1: Primary auditory cortex; AuV: Secondary auditory cortex ventral area; Ect: ectorhinal cortex; FrA: frontal association cortex; GI: granular insular cortex; M1: primary motor cortex; PRh: perirhinal cortex; RSd: Retrosplenial dorsal; S2: secondary somatosensory cortex; TeA: temporal association cortex I; V1B: primary visual cortex binocular area.

Table 4: Characteristics of cortical connections in the rat brain with weak meso- and macro-scale structural connectivity and strong functional connectivity.

Seed	Target	Neuronal tracer-based structural connectivity strength	Diffusion-based structural connectivity strength	Functional connectivity strength (Z')	Euclidean distance (mm)	Connection type (network)	Connection type (regional)
Right S2	Left GI	1.00	0.30	1.14	12.12	Sensorimotor network to another network	Heterotopic interhemispheric
Right DI	Right mPFC	1.44	0.30	1.01	6.70	Default mode network to another network	Intrahemispheric right
Right M1	Right Au1	1.00	0.60	1.00	8.57	Default mode network to sensorimotor network	Intrahemispheric right
Right Au1	Right M1	1.00	0.60	1.00	8.57	Default mode network to sensorimotor network	Intrahemispheric right
Left M1	Left Au1	1.00	0.40	0.99	8.57	Default mode network to sensorimotor network	Intrahemispheric left
Left Au1	Left M1	1.00	0.40	0.99	8.57	Default mode network to sensorimotor network	Intrahemispheric left
Left DI	Left mPFC	1.44	0.20	0.98	6.71	Default mode network to another network	Intrahemispheric left
Right M1	Left S1BF	1.00	0.50	0.96	9.20	Within sensorimotor network	Heterotopic interhemispheric
Left GI	Left mPFC	1.43	0.20	0.95	6.84	Default mode network to another network	Intrahemispheric left

Right GI	Right mPFC	1.43	0.10	0.93	6.83	Default mode network to another network	Intrahemispheric right
Left V1	Right M2	1.00	0.20	0.92	9.63	Sensorimotor network to another network	Heterotopic interhemispheric
Left RSd	Left AID	1.00	0.10	0.90	9.90	Default mode network to another network	Intrahemispheric left
Right V1	Left M2	1.00	0.20	0.90	9.64	Sensorimotor network to another network	Heterotopic interhemispheric
Right Cg1	Right AID	0.50	0.10	0.89	5.28	Default mode network to another network	Intrahemispheric right
Left RSd	Left LO	0.50	0.10	0.89	10.65	Within default mode network	Intrahemispheric left
Right Cg1	Right V1	1.00	0.50	0.88	7.72	Default mode network to another network	Intrahemispheric right
Right S2	Left AID	0.75	0.10	0.87	11.21	Sensorimotor network to another network	Heterotopic interhemispheric
Right LO	Right V1	1.00	0.20	0.86	10.26	Default mode network to another network	Intrahemispheric right
Left M1	Right GI	1.07	0.50	0.85	9.70	Sensorimotor network to another network	Heterotopic interhemispheric
Right GI	Left M2	1.00	0.30	0.84	8.91	Sensorimotor network to another network	Heterotopic interhemispheric
Left Cg1	Left AID	0.50	0.10	0.83	5.28	Default mode network to another network	Intrahemispheric left
Left mPFC	Right S2	0.50	0.20	0.82	8.60	Default mode network to sensorimotor network	Heterotopic interhemispheric
Right RSd	Right AID	1.00	0.30	0.81	9.92	Default mode network to another network	Intrahemispheric right

Seed and target regions were determined from the NeuroVIISAS tracer database. AID: agranular insular cortex dorsal part; Au1: primary auditory cortex; Cg1: cingulate cortex area 1; DI: dysgranular insular cortex; GI: granular insular cortex; LO: lateral orbital cortex; M1: primary motor cortex; M2: secondary motor cortex; mPFC: medial prefrontal cortex; RSd: retrosplenial dorsal; S1BF: primary somatosensory cortex barrel field; S2: secondary somatosensory cortex; V1: primary visual cortex.



3

Non-linear relationships between structural and functional connectivity in the human and rat cerebral cortex

Milou Straathof¹, Willem M. Otte^{1,2} & Rick M. Dijkhuizen¹

¹ *Biomedical MR Imaging and Spectroscopy Group, Center for Image Sciences, University Medical Center Utrecht and Utrecht University, Utrecht, The Netherlands.*

² *Department of Pediatric Neurology, UMC Utrecht Brain Center, University Medical Center Utrecht and Utrecht University, Utrecht, the Netherlands.*

Submitted.

Abstract

Understanding how structural and functional networks are related will help to unravel the complex organization of brain networks. These networks are complex because the overall topological behavior is difficult to explain by the constituent parts, such as local connectivity. The complex, potentially non-linear nature of the structure-function relationship may not be adequately assessed with a simple linear correlation analysis between structural and functional connectivity. Therefore, we mapped the cortical structure-function relationship considering non-linear behavior using an additive model. We determined whole-brain structural connectivities with diffusion-weighted MRI and functional connectivities with resting-state fMRI. We compared the results obtained from human and rodent brains to assess this within a perspective of translational neuroscience. Our results show that structure-function relationships in both the human and rat cortex are positive but non-linear, with stronger correlations at higher connectivity levels. We quantified a structure-function tipping point, which is the lowest structural connectivity weight from which onwards structural and functional connectivity become strongly associated. This structure-function tipping point was lower in the human compared to the rat cortex (human: median = 1.60 (1.36–1.69) (interquartile range), range = 0–8.79; rat: median = 5.69 (5.48–5.76), range = 0–8.31; $p=0.0005$). In the human cortex, non-linear structure-function relationships were similar in primary and secondary brain regions. However, in the rat cortex, a structure-function relationship was less evident in secondary brain regions. Our data highlights the inherent non-linear structure-function relationship in the human and rodent cortex and exposes organizational differences in functional networks between humans and rodents.

Introduction

In the last decades, neuroscientists have tried to unravel the organization of networks in the brain. There are two ways to look at brain networks: from a structural or a functional perspective. Structural networks represent the physical connections between brain regions (Johansen-Berg and Behrens, 2013). In comparison, functional connectivity represents the communication between brain regions, often measured as a statistical correlation between activity patterns in two brain regions (Biswal et al., 1995; Fox and Raichle, 2007). Identifying how these structural and functional connectivities are interrelated helps to understand how brain networks are organized and how disconnection can lead to functional abnormalities seen in brain disorders. A general straightforward linear correlation exists between structural and functional connectivity across different species, including humans and rodents (Damoiseaux and Greicius, 2009; Díaz-Parra et al., 2017; Honey et al., 2009; Stafford et al., 2014; Straathof et al., 2020b, 2019a). At a close look, the structure-function relationship differs across a range of strengths and depends on the type of connection. Consequently, a whole-brain linear fit, which ignores these complexities, often results in moderate correlations (Straathof et al., 2019a; Suárez et al., 2020). There are brain regions with a structural connection but without a measurable functional connection and the other way around (Greicius et al., 2009; Honey et al., 2009; van den Heuvel et al., 2009). In addition, there are brain regions where strong structural connectivity is accompanied by weak functional connectivity and vice versa (Lee and Xue, 2018). As a result, the structure-function relationship varies highly across brain regions (Grandjean et al., 2017; Wang et al., 2012; Zimmermann et al., 2016). In humans, structural and functional connectivity generally correspond in primary unimodal sensory regions, whereas they may essentially differ in secondary transmodal nonsensory-specific regions (Vázquez-Rodríguez et al., 2019). Correspondingly, an agreement between structural and functional connectivity strength was found in the sensorimotor network of the rat brain. In contrast, disagreement was seen in higher-order areas, including the insular cortex and parahippocampal regions (Straathof et al., 2020b).

Although correlation analyses or linear model approaches offer a transparent and easily interpretable way to determine structure-function relationships, they do not completely cover the complex nature of this relationship. We know that structural networks constrain but do not strictly determine functional networks. One factor responsible for the complex relationship between structural and functional connectivity is the dynamic nature

of functional connectivity. Functional connectivity is often characterized as a static property, but the underlying signal dynamically changes during seconds and minutes (Chang and Glover, 2010; Hutchison et al., 2013). The presence and strength of structural connections influence the stability of dynamic functional connectivity (Liao et al., 2015; Shen et al., 2015). A recent study suggested that structural and functional connectivity may be non-linearly related, mainly depending on direct structural connections and marginally on indirect connections (Liang and Wang, 2017). Therefore, models that incorporate non-linear components of the relationship between structural and functional connectivity may provide a more accurate representation of and offer new insights into the complex organization of brain networks.

In this study, we mapped the relationship between structural and functional connectivity in the cerebral cortex by taking non-linearity into account. To that aim, we applied a generalized additive model to structural connectivity measured with diffusion-weighted MRI and functional connectivity with resting-state fMRI. The combination of diffusion-weighted MRI and resting-state fMRI offers a unique translational way to study brain networks' structural and functional organization non-invasively in animals and humans. Therefore, we used this generalized additive model to compare the non-linearity of the structure-function relationship in the rat and human cortex, which are both intensively studied in the field of (translational) neuroscience. In addition, to understand the basis of the non-linear nature of the structure-function relationship, we assessed the impact of two factors that affect the linear structure-function relationship in the brain. First, we investigated whether our non-linear analyses show differences between primary and secondary brain regions. Second, we compared the effect of static and dynamic functional connectivity analyses on the non-linear structure-function relationship. Lastly, to validate our findings, we compared all non-linear analyses against straightforward linear analyses as a benchmark for structure-function relationships in the brain.

Materials & Methods

Human brain imaging

Resting-state fMRI

To determine functional connectivity in the human brain, we obtained resting-state fMRI data from the OpenfMRI database (nr. ds000224). This data is part of the Midnight Scan

Club, which includes various fMRI measurements from ten healthy right-handed young adult individuals (five females; age 24-34 years) (Gordon et al., 2017). Informed consent was obtained from all participants. The study was approved by the Washington University School of Medicine Human Studies Committee and Institutional Review Board. We used the first resting-state fMRI acquisition from each participant. Resting-state fMRI was acquired with a 2D gradient-echo EPI scan on a Siemens Trio 3T MRI scanner, with the following acquisition parameters: TR / TE = 2.2 s / 27 ms; flip angle = 90°; voxel size = 4 × 4 × 4 mm³; 36 slices; total acquisition time = 30 min.

Diffusion-weighted MRI

To determine structural connectivity in the human brain, we used the “Massive” (Multiple Acquisitions for Standardization of Structural Imaging Validation and Evaluation) Brain Dataset (Froeling et al., 2017). This dataset was acquired from a healthy subject (female, 25 years) on a clinical 3 T system (Philips Achieva) with an eight-channel head coil, who gave informed consent to participate in this study under a protocol approved by the University Medical Center Utrecht ethics board. The subject was scanned on 18 different occasions (total acquisition time: 22.5h). Each of the scanning sessions consisted of four diffusion-weighted MRI acquisition blocks of 15 minutes, providing a unique subset of the total 8000 diffusion-weighted volumes. The gradient directions were distributed over five shells and two Cartesian grids. The five shells consisted of 125, 250, 250, 250, and 300 gradient orientations on a half-sphere with b-values of respectively 500, 1000, 2000, 3000, and 4000 s/mm². The diffusion-weighted MRI data were acquired at an isotropic resolution of 2.5 mm³.

Rat brain imaging

Resting-state fMRI

To determine functional connectivity in the rat brain, we re-used a resting-state fMRI dataset previously acquired from thirteen healthy adult male Wistar rats at twelve to thirteen weeks of age (see (Straathof et al., 2019b) for details).

MRI experiments were conducted on a 4.7 T horizontal bore MR system. We used a homebuilt Helmholtz volume coil (90 mm diameter) and an inductively coupled surface coil (25 mm diameter) for signal excitation and detection, respectively. Rats were endotracheally intubated for mechanical ventilation (TOPO, Kent Scientific, Torrington, CT) with 1% isoflurane in a mixture of air with 30% O₂ (55 breaths per minute). Rats were subsequently immobilized in a specially designed MR-compatible stereotactic holder. During MRI, end-tidal CO₂, blood oxygen saturation, and heart rate were continuously monitored

with a capnograph (Multinex 4200, Datascope Corporation, Paramus, NJ) and pulse oximeter (8600 V, Nonin Medical, Plymouth, MN), respectively. Body temperature was maintained at 37.0 ± 0.5 °C. For resting-state fMRI, T_2^* -weighted blood oxygenation level-dependent (BOLD) images were acquired with a ventilation-triggered single-shot 3D gradient-echo echo-planar imaging (EPI) sequence with the following parameters: repetition time (TR) / echo time (TE) = 32 / 19 ms (effective TR = 1.024 s); 12° pulse angle; field-of-view (FOV) = $32 \times 24 \times 12$ mm³; $64 \times 48 \times 32$ acquisition matrix; $0.5 \times 0.5 \times 0.5$ mm³ voxels; 600 BOLD images in approximately 10 min.

Diffusion-weighted MRI

We acquired postmortem diffusion-weighted MRI data from a perfusion-fixed brain of a healthy adult male Wistar rat with an age of around twelve weeks to determine structural connectivity in the rat cortex. This dataset was part of a previous study (Sarabdjitsingh et al., 2017). The brain was kept inside the skull, and all extracranial tissue was removed. The sample was placed in a proton-free oil (Fomblin®) before MRI to minimize susceptibility artifacts. For diffusion-weighted MRI, we used a custom-made solenoid coil with an internal diameter of 26 mm. High spatial and angular resolution diffusion imaging (HARDI) was performed on a 9.4 T horizontal bore Varian MR system equipped with a 400 mT/m gradient coil (Agilent) using an 8-shot 3D EPI sequence. The acquisition parameters were TR / TE = 500 / 32.4 ms, Δ / δ = 15 / 4 ms; b-value = 3842 s/mm²; FOV = $19.2 \times 16.2 \times 33$ mm³; acquisition matrix = $128 \times 108 \times 220$; spatial resolution: $150 \times 150 \times 150$ μm³. Diffusion-weighting was executed in 60 non-collinear directions on a half sphere and included five non-diffusion-weighted (b0) images, with a total scan time of 8 hours.

Data availability

Rat resting-state fMRI and diffusion-weighted MRI data will be made freely available upon publication at the Open Science Framework (Straathof et al., 2020a).

Image processing

All MRI analyses were performed using FMRIB's Software Library (FSL) v5.0 unless otherwise stated.

Resting-state fMRI

The preprocessing of human and rat resting-state fMRI data included excluding the first ten images to ensure steady-state; motion-correction with *MCFLIRT* (Jenkinson et al., 2002); and brain extraction with *BET* (Smith, 2002). Motion-correction parameters, first-order temporal

derivatives, and the average ventricular signal were used as regressors for the resting-state signal. In addition, average white matter signal regression was applied for human datasets. The latter was excluded for rats because of the small white matter volume in rats and possible partial volume effects from grey matter signals. Low-frequency BOLD fluctuations were obtained by applying temporal filtering between 0.01 and 0.1 Hz and nuisance regression in a single regression model using 3dTproject in AFNI (Cox, 1996); the latter to reduce potential artifacts due to modular preprocessing (Caballero-Gaudes and Reynolds, 2017; Lindquist et al., 2019). We performed an independent component analysis with 20 components to identify biologically plausible resting-state networks in the rat cortex under our experimental conditions (Supplementary Figure S1). We used Fisher's Z-transformed correlation coefficients to measure inter- and intrahemispheric functional connectivity between regions of interest. We used a sliding-window approach for dynamic analyses, with a window size of 60 s and a step size of one TR. We calculated the Fisher's Z-transformed correlation coefficient between the time series from regions of interest for each window to measure dynamic functional connectivity.

Diffusion-weighted MRI

The human diffusion-weighted MRI scans were corrected for subject motion, eddy currents, and EPI artifacts (Froeling et al., 2017). Correction for eddy currents or bias fields was not necessary for the rat dataset because we used a special volume coil and MRI pulse sequence (with extra delays after sinus-shaped gradient pulses) that allowed homogenous imaging of post mortem brain tissue (Sinke et al., 2018). We used single shell constrained spherical deconvolution (CSD) to construct a fiber orientation distribution (FOD) map. Next, CSD-based tractography, using the iFOD2 algorithm, was performed in MRtrix3® (<http://www.mrtrix.org/>) (Tournier et al., 2012, 2010). Whole-brain tractography was done using dynamic seeding, generating 1 million streamlines and a FOD threshold of 0.06 for the human dataset. For the rat dataset, whole-brain tractography generated 2.5 million streamlines with a step size of 75 μm , an angle threshold of 40°, and a FOD threshold of 0.2 (Sinke et al., 2018). The generated tractogram was filtered by Spherical deconvolution Informed Filtering of Tracts (SIFT) (Smith et al., 2015, 2013). Regions-of-interest were considered structurally connected if one or multiple streamlines had their endpoints in both regions. The filtered number of inter-regional streamlines was indicative of structural connectivity strength. We log-transformed the structural connectivity strengths because they were skewed towards smaller weights enabling linear correlation analyses.

Regions-of-interest

For the rat data, we selected 46 regions covering the rat cortex, divided into left and right regions, resulting in a total of 92 cortical regions-of-interest. The 3D atlas rendering, with the region specifications and the corresponding MRI reference images, are available online (https://github.com/wmotte/rat_brain_atlas). For the human analyses, we used the cortical probabilistic Harvard-Oxford atlas, which includes 48 cortical regions across the cerebral cortex, divided into left and right cortical regions, resulting in 96 cortical regions. To enable the selection of regions-of-interest, mean resting-state fMRI and non-diffusion-weighted MRI images were linearly and non-linearly registered to the atlas space (i.e., reference brain (rat) or MNI space (human)) using *FLIRT* (Jenkinson and Smith, 2001) and *FNIRT* (Jenkinson et al., 2012). We used these registrations to transform the regions into individual resting-state fMRI and diffusion MRI spaces. We masked the regions with a temporal signal-to-noise ratio mask of ten for resting-state fMRI analyses. We only included regions comprised of seven or more voxels in individual resting-state space to ensure sufficient quality of resting-state fMRI signals. As a result, we included 80 cortical regions to analyze the rat brain and all 96 cortical regions for the human brain. For a complete list of included regions-of-interest, see Table 1.

In addition, we selected primary unimodal and secondary transmodal regions of interest according to a previous study (Vázquez-Rodríguez et al., 2019). In that study, the division into primary and secondary regions was based on the gradient of cortical organization in the human and macaque brain, with primary regions implicated in acting and perceiving at one end and transmodal association regions, such as the default mode network, at the other end (Margulies et al., 2016). For the human brain, primary regions included the pre- and post-central gyrus and visual processing areas (including occipital and temporo-occipital areas). Secondary areas included regions of the default mode and salience network (insular, cingulate, and temporal cortex and precuneus). For the rat brain, primary areas included primary and secondary visual, motor, and somatosensory cortices, and secondary transmodal areas included association, insular, cingulate and retrosplenial cortices.

Structure-function relationship*Generalized additive models*

To determine the structure-function relationship without an a priori determined linear model, we fitted generalized additive models using five knots and the restricted maximum

Table 1: Included regions-of-interest for analyses of structural and functional connectivity in human and rat brains.

<i>Human brain regions-of-interest</i>	<i>Rat brain regions-of-interest</i>
Left and right frontal pole	<i>Left and right agranular insular cortex dorsal part</i>
<i>Left and right insular cortex</i>	<i>Left and right agranular insular cortex posterior part</i>
Left and right superior frontal cortex	<i>Left and right agranular insular cortex ventral part</i>
Left and right middle frontal gyrus	Left and right primary auditory cortex
Left and right inferior frontal gyrus pars triangularis	Left and right secondary auditory cortex dorsal area
Left and right inferior frontal gyrus pars opercularis	Left and right secondary auditory cortex ventral area
Left and right precentral gyrus	<i>Left and right cingulate cortex area 1</i>
Left and right temporal pole	<i>Left and right cingulate cortex area 2</i>
<i>Left and right superior temporal gyrus anterior division</i>	<i>Left and right dysgranular insular cortex</i>
<i>Left and right superior temporal gyrus posterior division</i>	Left and right ectorhinal cortex
<i>Left and right middle temporal gyrus anterior division</i>	Left and right frontal cortex area 3
<i>Left and right middle temporal gyrus posterior division</i>	<i>Left and right frontal association cortex</i>
<i>Left and right middle temporal gyrus temporooccipital part</i>	<i>Left and right granular insular cortex</i>
<i>Left and right inferior temporal gyrus anterior division</i>	Left and right lateral orbital cortex
<i>Left and right inferior temporal gyrus posterior division</i>	<i>Left and right lateral parietal association cortex</i>
<i>Left and right inferior temporal gyrus temporooccipital part</i>	Left and right primary motor cortex
Left and right postcentral gyrus	Left and right secondary motor cortex
Left and right superior parietal lobule	Left and right medial orbital cortex
Left and right supramarginal gyrus anterior division	<i>Left and right medial parietal association cortex</i>
Left and right supramarginal gyrus posterior division	Left and right perirhinal cortex
Left and right angular gyrus	<i>Left and right retrosplenial dorsal</i>
Left and right lateral occipital cortex superior division	<i>Left and right retrosplenial granular cortex a region</i>
Left and right lateral occipital cortex inferior division	<i>Left and right retrosplenial granular cortex b region</i>
Left and right intracalcarine cortex	Left and right primary somatosensory cortex
Left and right frontal medial cortex	Left and right primary somatosensory cortex barrel field
Left and right juxtapositional lobule cortex	Left and right primary somatosensory cortex dysgranular region
<i>Left and right subcallosal cortex</i>	Left and right primary somatosensory cortex fore limb region
Left and right paracingulate gyrus	Left and right primary somatosensory cortex hind limb region
<i>Left and right cingulate gyrus anterior division</i>	Left and right primary somatosensory cortex jaw region
<i>Left and right cingulate gyrus posterior division</i>	Left and right primary somatosensory cortex trunk region
<i>Left and right precuneous cortex</i>	Left and right primary somatosensory cortex upper lip region
Left and right cuneal cortex	Left and right secondary somatosensory cortex
Left and right frontal orbital cortex	<i>Left and right temporal association cortex</i>
Left and right parahippocampal gyrus anterior division	Left and right primary visual cortex
Left and right parahippocampal gyrus posterior division	Left and right primary visual cortex binocular area
Left and right lingual gyrus	Left and right primary visual cortex monocular area
Left and right temporal fusiform cortex anterior division	Left and right secondary visual cortex lateral area
Left and right temporal fusiform cortex posterior division	Left and right secondary visual cortex mediolateral area
Left and right temporal occipital fusiform cortex	Left and right secondary visual cortex mediomedial area
Left and right occipital fusiform gyrus	Left and right ventral orbital cortex
Left and right frontal operculum cortex	
Left and right central opercular cortex	
Left and right parietal operculum cortex	
Left and right planum polare	
Left and right heschls gyrus	
Left and right planum temporale	
Left and right supracalcarine cortex	
Left and right occipital pole	

Brain regions in bold are primary unimodal regions, brain regions in italics are secondary transmodal regions.

likelihood approach in R (*mgcv* package) (Wood, 2017), functional connectivity being dependent on structural connectivity. Compared to the often-used generalized linear models, which only include linear covariate effects, generalized additive models are composed of a

sum of smooth or non-linear functions of covariates instead of or in addition to the linear effects. Based on these generalized additive models, we proposed a novel measure of structure-function correlations, which we named the structure-function tipping point. To determine this tipping point, we calculated the first derivative of the generalized additive model and its corresponding 95% confidence interval based on 10,000 iterations. This first derivative represents the change in functional connectivity for each increasing step of structural connectivity. Thus, structure-function tipping points are structural connectivity values where the increasing step of structural connectivity is associated with a deviation from an equilibrium state, characterized by a change in functional connectivity that is significantly higher or lower than zero (i.e., the 95% confidence interval of the first derivative does not include zero). The script that we used to determine the non-linear structure-function relationship and the associated structure-function tipping point is available online (<https://github.com/wmotte/tipping-point>). Next, we performed generalized additive models and calculated corresponding structure-function tipping points for each whole-brain static functional connectivity dataset. In addition, we ran similar analyses for primary and secondary regions of interest separately. Lastly, we determined the dynamic structure-function tipping point by calculating the tipping point for each dynamic window in the sliding window analyses, at the whole-brain level and for primary and secondary regions separately.

Tipping points were compared between the rat and human brain using a Mann-Whitney U test. In contrast, differences in tipping points between primary and secondary areas within species were compared with a paired Wilcoxon-signed rank test.

Linear correlation analysis

To validate our non-linear analyses, we performed a straightforward linear correlation analysis of structural versus functional connectivity as a benchmark for structure-function relationships in the brain. We determined the linear structure-function relationship using a Pearson correlation between log-transformed structural connectivity and functional connectivity per individual human or rat dataset. We performed correlation analyses at the whole-brain level and for primary and secondary regions separately for static functional connectivity analyses. For the dynamic functional connectivity analyses, we calculated the structure-function relationship for each dynamic window, which was averaged over all windows to determine a mean dynamic structure-function relationship per individual for the whole cortex and primary and secondary regions specifically.

Results

Non-linear relationship between structural and static functional connectivity in the human and rat cerebral cortex

We performed analyses of linear correlation between structural and static functional connectivity in each individual rat and human dataset as a benchmark for the structure-function relationship. Structural and static functional connectivity were significantly and positively correlated in the rat ($r = 0.26$ (0.23 – 0.29) (median (interquartile range (IQR))); all individual datasets $p < 0.0001$) and the human cortex ($r = 0.31$ (0.27 – 0.35); all individual datasets $p < 0.0001$).

The generalized additive model revealed a non-linear relationship between structural and static functional connectivity in both the rat and human cortex (Figures 1A and 1B). There was no or minimal correlation at low connectivity values, which changed to a significant positive linear- to an exponential-like relationship at higher values, reflective of a tipping point in the structure-function relation. From this tipping point onward, structural, and functional connectivity values became significantly positively correlated in both species. In the human cortex, structural and functional connectivity became significantly correlated at a structural connectivity strength of 1.60 (1.36 – 1.69) [min: 0; max: 8.71], and the structure-function relationship was only slightly non-linear. In the rat cortex, the structure-function relationship fluctuated around zero at low structural connectivity values but showed a clear structure-function tipping point at a structural connectivity strength of 5.69 (5.48 – 5.76) [min: 0; max: 8.31], which was significantly higher than the tipping point in the human cortex (Figure 1C; $W = 6$; $p = 5.1 \times 10^{-4}$). Comparison of the distributions of structural connectivity values in human and rat cortex revealed a highly similar pattern with slightly lower structural connectivity values in the rat brain (rat: 1.61 (0 – 3.83); human: 2.20 (0.69 – 3.95); $U = 2078400$, $p < 0.0001$) (Figure 1D).

We identified the connections with structure-function relationships beyond the structure-function tipping point in more than half of the humans (Figure 1E) and rats (Figure 1F). In the human brain, this resulted in 1622 connections distributed across the entire cortex (Figure 1E). In the rat brain, we identified only 137 cortical connections, of which 96% were intrahemispheric, and 95% were symmetrical in the left and right hemispheres (Figure 1F). Fifty-eight percent of these connections included at least one primary brain region, while thirty-three percent of these connections were between two primary brain regions.

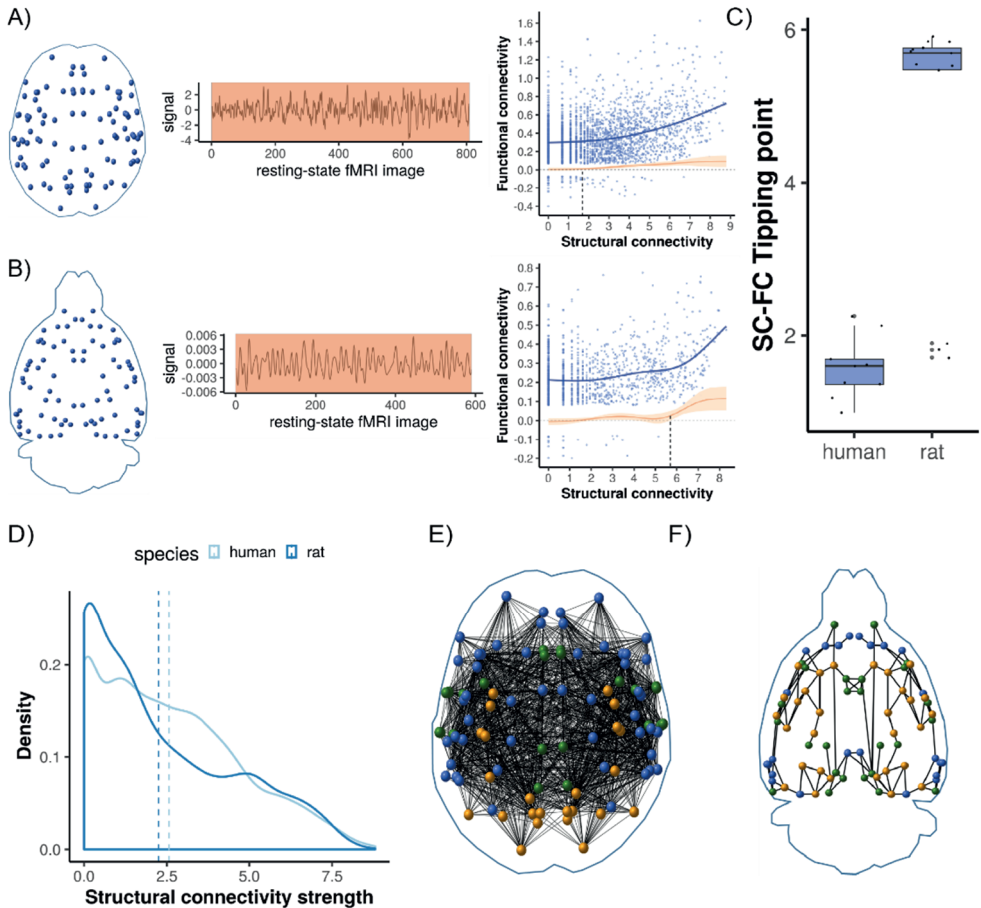


Figure 1: Non-linear relationship between structural and static functional connectivity in the human and rat cerebral cortex. Regions-of-interest projected as blue circles on a horizontal section outline of the human (A; left) and rat brain (B; left). Timeseries of low-frequency bandpass-filtered resting-state fMRI signal in the left motor cortex, with an orange window covering the whole-time range for static functional connectivity analyses in the human (A; middle) and rat brain (B; middle). Representative example of the generalized additive model fit between functional connectivity and structural connectivity (in blue) and the first derivative (in orange), with shades representing the 95% confidence interval for the human (A; right) and rat brain (B; right). Structure-function (SC-FC) tipping point, i.e., the structural connectivity value from which onwards structural and functional connectivities were significantly associated, in human and rat cortex (C). Boxplots show median and inter-quartile range (IQR) whiskers representing 1.5 times the IQR and dots represent individual results. Density plot of structural connectivity strength values in the human and rat cortex, with the dashed line indicating the mean (D). Regions-of-interest (circles) including connections belonging to connections above the structure-function tipping point in more than 50% of the individuals (black lines) on a horizontal section outline of the human (E) and rat brain (F). Yellow circles represent primary brain regions, green circles represent secondary brain regions, and blue circles represent other brain regions.

Differences in structure-function relationships between primary and secondary cortical brain regions

Since linear structure-function relationships may vary across the brain, we also investigated possible differences in structure-function relationships for primary and secondary regions in the rat and human cortex. In the human brain, structural and functional connectivity were significantly positively correlated in primary ($r = 0.42$ (0.39 – 0.45) (median (IQR)); all $p < 0.0001$) and secondary cortical areas ($r = 0.27$ (0.26 – 0.33); all $p < 0.005$, except for one individual), with a higher structure-function correlation in primary compared to secondary regions ($U = 45$; $p = 0.004$). Similarly, in the rat brain, we found that structural and functional connectivity were significantly positively correlated in primary ($r = 0.29$ (0.25 – 0.33); all $p < 0.001$) and secondary cortical regions ($r = 0.41$ (0.39 – 0.46); all $p < 0.05$, except for two rats), but the structure-function correlation was higher in secondary compared to primary regions ($V = 0$, $p = 0.0001$).

Non-linear generalized additive model analyses demonstrated a more complex relationship between structural and functional connectivity in primary compared to secondary cortical regions in the rat brain (Figure 2B). In ten out of thirteen rats, we could not determine a structure-function tipping point between secondary brain regions, because structural and functional connectivity were either significantly correlated at all structural connectivity values or not significantly correlated at all. As a result, we only identified a structure-function tipping point in three rats (at structural connectivity value 3.66 (3.46 – 4.55); [min: 0; max: 7.71]). In comparison, primary brain regions showed fluctuations around zero at low structural connectivity values but with a clear structure-function tipping point in ten out of thirteen rats (at structural connectivity strength value 4.84 (4.02 – 5.80); [min: 0; max: 8.31]) (Figure 2C). In the human brain, we could identify a tipping point in seven of the ten individuals in primary and eight out of ten individuals in secondary cortical regions (Figure 2A). Nevertheless, in some individuals, the structure-function relationship became non-significant again at high structural connectivity values due to a large 95% confidence interval, making a tipping point less evident. The structure-function tipping point occurred at a lower structural connectivity value in primary (2.28 (2.14 – 3.67); [min: 0; max: 8.61]) compared to secondary brain regions (3.89 (3.72 – 4.09); [min: 0; max: 8.11]) in the human cortex, but this was not statistically significant ($V = 2$; $p = 0.09$) (Figure 2C).

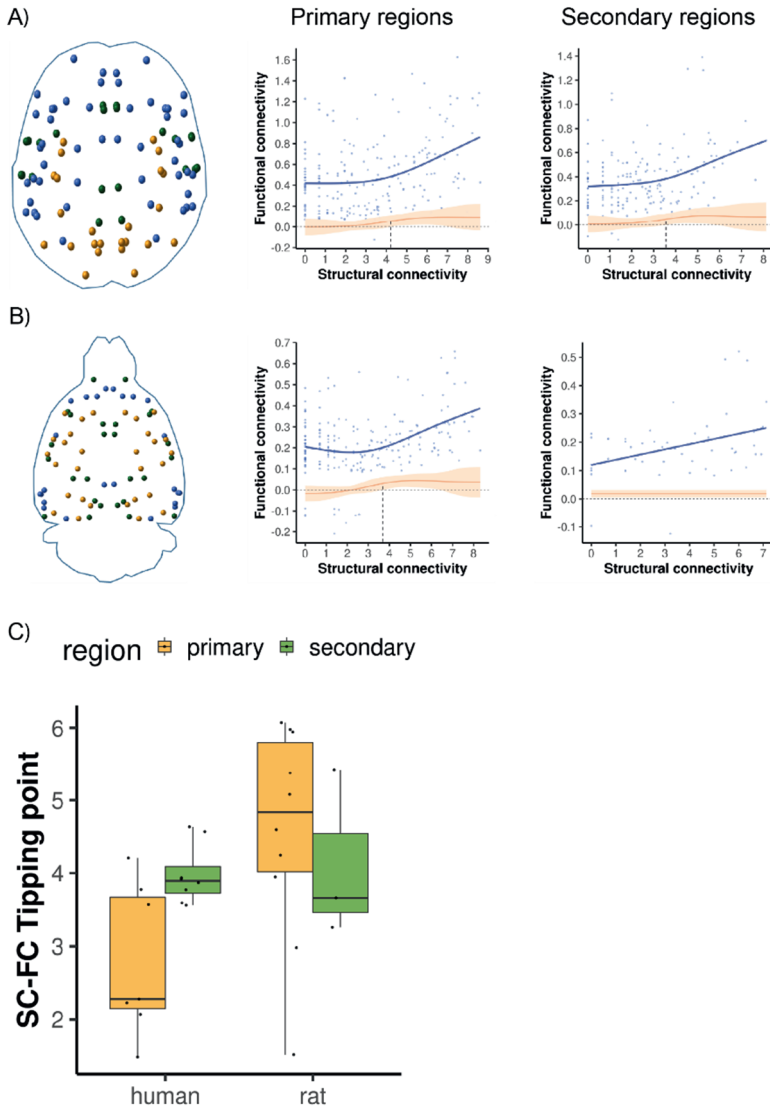


Figure 2: Structure-function relationships in primary and secondary brain regions in the human and rat cortex. Regions of interest projected as circles on a horizontal section outline of the brain (left) (primary regions in yellow, secondary regions in green, and other regions in blue), and representative examples of the generalized additive model fit in blue and the first derivative in orange, with shades representing the 95% confidence interval, in primary (middle) and secondary cortical regions (right) of an individual human (A) and rat brain (B). Structure-function (SC-FC) tipping point, i.e., the structural connectivity value from which onwards structural and functional connectivities were significantly associated, for primary (yellow) and secondary brain regions (green) in the rat and human brain (C). Boxplots show median and inter-quartile range (IQR), whiskers representing 1.5 times the IQR, and dots represent individual results.

Dynamic functional connectivity analyses reveal similar complex structure-function relationships

To determine whether the dynamic nature of functional connectivity influenced structure-function tipping points, we also applied generalized additive modeling to dynamic functional connectivity data. Similar to the static functional connectivity results, we found a significantly lower structural connectivity value as whole-brain structure-function tipping point in the human compared to the rat cortex (human: 2.48 (2.33 – 2.68); rat: 3.75 (3.41 – 3.88); $W = 1$; $p < 0.0001$) (Figure 3A). In separate assessments of primary and secondary brain regions, we did not find a difference in structure-function tipping point values between primary and secondary brain regions in the human cortex (primary regions: 4.05 (3.43 – 5.43); secondary regions: 5.04 (2.87 – 5.18); $V = 4$; $p = 0.75$) (Figure 3B), although we could only determine a tipping point in secondary brain regions in three out of ten individuals. In the rat cortex, we could determine tipping points for all individual rats and found a higher tipping point value in primary compared to secondary brain regions, but this was not statistically significant (primary regions: 3.38 (2.60 – 3.71); secondary regions: 2.42 (1.89 – 2.73); $V = 70$; $p = 0.09$).

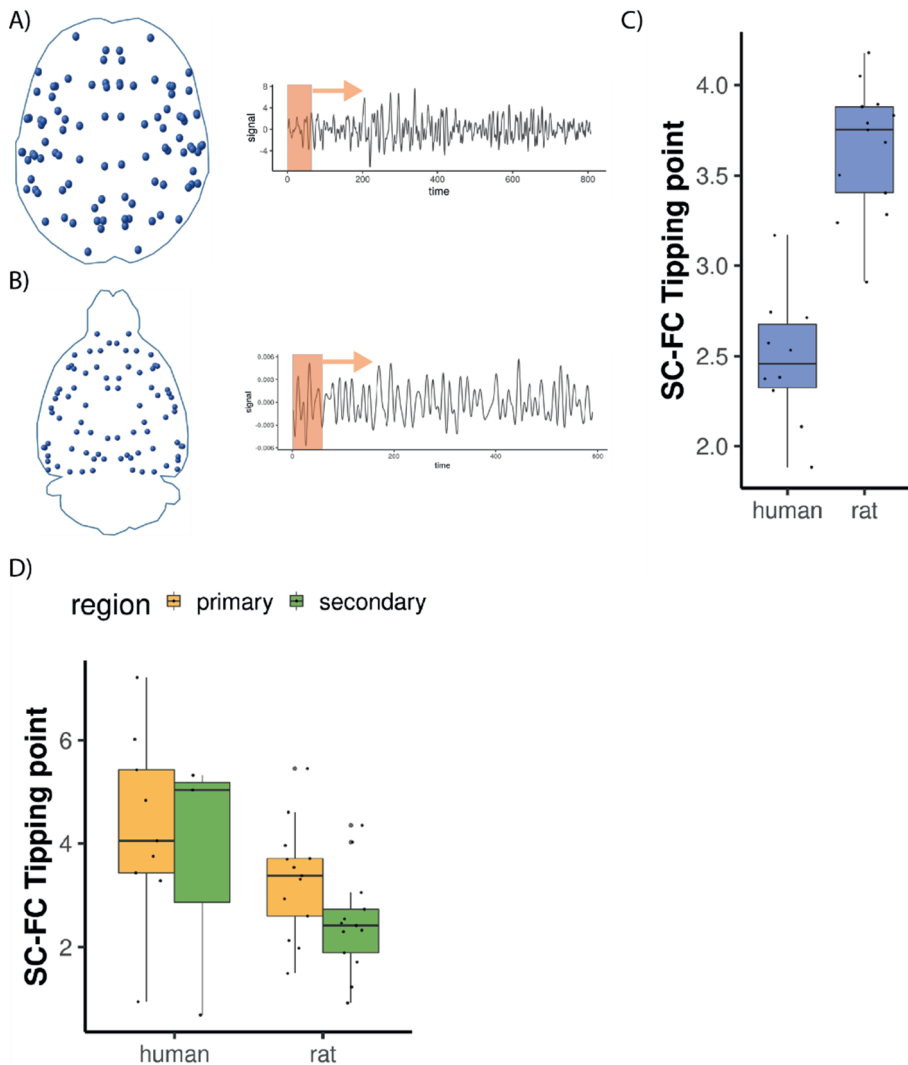


Figure 3: Tipping points for the relationship between structural connectivity and dynamic functional connectivity in the human and rat cortex. Regions-of-interest projected as blue circles on a horizontal section outline of the brain, and time series of low frequency bandpass-filtered resting-state fMRI signal in the left motor cortex, for human (A) and rat brain (B). The orange window represents the sliding-window approach to dynamically calculate functional connectivity and corresponding structure-function tipping point per window. The window length was 60 s (27 images for the human and 58 images for the rat brain), which was moved with the repetition time (2.2 s for the human and 1.024 s for the rat dataset). Structure-function (SC-FC) tipping points are shown for the whole brain (C) and primary (yellow) and secondary regions (green) in the human and rat brain (D). Boxplots show median and inter-quartile range (IQR), whiskers representing 1.5 times the IQR, and dots represent individual results.

Discussion

We mapped the relationship between structural and functional connectivity and evaluated the possible non-linearity of this relationship. Structure-function relationships in both the human and rat cortex were found to have non-linear profiles. Structural and functional connectivity were not significantly associated with weak structural connections, but their relationship became positive and statistically significant at higher connectivity levels. The structural connectivity weight at which this occurred was defined as the structure-function tipping point. This structure-function tipping point was lower in the human cortex than in the rat cortex. We found non-linear structure-function relationships in primary and secondary cortical brain regions, with no clear difference in the structure-function tipping point values.

Lower whole-brain structure-function tipping point in human compared to rat cortex

We confirmed that structural and functional connectivity were moderately correlated in all individual rat and human datasets, using frequently applied linear correlation analysis, in line with previous reports (Honey et al., 2009; Straathof et al., 2020b, 2019a). Our analyses of non-linear correlations showed that the relationship between cortical structural and (static and dynamic) functional connectivity is more complex, characterized by a significant positive structure-function correlation from the structure-function tipping point onwards. This non-linear relationship and the observed structure-function tipping point may relate to the small-world organization of structural brain networks (Sporns and Zwi, 2004). Small-world networks are characterized by strong structural connections within specialized functional modules, which may strongly associate with functional connectivity, and sparse weak structural connections between those functional modules, which are less strongly associated with functional connectivity. These weak structural connections are believed to be important for integrating information in the brain (Markov et al., 2014, 2013). However, they often span long distances and may introduce diverse inputs to and outputs from brain regions (Betz et al. and Bassett, 2018), resulting in limited association with functional connectivity. Stronger structural connections, particularly intrahemispherically, have a higher correlation with functional connectivity.

This significant and positive relationship, starting at the structure-function tipping point, was found to occur at lower structural connectivity strengths in the human compared to the rat cortex, despite a largely similar distribution of structural connectivity weights.

While the human brain appears to be organized as a small-world network (Liao et al., 2017; Sporns and Zwi, 2004), the organization of the rodent brain network may be more in-between a small-world and scale-free topology, characterized by less interconnected modules and more inter-modular connections (Henriksen et al., 2016; Oh et al., 2014; Sporns and Bullmore, 2014). The latter may result in a larger range of structural connections that are weakly or not associated with functional connectivity in the rat brain, reflected by fluctuations in the structure-function relationship at low structural connectivity values and a higher structure-function tipping point value. In the human brain, consistent connections with a structural connectivity strength above the tipping point were distributed all over the cortex. In comparison, in the rat cortex, we found that stronger structural connections above the structure-function tipping point were mostly intrahemispheric and involved primary brain regions, which have previously been identified as hub-regions in the structural network of the rat brain (van den Heuvel et al., 2016b). Weak structural connections in the rodent brain may have a random organization and cover long distances, whereas strong structural connections would be more ordered (van den Heuvel et al., 2016b; Ypma and Bullmore, 2016). This arrangement of strong and weak structural connections could be due to developmental processes like pruning, with structurally solid connections being mainly activated and functionally strengthened during development. In contrast, the structure-function relationship in weak structural connections may be more variable (van den Heuvel et al., 2016b). Synaptic pruning happens over a much shorter life period in the rat than in the human brain (Petanjek et al., 2011; Semple et al., 2013), potentially resulting in more “random” structural connections with a weak functional association in the rat brain.

Different structure-function relationships between human and rat cortex in primary and secondary regions

Since linear structure-function relationships vary across the brain (Straathof et al., 2020b; Vázquez-Rodríguez et al., 2019), we investigated the non-linear relationship in primary unimodal and secondary transmodal regions separately. Primary unimodal sensory regions showed higher linear structure-function correlations than transmodal secondary areas in the human brain, in line with a previous study that explained this by stronger participation of secondary brain regions in dynamic networks (Vázquez-Rodríguez et al., 2019). However, despite these differences in linear structure-function relationships, our non-linear correlation analyses showed similar non-linear structure-function relationships in primary and secondary regions in the human cortex. Speculatively, the large cortical expansion in the

human brain may have shifted the importance of primary sensory information processing towards the integration of information in secondary regions (Buckner and Krienen, 2013), resulting in similar complex structure-function relationships.

In the rat cortex, the structure-function relationship displayed more non-linearity in primary regions than in secondary regions, expressed by a noticeably clear structure-function tipping point. Since primary sensory cortices can integrate multisensory information in the rodent brain (Laramée and Boire, 2015; Stehberg et al., 2014), multimodal secondary regions may be less developed. This could explain the lack of non-linearity in the structure-function relationship, less dynamical interactions, and a consequently stronger linear structure-function correlation. Thus, our results indicate that the functional networks across the rat cortex are differently organized, with primary sensory areas showing non-linearity of the structure-function relationship resembling the organization of the human cortex. In contrast, higher-order transmodal areas appear less developed in their structure-function relationship.

Another factor that may explain the differences in structure-function correlations between rats and humans in primary and secondary regions, which may complicate the species comparison, is the anesthesia used in rodent studies. Light anesthesia during resting-state fMRI may increase the coherence between functional and structural networks (Barttfeld et al., 2015). In addition, light anesthesia in rats has been shown to impact signaling in secondary brain regions more than in primary brain regions (Liang et al., 2015). Higher-order brain regions are more inhibited under light anesthesia. In contrast, primary brain regions remain functioning and may continue to be involved in dynamic processes. However, another study that compared resting-state fMRI signals in awake humans and anesthetized monkeys demonstrated that functional signaling remains present under anesthesia in dynamic functional network areas, like associative cortices (Yin et al., 2019). Therefore, how anesthesia exactly influences the dynamics of functional networks and its role in the (non-) linear structure-function relationship across the brain, remains unclear, which could be a topic in future studies.

Different non-linear structure-function relationships in secondary brain regions using dynamic functional connectivity analyses

Our dynamic analyses showed similar non-linear structure-function relationships in our whole-brain assessments and in primary cortical regions as we found with the static analyses. Although functional connectivity values dynamically changed over the applied temporal

windows, the structural connectivity value from which structural and functional connectivity became significantly associated was similar. This suggests that the structure-function tipping point is inherent to structural brain networks, which may be determined by the topology of the network (small-world versus scale-free). However, we found differences in the non-linearity of structure-function relationships in secondary brain regions between static and dynamic functional connectivity analyses. In our static functional connectivity analyses, we could determine tipping points in the secondary regions in human but not in rat cortex. In contrast, in our dynamic functional connectivity analyses, we could determine tipping points in rat but not in human cortex. This difference may reflect dissimilarities in the dynamic nature of functional connectivity in secondary brain regions between humans and rats. In the human brain, functional connectivity between secondary transmodal regions may be highly dynamic. Still, it may not clearly reflect structural connectivity in these dynamic periods, resulting in the absence of structure-function tipping points in our dynamic analyses. In comparison, while functional connectivity between secondary regions in the rat brain may be dynamic, it may still resemble structural connectivity, resulting in clear tipping points in the dynamic analyses. These results support our hypothesis that brain networks are differently organized in the rat brain, and that secondary brain regions may functionally be less dynamic and developed. In addition, the specific differences between static and dynamic analysis in human and rat datasets suggest that potentially altered functional connectivity dynamics induced by light anesthesia cannot solely explain the observed differences in the structure-function relationship between the human and rat brain.

Future perspective

Our study fits within the field of comparative connectomics, which investigates the similarities and differences in brain network organization across species (van den Heuvel et al., 2016a). Although there is a large agreement between brain networks across species, differences facilitate distinctive behavior. Our non-linear correlation analyses identified clear differences in network organization between the rat and human cortex, characterized by less non-linearity and more homogeneous non-linear structure-function relationships across the human brain, compared to very clear non-linear components in the structure-function relationship in the rat brain that differed between primary and secondary brain regions. Whether this is simply due to differences in brain size, with more specialization and relatively less long-distance connections in the larger human brain, or species differences in the development of specific brain regions is currently unknown. Future studies are needed to

investigate the potential value of the introduced structure-function tipping point as a network marker for aging (Damoiseaux, 2017; Liu et al., 2017; Sala-Llonch et al., 2014; Zimmermann et al., 2016) or (risk of) disease (Bullmore and Sporns, 2009; van den Heuvel and Sporns, 2019).

Limitations

Our study has some limitations. First, we did not compare structural and functional connectivity within the same individuals or animals. This might have led to some underestimation of the structure-function relationships due to inter-individual variation. However, our ultrahigh-resolution diffusion-weighted data provided high-quality information on structural connectivity, necessary for reconstructing structural networks with a minimum of false positives (Maier-Hein et al., 2017). Second, as already mentioned above, resting-state fMRI in rats was acquired under light anesthesia, which may have influenced our functional connectivity analyses (Paasonen et al., 2018) and measures of structure-function correlation (Barttfeld et al., 2015; Uhrig et al., 2018). However, anesthesia-induced changes in functional connectivity have been shown to have no or minimal effects on the global organization of functional networks in rodents (Liang et al., 2012). Previous studies have demonstrated the reliability of comparisons of structure-function relationships between anesthetized rodents and awake humans (Díaz-Parra et al., 2017; Grandjean et al., 2017; Straathof et al., 2020b, 2019a). Lastly, since we used publicly available human datasets and previously acquired rat datasets, MRI acquisition parameters differed between species. Although we cannot rule out the effect of different parameter settings on our outcomes, the applied MRI protocols belong to the standards for structural and functional connectivity measurement in human and rodent brains.

Conclusion

Differences in the non-linear structure-function relationship between primary and secondary brain regions in the rat cortex, which were not apparent in the human cortex, reflect organizational differences in functional networks with a possible evolutionary origin. Thus, non-linear correlation analyses provide an original means to assess the complex interaction between functional and structural connectivity in neural networks and may reveal unique markers of brain development, aging and dysfunction.

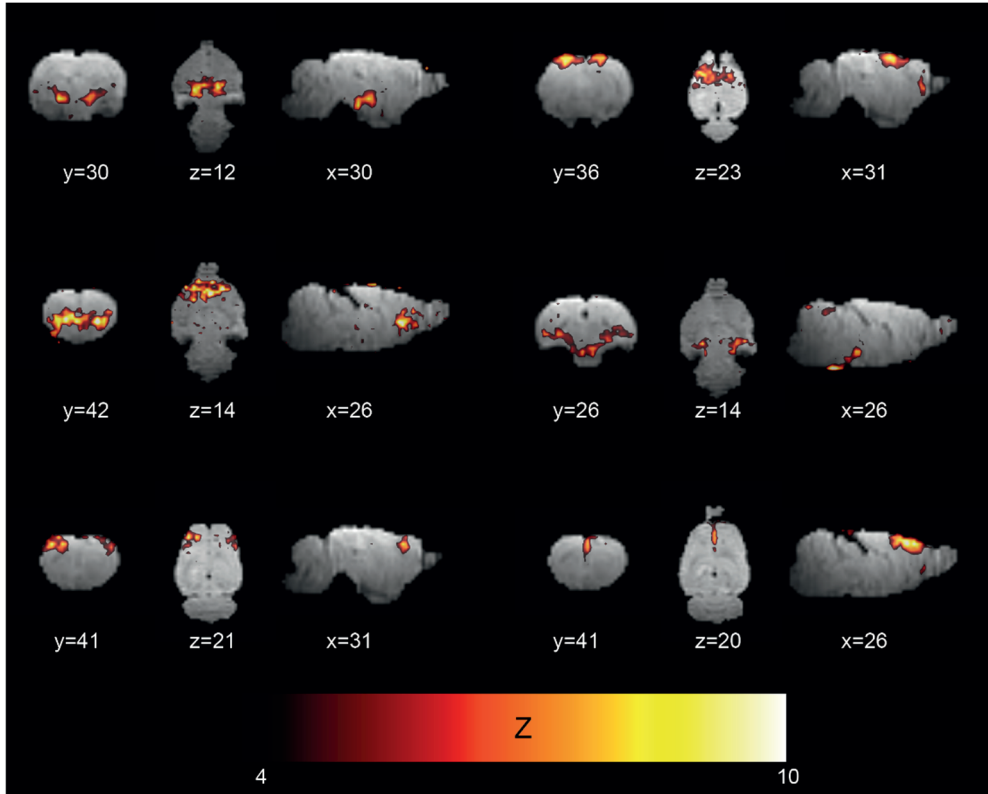
References

- Barttfeld, P., Uhrig, L., Sitt, J.D., Sigman, M., Jarraya, B., Dehaene, S., 2015. Signature of consciousness in the dynamics of resting-state brain activity. *Proc. Natl. Acad. Sci. U. S. A.* 112, 887–892. <https://doi.org/10.1073/pnas.1515029112>
- Betz, R.F., Bassett, D.S., 2018. Specificity and robustness of long-distance connections in weighted, interareal connectomes. *Proc. Natl. Acad. Sci. U. S. A.* 115, E4880–E4889. <https://doi.org/10.1073/pnas.1720186115>
- Biswal, B., Yetkin, F., Haughton, V., Hyde, J., 1995. Functional connectivity in the motor cortex of resting human brain using echo-planar MRI. *Magn. Reson. Med.* 34, 537–541. <https://doi.org/10.1002/mrm.1910340409>
- Buckner, R.L., Krienen, F.M., 2013. The evolution of distributed association networks in the human brain. *Trends Cogn. Sci.* 17, 648–665. <https://doi.org/10.1016/j.tics.2013.09.017>
- Bullmore, E., Sporns, O., 2009. Complex brain networks: Graph theoretical analysis of structural and functional systems. *Nat. Rev. Neurosci.* 10, 186–198. <https://doi.org/10.1038/nrn2575>
- Caballero-Gaudes, C., Reynolds, R.C., 2017. Methods for cleaning the BOLD fMRI signal. *Neuroimage* 154, 128–149. <https://doi.org/10.1016/j.neuroimage.2016.12.018>
- Chang, C., Glover, G.H., 2010. Time-frequency dynamics of resting-state brain connectivity measured with fMRI. *Neuroimage* 50, 81–98. <https://doi.org/10.1016/j.neuroimage.2009.12.011>
- Cox, R.W., 1996. AFNI: Software for Analysis and Visualization of Functional Magnetic Resonance Neuroimages. *Comput. Biomed Res.* 29, 162–173.
- Damoiseaux, J.S., 2017. Effects of Aging on Functional and Structural Brain Connectivity. *Neuroimage* 160, 32–40. <https://doi.org/10.1016/j.neuroimage.2017.01.077>
- Damoiseaux, J.S., Greicius, M.D., 2009. Greater than the sum of its parts : a review of studies combining structural connectivity and resting-state functional connectivity. *Brain Struct. Funct.* 213, 525–533. <https://doi.org/10.1007/s00429-009-0208-6>
- Díaz-Parra, A., Osborn, Z., Canals, S., Moratal, D., Sporns, O., 2017. Structural and functional, empirical and modeled connectivity in the cerebral cortex of the rat. *Neuroimage* 159, 170–184. <https://doi.org/10.1016/j.neuroimage.2017.07.046>
- Fox, M.D., Raichle, M.E., 2007. Spontaneous fluctuations in brain activity observed with functional magnetic resonance imaging. *Nat. Rev. Neurosci.* 8, 700–711. <https://doi.org/10.1038/nrn2201>
- Froeling, M., Tax, C.M.W., Vos, S.B., Luijten, P.R., Leemans, A., 2017. “MASSIVE” brain dataset: Multiple acquisitions for standardization of structural imaging validation and evaluation. *Magn. Reson. Med.* 77, 1797–1809. <https://doi.org/10.1002/mrm.26259>
- Gordon, E.M., Laumann, T.O., Gilmore, A.W., Newbold, D.J., Greene, D.J., Berg, J.J., Ortega, M., Hoyt-Drazen, C., Gratton, C., Sun, H., Hampton, J.M., Coalson, R.S., Nguyen, A.L., McDermott, K.B., Shimony, J.S., Snyder, A.Z., Schlaggar, B.L., Petersen, S.E., Nelson, S.M., Dosenbach, N.U.F., 2017. Precision Functional Mapping of Individual Human Brains. *Neuron* 95, 791–807. <https://doi.org/10.1016/j.neuron.2017.07.011>
- Grandjean, J., Zerbi, V., Balsters, J.H., Wenderoth, N., Rudin, M., 2017. Structural basis of large-scale functional connectivity in the mouse. *J. Neurosci.* 37, 8092–8101. <https://doi.org/10.1523/JNEUROSCI.0438-17.2017>
- Greicius, M.D., Supekar, K., Menon, V., Dougherty, R.F., 2009. Resting-state functional connectivity reflects structural connectivity in the default mode network. *Cereb. Cortex* 19, 72–78. <https://doi.org/10.1093/cercor/bhn059>
- Henriksen, S., Pang, R., Wronkiewicz, M., 2016. A simple generative model of the mouse mesoscale connectome. *Elife* 5, 1–19. <https://doi.org/10.7554/eLife.12366>
- Honey, C.J., Sporns, O., Cammoun, L., Gigandet, X., Thiran, J.P., Meuli, R., Hagmann, P., 2009. Predicting human resting-state functional connectivity from structural connectivity. *Proc. Natl. Acad. Sci. U. S. A.* 106, 2035–2040. <https://doi.org/10.1073/pnas.0811168106>
- Hutchison, R.M., Womelsdorf, T., Allen, E.A., Bandettini, P.A., Calhoun, V.D., Corbetta, M., Della Penna, S., Duyn, J.H., Glover, G.H., Gonzalez-Castillo, J., Handwerker, D.A., Keilholz, S., Kiviniemi, V., Leopold, D.A., de Pasquale, F., Sporns, O., Walter, M., Chang, C., 2013. Dynamic functional connectivity: Promise, issues, and interpretations. *Neuroimage* 80, 360–78. <https://doi.org/10.1016/j.neuroimage.2013.05.079>
- Jenkinson, M., Bannister, P., Brady, M., Smith, S., 2002. Improved optimization for the robust and accurate linear registration and motion correction of brain images. *Neuroimage* 17, 825–841. <https://doi.org/10.1006/nimg.2002.1132>
- Jenkinson, M., Beckmann, C.F., Behrens, T.E.J., Woolrich, M.W., Smith, S.M., 2012. Fsl. *Neuroimage* 62, 782–790. <https://doi.org/10.1016/j.neuroimage.2011.09.015>
- Jenkinson, M., Smith, S., 2001. A global optimisation method for robust affine registration of brain images. *Med. Image Anal.* 5, 143–156. [https://doi.org/10.1016/S1361-8415\(01\)00036-6](https://doi.org/10.1016/S1361-8415(01)00036-6)
- Johansen-Berg, H., Behrens, T.E.J., 2013. Diffusion MRI: From quantitative measurement to in-vivo neuroanatomy, Second ed. ed. Elsevier/Academic Press.
- Laramée, M.E., Boire, D., 2015. Visual cortical areas of the mouse: Comparison of parcellation and network structure with primates.

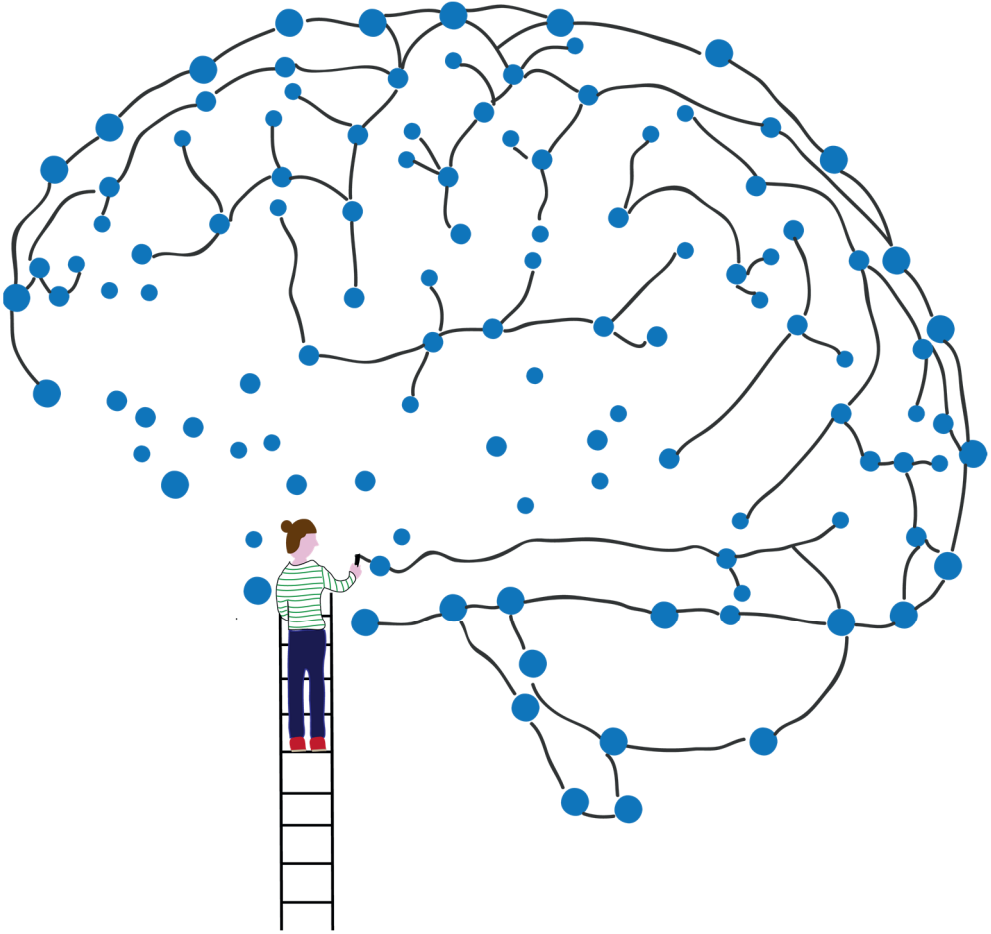
- Front. Neural Circuits 8, 149. <https://doi.org/10.3389/fncir.2014.00149>
- Lee, T., Xue, S., 2018. Revisiting the functional and structural connectivity of large-scale cortical networks. *Brain Connect.* 8, 129–138. <https://doi.org/10.1089/brain.2017.0536>
- Liang, H., Wang, H., 2017. Structure-Function Network Mapping and Its Assessment via Persistent Homology. *PLOS Comput. Biol.* 13, e1005325. <https://doi.org/10.1371/journal.pcbi.1005325>
- Liang, Z., King, J., Zhang, N., 2012. Intrinsic organization of the anesthetized brain. *J. Neurosci.* 32, 10183–10191. <https://doi.org/10.1523/JNEUROSCI.1020-12.2012>
- Liang, Z., Liu, X., Zhang, N., 2015. Dynamic Resting State Functional Connectivity in Awake and Anesthetized Rodents. *Neuroimage* 104, 89–99. <https://doi.org/doi:10.1016/j.neuroimage.2014.10.013>
- Liao, X., Vasilakos, A. V., He, Y., 2017. Small-world human brain networks: Perspectives and challenges. *Neurosci. Biobehav. Rev.* 77, 286–300. <https://doi.org/10.1016/j.neubiorev.2017.03.018>
- Liao, X., Yuan, L., Zhao, T., Dai, Z., Shu, N., Xia, M., Yang, Y., Evans, A., He, Y., 2015. Spontaneous functional network dynamics and associated structural substrates in the human brain. *Front. Hum. Neurosci.* 9, 478. <https://doi.org/10.3389/fnhum.2015.00478>
- Lindquist, M.A., Geuter, S., Wager, T.D., Caffo, B.S., 2019. Modular preprocessing pipelines can reintroduce artifacts into fMRI data. *Hum. Brain Mapp.* 40, 2358–2376. <https://doi.org/10.1002/hbm.24528>
- Liu, K., Yao, S., Chen, K., Zhang, J., Yao, L., Li, K., Jin, Z., Guo, X., 2017. Structural brain network changes across the adult lifespan. *Front. Aging Neurosci.* 9, 275. <https://doi.org/10.3389/fnagi.2017.00275>
- Maier-Hein, K.H., Neher, P.F., Houde, J.-C., Coté, M.-A., Garyfallidis, E., Zhong, J., Chamberland, M., Yeh, F.-C., Lin, Y.-C., Ji, Q., Reddick, W.E., Glass, J.O., Chen, D.Q., Feng, Y., Gao, C., Wu, Y., Ma, J., Renhjie, H., Li, Q., Westin, C.-F., Deslauriers-Gauthier, S., Omar Ocegueda González, J., Paquette, M., St-Jean, S., Girard, G., Rheault, F., Sidhu, J., Tax, C.M.W., Guo, F., Mesri, H.Y., Szabolcs, D., Froeling, M., Heemskerk, A.M., Leemans, A., Boré, A., Pinsard, B., Bedetti, C., Desrosiers, M., Brambati, S., Doyon, J., Sarica, A., Vasta, R., Cerasa, A., Quattrone, A., Yeatman, J., Khan, A.R., Hodges, W., Alexander, S., Romascano, D., Barakovic, M., Auria, A., Esteban, O., Lemkaddem, A., Thiran, J.-P., Ertan Cetingul, H., Odry, B.L., Mailhe, B., Nadar, M.S., Pizzagalli, F., Prasad, G., Villalón-Reina, J.E., Galvis, J., Thompson, P.M., De Santiago Requejo, F., Luque Laguna, P., Lacerda, L.M., Barrett, R., Dell'Acqua, F., Catani, M., Petit, L., Caruyer, E., Daducci, A., Dyrby, T.B., Holland-Letz, T., Hilgetag, C.C., Stieltjes, B., Descoteaux, M., 2017. The challenge of mapping the human connectome based on diffusion tractography. *Nat. Commun.* 8, 1349. <https://doi.org/10.1038/s41467-017-01285-x>
- Margulies, D.S., Ghosh, S.S., Goulas, A., Falkiewicz, M., Huntenburg, J.M., Langs, G., Bezgin, G., Eickhoff, S.B., Castellanos, F.X., Petrides, M., Jefferies, E., Smallwood, J., 2016. Situating the default-mode network along a principal gradient of macroscale cortical organization. *Proc. Natl. Acad. Sci. U. S. A.* 113, 12574–12579. <https://doi.org/10.1073/pnas.1608282113>
- Markov, N.T., Ercsey-Ravasz, M., Lamy, C., Gomes, A.R.R., Magrou, L., Misery, P., Giroud, P., Barone, P., Dehay, C., Toroczka, Z., Knoblauch, K., Van Essen, D.C., Kennedy, H., 2013. The role of long-range connections on the specificity of the macaque interareal cortical network. *Proc. Natl. Acad. Sci. U. S. A.* 110, 5187–5192. <https://doi.org/10.1073/pnas.1218972110>
- Markov, N.T., Ercsey-Ravasz, M.M., Ribeiro Gomes, A.R., Lamy, C., Magrou, L., Vezoli, J., Misery, P., Falchier, A., Quilodran, R., Gariel, M.A., Sallet, J., Gamanut, R., Huissoud, C., Clavagnier, S., Giroud, P., Sappey-Marinié, D., Barone, P., Dehay, C., Toroczka, Z., Knoblauch, K., Van Essen, D.C., Kennedy, H., 2014. A weighted and directed interareal connectivity matrix for macaque cerebral cortex. *Cereb. Cortex* 24, 17–36. <https://doi.org/10.1093/cercor/bhs270>
- Oh, S.W., Harris, J.A., Ng, L., Winslow, B., Cain, N., Mihalas, S., Wang, Q., Lau, C., Kuan, L., Henry, A.M., Mortrud, M.T., Ouellette, B., Nguyen, T.N., Sorensen, S.A., Slaughterbeck, C.R., Wakeman, W., Li, Y., Feng, D., Ho, A., Nicolas, E., Hirokawa, K.E., Bohn, P., Joines, K.M., Peng, H., Hawrylycz, M.J., Phillips, J.W., Hohmann, J.G., Wahnoutka, P., Gerfen, C.R., Koch, C., Bernard, A., Dang, C., Jones, A.R., Zeng, H., 2014. A mesoscale connectome of the mouse brain. *Nature* 508, 207–214. <https://doi.org/10.1038/nature13186>
- Paasonen, J., Stenroos, P., Salo, R.A., Kiviniemi, V., Gröhn, O., 2018. Functional connectivity under six anesthesia protocols and the awake condition in rat brain. *Neuroimage* 172, 9–20. <https://doi.org/10.1016/j.neuroimage.2018.01.014>
- Petanjek, Z., Judaš, M., Šimić, G., Rašin, M.R., Uylings, H.B.M., Rakic, P., Kostović, I., 2011. Extraordinary neoteny of synaptic spines in the human prefrontal cortex. *Proc. Natl. Acad. Sci. U. S. A.* 108, 13281–13286. <https://doi.org/10.1073/pnas.1105108108>
- Sala-Llloch, R., Junqué, C., Arenaza-Urquijo, E.M., Vidal-Piñero, D., Valls-Pedret, C., Palacios, E.M., Domènech, S., Salvà, A., Bargalló, N., Bartrés-Faz, D., 2014. Changes in whole-brain functional networks and memory performance in aging. *Neurobiol. Aging* 35, 2193–2202. <https://doi.org/10.1016/j.neurobiolaging.2014.04.007>
- Sarabdjitsingh, R.A., Loi, M., Joels, M., Dijkhuizen, R.M., van der Toorn, A., 2017. Early life stress-induced alterations in rat brain structures measured with high resolution MRI. *PLoS One* 12, e0185061. <https://doi.org/10.1371/journal.pone.0185061>
- Semple, B.D., Blomgren, K., Gimlin, K., Ferriero, D.M., Noble-Haeusslein, L.J., 2013. Brain development in rodents and humans: Identifying benchmarks of maturation and vulnerability to injury across species. *Prog. Neurobiol.* 106–107, 1–16. <https://doi.org/10.1016/j.pneurobio.2013.04.001>
- Shen, K., Hutchison, R.M., Bezgin, G., Everling, S., McIntosh, A.R., 2015. Network Structure Shapes Spontaneous Functional

- Connectivity Dynamics. *J. Neurosci.* 35, 5579–5588. <https://doi.org/10.1523/JNEUROSCI.4903-14.2015>
- Sinke, M.R.T., Otte, W.M., Christiaens, D., Schmitt, O., Leemans, A., van der Toorn, A., Sarabdjitsingh, R.A., Joëls, M., Dijkhuizen, R.M., 2018. Diffusion MRI-based cortical connectome reconstruction: dependency on tractography procedures and neuroanatomical characteristics. *Brain Struct. Funct.* 223, 2269–2285. <https://doi.org/10.1007/s00429-018-1628-y>
- Smith, R.E., Tournier, J.D., Calamante, F., Connelly, A., 2015. The effects of SIFT on the reproducibility and biological accuracy of the structural connectome. *Neuroimage* 104, 253–265. <https://doi.org/10.1016/j.neuroimage.2014.10.004>
- Smith, R.E., Tournier, J.D., Calamante, F., Connelly, A., 2013. SIFT: Spherical-deconvolution informed filtering of tractograms. *Neuroimage* 67, 298–312. <https://doi.org/10.1016/j.neuroimage.2012.11.049>
- Smith, S.M., 2002. Fast robust automated brain extraction. *Hum. Brain Mapp.* 17, 143–155. <https://doi.org/10.1002/hbm.10062>
- Sporns, O., Bullmore, E.T., 2014. From connections to function: The mouse brain connectome atlas. *Cell* 157, 773–775. <https://doi.org/10.1016/j.cell.2014.04.023>
- Sporns, O., Zwi, J.D.Z., 2004. The small world of the cerebral cortex. *Neuroinformatics* 2, 145–162. <https://doi.org/10.1385/NI:2:2:145>
- Stafford, J.M., Jarrett, B.R., Miranda-Dominguez, O., Mills, B.D., Cain, N., Mihalas, S., Lahvis, G.P., Lattal, K.M., Mitchell, S.H., David, S. V., Fryer, J.D., Nigg, J.T., Fair, D.A., 2014. Large-scale topology and the default mode network in the mouse connectome. *Proc. Natl. Acad. Sci. U. S. A.* 111, 18745–18750. <https://doi.org/10.1073/pnas.1404346111>
- Stehberg, J., Stehberg, J., Dang, P.T., Frostig, R.D., 2014. Unimodal primary sensory cortices are directly connected by long-range horizontal projections in the rat sensory cortex. *Front. Neuroanat.* 8, 1–19. <https://doi.org/10.3389/fnana.2014.00093>
- Straathof, M., Otte, W.M., Dijkhuizen, R.M., 2020a. Structure-function tipping points in rat brain. *Open Sci. Framework.*
- Straathof, M., Sinke, M.R., Dijkhuizen, R.M., Otte, W.M., on behalf of the TACTICS consortium, 2019a. A systematic review on the quantitative relationship between structural and functional network connectivity strength in mammalian brains. *J. Cereb. Blood Flow Metab.* 39, 189–209. <https://doi.org/10.1177/0271678X18809547>
- Straathof, M., Sinke, M.R.T., Roelofs, T.J.M., Blezer, E.L.A., Sarabdjitsingh, R.A., van der Toorn, A., Schmitt, O., Otte, W.M., Dijkhuizen, R.M., 2020b. Distinct structure-function relationships across cortical regions and connectivity scales in the rat brain. *Sci. Rep.* 10, 56. <https://doi.org/10.1038/s41598-019-56834-9>
- Straathof, M., Sinke, M.R.T., van der Toorn, A., Weerheim, P.L., Otte, W.M., Dijkhuizen, R.M., 2019b. Differences in structural and functional networks between young adult and aged rat brains before and after stroke lesion simulations. *Neurobiol. Dis.* 126, 23–35. <https://doi.org/10.1016/j.nbd.2018.08.003>
- Suárez, L.E., Markello, R.D., Betzel, R.F., Misisic, B., 2020. Linking Structure and Function in Macroscale Brain Networks. *Trends Cogn. Sci.* xx, 1–14. <https://doi.org/10.1016/j.tics.2020.01.008>
- Tournier, J.D., Calamante, F., Connelly, A., 2012. MRtrix: Diffusion tractography in crossing fiber regions. *Int. J. Imaging Syst. Technol.* 22, 53–66. <https://doi.org/10.1002/ima.22005>
- Tournier, J.D., Calamante, F., Connelly, A., 2010. Improved probabilistic streamlines tractography by 2nd order integration over fibre orientation distributions. *Proc. Int. Soc. Magn. Reson. Med.* 1670.
- Uhrig, L., Sitt, J.D., Jacob, A., Tasserie, J., Bartfeld, P., Dupont, M., Dehaene, S., Jarraya, B., 2018. Resting-state Dynamics as a Cortical Signature of Anesthesia in Monkeys. *Anesthesiology* 129, 942–958. <https://doi.org/10.1097/ALN.0000000000002336>
- van den Heuvel, M.P., Bullmore, E.T., Sporns, O., 2016a. Comparative Connectomics. *Trends Cogn. Sci.* 20, 345–361. <https://doi.org/10.1016/j.tics.2016.03.001>
- van den Heuvel, M.P., Mandl, R.C.W., Kahn, R.S., Hulshoff Pol, H.E., 2009. Functionally Linked Resting-State Networks Reflect the Underlying Structural Connectivity Architecture of the Human Brain. *Hum. Brain Mapp.* 30, 3127–3141. <https://doi.org/10.1002/hbm.20737>
- van den Heuvel, M.P., Scholtens, L.H., de Reus, M.A., 2016b. Topological organization of connectivity strength in the rat connectome. *Brain Struct. Funct.* 221, 1719–1736. <https://doi.org/10.1007/s00429-015-0999-6>
- van den Heuvel, M.P., Sporns, O., 2019. A cross-disorder connectome landscape of brain dysconnectivity. *Nat. Rev. Neurosci.* 20, 435–446. <https://doi.org/10.1038/s41583-019-0177-6>
- Vázquez-Rodríguez, B., Suárez, L.E., Markello, R.D., Shafiei, G., Paquola, C., Hagmann, P., van den Heuvel, M.P., Bernhardt, B.C., Spreng, R.N., Misisic, B., 2019. Gradients of structure – function tethering across neocortex. *Proc. Natl. Acad. Sci. U. S. A.* 116, 21219–21227. <https://doi.org/10.1073/pnas.1903403116>
- Wang, L., Su, L., Shen, H., Hu, D., 2012. Decoding lifespan changes of the human brain using resting-state functional connectivity MRI. *PLoS One* 7, e44530. <https://doi.org/10.1371/journal.pone.0044530>
- Wood, S.N., 2017. *Generalized Additive Models: An Introduction with R*, 2nd ed. Chapman & Hall / CRC Texts in Statistical Science.
- Yin, D., Zhang, Z., Wang, Zhiwei, Zeljic, K., Lv, Q., Cai, D., Wang, Y., Wang, Zheng, 2019. Brain map of intrinsic functional flexibility in anesthetized monkeys and awake humans. *Front. Neurosci.* 13, 174. <https://doi.org/10.3389/fnins.2019.00174>
- Ypma, R.J.F., Bullmore, E.T., 2016. Statistical Analysis of Tract-Tracing Experiments Demonstrates a Dense, Complex Cortical Network in the Mouse. *PLoS Comput. Biol.* 12, 1–22. <https://doi.org/10.1371/journal.pcbi.1005104>
- Zimmermann, J., Ritter, P., Shen, K., Rothmeier, S., Schirner, M., McIntosh, A.R., 2016. Structural architecture supports functional organization in the human aging brain at a regionwise and network Level. *Hum. Brain Mapp.* 37, 2645–2661.

Supplementary materials



Supplementary Figure S1: Group independent component analyses for rat resting-state fMRI dataset. Six different functional connectivity strength components are overlaid on a mean resting-state fMRI image. Color-coding reflects Z-scores. Rat brain images are shown in coronal view with y-slice numbers (left side), axial view with z-slice numbers (middle) and in sagittal view with corresponding x-slice numbers (right side).



Structural and functional MRI of altered brain development in a novel adolescent rat model of quinpirole-induced compulsive checking behavior

Milou Straathof¹, Erwin L.A. Blezer¹, Caroline van Heijningen¹, Christel E. Smeele¹, Annette van der Toorn¹, TACTICS Consortium², Jan K. Buitelaar^{3,4}, Jeffrey C. Glennon³, Willem M. Otte^{1,5}, Rick M. Dijkhuizen¹

¹ *Biomedical MR Imaging and Spectroscopy Group, Center for Image Sciences, University Medical Center Utrecht and Utrecht University, the Netherlands.*

² *Members of the TACTICS consortium are listed in the Acknowledgments.*

³ *Department of Cognitive Neuroscience, Donders Institute for Brain, Cognition and Behavior, Radboud University Medical Center, Nijmegen, the Netherlands.*

⁴ *Karakter Child and Adolescent Psychiatry University Center, Nijmegen, the Netherlands.*

⁵ *Department of Pediatric Neurology, UMC Utrecht Brain Center, University Medical Center Utrecht and Utrecht University, the Netherlands.*

European Neuropsychopharmacology 2020; 33, 58-70.

Supplementary material is available at European Neuropsychopharmacology online.

Abstract

Obsessive-compulsive disorder (OCD) is increasingly considered to be a neurodevelopmental disorder. However, despite insights in neural substrates of OCD in adults, less is known about mechanisms underlying compulsivity during brain development in children and adolescents. Therefore, we developed an adolescent rat model of compulsive checking behavior and investigated developmental changes in structural and functional measures in the frontostriatal circuitry. Five-weeks old Sprague Dawley rats were subcutaneously injected with quinpirole (n=21) or saline (n=20) twice a week for five weeks. Each injection was followed by placement in the middle of an open field table, and compulsive behavior was quantified as repeated checking behavior. Anatomical, resting-state functional and diffusion MRI at 4.7T were conducted before the first and after the last quinpirole/saline injection to measure regional volumes, functional connectivity, and structural integrity in the brain, respectively. After consecutive quinpirole injections, adolescent rats demonstrated clear checking behavior and repeated travelling between two open-field zones. MRI measurements revealed an increase of regional volumes within the frontostriatal circuits and an increase in fractional anisotropy (FA) in white matter areas during maturation in both experimental groups. Quinpirole-injected rats showed a larger developmental increase in FA values in the internal capsule and forceps minor compared to control rats. Our study points toward a link between development of compulsive behavior and altered white matter maturation in quinpirole-injected adolescent rats, in line with observations in pediatric patients with compulsive phenotypes. This novel animal model provides opportunities to investigate novel treatments and underlying mechanisms for patients with early-onset OCD specifically.

Introduction

Obsessive-compulsive disorder (OCD) is a mental illness in which people have recurrent thoughts, impulses or images that inflict anxiety, distress, and repetitive behaviors. OCD has been recognized as a relatively common psychiatric disorder with a lifetime prevalence of 1-3% in the general population (Kessler et al., 2005; Veale and Roberts, 2014). Although the key symptoms are obsessions and compulsions, people suffering from OCD may experience substantial variation in the severity of symptoms, the time of onset and the effect of treatment (Butwicka and Gmitrowicz, 2010; Eisen et al., 2013; Leckman et al., 2010; Lochner and Stein, 2013). These variations in OCD manifestations suggest that there are multiple mechanisms that could underlie the development of this disorder. Nevertheless, in recent years a consistent picture has emerged that shows that OCD is associated with structural and functional changes in brain areas that form the frontostriatal circuitry. Neuroimaging modalities, including positron emission tomography, single-photon emission computed tomography and MRI, have been used to characterize these changes (Frydman et al., 2016; Koch et al., 2014; Piras et al., 2015). Although results are variable, studies in adults with OCD point to a decreased grey matter volume in frontal cortical regions such as the orbitofrontal, parietal and anterior cingulate cortex, and increased volume in subcortical structures such as the putamen, thalamus and caudate nucleus (Boedhoe et al., 2018; Piras et al., 2015; Radua and Mataix-Cols, 2009). Structural changes in main white matter tracts have also been reported in adults with OCD. Decreased fractional anisotropy (FA) values, potentially reflective of reduced white matter integrity, have been measured in several white matter tracts, of which the cingulate bundle, corpus callosum and internal capsule appear to be most commonly affected (Koch et al., 2014).

The OCD phenotype may not only be related to the above-mentioned changes in brain structures, but also to changes in neural network activation patterns. Functional imaging techniques have revealed abnormal activity in specific regions of the frontostriatal circuitry (Del Casale et al., 2011). Symptom provocation-induced hyper- and hypo-activity have been detected in the orbitofrontal cortex, the caudate nucleus, and the thalamus in adults and adolescents (Adler et al., 2000; Gilbert et al., 2009). Studies using resting-state functional MRI (rs-fMRI) have shown that functional connectivity between specific areas of the frontostriatal circuitry may be increased or decreased in people with OCD (Calzà et al., 2019; Posner et al., 2014; Sakai et al., 2011).

Despite increasing insights in neural substrates of OCD in adults, less is known about potential underlying mechanisms during brain development in children and adolescents. The first appearance of clinical symptoms divides the OCD population into two groups, i.e., early, and late onset OCD patients that experience their first clinical symptoms before or after adulthood, respectively. The early onset group is the most prevalent since approximately three quarters of patients experience their first symptoms at a young age (Taylor, 2011). OCD may therefore be considered a neurodevelopmental disorder for the majority of affected persons.

In recent years a variety of translational animal models has been developed to study the pathophysiology of OCD and to test the effects of novel molecules (Albelda and Joel, 2012a, 2012b; Alonso et al., 2015). A frequently applied and well-defined model involves repeated injections of the dopamine D2/D3 receptor agonist quinpirole in adult rats (Szechtman et al., 1998). This results in sensitization of the D2/D3 receptor and compulsive checking behavior, a specific symptom of OCD. We set out to adapt this model to study the development of compulsive behavior during brain maturation in rats from juvenile to adolescent stages, with the specific goal to identify abnormal developmental changes in structural and functional aspects of the frontostriatal circuitry. To this aim, we applied serial structural and functional MRI of the brain, in combination with behavioral testing of compulsivity.

Experimental procedures

Animal model

All animal procedures were approved by the local Committee for Animal Experiments of the University Medical Center Utrecht, The Netherlands (DEC: 2014.I.12.104) and were performed in accordance with the guidelines of the European Communities council directive (EU Directive 2010/63/EU). All efforts were made to reduce animal suffering.

To study compulsive behavior in adolescent rats, we modified an established rat model for compulsive checking behavior. Forty-one juvenile Sprague Dawley rats (Harlan, Zeist) were housed individually and habituated to environmental conditions (temperature 22-24° and 12 h light/dark cycle with lights on at 7:00 AM) for at least seven days prior to the experiment with access to food and water ad libitum. From the age of five weeks (body weight: 104 ± 24 g (mean \pm standard deviation (SD))), we subcutaneously injected rats with

quinpirole (Tocris, UK; 0.5 mg/kg; n=21; Quinpirole group) or saline (n=20; Control group), twice a week for five weeks (a total of 10 injections). We randomly assigned the treatment (quinpirole or saline), but experimenters could not be blinded, due to the obvious behavioral effects of quinpirole treatment. Each injection was followed by placement of the rat in the middle of a large open field table for 30 minutes. On the open field table (160×160 cm², 60 cm above the floor), four objects (two black, two white; 8×8×8 cm³) were placed on fixed locations: two near the middle and two near the corners of the open field. Each rat's activity on the open field table was recorded with a camera fixed to the ceiling.

Behavioral analysis

Ethovision software (Noldus Information Technology B.V., Netherlands) was used to automatically trace the trajectories of locomotion for the open field tests after the fifth and tenth quinpirole/saline injection. The open field area was virtually divided into 25 rectangles of 40×40 cm² of which the outer zones extended outside the open field. For all analyses, we used the last 15 minutes for the quinpirole-injected rats, and the complete 30 minutes for the control rats, similar to the original study by Szechtman and colleagues who used the last 30 of 60 minutes for quinpirole-injected rats and the full 60 minutes for control rats (Szechtman et al., 1998). We calculated the frequency of visits for each zone during this observation period and defined the home-base as the most frequently visited zone.

Locomotor behavior

Compulsive checking behavior parameters were characterized relative to the home-base, and included frequency of checking (the total number of visits at the home-base), length of checks (the average time of a visit at the home-base), recurrence time of checking (the average time spent at other areas before returning to the home-base) and stops before returning to the home-base (the average number of areas an animal visited before returning to the home-base) (Szechtman et al., 1998; Tucci et al., 2014a). In addition, we determined the predictability of the visited zones as the Lempel-Ziv source entropy (Song et al., 2010) using a maximal substring of three zones and only including animals that visited at least nine different zones. The higher the source entropy, the less predictable the locomotion. Besides the compulsive behavior, we calculated hyperactivity measures, including the total travelled distance, average velocity of movement and immobility time (<0.01 cm movement per video frame).

Behavior during stops

We manually quantified stereotypic behaviors the rats showed during a stop at their own home-base (Szechtman et al., 1998). Like in the adult model, only the first 20 visits during the observation period were scored. However, because control rats were less active, all their visits were scored if required. First, for each visit we scored the entering or leaving direction to and from the home-base, to determine a potential directional preference. Directions were determined using a compass divided into eight different directions (per 45 degrees). Second, we counted the number of clockwise and anti-clockwise turns as horizontal movements per visit and the number of head dips as vertical movements. Third, we scored the interaction of the rat with the object by counting the number of sniffs and placement of the forelegs at the object per visit. Fourth, we determined the grooming time per visit. These individual behavioral scores were combined into a total number of behavioral acts per visit.

Experimental MRI protocol

MRI experiments were done before the first and after the tenth injection of quinpirole or saline. MRI experiments were executed on a 4.7T horizontal bore magnet (Varian, Palo Alto, USA) with a homebuilt Helmholtz volume coil for radiofrequency transmission and an inductively coupled surface coil for signal detection.

Animals were anesthetized with isoflurane anesthesia (4% for induction and 2% for maintenance) in a mixture of O₂ and air (30/70%). Subsequently, the animals were prepared for mechanical ventilation by endotracheal intubation. Animals were immobilized in a specially designed stereotactic holder and cradle to minimize movement during the MRI experiment. During MRI, end-tidal CO₂ was continuously monitored, and body temperature was maintained at 37.0 ± 1.0 °C. An infrared sensor (Nonin Medical Inc., Plymouth, MN, USA) was attached to the hind paw to monitor the heart rate and blood oxygen saturation.

Anatomical MRI: For volumetric analyses and registration, we performed a 3D balanced steady-state free precession scan. Repetition time (TR) = 5 ms; echo time (TE) = 2.5 ms; flip angle 20°; three averages; four pulse angle shifts; field-of-view (FOV) = 40×32×24 mm³; acquisition matrix = 160×128×96 points; resolution = 250 μm isotropic. Total acquisition time was ten minutes. Isoflurane anesthesia level was reduced to 1.5% at the start of the anatomical MRI acquisition, to lower the anesthetic depth for the following resting-state fMRI acquisition.

Resting-state functional MRI: For functional connectivity analyses, we acquired T2*-weighted blood oxygenation level-dependent images using a single shot multi-slice 2D

gradient echo-echo planar imaging (EPI) sequence under 1.5% isoflurane anesthesia. TR = 700 ms; TE = 20 ms; FOV = 32×27.2 mm²; acquisition matrix = 40×34 points; slice thickness = 0.80 mm, 17 slices, isotropic resolution of 800 μm, 850 images. The acquisition time was ten minutes. Resting-state fMRI acquisition was always started at 90 minutes after quinpirole injection, to standardize the effects of quinpirole across animals.

Diffusion MRI: For structural connectivity analyses we acquired multi-slice diffusion-weighted spin-echo images using four-shot EPI encoding. Diffusion MRI acquisition was performed under 2.0% of isoflurane anesthesia to minimize animal motion. Acquisition parameters were as follows: TR = 3000 ms; TE = 26.2 ms; FOV = 32×32 mm²; acquisition matrix = 64×128 points; in plane resolution = 500×250 μm², slice thickness = 500 μm; 25 slices; δ/Δ = 10.84/4 ms; b-value = 1,335 s/mm²; 60 directions. The acquisition time was 65 minutes.

Data analyses MRI

Regions-of-interest

For the structural connectivity analyses, several white matter tracts, known to be affected in adults and children with OCD, were used as regions-of-interest (Figure 1A): the external capsule (only the lateral part relative to the cingulum, 2.92 to 1.56 mm from bregma), the internal capsule (2.92 to -1.08 mm from bregma), the forceps minor of the corpus callosum (2.52 to 2.76 mm from bregma), the genu of the corpus callosum (1.80 to 2.28 mm from bregma) and the central part of the corpus callosum (defined as areas posterior to the genu of the corpus callosum (1.80 mm from bregma) and anterior to the dorsal part of the third ventricle (-0.60 mm from bregma, whereby only areas medial to the cingulum were included)).

Regions of interest for the functional connectivity and volumetric analyses were taken from a 3D rendering of the Paxinos and Watson atlas (G. Paxinos and Watson, 2005). The 3D atlas rendering, with the region specifications and the corresponding MRI images, are available online (https://github.com/wmotte/rat_brain_atlas). We selected regions within the frontostriatal circuitry: the caudate putamen (CPu), nucleus accumbens (NAcc: accumbens nucleus shell, accumbens nucleus core and lateral accumbens shell), anterior cingulate cortex (ACC: cingulate cortex areas 1 and 2), medial prefrontal cortex (mPFC: prelimbic and infralimbic cortex) and orbitofrontal cortex (OFC: dorsolateral, lateral, medial, and ventral orbital cortex) (Figure 1B).

Diffusion MRI

The diffusion-weighted images were brain-extracted with BET and motion- and eddy current-corrected with mutual information-based affine transformations of all images to the baseline image (Mangin et al., 2002). The diffusion tensor, the corresponding eigensystem, and the subsequently derived fractional anisotropy (FA) was computed for each voxel within the brain mask (Basser and Pierpaoli, 1996). Mean FA values, reflecting the degree of anisotropy (degree of restricted diffusion along the main directions of the diffusion tensor), were calculated for all white matter tracts of interest at each time point as a measure of structural connectivity (Koay et al., 2006).

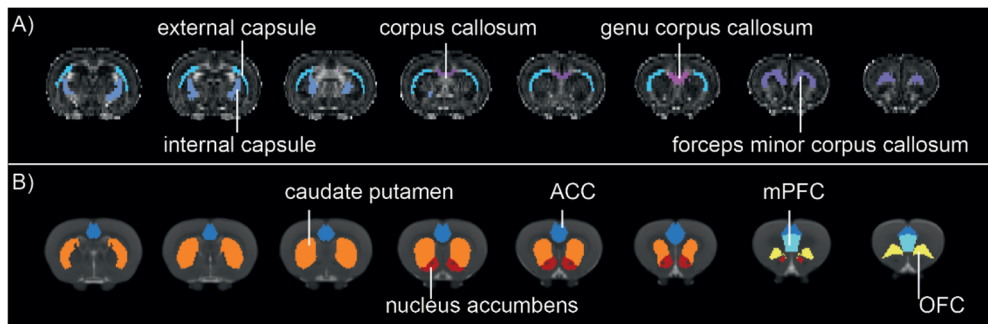


Figure 1. Grey and white matter regions-of-interest. Regions-of-interest for the structural connectivity analyses projected on a fractional anisotropy (FA) map (A), and for the volumetric and functional connectivity analyses, projected on an anatomical image (B). For the functional connectivity analyses, frontal and striatal areas were combined into two regions-of-interest: the frontal cortex (consisting of the anterior cingulate, medial prefrontal and orbitofrontal cortex) and striatum (consisting of the nucleus accumbens and caudate putamen). ACC: anterior cingulate cortex; mPFC: medial prefrontal cortex; OFC: orbitofrontal cortex.

Resting-state functional MRI

Preprocessing steps of the resting-state fMRI scans included removal of the first 20 images to reach a steady state; motion-correction with MCFLIRT (Jenkinson et al., 2002); and brain-extraction with BET (Smith, 2002). Motion-correction parameters were used as regressor for the resting-state signal, and low-frequency blood oxygenation level-dependent fluctuations were obtained by applying temporal filtering between 0.01 and 0.1 Hz in AFNI (Cox, 1996). To verify the ability to measure specific functional connectivity under our experimental conditions, we evaluated the functional connectivity of the left anterior cingulate cortex from seed-based analyses. We calculated Fisher's Z-transformed correlation coefficients for inter- and intrahemispheric functional connectivity between regions-of-interest. To preserve sufficient signal-to-noise ratio for these analyses, we combined the orbitofrontal, anterior cingulate and medial prefrontal cortex into one frontal cortical region-of-interest, and the

nucleus accumbens and caudate putamen into a striatal region. In addition, we performed functional connectivity analyses for the individual sub-regions of interest. The nucleus accumbens was excluded from this sub-region analysis, as the volume of this region in young rats was considered too small for reliable measurements.

Volumetric MRI

For the volumetric analyses of the regions of interest in the frontostriatal circuitry, we determined their volume in individual anatomical MRI space. For total grey matter and white matter volumes, we determined the volume in individual diffusion MRI space. The total cerebral white matter and grey matter volumes were calculated between the cerebellum and the olfactory bulb. For segmentation of the white matter, we used a minimum FA threshold of 0.25, and for segmentation of the grey matter we used a maximum FA threshold of 0.25, and a mean diffusivity below 0.001. Total volumes were calculated by multiplying the number of voxels with the volume of a voxel in either anatomical or diffusion MRI space.

Matching individual data with atlas coordinates

Individual anatomical images were non-linearly registered with the atlas rendering using FNIRT software (Jenkinson et al., 2012). Individual resting-state fMRI and diffusion MRI images were linearly registered to the individual anatomical image using FLIRT software (Jenkinson and Smith, 2001), followed by the non-linear registration from the individual anatomical space to the atlas as described above. Regions-of-interest were transformed to individual anatomical, functional and diffusion MRI space by taking the inverse of these registrations. The regions for the functional connectivity analyses were masked with a temporal signal-to-noise ratio mask of 10, and the regions for the structural connectivity analyses were masked with a white matter mask (FA higher than 0.25 (Giannelli et al., 2010)).

Statistical analyses

Statistical analyses were performed in R (3.2.3) and R-studio 0.99 (R Core Team, 2014). Differences in behavioral metrics (compulsive checking behavior, hyperactivity measures and behavior during stops) between control and quinpirole-injected rats after the fifth and tenth quinpirole/saline injection were analyzed with a Mann-Whitney U test.

We performed a mixed design ANOVA for all MRI parameters (regional brain volume, functional connectivity, and structural connectivity) separately to assess brain development, with the factor *time* as within-subject variable, and treatment effect, with the factor *group* (Control or Quinpirole) as between-subject variable, followed by post-hoc

paired Wilcoxon signed rank tests. In addition, we determined whether MRI parameters significantly differed between control and quinpirole-injected rats after the tenth quinpirole/saline injection with Mann-Whitney U tests.

For all MRI-based measures we assessed possible correlation with compulsive behavior measures after the tenth quinpirole/saline injection in the quinpirole and control group separately, using linear regression. All analyses were corrected for multiple testing using the false-discovery rate correction (Benjamini and Hochberg, 1995). Results with a corrected $p < 0.05$ were considered statistically significant.

Results

MRI acquisitions of two control and two quinpirole-injected rats were not complete, and behavioral data recording failed for two control rats and one quinpirole-injected rat. Therefore, final groups consisted of 18 quinpirole-injected and 16 control rats.

Locomotor, compulsive, and grooming behavior

Figure 2 shows a representative locomotor trajectory of one quinpirole-injected and one control rat after the tenth quinpirole/saline injection and the compulsive checking behavioral metrics that were calculated from the motor trajectories after the fifth and tenth quinpirole/saline injection. Compared to control rats, quinpirole-injected rats travelled more repeatedly between two zones of the open field (Figure 2A and 2B). Both after the fifth and after the tenth quinpirole/saline injection, quinpirole-injected rats showed a higher frequency of checks (fifth injection: Control: 12.7 ± 6.6 (mean \pm standard deviation (SD)); Quinpirole: 24.1 ± 12.3 ; $p=0.003$; tenth injection: Control: 15.9 ± 9.4 ; Quinpirole: 51.6 ± 33.6 ; $p=0.0004$), lower recurrence time of checking (fifth injection: Control: 122.4 ± 83.7 s; Quinpirole: 33.6 ± 29.0 s; $p=0.0003$; tenth injection: Control: 115.5 ± 69.2 s; Quinpirole: 18.9 ± 10.8 s; $p < 0.0001$) and lower number of stops before returning to the home-base (fifth injection: Control: 10.1 ± 3.4 ; Quinpirole: 5.8 ± 2.0 ; $p < 0.0001$; tenth injection: Control: 10.6 ± 3.4 ; Quinpirole: 6.9 ± 1.7 ; $p=0.0004$) than control rats (Figure 2C). The average length of a visit at the home-base was not statistically significantly different between quinpirole-injected and control rats after the fifth (Control: 71.8 ± 91.1 s; Quinpirole: 25.7 ± 65.5 s; $p=0.10$) and tenth quinpirole/saline injection (Control: 42.6 ± 84.4 ; Quinpirole: 6.3 ± 10.4 ; $p=0.08$) (Figure 2C).

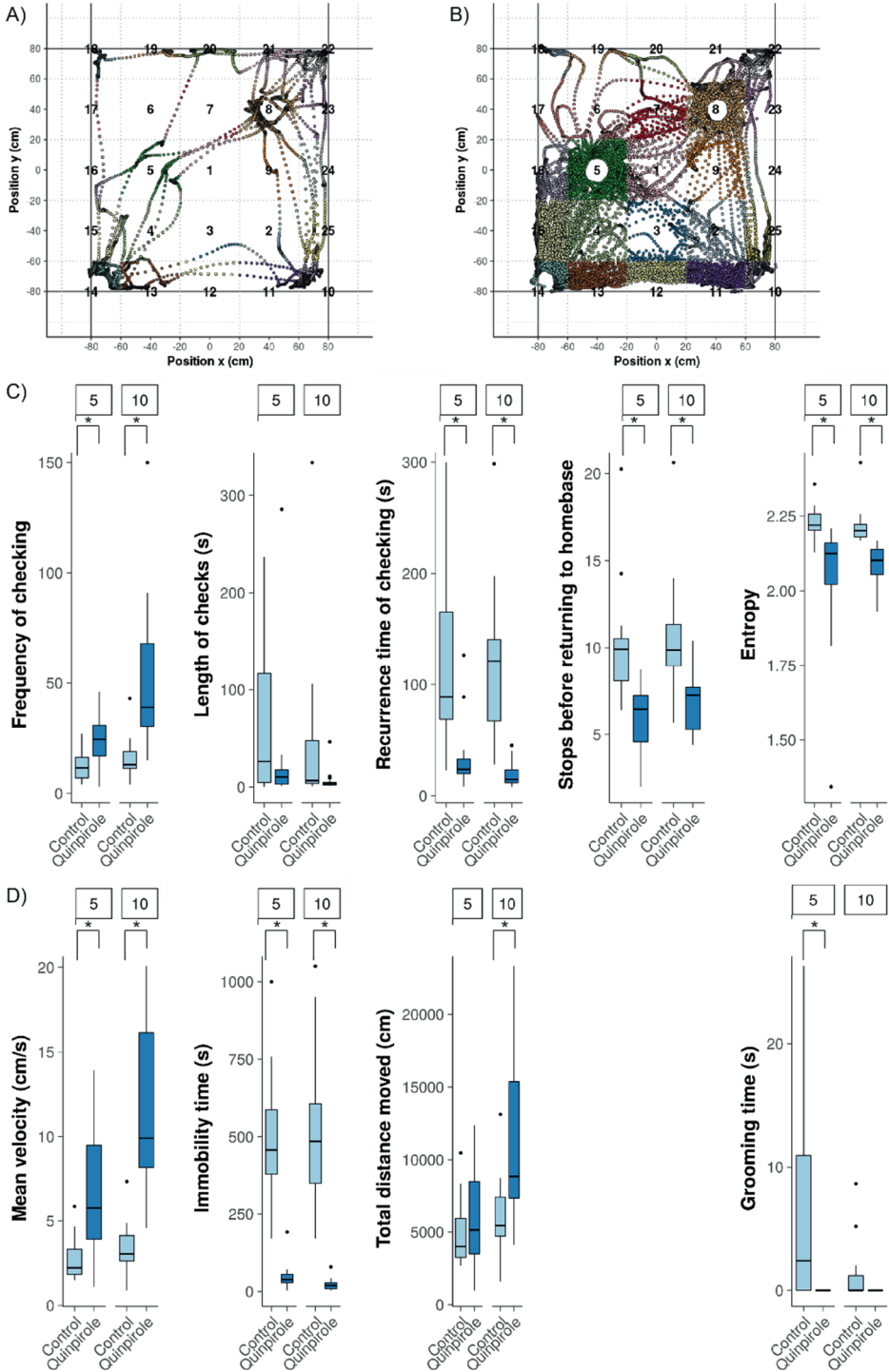


Figure 2: Locomotor trajectories and compulsive and hyperactive behavioral metrics for control and quinpirole-injected adolescent rats during the open field test. Locomotor trajectory of a control (A) and a quinpirole-injected adolescent rat (B). The different zones of the open field are numbered, and the locomotor trajectories are colored corresponding to these zones. We characterized behavior during the open field test for the last 15 minutes for quinpirole-injected rats and the full 30 minutes for control rats. Boxplots of compulsive behavior, including the frequency of checking (total number of visits at the home-base during observation), length of checks (average time (s) spent at the home-base), recurrence time of checking (average time (s) before returning to the home-base), stops before returning to the home-base (average number of zones visited in between two visits at the home-base) and entropy (predictability of the visited zones) for control and quinpirole-injected rats after the fifth and tenth injection of quinpirole/saline (C). Boxplots of hyperactive behavior, including the mean velocity, immobility time (<0.01 cm movement per video frame) and the total distance moved for control and quinpirole-injected rats after the fifth and tenth injection of quinpirole/saline (D). Grooming time (average time (s) grooming per visit at the home-base) for control and quinpirole-injected rats after the fifth and tenth injection of quinpirole/saline (E). * Corrected $p < 0.01$. Error bars represent the interquartile range and dots represent outliers.

The entropy of the visited zones was lower in quinpirole-injected rats compared to control rats after both the fifth and tenth injection (fifth injection: Control: 2.2 ± 0.005 ; Quinpirole: 2.0 ± 0.2 ; $p=0.002$; tenth injection: Control: 2.2 ± 0.006 ; Quinpirole: 2.1 ± 0.007 ; $p < 0.0001$). This lower entropy in quinpirole-injected rats means that the order of visited zones is less random and shows a higher degree of predictability and repeatability.

Next to compulsive behavior, we characterized hyperactivity measures in control and quinpirole-injected rats after the fifth and tenth quinpirole/saline injection (Figure 2D). At both time-points, quinpirole-injected rats moved with a higher mean velocity (fifth injection: Control: 2.8 ± 1.3 cm/s; Quinpirole: 6.6 ± 3.6 cm/s; $p=0.0004$; tenth injection: Control: 3.3 ± 1.5 cm/s; Quinpirole: 11.7 ± 5.1 cm/s; $p=0.002$) and had a lower immobility time (fifth injection: Control: 495.4 ± 207.8 s; Quinpirole: 47.2 ± 41.4 s; $p < 0.0001$; tenth injection: Control: 519.1 ± 236.7 s; Quinpirole: 22.1 ± 18.0 s; $p < 0.0001$). After the tenth quinpirole/saline injection, the quinpirole-injected rats moved over a longer distance (Control: 5954 ± 2664 cm; Quinpirole: 11112 ± 5454 cm; $p=0.002$). The total distance moved was not significantly different between quinpirole-injected and control rats after the fifth quinpirole injection (Control: 4963 ± 2316 cm; Quinpirole: 5899 ± 3178 cm; $p=0.34$).

After the fifth injection, control rats groomed significantly more during a visit of the home-base than quinpirole-injected rats (Figure 2E; Control: 6.7 ± 8.7 s; Quinpirole: no detectable grooming; $p=0.004$). The average grooming time per visit was not significantly different between control and quinpirole-injected rats after the tenth injection, although quinpirole-injected rats did not groom at all (Control: 1.21 ± 2.40 s; $p=0.21$). All other behaviors we quantified during home-base visits were not statistically significantly different between quinpirole-injected and control rats at both time-points.

Structural integrity and functional connectivity

Figures 3A and 3B show the structural connectivity in the white matter tracts of interest and the functional connectivity within the frontostriatal system, respectively, before the first and after the tenth quinpirole/saline injection.

For the structural integrity analyses, the mixed design ANOVA demonstrated a significant main effect of time for all included white matter tracts ($p < 0.0001$). Correspondingly, the post-hoc analyses revealed an increased FA value in all white matter tracts of interest in the control and quinpirole group after the tenth quinpirole/saline injection ($p < 0.0001$; Figure 3A). In addition, the mixed design ANOVA showed a significant interaction effect of group and time for the internal capsule and the forceps minor, indicating that the change in FA over time in these white matter tracts was different between quinpirole-injected and control rats. The increase in FA over time in these two white matter areas was larger in quinpirole-injected rats than in control rats (internal capsule: Control: 0.041 ± 0.019 ; Quinpirole: 0.063 ± 0.019 ; $p = 0.007$; forceps minor: Control: 0.035 ± 0.016 ; Quinpirole: 0.053 ± 0.019 ; $p = 0.01$). After the tenth quinpirole/saline injection, we found trends towards higher FA values in quinpirole-injected vs. control rats in the internal capsule (Control: 0.45 ± 0.01 ; Quinpirole: 0.46 ± 0.01 ; $p = 0.06$), the forceps minor (Control: 0.44 ± 0.008 ; Quinpirole: 0.45 ± 0.01 ; $p = 0.14$) and the center of the corpus callosum (Control: 0.52 ± 0.03 ; Quinpirole: 0.53 ± 0.02 ; $p = 0.14$).

Seed-based analysis of functional connectivity of the left anterior cingulate cortex showed that our approach enabled measurement of specific and localized functional connectivity effects in quinpirole-injected and control rats (Supplementary Figure S1). The mixed design ANOVA, with the factor time as within-subject variable, and the factor group as between-subject variable, demonstrated a significant main effect of group, irrespective of time, for the interhemispheric connection between the two frontal cortices ($p = 0.01$). However, post-hoc analyses did not reveal statistically significant differences in interhemispheric frontal connectivity between quinpirole-injected and control rats after the tenth quinpirole/saline injection. In addition, we did not find any time or interaction effects, or differences between quinpirole-injected and control rats after the tenth quinpirole/saline injection. Functional connectivity analyses in individual sub-regions, also did not reveal significant differences between quinpirole-injected and control rats after the tenth quinpirole/saline injection (Supplementary Figure S2).

Regional brain volumes

The volumes of regions within the frontostriatal system and the total grey and white matter volumes were determined before the first and after the tenth quinpirole/saline injection (Figure 4). The mixed design ANOVA, with the within-subject factor time and between-subject factor group, demonstrated a significant time effect for all volumes of interest ($p < 0.0001$). Correspondingly, post-hoc analyses revealed that all the investigated cerebral volumes increased between the first (before the first injection) and the final measurement (after the tenth injection), in the saline- and quinpirole-injected groups ($p < 0.0001$; Figure 4). There was no significant interaction effect between time and group. In addition, after the tenth quinpirole/saline injection, there were no significant differences in regional volumes between quinpirole-injected and control rats.

Relationship between compulsive behavior and MRI measures

We checked for possible relationships between MRI-based parameters and compulsive behavior measures after the tenth quinpirole/saline injection in the control and quinpirole group. None of the regressions demonstrated a significant correlation.

Discussion

We conducted a multi-parametric MRI examination of the development of compulsive behavior in a novel adolescent rat model of quinpirole-induced compulsive checking behavior. After five weeks of consecutive quinpirole injections, adolescent rats demonstrated clear compulsive checking behavior, repeated travelling between two open-field zones and no grooming. Our MRI measurements revealed developmental increases in regional brain volumes and white matter integrity in control and quinpirole-injected rats. Quinpirole-injected rats showed a larger increase in FA values in the internal capsule and forceps minor as compared to control rats, and a trend towards higher integrity values in the internal capsule, forceps minor and central part of the corpus callosum after five weeks of quinpirole treatment as compared to saline treatment.

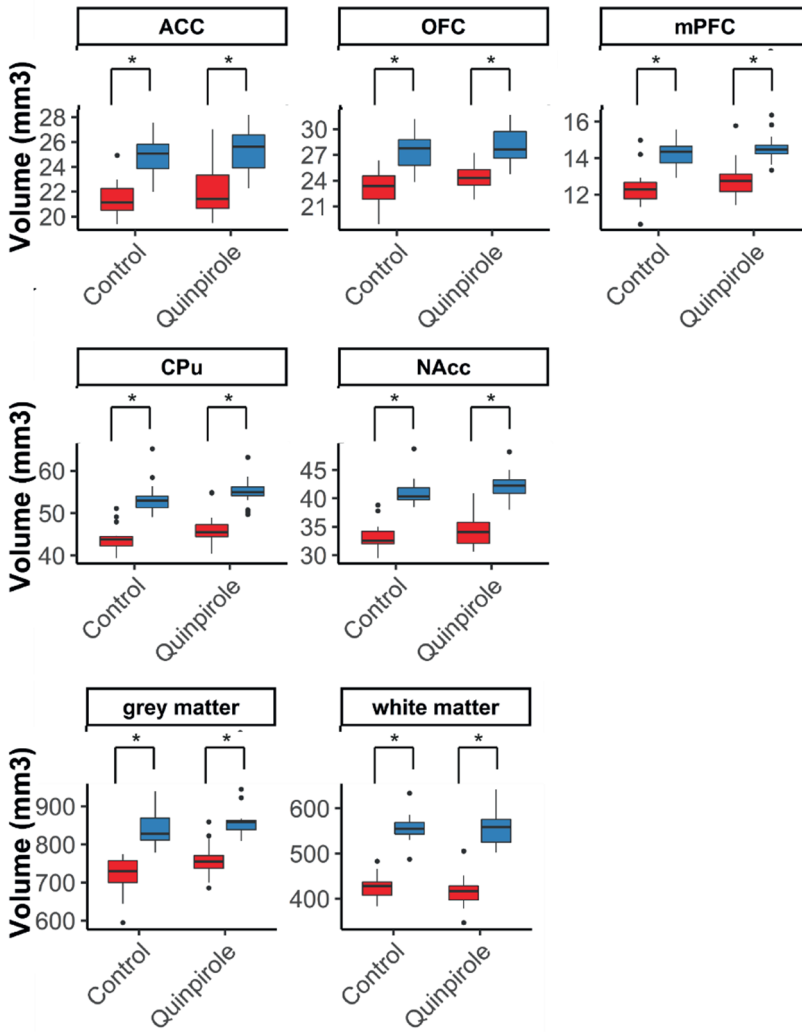


Figure 4: Regional brain volumes before and after repeated quinpirole/saline injections. Boxplots of the volumes (mm³) of regions-of-interest in the frontostriatal system, and the total white and grey matter volume for control and quinpirole-injected rats before the first (5-weeks old rats; red) and after the tenth injection (10-weeks old rats; blue) of quinpirole/saline. Error bars represent $1.5 \times$ interquartile range and dots represent outliers. ACC: anterior cingulate cortex; OFC: orbitofrontal cortex; mPFC: medial prefrontal cortex; CPu: caudate putamen; NAcc: nucleus accumbens. * Corrected $p < 0.01$.

Compulsive-like behavioral phenotype

While the model of quinpirole-induced compulsive checking in adult rats has shown good face validity to OCD (Stuchlik et al., 2016), compulsive behavior and OCD in humans generally develops during early adolescence (Boileau, 2011). Therefore, we have adapted the quinpirole-induced compulsive checking model in adult rats by starting quinpirole injections during early adolescence. Our study shows that quinpirole-injected adolescent rats meet three of four reported criteria for compulsive checking behavior after the fifth and tenth quinpirole/saline injection (Szechtman et al., 1998; Tucci et al., 2014a). By including the measurement after the fifth quinpirole/saline injection (8-9 weeks of age), we assured that the compulsive behavior developed during the adolescent phase and was established before adulthood. An additional feature that we observed in the quinpirole-injected adolescent rats was repeated traveling between two sides of the open field. This is also observable in adult rats with an OCD-like phenotype (Eilam, 2017). Next to these compulsive checking behaviors, we also characterized hyperactivity measures and specific behavioral acts the rats performed during a visit at the home-base. Quinpirole-injected adolescent rats travelled over a longer total distance and with higher velocity than control rats, corresponding to hyperactivity, which has also been observed in the adult model (Servaes et al., 2019). In addition, in contrast to control animals showing clear grooming behavior during a home-base visit, quinpirole-injected adolescent rats did not groom, similar to what has been observed in the adult rat model (Szechtman et al., 1998). However, other behavioral acts, such as interaction with objects or preferences for entering or leaving directions, that were significantly altered in the adult model, were not significantly different between quinpirole-injected and control adolescent rats.

The development of compulsive-like behavior after repeated quinpirole injections is believed to reflect modifications in the brain due to the sensitization to the dopamine D2-receptor agonist quinpirole (Tucci et al., 2014a), such as an increased D2 receptor density (Servaes et al., 2019). The reduced expression of compulsive checking behavior in the adolescent rat model may be explained by maturational differences in dopaminergic receptors in the striatum between day 40 (adolescence) and day 60 (adulthood) (Teicher et al., 1995), potentially resulting in reduced sensitivity to dopaminergic agonists in young rats (Bolanos et al., 1998; Ulloa et al., 2004). Nevertheless, we feel that the behavioral profile that we observed in response to repeated quinpirole injections during adolescence in rats effectively reflects a compulsive-like phenotype.

Structural and functional brain alterations

MRI-based measures of regional brain volume and white matter structural integrity revealed clear developmental changes in quinpirole-injected and control rats between pre- (early adolescence) and post-treatment (late adolescence/adulthood) time-points. The volumes of regions within the frontostriatal system, as well as the total grey and white matter volume, significantly increased during this developmental phase of adolescence. These findings are in line with previous research demonstrating that cortical and subcortical regions increase in volume up to at least two months of age in rats (Calabrese et al., 2013; Mengler et al., 2014), representing maturation of brain regions. White matter structural integrity also changed during this developmental period. We found increasing FA values in white matter tracts, between postnatal weeks five and ten. Previous studies also demonstrated an increase in FA values of white matter tracts during development in rats (Bockhorst et al., 2008; Calabrese and Johnson, 2013), which may continue during (early) adulthood (van Meer et al., 2012). Likewise, in humans, developmental increases in FA values of white matter tracts have been demonstrated to continue until the end of adolescence or the beginning of adulthood (Barnea-Goraly et al., 2005; Chen et al., 2016). These increasing FA values in white matter tracts during development may reflect ongoing myelination (Bockhorst et al., 2008). The increased FA values at postnatal week 10 may have resulted in more voxel inclusions and hence an apparent increase in white matter volume over time. Nevertheless, white matter volumes calculated from different MRI scans (not solely based on FA values) have been demonstrated to increase up until postnatal week 19 (Otte et al., 2015b). Therefore, we believe that the white matter volume increase during development, as observed in the current study, is not merely explained by increased FA values over time, but truly reflects an increase in white matter volume.

Regional brain volumes and functional connectivity within the frontostriatal system did not differ between quinpirole-injected and control rats after the tenth quinpirole/saline injection. In children with OCD, conflicting results have been reported regarding brain volume and functional connectivity changes. Increases or decreases, or even no differences, in the size of frontal cortical areas have been measured (Boedhoe et al., 2018; Christian et al., 2008; Lázaro et al., 2009). Furthermore, increased as well as decreased functional connectivity between frontostriatal regions has been reported (Bernstein et al., 2016; Fitzgerald et al., 2011b). These differences may be related to the heterogeneous nature of OCD but could also be due to methodological variation between studies. This underscores the need for

standardization of neuroimaging protocols and investigations in well-controlled experimental designs.

The developmental rise in FA in the internal capsule and forceps minor was larger in quinpirole-injected animals as compared to controls, suggesting differences in white matter maturation. As a result, we found a trend towards higher FA values in these white matter tracts and in the center of the corpus callosum in quinpirole-injected as compared to saline-injected rats after the five weeks treatment period. Elevated FA values in white matter tracts, including the corpus callosum and internal capsule, have also been observed in children and adolescents with OCD (Gruner et al., 2012; Zarei et al., 2011). The higher FA values in children with OCD are suggested to reflect premature myelination of white matter tracts (Zarei et al., 2011). In addition, FA values in the internal capsule have been shown to be positively correlated to symptom severity in children with OCD (Zarei et al., 2011). Together, these findings underline the involvement of white matter structural integrity disturbances in disease processes of OCD in children and adolescents.

The rat model of quinpirole-induced OCD-like behavior offers opportunities for standardized and well-controlled investigation of the neural underpinnings of compulsive checking behavior. Since approximately three quarters of patients experience their first symptoms at a young age (Taylor, 2011), the adolescent quinpirole rat model described in this study enables studying the neurodevelopmental processes underlying early-onset OCD specifically. For optimal translation, we used similar MR protocols as in human neuroimaging studies, including diffusion MRI and resting-state functional MRI. However, diffusion-based measures are proxies of the true neuroanatomical features, and the (sub)cellular processes underlying changes in FA remain largely unclear (Johansen-Berg and Behrens, 2013). In addition, in contrast to human neuroimaging studies, animals in our study were anesthetized during MRI acquisitions, which is known to influence functional connectivity measurements (Paasonen et al., 2018).

Despite the good face validity of the adult quinpirole-induced compulsivity model, its construct and predictive validity have not yet been extensively validated. The adolescent quinpirole-induced compulsive checking behavior model introduced in this study demonstrated face validity with regards to compulsive checking behavior and construct validity from disturbances in white matter integrity. However, despite clear behavioral effects, we did not find quinpirole-induced effects on resting-state functional connectivity. Quinpirole effects should still be present during the time of resting-state fMRI (90 minutes

after injection) as the half-life time of quinpirole in rat plasma is 9.5 hours (Whitaker and Lindstrom, 1987) and behavioral effects of quinpirole have been measured up to two hours after injection (Eilam et al., 1989). It may be that the use of anesthesia during our MRI acquisition has covered the effects of quinpirole on MRI-based measures of functional connectivity. Isoflurane anesthesia has been shown to affect the binding of agonistic PET tracers to the dopamine D2/D3 receptor (McCormick et al., 2011). Since quinpirole is a D2/D3 receptor agonist, the use of isoflurane anesthesia may have influenced the effects of quinpirole. Nonetheless, we expect a minimal contribution of this mechanism on the functional connectivity measurements in our study, since we administered quinpirole nine times without isoflurane anesthesia, and once at 40 minutes before the induction of isoflurane anesthesia. The clear behavioral effects in quinpirole-injected rats may be a direct result of the preceding quinpirole injection, rather than from a change in the macro-scale functional or structural brain connections. Since previous studies have shown abnormalities at the neurotransmitter and receptor level in the quinpirole model (Servaes et al., 2019, 2017), differences in structural and functional connectivity may be more subtle and at the micro-scale. Differences that are not detectable with macro-scale MRI-based measures. In addition, we cannot completely rule out that motion- and physiological-related noise may have obscured model-related changes in structural and functional connectivity. Future studies could investigate the predictive validity of the adolescent quinpirole model by assessing the effects of pharmacological treatments that are already used for children and adolescents with OCD. In addition, the adolescent quinpirole-induced compulsivity model provides unique opportunities to study potential novel therapeutic strategies and their working mechanisms for this subgroup of OCD patients specifically.

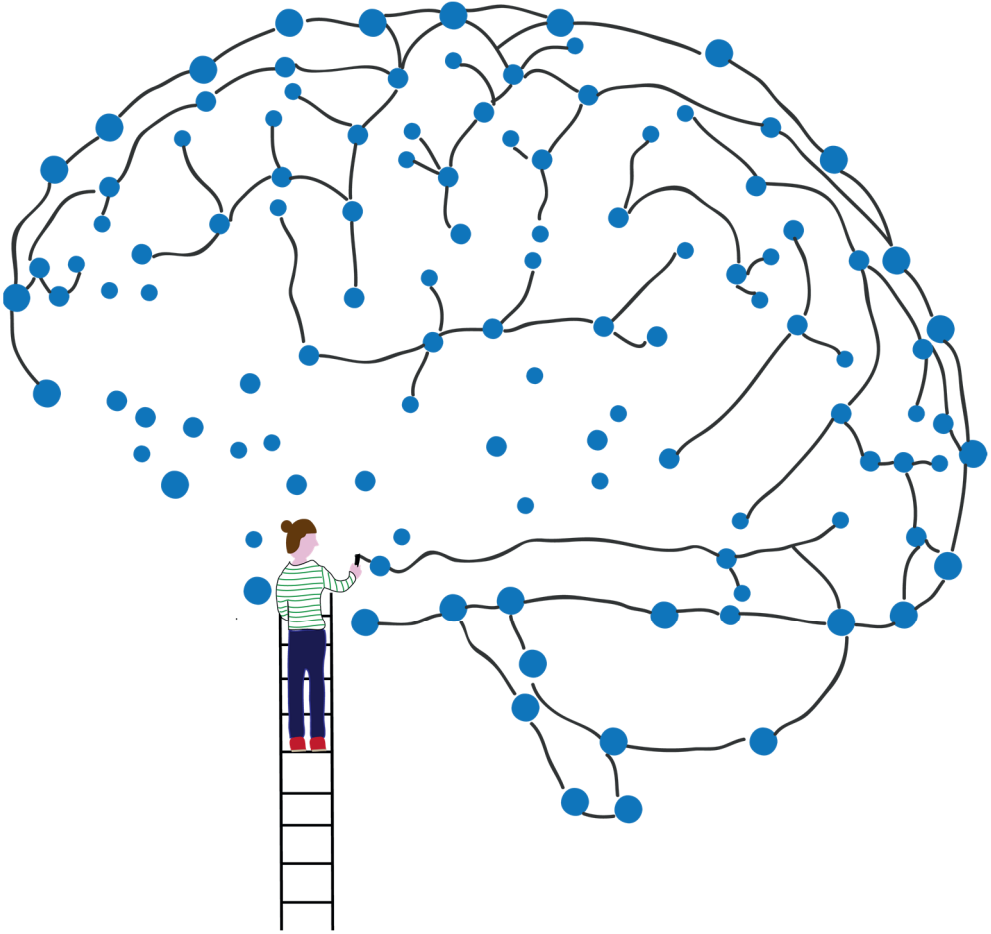
In conclusion, we found clear development of compulsive-like behavior and altered white matter maturation in a novel model of quinpirole-induced compulsivity in adolescent rats, which matched with reported substrates of early-onset OCD. Our study shows that MRI in animal models of specific symptoms of heterogeneous psychiatric disorders provides unique opportunities to assess the neurodevelopmental aspects and neurobiological substrates of these symptoms in a well-controlled experimental design.

References

- Adler, C.M., McDonough-Ryan, P., Sax, K.W., Holland, S.K., Arndt, S., Strakowski, S.M., 2000. fMRI of neuronal activation with symptom provocation in unmedicated patients with obsessive compulsive disorder. *J. Psychiatr. Res.* 34, 317–324. [https://doi.org/10.1016/S0022-3956\(00\)00022-4](https://doi.org/10.1016/S0022-3956(00)00022-4)
- Albelda, N., Joel, D., 2012a. Current animal models of obsessive compulsive disorder: an update. *Neuroscience* 211, 83–106. <https://doi.org/10.1016/j.neuroscience.2011.08.070>
- Albelda, N., Joel, D., 2012b. Animal models of obsessive-compulsive disorder: Exploring pharmacology and neural substrates. *Neurosci. Biobehav. Rev.* 36, 47–63. <https://doi.org/10.1016/j.neubiorev.2011.04.006>
- Alonso, P., López-Solà, C., Real, E., Segalàs, C., Menchón, J.M., 2015. Animal models of obsessive-compulsive disorder: utility and limitations. *Neuropsychiatr. Dis. Treat.* 11, 1939–1955. <https://doi.org/10.2147/NDT.S62785>
- Barnea-Goraly, N., Menon, V., Eckert, M., Tamm, L., Bammer, R., Karchemskiy, A., Dant, C.C., Reiss, A.L., 2005. White matter development during childhood and adolescence: A cross-sectional diffusion tensor imaging study. *Cereb. Cortex* 15, 1848–1854. <https://doi.org/10.1093/cercor/bhi062>
- Basser, P., Pierpaoli, C., 1996. Microstructural and physiological features of tissue elucidated by quantitative-diffusion tensor MRI. *J. Magn. Reson. Series B* 1, 209–219.
- Benjamini, Y., Hochberg, Y., 1995. Controlling the false discovery rate: A practical and powerful approach to multiple testing. *J. R. Stat. Soc. Ser. B* 57, 289–300.
- Bernstein, G.A., Mueller, B.A., Westlund Schreiner, M., Campbell, S.M., Regan, E.K., Nelson, P.M., Hour, A.K., Lee, S.S., Zagoloff, A.D., Lim, K.O., Yacoub, E.S., Cullen, K.R., 2016. Abnormal striatal resting-state functional connectivity in adolescents with obsessive-compulsive disorder. *Psychiatry Res. Neuroimaging* 247, 49–56. <https://doi.org/10.1016/j.psychres.2015.11.002>
- Bockhorst, K.H., Narayana, P.A., Liu, R., Ahobila-Vijjala, P., Ramu, J., Kamel, M., Wosik, J., Bockhorst, T., Hahn, K., Hasan, K.M., Perez-Polo, J.R., 2008. Early postnatal development of rat brain: In vivo diffusion tensor imaging. *J. Neurosci. Res.* 86, 1520–1528. <https://doi.org/10.1002/jnr.21607>
- Boedhoe, P.S.W., Schmaal, L., Abe, Y., Alonso, P., Ameis, S.H., Anticevic, A., Arnold, P.D., Batistuzzo, M.C., Benedetti, F., Beucke, J.C., Bollettini, I., Bose, A., Brem, S., Calvo, A., Calvo, R., Cheng, Y., Cho, K.I.K., Ciullo, V., Dallspezia, S., Denys, D., Feusner, J.D., Fitzgerald, K.D., Focher, J.-P., Fridgerisson, E.A., Gruner, G., Hanna, G.L., Hibar, D.P., Hoexter, M.Q., Hu, H., Huyser, C., Jahanshad, N., James, A., Kathmann, N., Kaufmann, C., Koch, K., Soo Kwon, J., Lazaro, L., Lochner, C., Marsh, R., Martinez-Zalacain, I., Mataix-Cols, D., Menchon, J.M., Minuzzi, L., Morer, A., Nakamae, T., Nakao, T., Narayanaswamy, J.C., Nishida, S., Nurmi, E., O'Neill, J., Piacentini, J., Piras, F., Piras, F., Janardhan Reddy, Y.C., Reess, T.J., Sakai, Y., Sato, J.R., Simpson, H.B., Soreni, N., Soriano-Mas, C., Spalletta, G., Stevens, M.C., Szeszo, P.R., Tolin, D.F., van Wingen, G.A., Venkatasubramanian, G., Walitza, S., Wang, Z., Yun, J.-Y., ENIGMA-OCD Working group, Thompson, P.M., Stein, D.J., van den Heuvel, O.A., 2018. Cortical abnormalities associated with pediatric and adult obsessive-compulsive disorder: Findings from the ENIGMA obsessive-compulsive disorder working group. *Am. J. Psychiatry* 175, 453–462. <https://doi.org/10.1176/appi.ajp.2017.17050485>
- Boileau, B., 2011. A review of obsessive-compulsive disorder in children and adolescents. *Dialogues Clin. Neurosci.* 13, 401–411.
- Bolanos, C.A., Glatt, S.J., Jackson, D., 1998. Subsensitivity to dopaminergic drugs in preadolescent rats: A behavioral and neurochemical analysis. *Dev. Brain Res.* 111, 25–33. [https://doi.org/10.1016/S0165-3806\(98\)00116-3](https://doi.org/10.1016/S0165-3806(98)00116-3)
- Butwick, A., Gmitrowicz, A., 2010. Symptom clusters in obsessive-compulsive disorder (OCD): influence of age and age of onset. *Eur. Child Adolesc. Psychiatry* 19, 365–370. <https://doi.org/10.1007/s00787-009-0055-2>
- Calabrese, E., Badea, A., Watson, C., Johnson, G.A., 2013. A quantitative magnetic resonance histology atlas of postnatal rat brain development with regional estimates of growth and variability. *Neuroimage* 71, 196–206. <https://doi.org/10.1016/j.neuroimage.2013.01.017>
- Calabrese, E., Johnson, G.A., 2013. Diffusion tensor magnetic resonance histology reveals microstructural changes in the developing rat brain. *Neuroimage* 79, 329–339. <https://doi.org/10.1016/j.neuroimage.2013.04.101>
- Calzà, J., Gürsel, D.A., Schmitz-Koep, B., Bremer, B., Reinholz, L., Berberich, G., Koch, K., 2019. Altered cortico-striatal functional connectivity during resting state in obsessive-compulsive disorder. *Front. Psychiatry* 10, 319. <https://doi.org/10.3389/fpsy.2019.00319>
- Chen, Z., Zhang, H., Yushkevich, P.A., Liu, M., Beaulieu, C., 2016. Maturation along white matter tracts in human brain using a diffusion tensor surface model tract-specific analysis. *Front. Neuroanat.* 10, 9. <https://doi.org/10.3389/fnana.2016.00009>
- Christian, C.J., Lencz, T., Robinson, D.G., Burdick, K.E., Ashtari, M., Malhotra, A.K., Betensky, J.D., Szeszo, P.R., 2008. Gray Matter Structural Alterations in Obsessive-Compulsive Disorder: Relationship to Neuropsychological Functions. *Psychiatry Res.* 164, 123–131. <https://doi.org/10.1016/j.psychres.2008.03.005>
- Cox, R.W., 1996. AFNI: Software for Analysis and Visualization of Functional Magnetic Resonance Neuroimages. *Comput.*

- Biomedical Res. 29, 162–173.
- Del Casale, A., Kotzalidis, G.D., Rapinesi, C., Serata, D., Ambrosi, E., Simonetti, A., Pompili, M., Ferracuti, S., Tatarelli, R., Girardi, P., 2011. Functional neuroimaging in obsessive-compulsive disorder. *Neuropsychobiology* 64, 61–85. <https://doi.org/10.1159/000325223>
- Eilam, D., 2017. From an animal model to human patients: An example of a translational study on obsessive compulsive disorder (OCD). *Neurosci. Biobehav. Rev.* 76, 67–76. <https://doi.org/10.1016/j.neubiorev.2016.12.034>
- Eilam, D., Golani, I., Szechtman, H., 1989. D2-agonist quinpirole induces perseveration of routes and hyperactivity but no perseveration of movements. *Brain Res.* 490, 255–267. [https://doi.org/10.1016/0006-8993\(89\)90243-6](https://doi.org/10.1016/0006-8993(89)90243-6)
- Eisen, J.L., Sibrava, N.J., Boisseau, C.L., Mancebo, M.C., Stout, R.L., Pinto, A., Rasmussen, S.A., 2013. Five-year course of obsessive-compulsive disorder: Predictors of remission and relapse. *J. Clin. Psychiatry* 74, 233–239. <https://doi.org/10.4088/JCP.12m07657>
- Fitzgerald, K.D., Welsh, R.C., Stern, E.R., Angstadt, M., Hanna, G.L., Abelson, J.L., Taylor, S.F., 2011. Developmental alterations of frontal-striatal-thalamic connectivity in obsessive compulsive disorder. *J. Am. Acad. Child Adolesc. Psychiatry* 50, 938–948. <https://doi.org/10.1016/j.jaac.2011.06.011>
- Frydman, I., de Salles Andrade, J.B., Vigne, P., Fontenelle, L.F., 2016. Can neuroimaging provide reliable biomarkers for obsessive-compulsive disorder? A narrative review. *Curr. Psychiatry Rep.* 18, 90. <https://doi.org/10.1007/s11920-016-0729-7>
- Giannelli, M., Cosottini, M., Michelassi, M.C., Lazzarotti, G., Belmonte, G., Bartolozzi, C., Lazzeri, M., 2010. Dependence of brain DTI maps of fractional anisotropy and mean diffusivity on the number of diffusion weighting directions. *J. Appl. Clin. Med. Phys.* 11, 176–190.
- Gilbert, A.R., Akkal, D., Almeida, J.R.C., Mataix-Cols, D., Kalas, C., Devlin, B., Birmaher, B., Phillips, M.L., 2009. Neural correlates of symptom dimensions in pediatric obsessive-compulsive disorder: A functional magnetic resonance imaging study. *J. Am. Acad. Child Adolesc. Psychiatry* 48, 936–944. <https://doi.org/10.1097/CHI.0b013e3181b2163c>
- Gruner, P., Vo, A., Ikuta, T., Mahon, K., Peters, B.D., Malhotra, A.K., Uluğ, A.M., Szeszo, P.R., 2012. White matter abnormalities in pediatric obsessive-compulsive disorder. *Neuropsychopharmacology* 37, 2730–2739. <https://doi.org/10.1038/npp.2012.138>
- Jenkinson, M., Bannister, P., Brady, M., Smith, S., 2002. Improved optimization for the robust and accurate linear registration and motion correction of brain images. *Neuroimage* 17, 825–841. <https://doi.org/10.1006/nimg.2002.1132>
- Jenkinson, M., Beckmann, C.F., Behrens, T.E.J., Woolrich, M.W., Smith, S.M., 2012. Fsl. *Neuroimage* 62, 782–790. <https://doi.org/10.1016/j.neuroimage.2011.09.015>
- Jenkinson, M., Smith, S., 2001. A global optimisation method for robust affine registration of brain images. *Med. Image Anal.* 5, 143–156. [https://doi.org/10.1016/S1361-8415\(01\)00036-6](https://doi.org/10.1016/S1361-8415(01)00036-6)
- Johansen-Berg, H., Behrens, T.E.J., 2013. *Diffusion MRI: From quantitative measurement to in-vivo neuroanatomy*, Second ed. ed. Elsevier/Academic Press.
- Kessler, R.C., Berglund, P., Demler, O., Jin, R., Merikangas, K.R., Walters, E.E., 2005. Lifetime prevalence and age-of-onset distributions of DSM-IV disorders in the national comorbidity survey replication. *Arch. Gen. Psychiatry* 62, 593–602.
- Koay, C.G., Chang, L., Carew, J.D., Pierpaoli, C., Basser, P.J., 2006. A unifying theoretical and algorithmic framework for least squares methods of estimation in diffusion tensor imaging. *J. Magn. Reson.* 182, 115–125. <https://doi.org/10.1016/j.jmr.2006.06.020>
- Koch, K., Reef, T.J., Rus, O.G., Zimmer, C., Zaudig, M., 2014. Diffusion tensor imaging (DTI) studies in patients with obsessive-compulsive disorder (OCD): A review. *J. Psychiatr. Res.* 54, 26–35. <https://doi.org/10.1016/j.jpsychires.2014.03.006>
- Lázaro, L., Bargalló, N., Castro-Fornieles, J., Falcón, C., Andrés, S., Calvo, R., Junqué, C., 2009. Brain changes in children and adolescents with obsessive-compulsive disorder before and after treatment: A voxel-based morphometric MRI study. *Psychiatry Res. - Neuroimaging* 172, 140–146. <https://doi.org/10.1016/j.psychresns.2008.12.007>
- Leckman, J.F., Denys, D., Simpson, H.B., Mataix-Cols, D., Hollander, E., Saxena, S., Miguel, E.C., Rauch, S.L., Goodman, W.K., Phillips, K.A., Stein, D.J., 2010. Obsessive-compulsive disorder: A review of the diagnostic criteria and possible subtypes for DSM-V. *Depress. Anxiety* 27, 507–527. <https://doi.org/10.1002/da.20669>
- Lochner, C., Stein, D.J., 2013. Heterogeneity of obsessive-compulsive disorder: a literature review. *Harv. Rev. Psychiatry* 11, 113–132. <https://doi.org/10.1080/10673220303949>
- Mangin, J.F., Poupon, C., Clark, C., Le Bihan, D., Bloch, I., 2002. Distortion correction and robust tensor estimation for MR diffusion imaging. *Med. Image Anal.* 6, 191–198. https://doi.org/10.1007/3-540-45468-3_23
- McCormick, P.N., Ginovart, N., Wilson, A.A., 2011. Isoflurane anaesthesia differentially affects the amphetamine sensitivity of agonist and antagonist D2/D3 positron emission tomography radiotracers: Implications for in vivo imaging of dopamine release. *Mol. Imaging Biol.* 13, 737–746. <https://doi.org/10.1007/s11307-010-0380-3>
- Mengler, L., Khmelinskii, A., Diedenhofen, M., Po, C., Staring, M., Lelieveldt, B.P.F., Hoehn, M., 2014. Brain maturation of the adolescent rat cortex and striatum: Changes in volume and myelination. *Neuroimage* 84, 35–44. <https://doi.org/10.1016/j.neuroimage.2013.08.034>
- Otte, W.M., van Meer, M.P.A., van der Marel, K., Zwartbol, R., Viergever, M.A., Braun, K.P.J., Dijkhuizen, R.M., 2015. Experimental

- focal neocortical epilepsy is associated with reduced white matter volume growth: results from multiparametric MRI analysis. *Brain Struct. Funct.* 220, 27–36. <https://doi.org/10.1007/s00429-013-0633-4>
- Paasonen, J., Stenroos, P., Salo, R.A., Kiviniemi, V., Gröhn, O., 2018. Functional connectivity under six anesthesia protocols and the awake condition in rat brain. *Neuroimage* 172, 9–20. <https://doi.org/10.1016/j.neuroimage.2018.01.014>
- Paxinos, G., Watson, W., 2005. The rat brain in stereotaxic coordinates 5th edition. Elsevier Academic Press, Amsterdam.
- Piras, Federica, Piras, Fabrizio, Chiapponi, C., Girardi, P., Caltagirone, C., Spalletta, G., 2015. Widespread structural brain changes in OCD: A systematic review of voxel-based morphometry studies. *Cortex* 62, 89–108. <https://doi.org/10.1016/j.cortex.2013.01.016>
- Posner, J., Marsh, R., Maia, T. V., Peterson, B.S., Gruber, A., Simpson, H.B., 2014. Reduced functional connectivity within the limbic cortico-striato-thalamo-cortical loop in unmedicated adults with obsessive-compulsive disorder. *Hum. Brain Mapp.* 35, 2852–2860. <https://doi.org/10.1002/hbm.22371>
- R Core Team, 2014. R: A language and environment for statistical computing.
- Radua, J., Mataix-Cols, D., 2009. Voxel-wise meta-analysis of grey matter changes in obsessive-compulsive disorder. *Br. J. Psychiatry* 195, 393–402. <https://doi.org/10.1192/bjp.bp.108.055046>
- Sakai, Y., Narumoto, J., Nishida, S., Nakamae, T., Yamada, K., Nishimura, T., Fukui, K., 2011. Corticostriatal functional connectivity in non-medicated patients with obsessive-compulsive disorder. *Eur. Psychiatry* 26, 463–469. <https://doi.org/10.1016/j.eurpsy.2010.09.005>
- Servaes, S., Glorie, D., Stroobants, S., Staelens, S., 2019. Neuroreceptor kinetics in rats repeatedly exposed to quinpirole as a model for OCD. *PLoS One* 14, e0213313. <https://doi.org/https://doi.org/10.1371/journal.pone.0213313>
- Servaes, S., Glorie, D., Verhaeghe, J., Stroobants, S., Staelens, S., 2017. Preclinical molecular imaging of glutamatergic and dopaminergic neuroreceptor kinetics in obsessive compulsive disorder. *Prog. Neuro-Psychopharmacology Biol. Psychiatry* 77, 90–98. <https://doi.org/10.1016/j.pnpbp.2017.02.027>
- Smith, S.M., 2002. Fast robust automated brain extraction. *Hum. Brain Mapp.* 17, 143–155. <https://doi.org/10.1002/hbm.10062>
- Song, C., Qu, Z., Blumm, N., Barabási, A.-L., 2010. Limits of Predictability in Human Mobility. *Science* (80-). 327, 1018–1021. <https://doi.org/10.1126/science.1177170>
- Stuchlik, A., Radoštová, D., Hatalova, H., Vales, K., Nekovarova, T., Koprivova, J., Svoboda, J., Horacek, J., 2016. Validity of quinpirole sensitization rat model of OCD: Linking evidence from animal and clinical studies. *Front. Behav. Neurosci.* 10, 209. <https://doi.org/10.3389/fnbeh.2016.00209>
- Szechtman, H., Sulis, W., Eilam, D., 1998. Quinpirole induces compulsive checking behavior in rats: A potential animal model of obsessive-compulsive disorder (OCD). *Behav. Neurosci.* 112, 1475–1485. <https://doi.org/10.1037/0735-7044.112.6.1475>
- Taylor, S., 2011. Early versus late onset obsessive-compulsive disorder: evidence for distinct subtypes. *Clin. Psychol. Rev.* 31, 1083–1100. <https://doi.org/10.1016/j.cpr.2011.06.007>
- Teicher, M.H., Andersen, S.L., Hostetter, J.C., 1995. Evidence for dopamine receptor pruning between adolescence and adulthood in striatum but not nucleus accumbens. *Dev. Brain Res.* 89, 167–172. [https://doi.org/10.1016/0165-3806\(95\)00109-Q](https://doi.org/10.1016/0165-3806(95)00109-Q)
- Tucci, M.C., Dvorkin-Gheva, A., Sharma, R., Taji, L., Cheon, P., Peel, J., Kirk, A., Szechtman, H., 2014. Separate mechanisms for development and performance of compulsive checking in the quinpirole sensitization rat model of obsessive-compulsive disorder (OCD). *Psychopharmacology (Berl)*. <https://doi.org/10.1007/s00213-014-3505-6>
- Ulloa, R.-E., Nicolini, H., Fernández-Guasti, A., 2004. Age differences in an animal model of obsessive-compulsive disorder: participation of dopamine - Dopamine in an animal model of OCD. *Pharmacol. Biochem. Behav.* 78, 661–666. <https://doi.org/10.1016/j.pbb.2004.04.009>
- van Meer, M.P.A., Otte, W.M., van der Marel, K., Nijboer, C.H., Kavelaars, A., Berkelbach van der Sprenkel, J.W., Viergever, M.A., Dijkhuizen, R.M., 2012. Extent of bilateral neuronal network reorganization and functional recovery in relation to stroke severity. *J. Neurosci.* 32, 4495–4507. <https://doi.org/10.1523/JNEUROSCI.3662-11.2012>
- Veale, D., Roberts, A., 2014. Obsessive-compulsive disorder. *BMJ* 348, g2183. <https://doi.org/10.1136/bmj.g2183>
- Whitaker, N.G.G., Lindstrom, T.D., 1987. Disposition and biotransformation of quinpirole, a new D-2 dopamine agonist antihypertensive agent, in mice, rats, dogs and monkeys. *Drug Metab. Dispos.* 15, 107–113.
- Zarei, M., Mataix-Cols, D., Heyman, I., Hough, M., Doherty, J., Burge, L., Winmill, L., Nijhawan, S., Matthews, P.M., James, A., 2011. Changes in gray matter volume and white matter microstructure in adolescents with obsessive-compulsive disorder. *Biol. Psychiatry* 70, 1083–1090. <https://doi.org/10.1016/j.biopsych.2011.06.032>



Memantine treatment does not affect compulsive behavior or frontostriatal connectivity in an adolescent rat model for quinpirole-induced compulsive checking behavior

Milou Straathof¹, Erwin L.A. Blezer¹, Christel E. Smeele¹, Caroline van Heijningen¹, Annette van der Toorn¹, TACTICS Consortium², Jan K. Buitelaar^{3,4}, Jeffrey C. Glennon^{3,5}, Willem M. Otte^{1,6} & Rick M. Dijkhuizen¹

¹ Biomedical MR Imaging and Spectroscopy Group, Center for Image Sciences, University Medical Center Utrecht & Utrecht University, the Netherlands.

² Members of the TACTICS consortium are listed in the Acknowledgments.

³ Department of Cognitive Neuroscience, Donders Institute for Brain, Cognition and Behavior, Radboud University Medical Center, Nijmegen, the Netherlands.

⁴ Karakter Child and Adolescent Psychiatry University Center, Nijmegen, the Netherlands.

⁵ Conway Institute of Biomolecular and Biomedical Research, School of Medicine, University College Dublin, Dublin 4, Ireland.

⁶ Department of Pediatric Neurology, UMC Utrecht Brain Center, University Medical Center Utrecht and Utrecht University, the Netherlands.

Submitted.

Abstract

Background: Compulsivity often develops during childhood and is associated with elevated glutamate levels within the frontostriatal system. This suggests that anti-glutamatergic drugs, like memantine, may be an effective treatment.

Aim: Our goal was to characterize the acute and chronic effect of memantine treatment on compulsive behavior and frontostriatal network structure and function in an adolescent rat model of compulsivity.

Methods: Juvenile Sprague Dawley rats received repeated quinpirole, resulting in compulsive checking behavior (n=32; Compulsive), or saline injections (n=32; Control). Eight compulsive and control rats received chronic memantine treatment, and eight compulsive and control rats received saline treatment, for seven consecutive days between the 10th and 12th quinpirole/saline injection. Compulsive checking behavior was assessed, and structural and functional brain connectivity was measured with diffusion MRI and resting-state fMRI before and after treatment. The other rats received an acute single memantine (Compulsive: n=12; Control: n=12) or saline injection (Compulsive: n=4; Control: n=4) during pharmacological MRI after the 12th quinpirole/saline injection. An additional group of rats received a single memantine injection after a single quinpirole injection (n=8).

Results: Memantine treatment did not affect compulsive checking, nor frontostriatal structural and functional connectivity in the quinpirole-induced adolescent rat model. While memantine activated the frontal cortex in control rats, no significant activation responses were measured after single or repeated quinpirole injections.

Conclusions: The lack of a memantine treatment effect in quinpirole-induced compulsive adolescent rats may be partly explained by the interaction between glutamatergic and dopaminergic receptors in the brain, which can be evaluated with functional MRI.

Introduction

Compulsivity is the repetitive, irresistible urge to perform certain behaviors without voluntary control, and can be considered to be a cross-disorder trait of psychiatric disorders like obsessive compulsive disorder (OCD) and autism spectrum disorder (ASD) (Jacob et al., 2009). Current treatment strategies for these disorders typically focus on diminishing symptoms associated with a specific diagnosis. For people with OCD, medication treatments with selective serotonin reuptake inhibitors (SSRIs) or combination treatments with cognitive behavioral therapy have been proven effective, but 40-60% of these patients have treatment-resistant symptoms (Franklin and Foa, 2011). There are no curative or even symptomatic treatments available for the key symptoms of ASD (Accordino et al., 2016), and SSRI treatment is not very effective (Williams et al., 2013). This stresses the need for alternative treatment approaches, for example by focusing on cross-disorder traits, e.g., compulsive behavior, so treatment can be tailored to specific symptom domains.

Development of treatment approaches that focus on compulsive behavior requires knowledge of the underlying neural circuits. Compulsive behavior has been associated with structural and functional abnormalities within the frontal cortico-striatal-thalamo-cortical circuits in humans, as demonstrated with magnetic resonance imaging (MRI) (Figeo et al., 2016; Montigny et al., 2013). Recent findings have implicated that compulsive behavior may involve four frontal cortico-striatal-thalamo-cortical circuits, each consisting of different cortical and striatal components (O. A. van den Heuvel et al., 2016). Within these circuits, compulsive behavior may either be caused by hyperactivity within the striatal component or by a failure of top-down control of the frontal cortical regions over the striatal component (Fineberg et al., 2010). It has been theorized that this top-down cortical control is mediated by the neurotransmitter glutamate (Sesack et al., 2003). This points towards a relationship between compulsive behavior and altered glutamate concentrations, which is further supported by the high density of glutamate receptors in the frontostriatal circuits (Monaghan et al., 1985) and dysregulation of glutamatergic signaling in individuals with ASD and OCD (Naaijen et al., 2015; Pittenger et al., 2011).

The role of glutamate in patients with OCD and ASD may imply that anti-glutamatergic drugs could be effective as medication against compulsivity (Mechler et al., 2017). One potential drug is the *N*-methyl-D-aspartate (NMDA) receptor antagonist memantine, an FDA approved drug used in the clinic for the symptomatic treatment of Alzheimer's disease (see for a systematic review and meta-analysis: Matsunaga *et al*, 2015).

Memantine is an open-channel NMDA receptor blocker with rapid response kinetics (Chen et al., 1992), which may protect neurons against glutamate excitotoxicity with limited side effects (Rammes et al., 2008). Memantine has shown some initial promise as a successful treatment against OCD symptoms in an animal model and in human adults with OCD. Memantine decreases marble-burying behavior in mice (Egashira et al., 2008), which is thought to reflect anxiety but also compulsive behavior. As an add-on treatment in human adults with OCD, memantine was found to reduce the severity of symptoms (Ghaleiha et al., 2013; Haghghi et al., 2013). Since three-quarters of people with OCD experience their first symptoms in mid childhood, OCD is suggested to be a neurodevelopmental disorder (Boileau, 2011). Therefore, it is important to assess the treatment potential of memantine in this developmental period (Mechler et al., 2017). In addition, mechanistically it remains unclear how memantine exerts its therapeutic effects on neural circuits involved in OCD.

Therefore, the objective of this study was to determine the therapeutic efficacy of memantine on the reduction of compulsive behavior during adolescence. To that aim we measured the behavioral effects of memantine administration in adolescent rats with quinpirole-induced compulsive checking behavior (Straathof et al., 2020a). In addition, we aimed to elucidate the possible mode of action of memantine on the development of structural and functional connectivity, and functional activation, within the frontostriatal system, which we measured with structural and functional MRI methods.

Methods

All experiments were approved by the Committee for Animal Experiments of the University Medical Center Utrecht, The Netherlands (2014.I.12.104), and all efforts were made to reduce the number of animals used and to minimize animal suffering.

Animal model

We used a recently described adolescent rat model of compulsive checking behavior (Straathof et al., 2020a), which is adapted from an established adult rat model of compulsive checking behavior (Szechtman et al., 1998).

Sixty-four juvenile Sprague Dawley rats (Harlan, the Netherlands) were housed individually and habituated to environmental conditions (temperature 22-24 °C and 12 h light/dark cycle with lights on at 7:00 AM) for at least 7 days prior to the experiment, with

access to food and water ad libitum. From the age of 5 weeks (body weight: 105 ± 18 grams (mean \pm standard deviation (SD)), corresponding to puberty (Sengupta, 2013), we subcutaneously injected the rats with the selective D2/D3 receptor agonist quinpirole (Tocris, UK, 0.5 mg/kg; n=32; Compulsive group) or saline (n=32; Control group), twice per week during 6 weeks (total of 12 injections). We randomly assigned the treatment (quinpirole or saline) to the animals. The experimenters (CvH, CES, MS and ELAB) could not be blinded for the factor group (Compulsive or Control), due to the obvious behavioral effects of quinpirole treatment. Nevertheless, the experimenters were blinded for memantine or saline treatment. Each injection was immediately followed by placement of the rat in the center of a large open field table (160×160 cm, 60 cm above the floor) for 30 minutes. On the open field table, four objects (2 black, 2 white; 8×8×8 cm) were placed on fixed locations: two near the middle and two near the corners of the table. The combination of repetitive quinpirole injections and placement on the open field is essential for the development of compulsive checking behavior (Szechtman et al., 1998).

Experimental groups

The potency of memantine treatment to reduce compulsive behavior and its mode of action in the quinpirole-induced adolescent rat model of compulsive checking behavior was assessed in two studies.

In Study I, we measured the effects of a sub-chronic memantine treatment on compulsive behavior and structural and functional connectivity in the frontostriatal system of adolescent rats. Rats were randomly assigned to memantine or saline treatment, and the experimenters were blinded for this treatment assignment. Rats received daily intraperitoneal injections of the NMDA receptor antagonist memantine (20 mg/kg/day (Sekar et al., 2013), Boehringer Ingelheim Pharma, Germany) (Compulsive + memantine group: n=8, Control + memantine group: n=8) or saline (Compulsive + saline group: n=8, Control + saline group: n=8) for seven consecutive days, starting the day after the 10th quinpirole or saline injection. On days when both injections were given (11th and 12th quinpirole/saline injection), the memantine/saline treatment was given 30 minutes before the quinpirole/saline injection.

In Study II, we measured the acute effects of a single memantine injection on functional activation in the frontostriatal system. Rats received an acute intravenous memantine (20 mg/kg, Sigma-Aldrich, Germany; Compulsive + memantine: n=12, Control + memantine: n=12) or saline injection (Compulsive + saline: n=4, Control + saline group: n=4) 130 minutes after the 12th quinpirole/saline injection during pharmacological MRI.

Groups receiving saline during MRI were smaller because our previous study showed no significant effects of saline injections on pharmacological MRI (Roelofs et al., 2017). To assess the influence of possible pharmacological interactions between memantine and quinpirole, we included an extra experimental group of rats. In this group, rats (n=8) received only one quinpirole injection, followed by a single memantine injection 130 minutes after quinpirole injection during pharmacological MRI.

Behavioral analyses

Ethovision software (Noldus Information Technology B.V., the Netherlands) was used to automatically trace the locomotor trajectories of the rats on the open field table on the days of the MRI experiments. The open field area was virtually divided into 25 rectangles of 40×40 cm² of which the outer zones extended 20 cm outside the open field. For all analyses, we used the last 15 minutes for the compulsive rats, and the complete 30 minutes for the control rats (Straathof et al., 2020a). We calculated the frequency of visits for each zone during the observation period and defined the home-base as the most frequently visited zone.

We quantified compulsive-like checking behavior before and after memantine treatment in Study I (after the 10th and 12th quinpirole/saline injections), and before the single memantine injection in Study II (after the 12th quinpirole/saline injection). Compulsive checking behavior parameters were characterized relative to the home-base, and included frequency of checking (number of visits of the home-base per minute, observed during the observation period), length of checks (average time of a visit at the home-base), recurrence time of checking (average time spent in other areas before returning to the home-base) and stops before returning to the home-base (average number of other areas the rat visited before returning to the home-base) (Szechtman et al., 1998; Tucci et al., 2014b). In addition, we determined the predictability of the visited zones as the Lempel-Ziv source entropy (Song et al., 2010), using a maximal substring of three zones and only including animals that visited at least nine different zones.

To study the effects of memantine treatment on behavioral measures other than compulsive-like checking behavior, we performed additional behavioral measurements on the rats in Study I. We calculated hyperactivity measures, including the total travelled distance, average velocity of movement and immobility time (<0.01 cm movement per video frame). In addition, we manually quantified stereotypic behaviors the rats showed during a stop at their home-base (Straathof et al., 2020a; Szechtman et al., 1998), for the first twenty visits during the observation period. Because control rats were less active, all visits were

included when the total amount of home-base visits was below twenty. First, for each visit we scored the entering or leaving direction relative to the home-base, to determine a potential directional preference. We used a compass divided into eight different directions (per 45 degrees) to determine the directions. Second, to quantify the horizontal movements per visit we counted the number of anti-clockwise and clockwise turns, and for vertical movements we counted the number of head dips per visit. Third, the placement of the forelimbs and number of sniffs at the object were counted to score the interaction of the rat with the object per visit. Fourth, we determined the grooming time per visit. Lastly, these individual behavioral scores were combined into a total number of behavioral acts per visit.

MRI acquisition

All MRI experiments were conducted on a 9.4T MR system equipped with a 400 mT/m gradient coil (Varian, Palo Alto, CA, USA). A homebuilt 90 mm diameter Helmholtz volume coil was used for signal excitation and an inductively coupled 25 mm diameter surface coil for signal detection. On the days MRI was executed, rats were directly transferred from the open field test platform to the MRI scanner. Rats were anesthetized and endotracheally intubated for mechanical ventilation with 2% isoflurane in a mixture of air and O₂ (70% / 30%). Rats were subsequently immobilized in a specially designed stereotactic holder and placed in an animal cradle. For memantine or saline administration during MRI in Study II, one tail vein was cannulated under isoflurane anesthesia before placing the rat in the stereotactic holder. During MRI, end-tidal CO₂ was continuously monitored with a capnograph (Microcap, Oridion Medical 1987 Ltd., Jerusalem, Israel) and body temperature was maintained at 37.0 ± 1.0 °C. Heart rate and blood oxygen saturation were monitored with an infrared sensor attached to the hind paw. Parameter settings for the MRI acquisitions were as followed:

Anatomical MRI: 3D balanced steady-state free precession (BSSFP) scan with four phase cycling angles (0°, 90°, 180°, 270°). Repetition time (TR) / echo time (TE) = 5/2.5 ms; flip angle = 20°; field-of-view (FOV) = 40×32×24 mm³; acquisition matrix = 160×128×96; image resolution = 250 μm isotropic. Total acquisition time = 12.5 min. Isoflurane anesthesia level was reduced to 1.5% at the start of the anatomical MRI acquisition to lower the anesthetic depth for the following resting-state fMRI or pharmacological MRI acquisition.

Resting-state functional MRI: T₂^{*}-weighted blood oxygenation level-dependent (BOLD) images were acquired using a single shot 3D gradient echo planar imaging (EPI) sequence. TR/TE = 26.1/15 ms; FOV = 32.4×32.4×16.8 mm³; flip angle = 13°; acquisition matrix =

54×54×28; image resolution = 600 μm isotropic. Acquisition time = 730.8 ms per scan volume, with a total of 800 volumes resulting in a total scan time of 9 minutes and 45 seconds. Resting-state fMRI was always started at 90 minutes after quinpirole injection, to standardize the effects of quinpirole across animals.

Diffusion-weighted MRI: 2D 4-shot spin echo EPI sequence: TR/TE = 1700/34 ms; FOV = 32×32mm²; acquisition matrix = 64×128; 25 slices of 0.5 mm, image resolution = 500×250×500 μm^3 , zero-filled to 250×250×500 μm^3 ; b = 1611 s/mm²; δ/Δ = 6.5 / 10.27 ms. Five non-diffusion-weighted (b0) and sixty diffusion-weighted images were acquired. Diffusion-weighted MRI was performed at 2% isoflurane anesthesia to minimize animal motion.

Pharmacological MRI: 2D gradient echo multi-slice sequence: TR/TE = 500/15 ms; FOV = 32×32mm²; flip angle = 50°; acquisition matrix = 128×128; 25 slices of 0.5 mm, image resolution = 250×250×500 μm^3 ; acquisition time = 128 s per scan volume, with a total of 47 volumes resulting in a total scan time of 103 minutes. Nine baseline scans were acquired, followed by an intravenous memantine or saline injection during the tenth scan and 37 post-injection scans.

For study I, MRI acquisitions were done after the 10th (pre-treatment measurement) and 12th (post-treatment measurement) injection of quinpirole/saline. The MRI session consisted of anatomical MRI, followed by resting-state fMRI acquisition and diffusion-weighted MRI. For study II, MRI acquisition was done after the 12th injection of quinpirole/saline. The MRI session consisted of anatomical MRI, followed by pharmacological MRI.

MRI processing

Analyses were performed using FMRIB's Software Library (FSL) v5.0.9, unless otherwise stated.

Regions of interest

Regions-of-interest were taken from the 3D rendering of the Paxinos and Watson atlas (George Paxinos and Watson, 2005). Regions included the frontal cortex (consisting of the orbitofrontal cortex (OFC: dorsolateral, lateral, medial, and ventral orbital cortex), the anterior cingulate cortex (ACC: Cingulate cortex area 1 and 2) and the medial prefrontal cortex (mPFC: prelimbic and infralimbic cortex)) and the striatum (caudate putamen (CPU) and nucleus accumbens (NAcc)) for all MR analyses. We measured interhemispheric homologous connectivity for these regions as well as frontostriatal intrahemispheric

connectivity. Homotopic areas in the left and right hemisphere were combined for the pharmacological MRI analyses. In addition, resting-state fMRI and pharmacological MRI analyses were also performed for the different sub-regions (OFC, ACC, MPFC, CPu & NAcc) separately.

Registration

We linearly registered individual anatomical images to a three-dimensional model of the Paxinos and Watson atlas (George Paxinos and Watson, 2005) and created a study-specific template by taking the mean of these registered images. Individual mean resting-state fMRI scans were linearly registered to the individual anatomical scan using *FLIRT* (Jenkinson et al., 2002; Jenkinson and Smith, 2001), followed by non-linear registration to the study specific anatomical template using *FNIRT* (Andersson et al., 2007a). Individual averaged non-diffusion weighted (b0) images were non-linearly registered to the average b0 image of one individual rat (DWI template), followed by linear registration to the study-specific anatomical template. Individual pharmacological MR images were directly non-linearly registered to the study-specific anatomical template. Regions-of-interest were transformed to individual space with the inverse of these registrations. The resting-state fMRI regions-of-interest were masked with a temporal signal to noise ratio mask of 10 and the regions-of-interest for DWI-based tractography were masked with a grey matter mask (fractional anisotropy (FA) lower than 0.25).

Diffusion-weighted imaging – Study I

The diffusion-weighted images were brain-extracted with *BET* (Smith, 2002), motion- and eddy current-corrected with affine transformations in *MCFLIRT* (Jenkinson et al., 2002) and the diffusion tensor was fitted using *dtifit* within the FMRIB's Diffusion Toolbox (FDT package). Whole-brain tractography was performed using MrTrix3^{*} (www.mrtrix.org) (J.-D. Tournier et al., 2012). The response function estimation for single shell constrained spherical deconvolution (CSD) tractography was performed on individual datasets with a reimplement of the Tax-method for response function estimation (Tax et al., 2014). Subsequently, the individual response functions were averaged to obtain a group response function. We performed whole-brain CSD tractography on individual datasets with one million streamlines, and streamlines-of-interest were selected by using our regions-of-interest as start- and endpoints. The median fractional anisotropy (FA), reflecting the degree of diffusion anisotropy (degree of restricted diffusion along the main directions of the diffusion tensor), was used as a measure of structural connectivity (Koay et al., 2006).

Resting-state fMRI – Study I

Preprocessing steps of the resting-state fMRI scans included removal of the first 20 images to reach a steady state, motion-correction, brain-extraction and removal of noise components with single-subject independent component analysis (Beckmann and Smith, 2004). Moreover, the BOLD signal was normalized, and motion-correction parameters were used as regressors for the resting-state signal. Low-frequency BOLD fluctuations were obtained by applying temporal filtering between 0.01 and 0.1 Hz in AFNI (Cox, 1996). We calculated Fisher's Z-transformed correlation coefficients for inter- and intrahemispheric functional connectivity between regions-of-interest.

Pharmacological MRI – Study II

Preprocessing steps of the pharmacological MRI scans included removal of the first baseline scan, brain extraction and motion correction. The BOLD response to the memantine/saline injection was normalized to the mean baseline signal (mean of the first 8 images). To calculate brain activation maps, we used a repeating OFF/ON design as regressor for a voxel-wise generalized linear model (GLM) per group, in which “OFF” corresponded with the pre-injection scans and “ON” with the first 25 post-injection scans. Resulting z activation maps per group were false discovery rate (FDR)-corrected, with a threshold at $z=3.1$ corresponding to $p < 0.001$ after FDR correction. The brain activation response to memantine or saline injection was calculated as the positive area under the curve (AUC) of the BOLD signal time-course for each individual rat (negative values were excluded). This AUC represents the percentage of BOLD signal change per second.

Statistics

Statistical analyses were performed in R (3.2.3) and RStudio 0.99.903 (R Core Team, 2014). P-values were FDR corrected and considered significant below 0.05 after FDR correction.

Differences in compulsive behavioral metrics before memantine treatment (Study I and II separately) between the Compulsive and Control group were analyzed with a Mann-Whitney U test, to verify that compulsive-like behavior developed before memantine injections.

For Study I, effects of memantine/saline treatment on various types of behavior (compulsive checking behavior, hyperactivity measures and behavior during stops), bodyweight, functional connectivity and structural connectivity were determined with Wilcoxon signed-rank tests to compare the pre and post measurement for each group

separately. In addition, a mixed design ANOVA, with factor “time” as within-subject variable, and factors “group” (Control or Compulsive) and “treatment” (saline or memantine) as between-subject variables was performed. P-values were FDR-corrected per modality in the behavior, functional and structural connectivity analyses.

For statistical analysis of pharmacological MRI data in Study II, we compared the BOLD activation responses (AUC) between groups using a Kruskal-Wallis test, followed by post-hoc Dunn’s tests, adjusted for multiple comparisons using the Benjamini Yekutieli method for FDR correction (Benjamini and Yekutieli, 2001).

Results

In Study I, one control rat died during the post-memantine MRI acquisition because of respiratory problems caused by excessive mucus. In addition, the behavioral recording of one compulsive rat was incomplete and the MRI scans of one control and one compulsive rat were affected by artifacts. Therefore, final groups in Study I consisted of fourteen compulsive rats (Compulsive + saline treatment: n=7; Compulsive + memantine treatment: n=7) and fourteen control rats (Control + saline treatment: n=8; Control + memantine treatment: n=6). In Study II, all included animals could be used for analyses, resulting in final group sizes of sixteen compulsive rats (Compulsive + saline injection: n=4; Compulsive + memantine injection: n=12) and sixteen control rats (Control + saline injection: n=4; Control + memantine injection: n=12).

Study I: Memantine treatment does not reduce compulsive behavior and frontostriatal structural and functional connectivity in adolescent rats

Before memantine treatment in Study I or memantine injection in Study II, compulsive rats displayed clear patterns of repeated travelling between two zones of the open field, and compulsive-like checking behavior (Supplementary Figure S1).

As expected, we detected no statistically significant effect of saline treatment on any of the measures of compulsive behavior (Figure 1). Similarly, however, behavioral measures, exposing compulsivity in quinpirole-injected rats, were not significantly altered after memantine treatment in control and compulsive rats. Comparable results were found for the additional behavioral measures, which include hyperactivity measures and stereotypic behaviors during stops at the home-base (Supplementary Figure S2). Furthermore, no

significant interaction effects between factors “time” (pre- or post-treatment), “group” (Compulsive or Control) and “treatment” (saline or memantine) were found for any of the behavioral measures. Correspondingly, we also did not find a statistically significant effect of the memantine treatment on functional or structural connectivity in the frontostriatal system (Figure 2). Similarly, functional connectivity analyses on individual sub-regions of the frontal cortex and striatum did not reveal statistically significant effects of memantine treatment (Supplementary Figure S3).

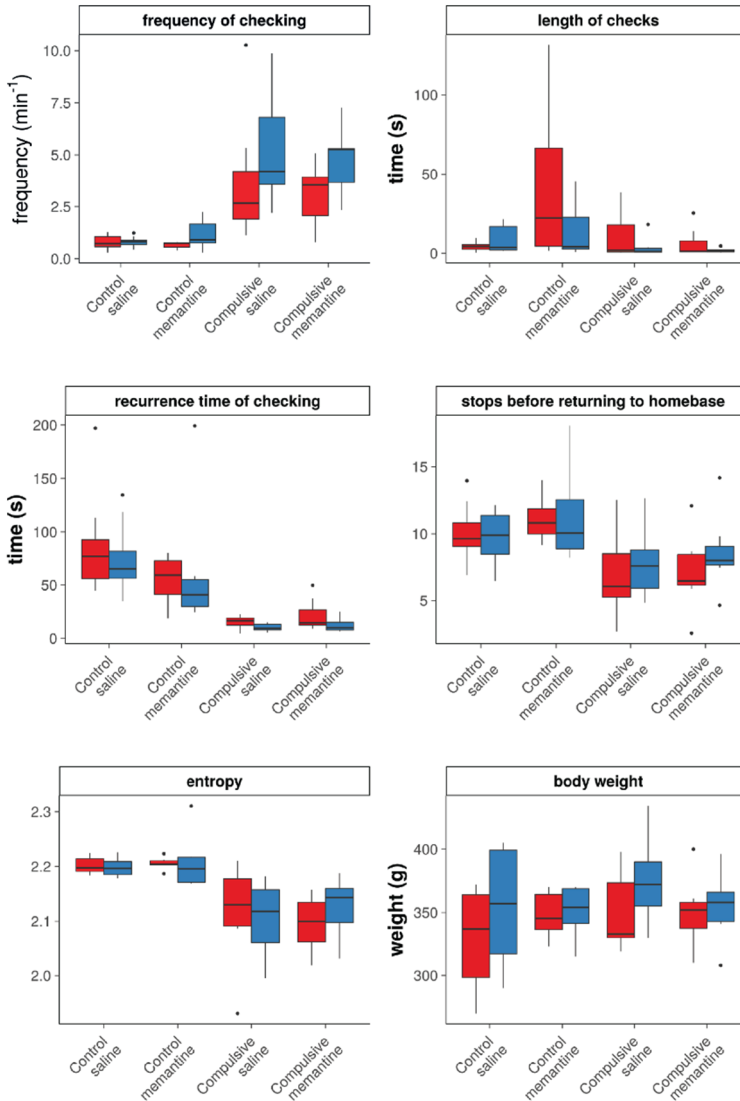


Figure 1: Measures of compulsive checking behavior and body weight, before and after saline/memantine treatment in control and compulsive rats. Compulsive behavior measures (frequency of checking (number of visits at the home-base per minute (observed during 15 minutes for compulsive rats, and during 30 minutes for controls)), length of checks (average time (s) spent at the home-base), recurrence time of checking (average time (s) before returning to the home-base), stops before returning to the home-base (average number of zones visited in between two visits of the home-base)), entropy (predictability of the visited zones), and body weight (g), before (red) and after (blue) seven days of daily saline/memantine treatment (Control + saline: n=8; Control + memantine: n=6; Compulsive + saline: n=7; Compulsive + memantine: n=7). Error bars represent 1.5 times the interquartile range, and dots represent values that exceeded 1.5 times the interquartile range.

We found a significant interaction effect between factors “time” and “treatment” (saline or memantine) on body weight ($p=0.0003$). Body weight of control and compulsive adolescent rats increased in the seven days between pre- and post-treatment with saline (Control: pre: 330 ± 38 g; post: 355 ± 45 g, $p=0.01$ before FDR correction; Quinpirole: pre: 351 ± 31 g; post: 375 ± 34 g, $p=0.01$ before FDR correction) (Figure 1), but not in rats that were treated with memantine.

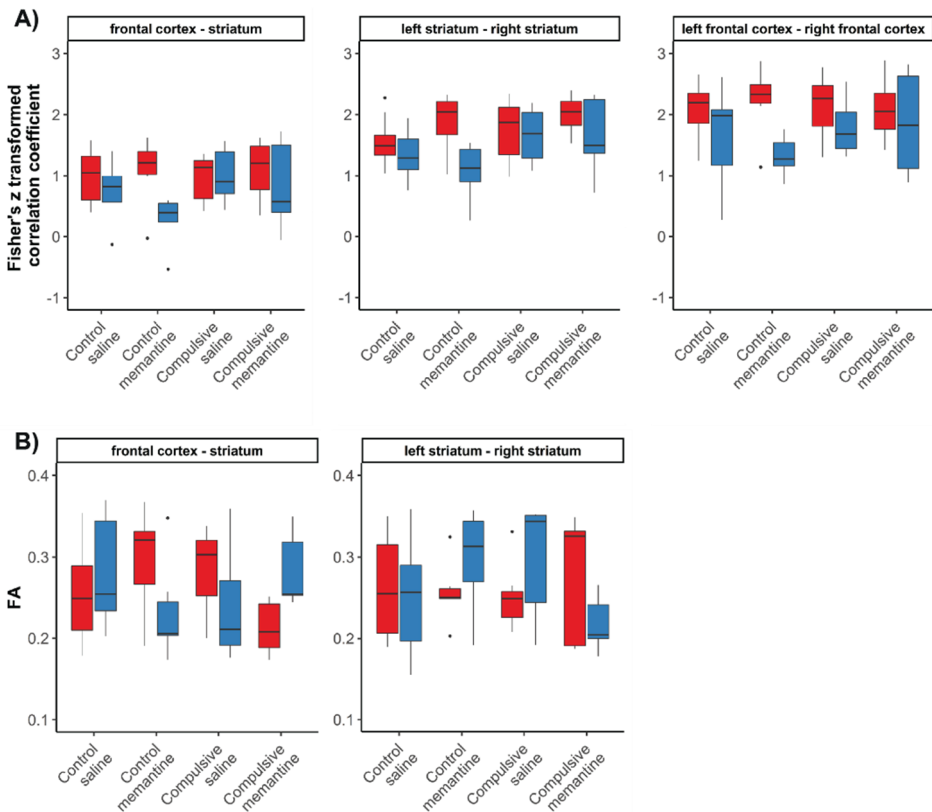


Figure 2: Functional and structural connectivity in the frontostriatal system before and after saline/memantine treatment in control and compulsive rats. Bar graphs of functional connectivity (Fisher's Z-transformed correlation coefficient) (A) and structural connectivity (median fractional anisotropy (FA)) (B) of intra- and interhemispheric connections within the frontostriatal system before (red) and after (blue) seven days of daily saline/memantine treatment (Control + saline: n=8; Control + memantine: n=6; Compulsive + saline: n=7; Compulsive + memantine: n=7). Structural connectivity between the left and right frontal cortex could not be determined because of unreliable tractography results. Error bars represent 1.5 times the interquartile range and dots represent values that exceed 1.5 times the interquartile range.

Study II: Memantine activates the frontal cortex, but not after quinpirole injection in adolescent rats

Figure 3A shows brain activation maps, which display regions where memantine/saline injection resulted in a significant activation response. As expected, saline injection did not activate brain areas in control nor in compulsive rats, as also illustrated from BOLD signal time courses in the frontal cortex and striatum (Figure 3B). However, memantine injection induced clear positive brain activation in frontal and occipital cortical areas in control rats, but not in compulsive rats.

In control rats, the AUC of the BOLD response in the frontal cortex was significantly higher after memantine injection as compared to saline injection (memantine: $AUC = 0.05 \pm 0.02$; saline: $AUC = 0.01 \pm 0.01$, $p=0.004$) (Figure 3C). In compulsive rats, the AUCs were similar between memantine- and saline-injected rats for all measured areas. Memantine-induced BOLD responses in the frontal cortex were statistically significantly higher in control than in compulsive rats (Control: $AUC=0.05 \pm 0.02$; Compulsive: $AUC=0.02 \pm 0.02$, $p=0.002$). The AUCs for the striatum after memantine or saline injection were similar between groups. We found similar results for analyses of the separate sub-regions of the frontal cortex (ACC, OFC, mPFC) and striatum (CPu and NAcc) (Supplementary Figure S4).

Lastly, to assess the influence of possible pharmacological interaction between memantine and quinpirole, we included an additional experimental group, in which each rat received only a single quinpirole injection, followed by a single memantine injection. Quantitative assessment revealed no statistically significant differences in the AUC of the BOLD response in the frontal cortex and striatum between compulsive and single quinpirole-injected rats (Figure 4).

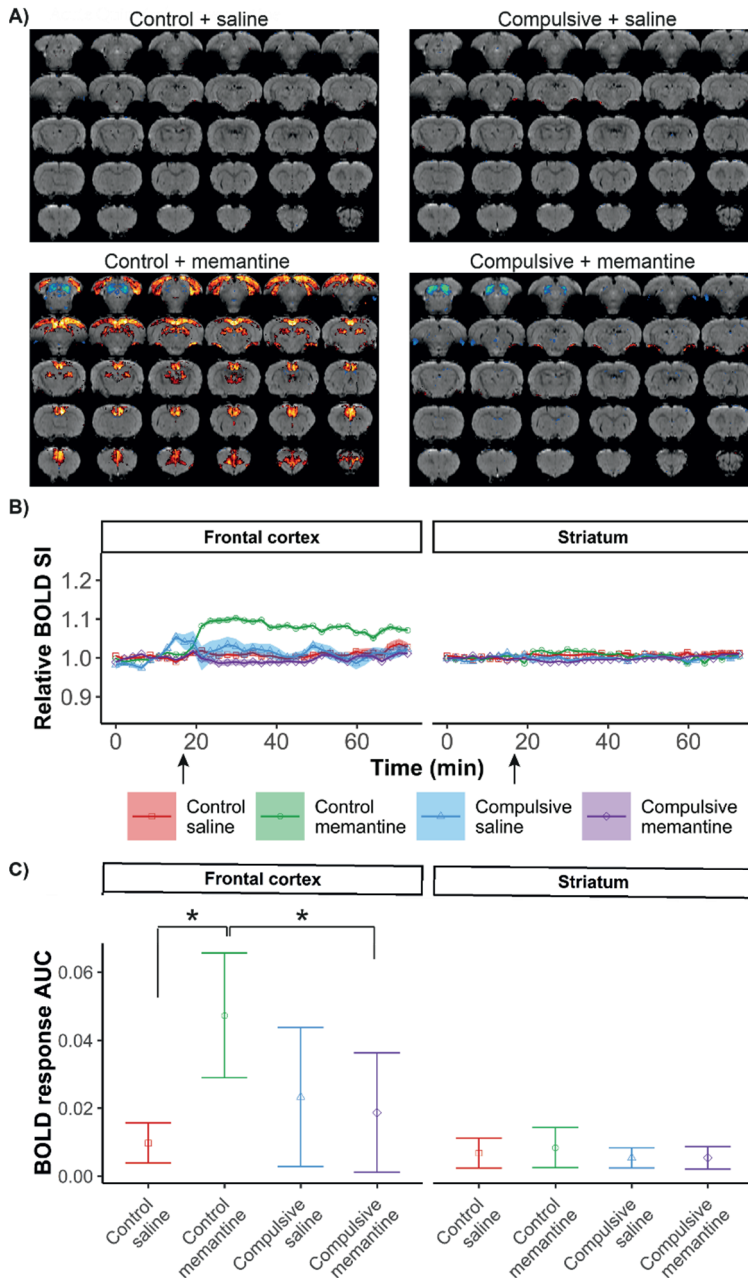


Figure 3: Brain activation directly after memantine/saline injection in control and compulsive rats. Brain activation maps, overlaid on anatomical images, show positive BOLD activation responses in yellow/red ($z > 3.1$) and negative responses in blue ($z < -3.1$) (A). The normalized BOLD signal intensity (SI) time-course is shown as averaged time series for the regions-of-interest, with the arrow indicating the time of memantine/saline injection

(B). BOLD responses to memantine or saline injection quantified as area under the curve (AUC) (relative positive BOLD SI change per second) (C). Control + saline: n=4; Control + memantine: n=12; Compulsive + saline: n=4; Compulsive + memantine: n=12. *Corrected $p < 0.05$. Shades in B represent the standard error. Error bars in C represent the standard deviation.

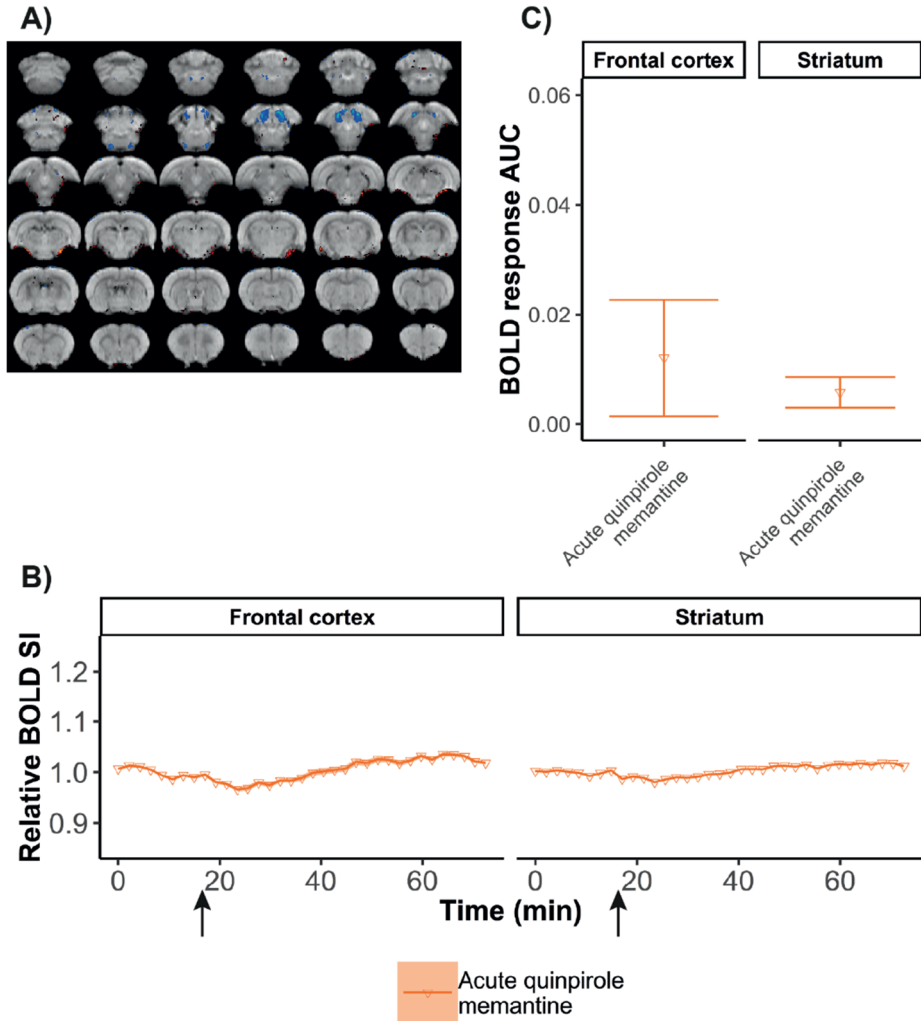


Figure 4: Brain activation directly after memantine injection following a single quinpirole injection. Brain activation maps, overlaid on anatomical images, show positive BOLD activation responses in yellow/red ($z > 3.1$) and negative responses in blue ($z < -3.1$) (A). The normalized BOLD signal intensity (SI) time-course is shown as averaged time series for the regions-of-interest, with the arrow indicating the time of memantine injection (B). BOLD responses to memantine injection quantified as area under the curve (AUC) (relative positive BOLD SI change per second) (C). Acute quinpirole + memantine: n=8. Shades in B represent the standard error. Error bars in C represent the standard deviation.

Discussion

In this study we determined the therapeutic efficacy of memantine to reduce compulsive-like behavior in adolescent rats and assessed its possible mode of action on the frontostriatal system (Study I). We showed that a repeated memantine treatment regimen did not reduce compulsive-like behavior in the adolescent rat model of quinpirole-induced compulsive checking behavior. Correspondingly, memantine treatment did not induce changes in structural and functional connectivity in the frontostriatal system. A single memantine injection activated frontal cortical regions in control but not in compulsive adolescent rats or rats that received a single quinpirole injection (Study II), which may explain the absence of memantine-induced treatment effects in Study I.

The main aim of our study was to identify and elucidate possible therapeutic effects of the NMDA receptor antagonist memantine in adolescent compulsive behavior (Study I). Several glutamatergic antagonists have been shown to be effective in reducing OCD symptoms in adults (Pittenger et al., 2011) and ASD-associated behavior in pediatric patients (Mechler et al., 2017). Before memantine treatment, quinpirole-injected rats demonstrated clear compulsive-like checking behavior, similar to our earlier study in the adolescent model (Straathof et al., 2020a) and comparable to the adult model (Szechtman et al., 1998). In line with clinical treatment regimes, we started the memantine treatment after the development of compulsive checking behavior (i.e., after the 10th quinpirole/saline injection). The repetitive quinpirole injections were continued during the memantine treatment period, to ensure persistence of quinpirole-induced compulsive behavior (de Haas et al., 2011). The applied memantine treatment regimen, however, did not reduce compulsive-like behavior and functional or structural connectivity in the frontostriatal circuitry. Similar to findings in OCD patients, varying results have been reported with regard to the ability of pharmacological agents to reduce compulsive behavior in animal models, including quinpirole-injected adult rats (Stuchlik et al., 2016). Since memantine and quinpirole can induce similar effects in the brain –for example, memantine and quinpirole both induce long-term depression in the striatum (Mancini et al., 2016)– treatment effects may have interacted, leading to obfuscation of possible behavioral consequences.

To assess the effect of memantine on brain network activity, we measured direct activation responses with pharmacological MRI (Study II). A previous study demonstrated that memantine can elicit increased as well as decreased activity in the prelimbic cortex in drug-naïve rats (Sekar et al., 2013). Micro-dialysis studies have suggested that NMDA-

receptor antagonists can activate prefrontal areas by increasing the glutamatergic tone (López-Gil et al., 2007; Moghaddam et al., 1997), which can activate other glutamatergic receptors. We found that memantine injection in control rats not only influences brain activity in the frontal cortex, but also resulted in activation of remote brain areas. However, this memantine-induced activation was largely absent in quinpirole-induced compulsive rats or in rats that received only a single quinpirole injection. This suggests that the absence of memantine-induced activation in the compulsive group in Study II was not fundamentally associated with the compulsive-like phenotype by sensitization of dopamine D2/D3 receptors, but more likely a result of interactions between pathways activated by memantine and quinpirole. There is a tight interaction between glutamatergic and dopaminergic receptors in the brain (Cepeda et al., 2009). Quinpirole has been shown to attenuate the excitatory effects of NMDA and AMPA receptors in the prefrontal cortex (Tseng and O'Donnell, 2004) and striatum (Cepeda et al., 1993). This attenuating effect of quinpirole on glutamatergic neurotransmission may explain the absence of memantine-induced prefrontal activation in quinpirole-injected adolescent rats. This suggests that anti-glutamatergic drugs may not be effective in individuals with altered dopaminergic neurotransmission. In addition, interactions between quinpirole and memantine may have occurred at the dopamine D2/D3 receptor level, because both substances are dopamine D2 receptor agonists (Mancini et al., 2016; Seeman et al., 2008). Such direct or indirect interactions between quinpirole and memantine may have obscured the treatment effects of memantine on compulsive behavior in this adolescent rat model in Study I.

A possible limitation of the current study is the use of isoflurane anesthesia during resting-state fMRI acquisition. It has been shown that anesthesia with a comparable level of isoflurane (1.3%) as used in our study (1.5%) leads to enhanced functional connectivity values in cortico-striatal connections and diminished functional connectivity values between subcortical regions, as compared to awake rats (Paasonen et al., 2018). Thus, isoflurane anesthesia-induced changes in cortico-striatal functional connectivity may have obscured effects of quinpirole or memantine on functional connectivity in this circuitry. However, since all groups were scanned under the same anesthesia conditions, we expect that specific group differences in functional connectivity would still have been detectable.

In conclusion, our study did not reveal beneficial effects of memantine treatment on quinpirole-induced compulsive checking behavior in adolescent rats. This absence of a treatment effect of memantine may be at least partly explained by model-treatment interactions between the dopaminergic and glutamatergic system. Future studies that apply

this model should carefully consider possible interactions between quinpirole and pharmacological treatments, which may be verified in parallel pharmacological MRI experiments.

References

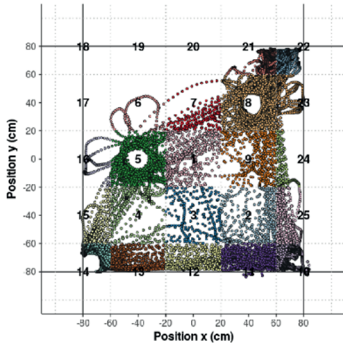
- Accordino, R.E., Kidd, C., Politte, L.C., Henry, C.A., McDougle, C.J., 2016. Psychopharmacological interventions in autism spectrum disorder. *Expert Opin. Pharmacother.* 17:7, 937–952. <https://doi.org/10.1517/14656566.2016.1154536>
- Andersson, J.L.R., Jenkinson, M., Smith, S., 2007. Non-linear registration aka Spatial normalisation. *FMRIB Tech. Rep. TR07JA2*.
- Beckmann, C.F., Smith, S.M., 2004. Probabilistic independent component analysis for functional magnetic resonance imaging. *IEEE Trans. Med. Imaging* 23, 137–152. <https://doi.org/10.1109/TMI.2003.822821>
- Benjamini, Y., Yekutieli, D., 2001. The control of the false discovery rate in multiple testing under dependence. *Ann. Stat.* 29, 1165–1188.
- Boileau, B., 2011. A review of obsessive-compulsive disorder in children and adolescents. *Dialogues Clin. Neurosci.* 13, 401–411.
- Cepeda, C., André, V.M., Jocoy, E.L., Levine, M.S., 2009. Chapter 3: NMDA and Dopamine: Diverse mechanisms applied to interacting receptor systems, in: VanDongen, A.M. (Ed.), *Biology of the NMDA Receptor*. CRC Press Taylor & Francis Group, pp. 41–59.
- Cepeda, C., Buchwald, N.A., Levine, M.S., 1993. Neuromodulatory actions of dopamine in the neostriatum are dependent upon the excitatory amino acid receptor subtypes activated. *Proc. Natl. Acad. Sci. USA* 90, 9576–9580.
- Chen, H.S. V., Pellegrini, J.W., Aggarwal, S.K., Lei, S.Z., Warach, S., Jensen, F.E., Lipton, S.A., 1992. Open-channel block of N-methyl-D-aspartate (NMDA) responses by memantine: therapeutic advantage against NMDA receptor-mediated neurotoxicity. *J. Neurosci.* 12, 4427–36.
- Cox, R.W., 1996. AFNI: Software for Analysis and Visualization of Functional Magnetic Resonance Neuroimages. *Comput. Biomed Res.* 29, 162–173.
- de Haas, R., Nijdam, A., Westra, T.A., Kas, M.J.H., Westenberg, H.G.M., 2011. Behavioral pattern analysis and dopamine release in quinpirole-induced repetitive behavior in rats. *J. Psychopharmacol.* 25, 1712–1719. <https://doi.org/10.1177/0269881110389093>
- Egashira, N., Okuno, R., Harada, S., Matsushita, M., Mishima, K., Iwasaki, K., Nishimura, R., Oishi, R., Fujiwara, M., 2008. Effects of glutamate-related drugs on marble-burying behavior in mice: Implications for obsessive-compulsive disorder. *Eur. J. Pharmacol.* 586, 164–170. <https://doi.org/10.1016/j.ejphar.2008.01.035>
- Figee, M., Pattij, T., Willuhn, I., Luijckes, J., van den Brink, W., Goudriaan, A., Potenza, M.N., Robbins, T.W., Denys, D., 2016. Compulsivity in obsessive-compulsive disorder and addictions. *Eur. Neuropsychopharmacol.* 26, 856–868. <https://doi.org/10.1016/j.euroneuro.2015.12.003>
- Fineberg, N.A., Potenza, M.N., Chamberlain, S.R., Berlin, H.A., Menzies, L., Bechara, A., Sahakian, B.J., Robbins, T.W., Bullmore, E.T., Hollander, E., 2010. Probing compulsive and impulsive behaviors, from animal models to endophenotypes: a narrative review. *Neuropsychopharmacology* 35, 591–604. <https://doi.org/10.1038/npp.2009.185>
- Franklin, M.E., Foa, E.B., 2011. Treatment of obsessive compulsive disorder. *Annu. Rev. Clin. Psychol.* 7, 229–243. <https://doi.org/10.1146/annurev-clinpsy-032210-104533>
- Ghaleiha, A., Entezari, N., Modabbernia, A., Najand, B., Askari, N., Tabrizi, M., Ashrafi, M., Hajiaghache, R., Akhondzadeh, S., 2013. Memantine add-on in moderate to severe obsessive-compulsive disorder: Randomized double-blind placebo-controlled study. *J. Psychiatr. Res.* 47, 175–180. <https://doi.org/10.1016/j.jpsychires.2012.09.015>
- Haghighi, M., Jahangard, L., Mohammad-Beigi, H., Bajoghli, H., Hafezian, H., Rahimi, A., Afshar, H., Holsboer-Trachsler, E., Brand, S., 2013. In a double-blind, randomized and placebo-controlled trial, adjuvant memantine improved symptoms in inpatients suffering from refractory obsessive-compulsive disorders (OCD). *Psychopharmacology (Berl)*. 228, 633–640. <https://doi.org/10.1007/s00213-013-3067-z>
- Jacob, S., Landeros-weisenberger, A., Leckman, J.F., 2009. Autism Spectrum and Obsessive-Compulsive Disorders: OC Behaviors, Phenotypes and Genetics. *Autism Res.* 2, 293–311. <https://doi.org/10.1002/aur.108>
- Jenkinson, M., Bannister, P., Brady, M., Smith, S., 2002. Improved optimization for the robust and accurate linear registration and motion correction of brain images. *Neuroimage* 17, 825–841. <https://doi.org/10.1006/nimg.2002.1132>
- Jenkinson, M., Smith, S., 2001. A global optimisation method for robust affine registration of brain images. *Med. Image Anal.* 5, 143–156. [https://doi.org/10.1016/S1361-8415\(01\)00036-6](https://doi.org/10.1016/S1361-8415(01)00036-6)

- Koay, C.G., Chang, L., Carew, J.D., Pierpaoli, C., Basser, P.J., 2006. A unifying theoretical and algorithmic framework for least squares methods of estimation in diffusion tensor imaging. *J. Magn. Reson.* 182, 115–125. <https://doi.org/10.1016/j.jmr.2006.06.020>
- López-Gil, X., Babet, Z., Amargós-Bosch, M., Sunol, C., Artigas, F., Adell, A., 2007. Clozapine and Haloperidol Differently Suppress the MK-801-Increased Glutamatergic and Serotonergic Transmission in the Medial Prefrontal Cortex of the Rat. *Neuropsychopharmacology* 32, 2087–2097. <https://doi.org/10.1038/sj.npp.1301356>
- Mancini, M., Ghiglieri, V., Bageetta, V., Pendolino, V., Vannelli, A., Cacace, F., Mineo, D., Calabresi, P., Picconi, B., 2016. Memantine alters striatal plasticity inducing a shift of synaptic responses toward long-term depression. *Neuropharmacology* 101, 341–350. <https://doi.org/10.1016/j.neuropharm.2015.10.015>
- Matsunaga, S., Kishi, T., Iwata, N., 2015. Memantine monotherapy for Alzheimer's Disease: A systematic review and meta-analysis. *PLoS One* 10, e0123289. <https://doi.org/10.1371/journal.pone.0123289>
- Mechler, K., Häge, A., Schweinfurth, N., Glennon, J.C., Dijkhuizen, R.M., Murphy, D., Durston, S., Williams, S., Buitelaar, J.K., Banaschewski, T., Dittmann, R.W., TACTICS Consortium, 2017. Glutamatergic Agents in the Treatment of Compulsivity and Impulsivity in Child and Adolescent Psychiatry: a Systematic Review of the Literature. *Z. Kinder. Jugendpsychiatr. Psychother.* 1–18. <https://doi.org/10.1024/1422-4917/a000546>
- Moghaddam, B., Adams, B., Verma, A., Daly, D., 1997. Activation of Glutamatergic Neurotransmission by Ketamine: A Novel Step in the Pathway from NMDA Receptor Blockade to Dopaminergic and Cognitive Disruptions Associated with the Prefrontal Cortex. *J. Neurosci.* 17, 2921–2927.
- Monaghan, D.T., Yao, D., Cotman, C.W., 1985. L-[3H]Glutamate binds to kainate-, NMDA- and AMPA-sensitive binding sites: an autoradiographic analysis. *Brain Res.* 340, 378–383. [https://doi.org/10.1016/0006-8993\(85\)90936-9](https://doi.org/10.1016/0006-8993(85)90936-9)
- Montigny, C., Castellanos-Ryan, N., Whelan, R., Banaschewski, T., Barker, G.J., Büchel, C., Gallinat, J., Flor, H., Mann, K., Paillère-Martinot, M.L., Nees, F., Lathrop, M., Loth, E., Paus, T., Pausova, Z., Rietschel, M., Schumann, G., Smolka, M.N., Struve, M., Robbins, T.W., Garavan, H., Conrod, P.J., Consortium, I., 2013. A phenotypic structure and neural correlates of compulsive behaviors in adolescents. *PLoS One* 8, e80151. <https://doi.org/10.1371/journal.pone.0080151>
- Naaijen, J., Lythgoe, D.J., Amiri, H., Buitelaar, J.K., Glennon, J.C., 2015. Fronto-striatal glutamatergic compounds in compulsive and impulsive syndromes: A review of magnetic resonance spectroscopy studies. *Neurosci. Biobehav. Rev.* 52, 74–88. <https://doi.org/10.1016/j.neubiorev.2015.02.009>
- Paasonen, J., Stenroos, P., Salo, R.A., Kiviniemi, V., Gröhn, O., 2018. Functional connectivity under six anesthesia protocols and the awake condition in rat brain. *Neuroimage* 172, 9–20. <https://doi.org/10.1016/j.neuroimage.2018.01.014>
- Paxinos, G., Watson, C., 2005. *The Rat Brain in Stereotaxic Coordinates - The new coronal set.* Academic Press.
- Pittenger, C., Bloch, M.H., Williams, K., 2011. Glutamate abnormalities in obsessive compulsive disorder: Neurobiology, pathophysiology, and treatment. *Pharmacol. Ther.* 132, 314–332. <https://doi.org/10.1016/j.pharmthera.2011.09.006>
- R Core Team, 2014. *R: A language and environment for statistical computing.*
- Rammes, G., Danysz, W., Parsons, C.G., 2008. Pharmacodynamics of memantine: an update. *Curr. Neuropharmacol.* 6, 55–78. <https://doi.org/10.2174/157015908783769671>
- Roelofs, T.J.M., Verharen, J.P.H., van Tilborg, G.A.F., Boekhoudt, L., van der Toorn, A., de Jong, J.W., Luijendijk, M.C.M., Otte, W.M., Adan, R.A.H., Dijkhuizen, R.M., 2017. A novel approach to map induced activation of neuronal networks using chemogenetics and functional neuroimaging in rats: A proof-of-concept study on the mesocorticolimbic system. *Neuroimage* 156, 109–118. <https://doi.org/10.1016/j.neuroimage.2017.05.021>
- Seeman, P., Caruso, C., Lasaga, M., 2008. Memantine agonist action at dopamine D2High receptors. *Synapse* 62, 149–153. <https://doi.org/10.1002/syn.20472>
- Sekar, S., Jonckers, E., Verhoye, M., Willems, R., Veraart, J., Van Audekerke, J., Couto, J., Giugliano, M., Wuyts, K., Dedeurwaerdere, S., Sijbers, J., Mackie, C., Ver Donck, L., Steckler, T., Van Der Linden, A., 2013. Subchronic memantine induced concurrent functional disconnectivity and altered ultra-structural tissue integrity in the rodent brain: revealed by multimodal MRI. *Psychopharmacology (Berl.)* 227, 479–491. <https://doi.org/10.1007/s00213-013-2966-3>
- Sengupta, P., 2013. *The Laboratory Rat: Relating Its Age With Human's.* Int. J. Prev. Med. 4, 624–630.
- Sesack, S.R., Carr, D.B., Omelchenko, N., Pinto, A., 2003. Anatomical Substrates for Glutamate-Dopamine Interactions: Evidence for Specificity of Connections and Extrasynaptic Actions. *Ann. N. Y. Acad. Sci.* 1003, 36–52. <https://doi.org/10.1196/annals.1300.066>
- Smith, S.M., 2002. Fast robust automated brain extraction. *Hum. Brain Mapp.* 17, 143–155. <https://doi.org/10.1002/hbm.10062>
- Song, C., Qu, Z., Blumm, N., Barabási, A.-L., 2010. Limits of Predictability in Human Mobility. *Science (80-)*. 327, 1018–1021. <https://doi.org/10.1126/science.1177170>
- Straathof, M., Blezer, E.L.A., van Heijningen, C., Smelee, C.E., van der Toorn, A., Consortium Tactics, Buitelaar, J.K., Glennon, J.C., Otte, W.M., Dijkhuizen, R.M., 2020. Structural and functional MRI of altered brain development in a novel adolescent rat model of quipirole-induced compulsive checking behavior. *Eur. Neuropsychopharmacol.* 33, 58–70. <https://doi.org/10.1016/j.euroneuro.2020.02.004>
- Stuchlik, A., Radostová, D., Hatalova, H., Vales, K., Nekovarova, T., Koprivova, J., Svoboda, J., Horacek, J., 2016. Validity of

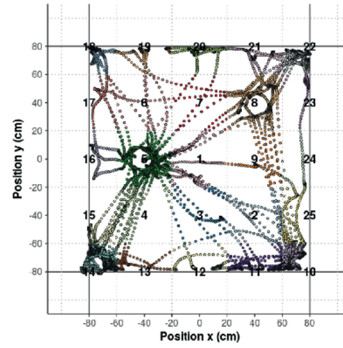
- quinpirole sensitization rat model of OCD: Linking evidence from animal and clinical studies. *Front. Behav. Neurosci.* 10, 209. <https://doi.org/10.3389/fnbeh.2016.00209>
- Szechtman, H., Sulis, W., Eilam, D., 1998. Quinpirole induces compulsive checking behavior in rats: A potential animal model of obsessive-compulsive disorder (OCD). *Behav. Neurosci.* 112, 1475–1485. <https://doi.org/10.1037/0735-7044.112.6.1475>
- Tax, C.M.W., Jeurissen, B., Vos, S.B., Viergever, M.A., Leemans, A., 2014. Recursive calibration of the fiber response function for spherical deconvolution of diffusion MRI data. *Neuroimage* 86, 67–80. <https://doi.org/10.1016/j.neuroimage.2013.07.067>
- Tournier, J.-D., Calamante, F., Connelly, A., 2012. MRtrix: Diffusion Tractography in crossing fiber regions. *Int. J. Imaging Syst. Technol.* 22, 53–66. <https://doi.org/10.1002/ima.22005>
- Tseng, K.Y., O'Donnell, P., 2004. Dopamine – Glutamate Interactions Controlling Prefrontal Cortical Pyramidal Cell Excitability Involve Multiple Signaling Mechanisms. *J. Neurosci.* 24, 5131–5139. <https://doi.org/10.1523/JNEUROSCI.1021-04.2004>
- Tucci, M.C., Dvorkin-Gheva, A., Sharma, R., Taji, L., Cheon, P., Peel, J., Kirk, A., Szechtman, H., 2014. Separate mechanisms for development and performance of compulsive checking in the quinpirole sensitization rat model of obsessive-compulsive disorder (OCD). *Psychopharmacology (Berl)*. 231, 3707–3718. <https://doi.org/10.1007/s00213-014-3505-6>
- van den Heuvel, O.A., van Wingen, G., Soriano-Mas, C., Alonso, P., Chamberlain, S.R., Nakamae, T., Denys, D., Goudriaan, A.E., Veltman, D.J., 2016. Brain circuitry of compulsivity. *Eur. Neuropsychopharmacol.* 26, 810–827. <https://doi.org/10.1016/j.euroneuro.2015.12.005>
- Williams, K., Brignell, A., Randall, M., Silove, N., Hazell, P., 2013. Selective serotonin reuptake inhibitors (SSRIs) for autism spectrum disorders (ASD). *Cochrane Database Syst. Rev.* CD994677. <https://doi.org/10.1002/14651858.CD004677.pub3>

Supplementary Material

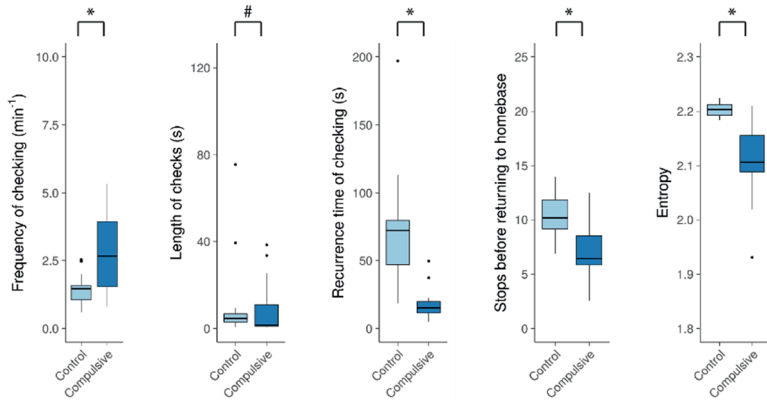
A) Compulsive



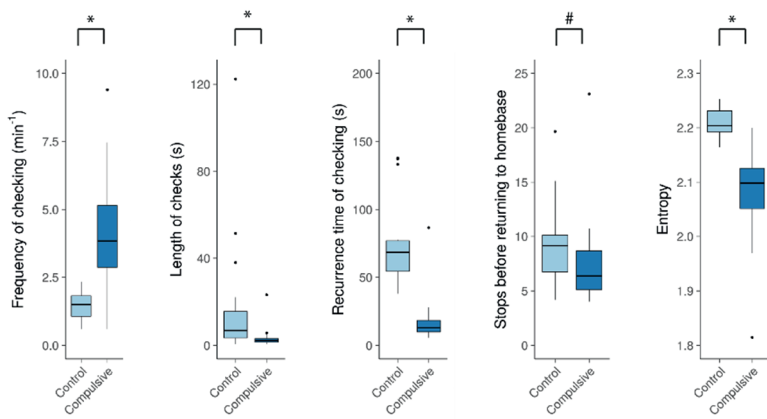
B) Control



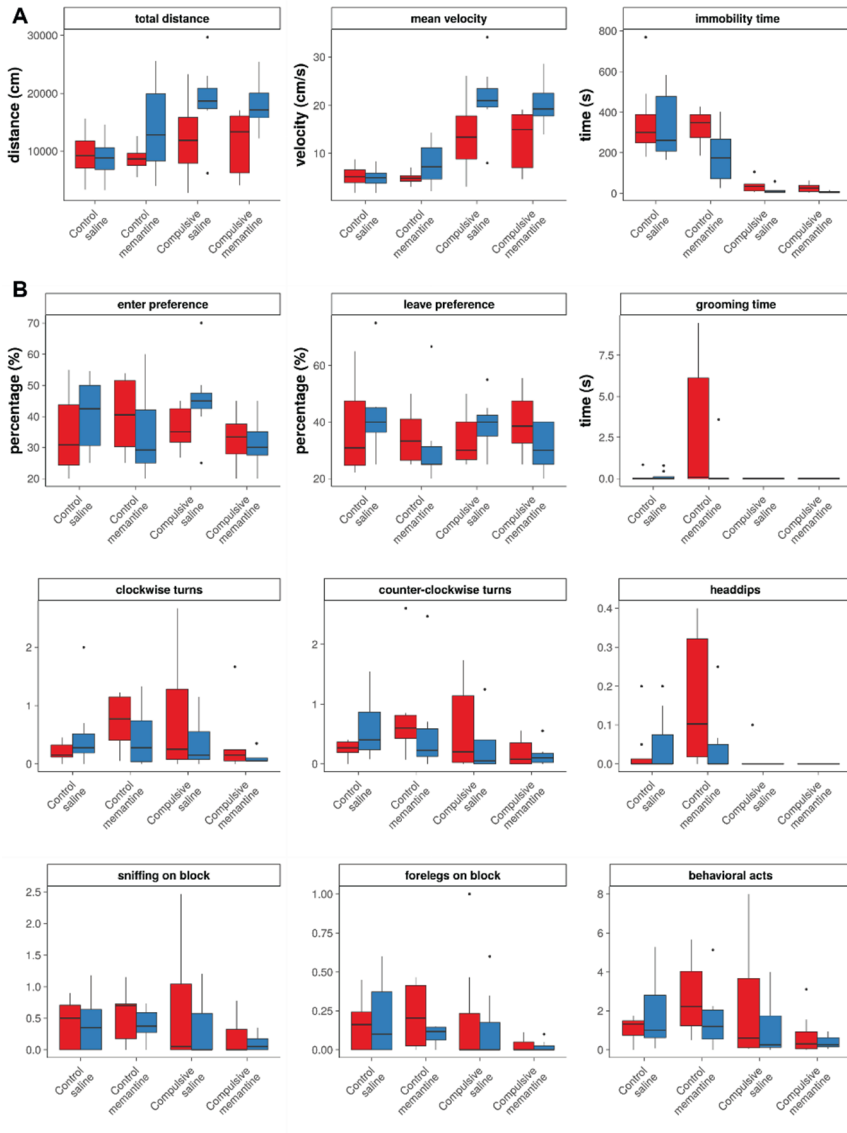
C) Study I



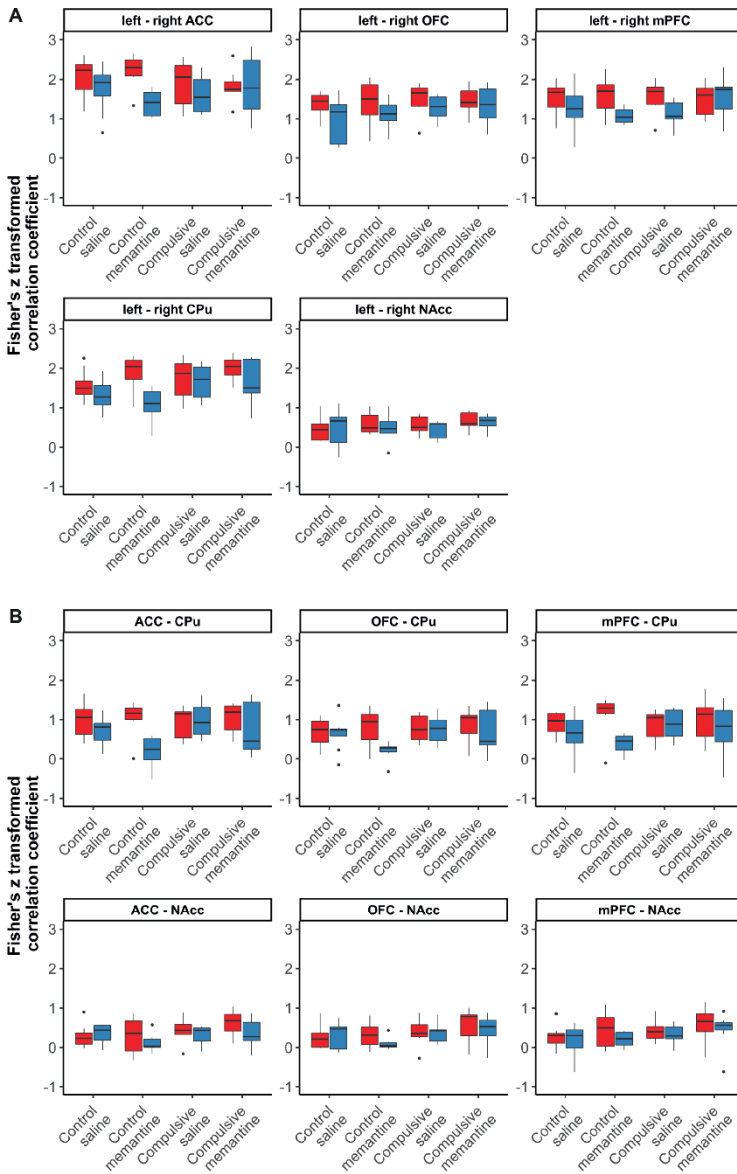
D) Study II



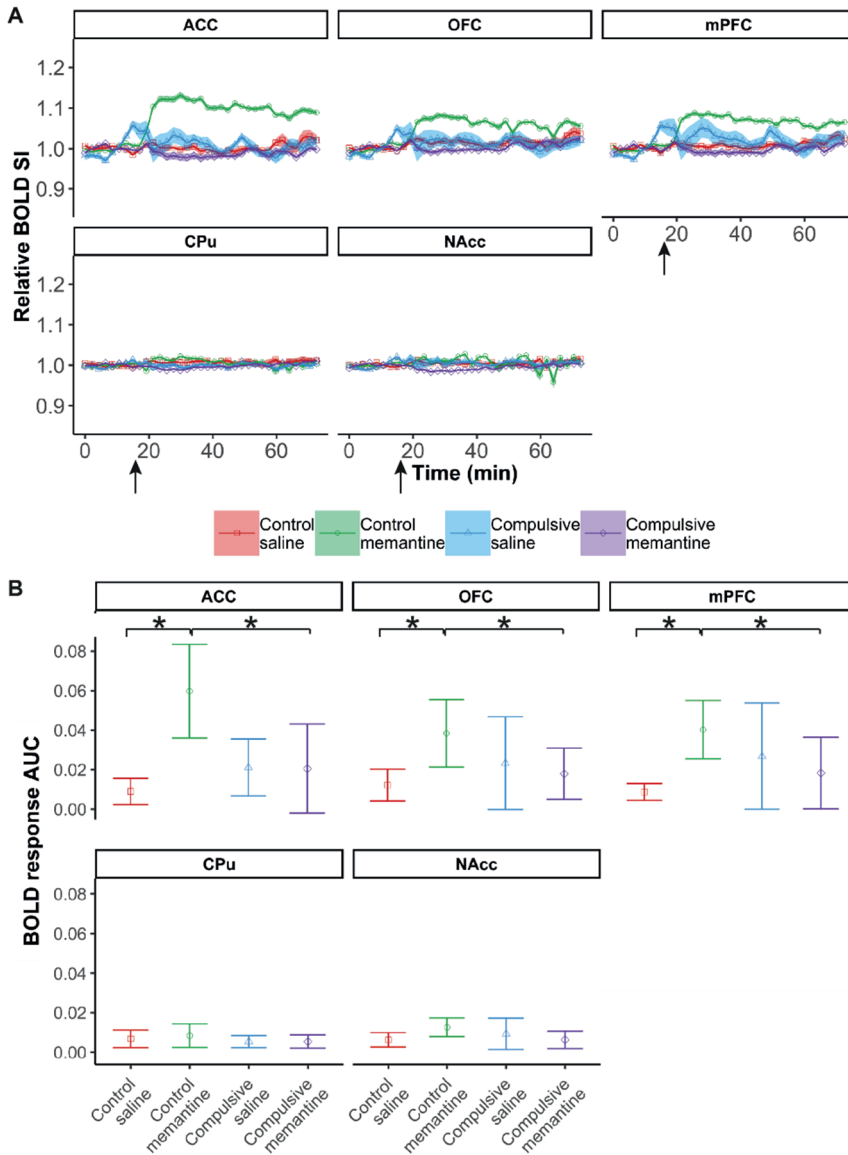
Supplementary Figure S1: Locomotor trajectories and behavioral metrics for control and compulsive adolescent rats before saline/memantine treatment. A representative locomotor trajectory of a compulsive (A) and a control adolescent rat (B) during the observation period after the 10th quinpirole/saline injection. The different zones on the open field are numbered, and locomotor trajectories are colored corresponding to these zones. We characterized behavior during the open field test for the last 15 minutes for compulsive rats and the full 30 minutes for control rats. Boxplots of the frequency of checking (number of visits at the home-base per minute (observed during 15 minutes for compulsive rats, and during 30 minutes for controls), length of checks (average time (s) spent at the home-base), recurrence time of checking (average time (s) before returning to the home-base), stops before returning to the home-base (average number of zones visited in between two visits of the home-base) and entropy (predictability of the visited zones) for control and compulsive rats prior to memantine/saline treatment in Study I (C, after the 10th quinpirole/saline injection: Compulsive: n=14; Control: n=14) and prior to memantine/saline injection in Study II (D, after the 12th quinpirole/saline injection: Compulsive: n=16; Control: n=16). * Corrected $p < 0.05$; # corrected $p < 0.1$. Error bars represent 1.5 times the interquartile range, and dots represent values that exceeded 1.5 times the interquartile range.



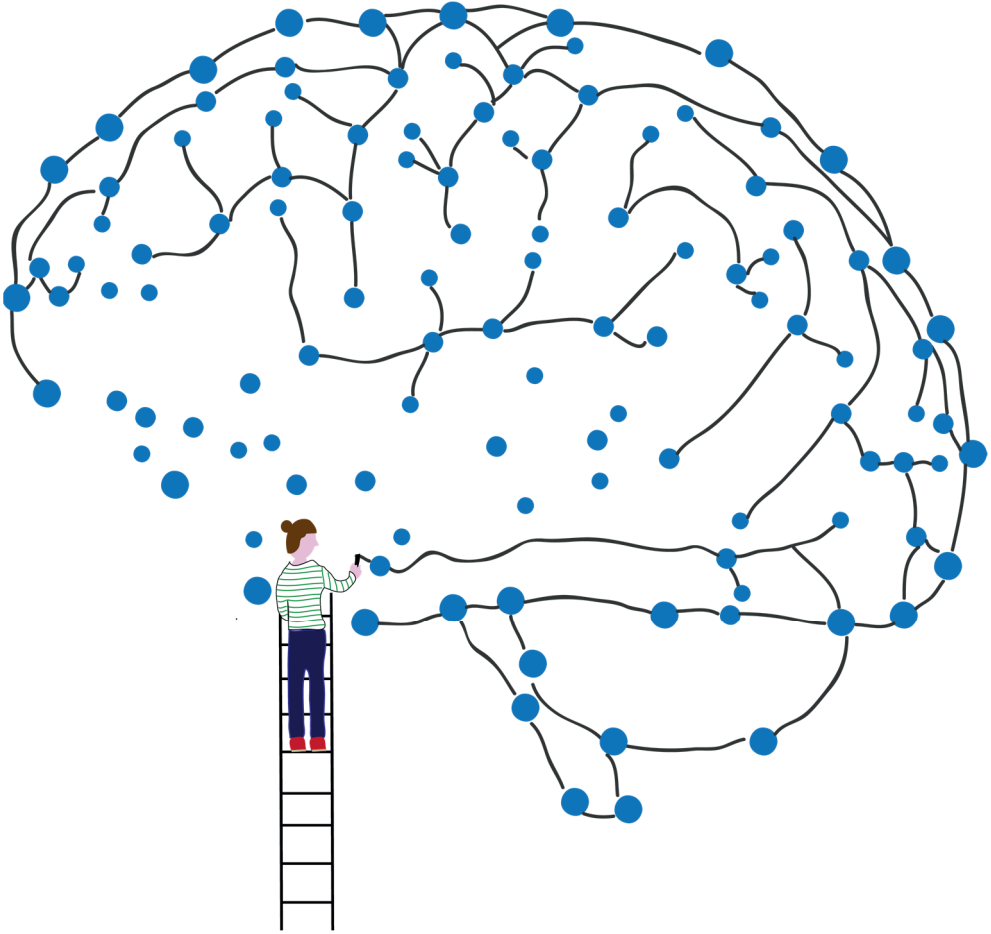
Supplementary Figure S2: Measures of hyperactivity and stereotypic behavior before and after saline/memantine treatment in control and compulsive rats. Hyperactivity measures (total distance moved, mean velocity and total immobility time (<0.01 cm movement per video frame)) (A) and stereotypic behaviors (enter preference (percentage of same enter direction of home-base zone), leave preference (percentage of same leave direction of home-base zone), average grooming time, number of clockwise turns, number of counter-clockwise turns, number of head dips, number of sniffs on block, number of placement of forelimbs on block, and total number of behavioral acts per home-base visit) (B) before (red) and after (blue) seven days of memantine/saline treatment. Error bars represent 1.5 times the interquartile range, and dots represent values that exceeded 1.5 times the interquartile range.



Supplementary Figure S3: Functional connectivity between individual brain regions in the frontostriatal system before and after saline/memantine treatment in control and compulsive rats. Bar graphs of interhemispheric (A) and intrahemispheric (B) functional connectivity (Fisher’s Z-transformed correlation coefficient) between individual sub-regions within the frontostriatal system before (red) and after (blue) seven days of daily saline/memantine treatment (Control + saline: n=8; Control + memantine: n=6; Compulsive + saline: n=7; Compulsive + memantine: n=7). Error bars represent 1.5 times the interquartile range, and dots represent values that exceeded 1.5 times the interquartile range.



Supplementary Figure S4: Brain activation directly after memantine/saline injection in control and compulsive rats in sub-regions of the frontostriatal system. The normalized BOLD signal intensity (SI) time-course is shown as averaged time series for the regions-of-interest, with the arrow indicating the time of memantine/saline injection (A). BOLD responses to memantine or saline injection quantified as AUC (relative positive BOLD SI change per second) (B). * Corrected $p < 0.05$. Shades in A represent the standard error. Error bars in B represent the standard deviation.



6

Differences in structural and functional networks between young adult and aged rat brains before and after stroke lesion simulations

Milou Straathof ^{a *}, Michel R.T. Sinke ^{a *}, Annette van der Toorn ^a, Paul L. Weerheim ^a, Willem M. Otte ^{a,b} & Rick M. Dijkhuizen ^a

** Shared first author*

^a Biomedical MR Imaging and Spectroscopy Group, Center for Image Sciences, University Medical Center Utrecht and Utrecht University, Utrecht, The Netherlands

^b Department of Pediatric Neurology, Brain Center Rudolf Magnus, University Medical Center Utrecht, Utrecht, The Netherlands

Neurobiology of Disease 2019; 126; 23-35.

Supplementary material is available at Neurobiology of Disease online.

Abstract

Neural network changes during aging may contribute to vulnerability and resilience to brain lesions in age-related neurological disorders, such as stroke. However, the relationship between age-related neural network features and stroke outcome is unknown. Therefore, we assessed structural and functional network status in young adult and aged rat brain and measured the effects of simulated stroke lesions.

Eleven rats underwent diffusion-weighted MRI and resting-state functional MRI at young adult age (post-natal day 88) and old age (between post-natal day 760 and 880). Structural and functional brain network features were calculated from graph-based network analysis. We performed three lesion simulations based on the brain injury pattern in frequently applied rodent stroke models, i.e., a small cortical lesion, a subcortical lesion, or a large cortical plus subcortical lesion, for which we computationally removed the involved network regions.

Global network characteristics, i.e., integration and segregation, were not significantly different between the two age groups. However, we detected local differences in structural and functional networks between young adult and old rats, mainly reflected by shifts of hub regions. Stroke lesion simulations induced significant global and local network changes, characterized by lower efficiency, and shifts of hub regions in structural and functional networks, which was most evident after a large cortical plus subcortical lesion. Functional and structural hub region shifts after lesion simulations differed between young adult and aged rats.

Our lesion simulation study demonstrates that age-dependent brain network status affects structural and functional network reorganization after stroke, particularly involving hub shifts, which may influence functional outcome. Computational lesion studies offer a cheap and simple alternative to empirical studies and can complement or guide more complicated experimental studies in animal models and patients.

Introduction

Stroke – i.e. a sudden loss of blood flow to the brain – is one of the main causes of long-term disability in adults, and affects almost 17 million people worldwide per year (Feigin et al., 2014). Despite the significant functional consequences, many patients show (partial) recovery of sensorimotor and cognitive functions during the weeks and months following stroke, which may be related to reorganization of surviving networks in the brain (Cramer, 2008; Grefkes and Fink, 2011; Jiang et al., 2013; Jones, 2017; Murphy and Corbett, 2009). Post-stroke brain remodeling occurs at different levels and locations, i.e. from micro- (e.g. synaptic plasticity) to macro-scale (e.g. cortical remapping) (Biernaskie and Corbett, 2001; Jones et al., 1996; Stroemer et al., 1995) and from peri- to contralesional sites (Cai et al., 2016; Crofts et al., 2011; Dacosta-Aguayo et al., 2014; Granziera et al., 2012; Gratton et al., 2012; Johansen-Berg et al., 2010; Schaechter et al., 2009), respectively. These insights have led to the notion that assessment of neural networks at whole-brain level is critical for optimal understanding of the functional consequences of stroke (Carter et al., 2012; Grefkes and Fink, 2011; Rehme and Grefkes, 2013).

Brain networks consist of spatially distributed regions that are connected and interacting with each other at micro-, meso- and macro-scales (Bassett and Sporns, 2017; Bullmore and Sporns, 2009a). Modern network science describes the brain as a collection of nodes (e.g., individual neurons, neuronal clusters, or functional brain regions) and edges or ties (e.g., structural, or functional connections between nodes). A healthy brain's network topology is described by an optimal balance between integration (i.e. global efficiency) and segregation (i.e. local specialization) of neural signaling, characterized by small-world organization, modularity and a 'rich club' of highly connected hub regions (Bassett and Bullmore, 2009; Bassett and Sporns, 2017; Bullmore and Sporns, 2009a; Sporns, 2010). These topological characteristics have been found across species (M. P. van den Heuvel et al., 2016a, 2016b; van den Heuvel et al., 2015) and deviation from optimal organization has been observed in relation to aging, brain dysfunction and cerebral injury, including stroke (Bassett and Bullmore, 2009; Bullmore and Sporns, 2009a; Sporns, 2010; Stam, 2014; van Meer et al., 2012). Moreover, network changes during aging may contribute to vulnerability and resilience to brain lesions in age-related neurological disorders, such as stroke. However, the relationship between age-related neural network features and stroke is largely unknown. Systematic studies on this relationship in stroke patients are complicated and may be more

straightforwardly conducted in laboratory rodents that age relatively fast and can be scanned serially in a fairly short timeframe.

Experimental animal stroke studies are generally performed in young adult rodents, even though the risk and prevalence of human stroke is higher at older age. Recently, this age discrepancy between animal stroke models and human stroke patients has been put forward as one of the causes of poor bench-to-bedside translation (Dirnagl, 2016). The age at which stroke is induced is known to influence stroke outcome and response to therapies in experimental models (Liang et al., 2016; Herson and Traystman, 2014; Liu et al., 2009). In the current study, we aimed to identify differences in brain networks of young adult and aged rats as well as their susceptibility and resilience to stroke lesions. We used data from rats that were longitudinally scanned with MRI from early adulthood to old age. The imaging protocol included resting-state functional MRI (resting-state fMRI) and diffusion MRI, which allowed assessment of large-scale functional and structural neural network status under healthy conditions. We simulated lesions in brain areas that are typically affected in different rodent stroke models, i.e. cortical photothrombosis (Watson et al., 1985), short transient middle cerebral artery occlusion (MCAO), and permanent or long transient MCAO (Garcia et al., 1995; Li et al., 1995). In addition, we simulated lesions in a single hub region and in a single non-hub region to measure their effect on the global network characteristics. We chose regions that are normally not affected in the abovementioned stroke models. We hypothesized that local and global network characteristics alter in relation to lesion extent, and that this relationship differs between young adult and aged rats.

Materials and Methods

Animals

Twenty healthy male Wistar rats (Harlan, Horst, The Netherlands) were housed in groups of four rats per cage. The rats had *ad libitum* access to food and water, were housed with a light/dark cycle of 12 h (lights on at 7:00 AM), and temperature was controlled between 22 and 24 °C. All experiments were approved by the committee for Animal Experiments of the University Medical Center Utrecht, The Netherlands (protocol number 2010.I.10.228) and were performed in accordance with the guidelines of the European Communities council directive.

MRI was done at multiple time-points during the lifespan of the rats, until their natural death. We analyzed data from eleven animals that were scanned during early adulthood (postnatal day 88), i.e., comparable to the age of rats in most preclinical stroke studies, as well as at old age (postnatal day 760 or 880), i.e., representative of the age during which clinical stroke is prevalent. Scans from animals that died before this age were not included in the analyses.

MRI acquisition

MRI experiments were conducted on a 4.7T horizontal bore MR system. We used a homebuilt Helmholtz volume coil (90 mm diameter) and an inductively coupled surface coil (25 mm diameter) for signal excitation and detection, respectively. Rats were anesthetized with 4% isoflurane and endotracheally intubated for mechanical ventilation (TOPO, Kent Scientific, Torrington, CT, USA) with 1-2% isoflurane in a mixture of air with 30% O₂ (55 breaths per minute). Rats were subsequently immobilized in a specially designed MR-compatible stereo-tactic holder, including earplugs and a tooth holder. During MRI, end-tidal CO₂ as well as blood oxygen saturation and heart rate were continuously monitored with a capnograph (Multinex 4200, Datascope Corporation, Paramus, NJ, USA) and pulse oximeter (8600V, Nonin Medical, Plymouth, MN, USA), respectively. Body temperature was maintained at 37.0 ± 0.5 °C.

For resting-state fMRI, T₂*-weighted blood oxygenation level-dependent (BOLD) images were acquired under 1.0% isoflurane anesthesia, with a ventilation-triggered single-shot 3D gradient-echo echo planar imaging (EPI) sequence (repetition time (TR) / echo time (TE) = 32 / 19 ms (effective TR = 1.024 s); 12° pulse angle; field-of-view (FOV) = 32 x 24 x 12 mm³; 64 x 48 x 32 acquisition matrix; 0.5 x 0.5 x 0.5 mm³ voxels; 600 BOLD images in approximately 10 minutes). Diffusion MRI was executed under 1.5-2.0% isoflurane with a 2D 5-shot EPI sequence (TR / TE = 1750 / 28.52 ms; 4 b₀ images, 4 b-values (650, 1285, 1919 and 2518 s/mm²); $\delta / \Delta = 5 / 10$ ms; 30 directions per b-value, three averages; 128 x 128 acquisition matrix; 0.195 x 0.195 mm² voxels; 19 1.0-mm slices). In addition, anatomical images were acquired with a 3D gradient-echo sequence (TR / TE = 6 / 2.25 ms; 40° flip angle; 4 averages; FOV = 40 x 25 x 20 mm³; 160 x 100 x 80 matrix; 0.25 x 0.25 x 0.25 mm³ voxels).

Image processing

Resting-state functional connectivity

Resting-state functional MR images were processed with FSL 5.0 (Jenkinson et al., 2012), unless otherwise stated. Preprocessing steps of the resting-state fMRI scans included removal of the first 10 images to reach a steady state, motion-correction with *MCFLIRT* (Jenkinson et al., 2002) and brain-extraction with *BET* (Smith, 2002). Motion-correction parameters were used as regressors for the resting-state signal (no linear detrending and global mean regression were performed). Low-frequency BOLD fluctuations were obtained by applying temporal filtering between 0.01 and 0.1 Hz in *AFNI* (Cox, 1996). We calculated Fisher's Z-transformed correlation coefficients to measure inter- and intrahemispheric functional connectivity between regions-of-interest (ROIs) (see below). Individual functional connectivity matrices were divided by their own mean to correct for individual differences in mean functional connectivity strength. This procedure is based on a normalization step in the analysis of structural networks described by van den Heuvel *et al.* (2010). They reported normalization by dividing all network edge values by the maximum network edge value. However, since many functional connectivity networks in our study were skewed towards lower correlation values with high value outliers (see Supplementary Figure 1), we normalized functional network values with the mean rather than the maximum value. For comparison, we performed a sensitivity analysis with the maximum value as normalization factor and data are presented in Supplementary Figure 2-5. Results were highly similar between mean and maximum normalization procedures.

Diffusion-based structural connectivity

Diffusion-weighted images were preprocessed with FSL 5.0 (Jenkinson et al., 2012) and MRtrix3 (J. D. Tournier et al., 2012). Motion and eddy current corrections were done with *dwi2preproc* (MRtrix3), which uses FSL tools (Andersson and Sotiropoulos, 2016). Calculation of diffusion parameters, i.e., fractional anisotropy (FA), mean diffusivity (MD), axial diffusivity (AD) and radial diffusivity (RD), was done with *dtifit* in FSL.

Further processing, tractography and connectome reconstruction were done in MRtrix3. We first determined multi-shell response functions for white matter (WM), gray matter (GM) and cerebral spinal fluid (CSF) using *dwi2response* and custom-made WM, GM, and CSF masks. Multi-shell multi-tissue constrained spherical deconvolution (CSD) (Jeurissen et al., 2014) was performed to generate WM, GM and CSF volume fraction maps,

and to obtain fiber orientation distribution (FOD) maps for WM, GM and CSF separately, of which the WM FOD map was used for tractography.

We performed CSD tractography using the iFOD2 algorithm (Tournier et al., 2010), with dynamic seeding over the WM FOD map, a step-size of 0.1 mm, an angle threshold of 45° and an FOD amplitude threshold of 0.2, thereby generating 1 million tracts over the entire brain. After whole-brain tractography we used *Spherical deconvolution Informed Filtering of Tractograms (SIFT)* to improve the accuracy of the reconstructed whole-brain connectome by fitting and optimizing tracts at whole-brain level to the underlying diffusion-weighted images, and by removing (i.e. filtering) inappropriate tracts from the connectome (Smith et al., 2015, 2013).

Whole-brain structural networks were constructed by matching the filtered tracts with ROIs in subject space. Two regions were considered connected if one or more tracts traversed – or had their endpoints in – both regions. The streamline count after SIFT was used as measure of structural connectivity strength.

Regions-of-interest

After preprocessing, resting-state fMRI and diffusion MRI images were linearly and non-linearly registered to a reference rat brain using *FLIRT* and *FNIRT* (Andersson et al., 2007b; Jenkinson and Smith, 2001), respectively. The reference rat brain was aligned with a custom-built 3D reconstruction of the Paxinos and Watson rat brain atlas (Majka et al., 2012; G. Paxinos and Watson, 2005). We included 88 cortical and subcortical regions from the atlas, covering most of the rat brain, with sufficient assurance of spatial alignment (i.e., inclusion of at least 8 voxels per ROI in the resting-state scans). Subsequently, all ROIs were back projected in subject space, where further analyses were performed.

Graph-based network analysis

To determine the effects of lesion simulations on global and local network characteristics of structural and functional brain networks, we used graph analyses (Bullmore and Sporns, 2009a). These graph analyses were performed on individual weighted networks, for resting-state fMRI and diffusion MRI networks separately. A weighted graph $G = (V, W)$ was constructed with V as the collection of all included regions N , and W as the collection of all edge weights w . Self-connections were excluded, and negative edge weights in the functional weighted graphs were set to 0. The Fisher's Z-transformed correlation coefficient was used as functional edge weight, while the SIFT-corrected streamline count was used as structural

edge weight. To characterize brain networks, we calculated global as well as local network parameters separately.

Table 1: Included regions-of-interest for resting-state fMRI and diffusion MRI analyses.

<i>Names (abbreviations) of Paxinos & Watson atlas regions</i>
Left and Right Agranular insular cortex dorsal part (AID)
Left and Right Agranular insular cortex posterior part (AIP)
Left and Right Agranular insular cortex ventral part (AIV)
Left and Right Primary auditory cortex (Au1)
Left and Right Secondary auditory cortex dorsal area (AuD)
Left and Right Secondary auditory cortex ventral area (AuV)
Left and Right Cingulate cortex area 1 (Cg1)
Left and Right Cingulate cortex area 2 (Cg2)
Left and Right Dysgranular insular cortex (DI)
Left and Right Dorsolateral entorhinal cortex (DLEnt)
Left and Right Ectorhinal cortex (Ect)
Left and Right Frontal cortex area 3 (Fr3)
Left and Right Frontal association cortex (FrA)
Left and Right Granular insular cortex (GI)
Left and Right Lateral orbital cortex (LO)
Left and Right Lateral parietal association cortex (LptA)
Left and Right Primary motor cortex (M1)
Left and Right Secondary motor cortex (M2)
Left and Right Medial parietal association cortex (MptA)
Left and Right Perirhinal cortex (Prh)
Left and Right Retrosplenial dorsal (RSD)
Left and Right Retrosplenial granular cortex a region (RSGa)
Left and Right Retrosplenial granular cortex b region (RSGb)
Left and Right Primary somatosensory cortex barrel field (S1BF)
Left and Right Primary somatosensory cortex dysgranular region (S1DZ)
Left and Right Primary somatosensory cortex forelimb region (S1FL)
Left and Right Primary somatosensory cortex hindlimb region (S1HL)
Left and Right Primary somatosensory cortex jaw region (S1J)
Left and Right Primary somatosensory cortex trunk region (S1Tr)
Left and Right Primary somatosensory cortex upper lib region (S1ULp)
Left and Right Secondary somatosensory cortex (S2)
Left and Right Temporal association cortex 1 (TeA)
Left and Right Primary visual cortex (V1)
Left and Right Primary visual cortex binocular area (V1B)
Left and Right Primary visual cortex monocular area (V1M)
Left and Right Secondary visual cortex lateral area (V2L)
Left and Right Secondary visual cortex mediolateral area (V2ML)
Left and Right Secondary visual cortex mediomedial area (V2MM)
Left and Right Ventral orbital cortex (VO)
Left and Right Thalamus (T)
Left and Right Globus Pallidum (GP)
Left and Right Caudate putamen (CPu)
Left and Right Accumbens nucleus (Acc)
Left and Right Hippocampus (Hipp)

Global parameters

To characterize the network topology we measured several global network parameters: the weighted-undirected clustering coefficient (C) (Fagiolo, 2007) as a measure of segregation, the weighted shortest path length (L) (Stam et al., 2009), as a measure of global efficiency or integration, and the small-worldness (Humphries and Gurney, 2008). All global parameters were calculated for structural and resting-state functional networks.

- **Clustering coefficient (C):** The weighted clustering coefficient provides a measure of the degree to which the nearest neighbors of each node are directly connected to each other. It sums the weights of the connections that exist between the nearest neighbors, divided by the potential maximum number of connections in triplets of nodes. We first calculated the weighted C for each node *i* in the entire graph:

$$C_i = \frac{\sum_{j \neq i} \sum_{h \neq (i,j)} w_{ij}^{\frac{1}{3}} w_{ih}^{\frac{1}{3}} w_{jh}^{\frac{1}{3}}}{d_i(d_i - 1)}$$

In which *d_i* is the number of connections of node *i*. This equation considers weights of all edges in a triplet and excludes weights that are not participating in a triplet. Subsequently, the weighted C was determined by taking the mean of the local clustering coefficients over all the nodes in the network:

$$C = N^{-1} \sum_{i=1}^N C_i$$

- **Weighted shortest path length (L):** The weighted shortest path length provides a measure of the average minimal distance between a node and all the other nodes in the network. This is measured as the inverse of the weights of the connections that have to be crossed to go from one node to another. We first calculated the weighted path length (*l_{ij}^w*) for each pair of nodes (*i* and *j*) in the entire graph using Dijkstra’s algorithm for weighted graphs (Dijkstra, 1959), by taking the minimum sum of the inverse weights (*d_{ij}*) to travel between node *i* and *j*:

$$l_{ij}^w = \min_{i \leftrightarrow j} \left(\text{sum}(d_{ij}) \right) \text{ and } d_{ij} = 1/w_{ij}$$

To handle disconnected edges, characterized by an infinite path length, we used the harmonic mean ($1/\infty \rightarrow 0$). The harmonic mean takes the reciprocal of the mean of the reciprocals (Newman, 2003):

$$L = \frac{N(N - 1)}{\sum_{i=1, j \neq i}^N \frac{1}{l_{ij}^w}}$$

- For each functional and structural network, C and L were normalized based on 10 randomly rewired surrogate networks (Maslov and Sneppen, 2002). The normalized weighted clustering (γ) and path length (λ) were defined as:

$$\gamma = \frac{C}{C_{random}} \quad \lambda = \frac{L}{L_{random}}$$

- **Small-worldness** was calculated as a measure of the optimal balance between segregation (clustering) and integration (path length), by γ/λ , according to Humphries and Gurney (Humphries and Gurney, 2008).

Local parameters

To investigate local (i.e. nodal) characteristics of the network, we identified most important nodes, i.e. the hubs, in the network, by quantifying the strength (weighted version of degree) (Barrat et al., 2004) and betweenness centrality (Brandes, 2001; Freeman, 1977) for each node separately.

- **Strength (S):** The connection strength of a node is the sum of all the edge weights connected to that node. This provides a measure of the total nodal connectivity (strength). We calculated the strength of each node in the entire graph:

$$S_i = \sum_{j=1}^N w_{ij}$$

- **Betweenness centrality (C_B):** The weighted betweenness centrality of a node provides a measure of the importance of the node in network connectivity. It measures the degree to which a node lies on the shortest path between two other nodes. We calculated the betweenness centrality for each node in the entire graph:

$$C_B(v) = \sum_{s \neq v \neq t \in V} \frac{\sigma_{st}(v)}{\sigma_{st}}$$

In this formula, $\sigma_{st}(v)$ is the number of shortest paths from s to t in which node v is partaking.

- **Hub nodes**, or hub regions, are regions in the brain with a central position, which play a crucial role in network communication. Hub regions can be defined by different metrics. They generally have a low clustering coefficient and shortest path length, and a high average strength and betweenness centrality (Bullmore and Sporns, 2009a; Sporns et al., 2007). Therefore, we determined the hubs based on these four characteristics, as previously described (van den Heuvel et al., 2010). First, we averaged these four characteristics for each region over all individual rats at each time-point separately. Subsequently, we determined which regions belonged to the top 20% for each of the four

characteristics separately (the regions with the 20% lowest clustering coefficients or path lengths, and/or the 20% highest strengths or betweenness centralities). When the node belonged to the top 20% for a category, the hub score for that category was one. Regions could get a hub score between 0 and 4, and hub regions were identified as regions with a hub score of 2 or higher.

Lesion simulations

To quantify effects of lesion simulations in young adult and aged rats, we simulated three different stroke lesion types that are typically observed in frequently applied rat stroke models (Fluri et al., 2015): small cortical lesions, subcortical lesions and large cortical plus subcortical lesions (see Figure 1). Lesions were simulated by elimination of edges from the nodes that were selected as part of the lesion (i.e., structural, and functional connections were set to 0). Subsequently, network parameters were calculated as described above, for each type of simulated stroke lesion in young adult and aged rats.

Small cortical lesion

A focal cortical lesion is a hallmark of the photothrombotic stroke model, which involves systemic injection of a photosensitive dye (Rose-Bengal) followed by focal illumination of the cortex through the intact skull (Watson et al., 1985). In the rat photothrombotic stroke model, lesion induction is often targeted to the forelimb area of the somatosensory cortex (S1FL). Therefore, we modeled photothrombotic stroke by eliminating S1FL nodes in our functional and structural networks.

Subcortical lesion

Probably the most frequently applied rat stroke model involves unilateral occlusion of the middle cerebral artery (MCA) with an intraluminal filament (Longa et al., 1989). Short temporary (30-60 min) MCA occlusion usually results in subcortical damage in the caudate putamen (CPu), modeled in our study by eliminating the CPu node in functional and structural networks.

Large cortical plus subcortical lesion

Longer (60-120 min) or permanent MCA occlusion induces extensive cortical and subcortical damage. We simulated these large lesions by eliminating the CPu node and nodes representing all sub-regions of the primary somatosensory cortex (S1) (i.e., the forelimb region (S1FL) and hindlimb region (S1HL), jaw region (S1J), upper lip region (S1ULp), barrel

field region (S1BF), trunk region (S1Tr) and the dysgranular zone of S1 (S1DZ)), the secondary somatosensory cortex (S2), and the insular cortex (i.e., AID, AIP, AIV, DI and GI).

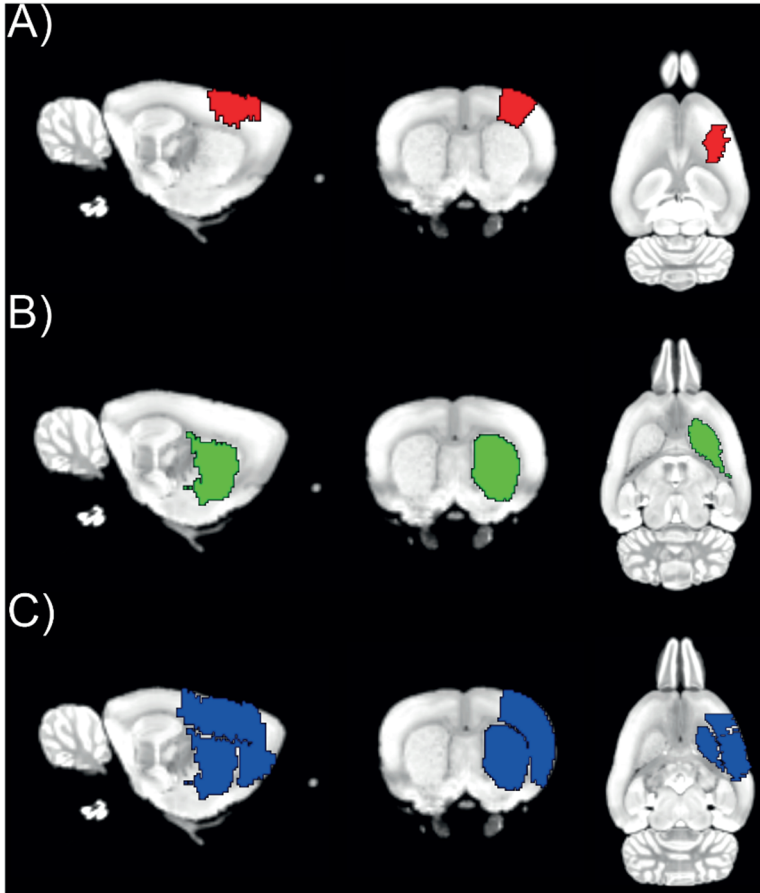


Figure 1. Lesion simulations. Regions overlaid on a sagittal (left), coronal (middle) and transversal (right) rat brain slice indicate typical lesion areas after cortical photothrombotic stroke (A (red)), and short (B (green)) or long (C (blue)) middle cerebral artery occlusion. Simulated lesion areas involved multiple slices throughout the brain but are here displayed on a single slice in each plane for illustration purposes.

Lesions in a single hub or non-hub region

We simulated lesions in two additional areas: (1) the right hippocampus, a hub region in both structural and functional networks in young adult and aged rats, and (2) the right medial parietal association cortex, a non-hub region in all networks.

Statistical analyses

To statistically determine whether global and local network characteristics differed between healthy young adult and aged rats, we performed paired t-testing for each global and nodal parameter. Because local characteristics were determined for 88 regions-of-interest, we corrected the nodal analyses for multiple testing using a false-discovery rate (FDR) correction (Benjamini and Hochberg, 1995). Comparisons with p-values lower than 0.05 after FDR correction were considered statistically significantly different. To test for homotopic symmetrical hubs, i.e. whether homotopic regions in the left and right hemispheres both belonged to the hub regions, we calculated the Dice index (Yin and Yasuda, 2006) for homotopic hub regions in young adult and aged rats separately.

To assess the effect of simulated stroke lesions, we calculated the difference value for each global or nodal characteristic between the healthy condition and lesion simulation: $\text{value}_{\Delta} = \text{value}_{\text{lesioned network}} - \text{value}_{\text{healthy network}}$. To measure the effect of a lesion on network characteristics, we first tested whether the network parameters changed significantly compared to the healthy condition with a one sample t-test for each simulated lesion type at each age separately. In addition, we compared the effects of different stroke lesion simulations on the network parameters with an ANOVA for each age separately. Secondly, we evaluated for each simulated lesion type, whether the lesion-induced change in network parameters differed between young adult and aged rats using a paired t-test. In addition, we calculated the Dice index for the hub regions in structural and functional networks before (healthy condition) and after each type of simulated lesion for young adult and aged rats separately.

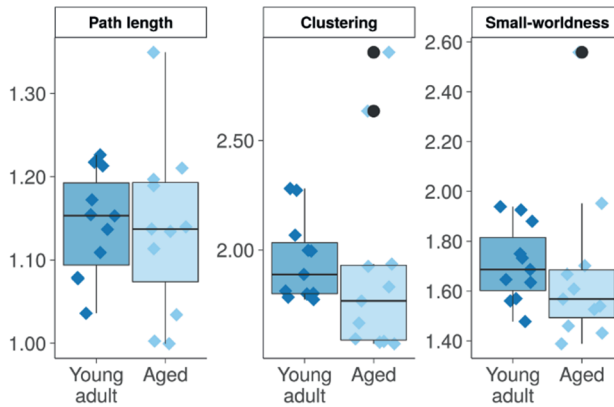
We constructed 95% confidence intervals for the Dice indices by means of bootstrapping. This involves repeated calculation of the Dice indices on 10.000 resampled sets, with replacement (Bland and Altman, 2015). Subsequently, we used bootstrapping to construct 95% confidence interval of delta Dice indices. To test whether the homotopic organization of hubs, as well as hub shifts after the simulated lesions, were significantly different between young and old rats we determined p-values from the 95% confidence intervals (Altman and Bland, 2011).

Results

Stable global structural and functional network features between young adulthood and old age

Figure 2 shows quantitative results from the graph-based whole-brain network analyses of functional connectivity and structural tractography data from young adult and aged rats. For structural (Figure 2A) as well as resting-state functional networks (Figure 2B), we found no significant differences in global network measures, i.e., clustering coefficient, path length and small-worldness, between young adult and aged rats.

A) Global structural network



B) Global functional network

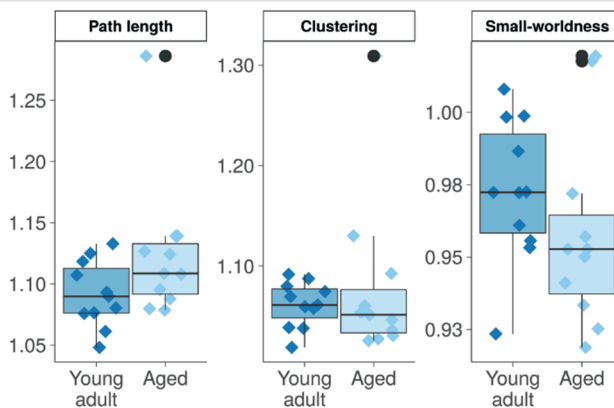


Figure 2: Global network parameters for whole-brain structural and resting-state functional networks in young adult and aged rats. Path length, clustering coefficient and small-worldness in (A) diffusion MRI-based whole-brain structural networks and (B) resting-state fMRI-based whole-brain functional networks in young adult (dark blue) and aged rats (light blue). Individual values are shown as diamonds with horizontal jitter for visualization purposes. Boxplots show median and inter-quartile range (IQR), whiskers representing 1.5 times the IQR, and dots representing outliers. Outliers are defined as values exceeding 1.5 times the IQR above the upper and below the lower quartile. Clustering = Clustering coefficient.

Higher nodal strength in structural network of aged rats

To investigate local network features in the rat brain, we calculated the nodal strength and betweenness centrality for each region-of-interest in the structural and resting-state functional networks. We found statistically significant differences in node strength between young adult rats and aged rats for several regions in the structural network, which are listed Table 2. In all these regions node strength – and betweenness centrality for the right frontal area 3, left cingulum area 2 and left lateral orbital cortex – was increased at old age, except for the left dysgranular insular cortex, which showed decreased node strength.

In contrast, there were no statistically significant differences in strength or betweenness centrality of the functional network nodes between young adult and aged rats.

Network hub nodes shift between young adulthood and old age

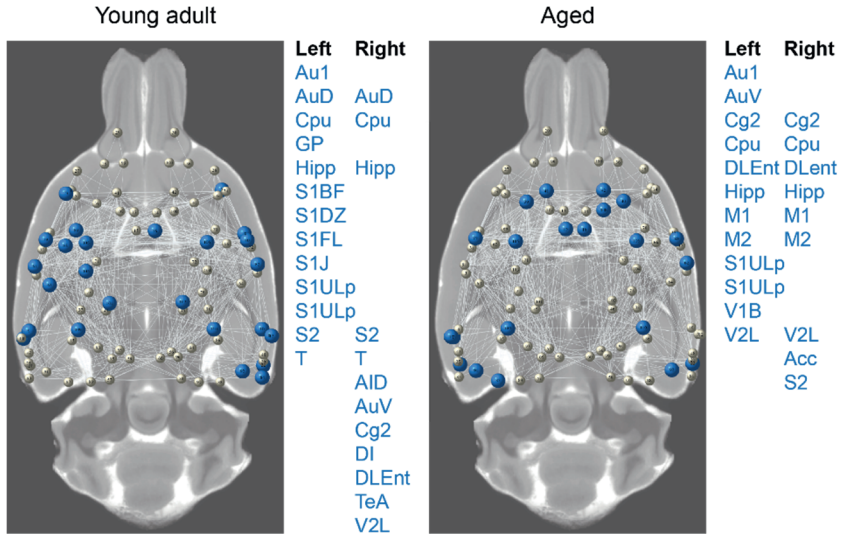
Hub nodes, i.e., the nodes with the highest degree of connectivity within the network, characterized by a low clustering coefficient and short path length, and a high strength and betweenness centrality, were found throughout the rat brain. The distribution of hub nodes in the structural brain network is shown in Figure 3A for young adult and aged rats. Consistent hub nodes in young adult and aged rats were, for example, the left and right caudate putamen and hippocampi. From young adulthood to old age, several regions (e.g., in the left somatosensory cortex) appeared to lose their hub status, whereas other regions (e.g., the left and right primary and secondary motor cortices) acquired a hub status. In aged rats, hubs tended to be more symmetrically distributed in bilateral homotopic areas (e.g., the left and right primary and secondary motor cortices, caudate putamen, and dorsolateral entorhinal cortices), and were located more medially as compared to young adult rats. The overlap in hub nodes in the young adult and aged structural network, expressed by the Dice coefficient was 0.29 (95% CI= 0.14-0.44). The Dice coefficient reflecting the overlap between hub regions in the left and right hemispheres was 0.61 (95% CI = 0.31 – 0.85) for aged rats,

compared to 0.32 (95% CI = 0.11 – 0.53) for young adult rats (Δ Dice = 0.30, 95% CI = -0.03 – 0.62, $p = 0.13$).

Table 2. Regions with significantly altered nodal network measures in aged rats compared to young adult rats.

<i>Region of interest</i>	<i>Nodal network feature</i>	<i>Δ Percentage</i>	<i>FDR corrected P-value</i>
Left Acc	Strength	80	< 0.01
Right Acc	Strength	100	< 0.01
Left AID	Strength	111	< 0.01
Right AID	Strength	111	< 0.01
Right AIP	Strength	88	0.02
Left AIV	Strength	167	< 0.001
Right AIV	Strength	184	< 0.001
Right AuV	Strength	75	0.04
Left Cg1	Strength	119	< 0.001
Right Cg1	Strength	85	< 0.01
Left Cg2	Betweenness	237	0.04
Left Cg2	Strength	65	< 0.01
Right Cg2	Strength	58	< 0.01
Left CPu	Strength	45	< 0.01
Right CPu	Strength	55	< 0.01
Left DI	Betweenness	-33	0.04
Right DI	Strength	88	< 0.01
Left Fr3	Strength	147	< 0.001
Right Fr3	Betweenness	84	0.02
Left FrA	Strength	1088	< 0.01
Left GP	Strength	43	0.02
Right GP	Strength	74	< 0.01
Left LO	Betweenness	172	0.03
Left LO	Strength	293	< 0.001
Right LO	Strength	193	< 0.001
Left M1	Strength	65	< 0.01
Right M1	Strength	105	< 0.001
Left M2	Strength	89	< 0.01
Right M2	Strength	125	< 0.01
Right MptA	Strength	82	0.02
Right Prh	Strength	50	0.02
Right RSGb	Strength	44	0.03
Right S1BFa	Strength	35	< 0.01
Right S1J	Strength	60	0.04
Left T	Strength	55	< 0.01
Right T	Strength	78	< 0.01
Left V1	Strength	60	0.02
Left V2ML	Strength	142	0.04
Right V2MM	Strength	102	0.04
Left VO	Strength	181	< 0.001
Right VO	Strength	170	< 0.001

A) Structural network



B) Functional network

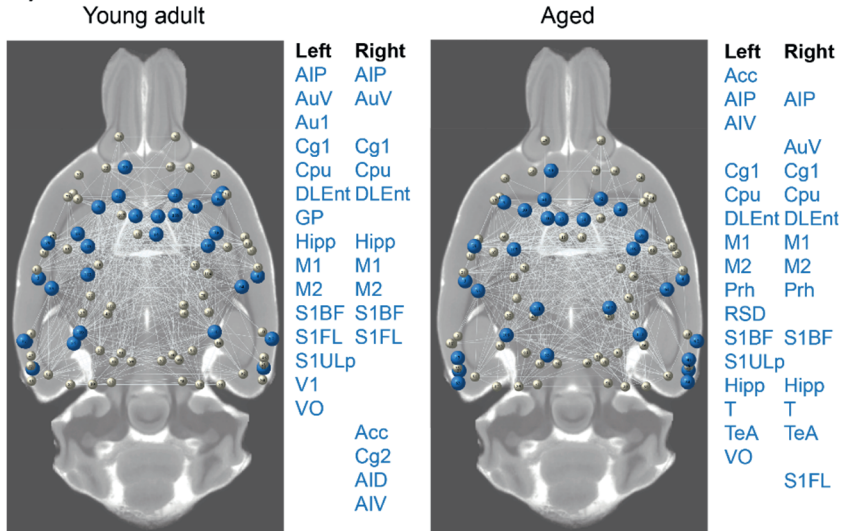


Figure 3: Hub regions in structural and functional whole-brain networks in young adult and aged rats. Hub regions in (A) structural networks and (B) resting-state functional networks, overlaid on an axial structural MR image of a rat brain slice, are displayed in the 3D network as large blue nodes, whereas the other (non-hub) regions are presented as small white nodes. Networks are shown for young adult (left) and aged rats (right). Hub regions are listed right from the maps.

The distribution of hub nodes in the resting-state functional network (Figure 3B) was different from that in the structural network. Nevertheless, consistent with the findings in the structural network, the left and right caudate putamen and hippocampi were also hub nodes in the functional networks of young adult and aged rats. There was a relatively higher density of functional network hub nodes in posterior and temporal regions (such as the temporal association area and perirhinal cortex) in aged rats as compared to young adult rats. The overlap in hub nodes in the young adult and aged functional network never reached 1 (mean Dice: 0.53; 95% CI= 0.37-0.68). Regions that lost their hub status in the resting-state functional network in aged rats included the right insular cortex, while other regions, such as the bilateral thalamus, acquired hub status. In line with the structural network hubs, functional network hub nodes in old rats tended to be more symmetrically distributed in homotopic areas in the left and right hemispheres. The Dice coefficient (reflecting the overlap between hub regions in the left and right hemisphere) was 0.61 (95% CI = 0.39 – 0.83) for old rats, compared to 0.53 (95% CI = 0.32 – 0.74) for young adult rats (Δ Dice = 0.08, 95% CI = -0.14 - 0.32, $p = 0.44$).

Lesion simulations

To determine the effect of stroke lesions on network parameters in young adult and old rats, we simulated the extent of network damage for different frequently applied stroke models (cortical photothrombosis, transient MCAO with only subcortical damage, and transient/permanent MCAO with cortical and subcortical damage). We calculated a delta-score for each network parameter as the change in the network parameter after lesion simulation as compared to the parameter for the healthy network.

Unilateral stroke lesion simulations affect global structural and functional network features at a whole-brain level

The effect of stroke lesion simulations on global structural network characteristics are shown in Figure 4A. Subtle, but statistically significant changes were measured after cortical (i.e., increased clustering ($p < 0.01$)) and subcortical stroke simulations (i.e., increased path length and decreased small-worldness ($p < 0.01$)), which were comparable between young adult and old aged rats. Subcortical plus cortical damage resulted in considerable increases in path length and clustering in both age groups ($p < 0.01$).

For whole-brain functional networks, stroke lesion simulations resulted in significant changes for all measured global network characteristics, i.e., increased path length, higher clustering and lower small-worldness ($p < 0.01$; Figure 4B). These changes were relatively small for the cortical and subcortical stroke simulations, and substantial for the large stroke lesions involving cortical plus subcortical regions. There were no significant differences in these global functional network changes between young adult and aged animals.

Additional analyses of lesion simulations in the right hippocampus (hub region) or right medial parietal association cortex (non-hub region) revealed subtle but significant effects on structural and functional networks, which were highly comparable with the effects of cortical stroke and sub-cortical stroke (Suppl. Figure 6).

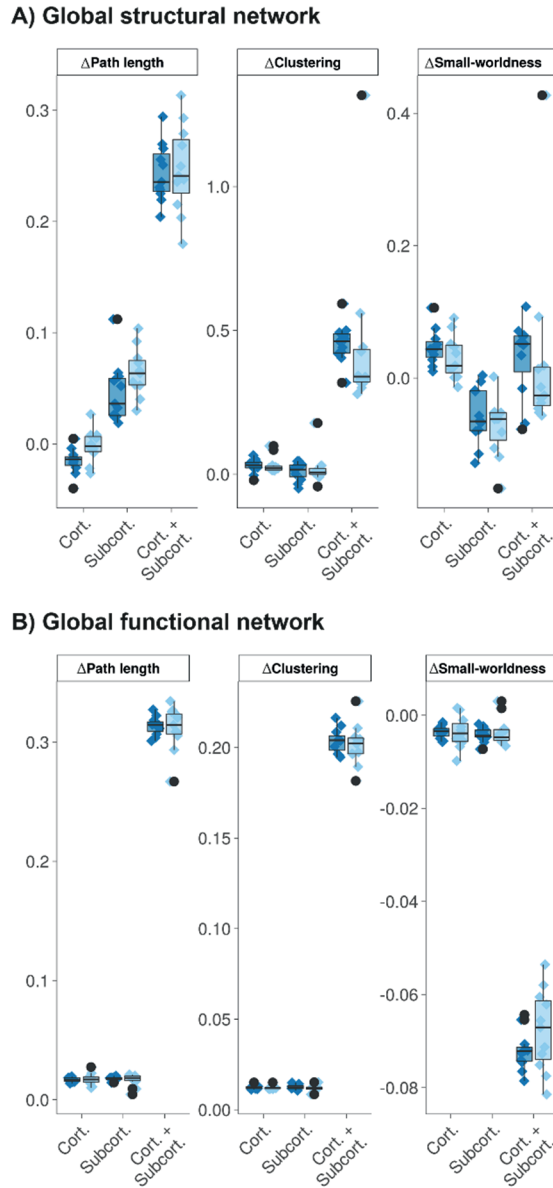


Figure 4: Effects of different stroke lesion simulations on global network measures in young adult and old rats. Changes in path length, clustering and small-worldness after stroke lesion simulation, calculated as metric delta values between the healthy control network and the network after stroke simulation, for (A) diffusion-based structural networks and (B) resting-state fMRI-based functional networks. Delta-scores were determined for different stroke lesion simulations, i.e., cort: cortical (phot thrombosis), subcort: subcortical (short transient

MCAO) and cort + subcort: cortical plus subcortical (long transient or permanent MCAO), for young adult rats (dark blue) and aged rats (light blue). Individual values are given as diamonds with horizontal jitter for visualization purposes. Boxplots show median and inter-quartile range (IQR), whiskers representing 1.5 times the IQR, and dots representing outliers. Outliers are defined as values exceeding 1.5 times the IQR above the upper and below the lower quartile.

Hub regions shift after stroke simulations

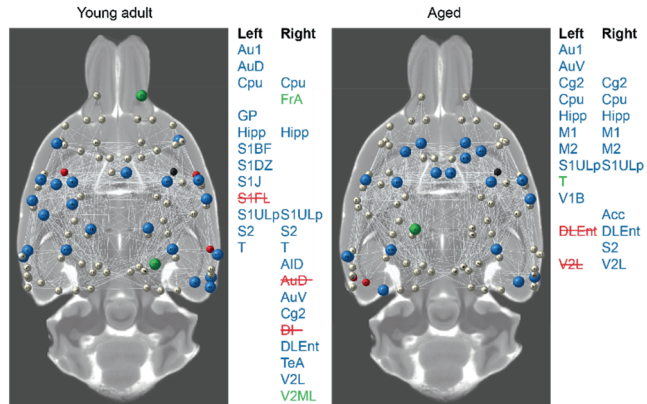
In addition to changes in global network features, stroke lesion simulations resulted in shifts of hub nodes in young adult and aged rats' structural and functional networks (Figures 5 and 6). These shifts were most apparent after simulation of a large cortical plus subcortical lesion. In structural networks, some regions acquired a hub status, whereas other regions lost their hub status after lesion simulations (Figure 5). In functional networks, regions mainly acquired a hub status after lesion simulations (Figure 6). The number of regions with shifted hub status was higher in structural networks than in functional networks, which was indicated by a lower Dice coefficient for the overlap in hub regions before and after stroke simulation (Table 3).

As can be observed in Figures 5 and 6, there were several local differences between young adult and old rats in the pattern of shifts in hub regions in structural and functional networks after stroke simulations. For example, in aged rats we found that the left, contralesional forelimb region of the primary somatosensory cortex acquired a functional network hub status after a unilateral lesion in subcortical or cortical plus subcortical tissue, which was not observed in young adult rats.

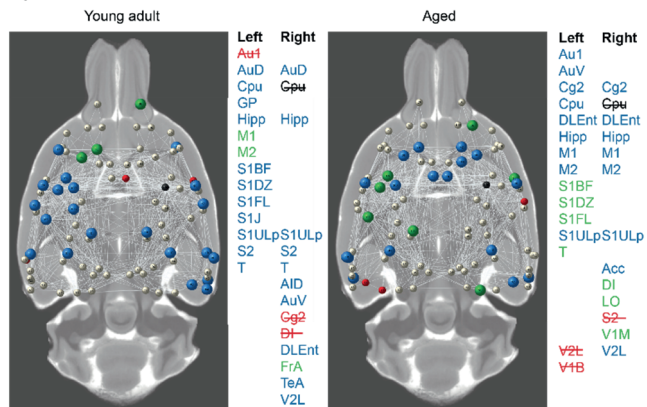
Table 3: Dice coefficients (95% CI) for the overlap in hub regions before and after stroke simulations, in structural and functional brain networks of young adult and old rats.

	Structural network		Functional network	
	<i>Young adult</i>	<i>Aged</i>	<i>Young adult</i>	<i>Aged</i>
Cortical stroke	0.78 (0.61-0.93)	0.86 (0.70-1.00)	0.90 (0.78-1.00)	0.93 (0.83-1.00)
Subcortical stroke	0.71 (0.54-0.88)	0.61 (0.42-0.79)	0.84 (0.70-0.96)	0.90 (0.79-1.00)
Cortical plus subcortical stroke	0.47 (0.30-0.64)	0.44 (0.26-0.62)	0.55 (0.39-0.71)	0.71 (0.55-0.85)

A) Small cortical lesion



B) Subcortical lesion



C) Large cortical and subcortical lesion

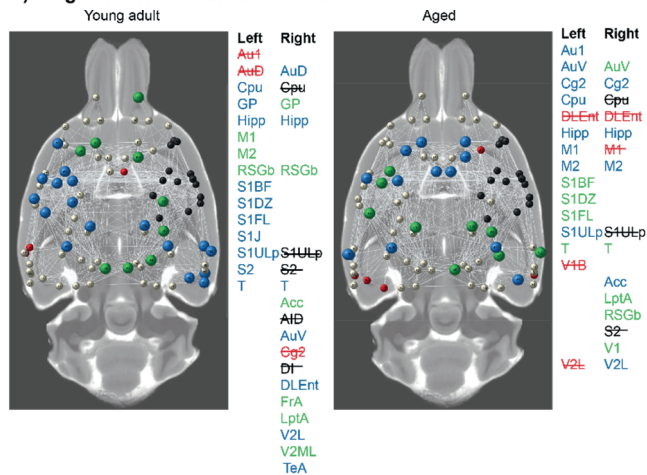
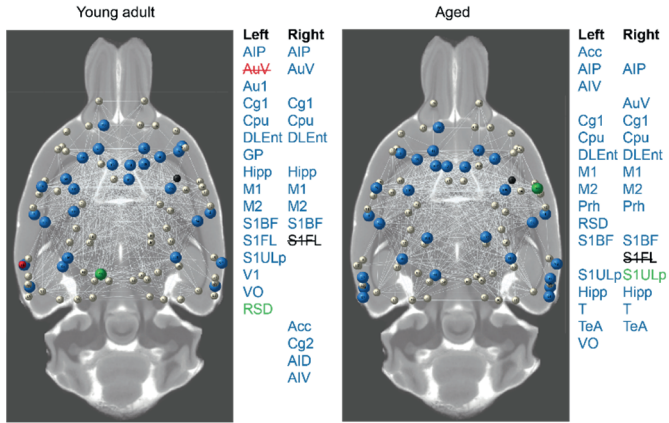


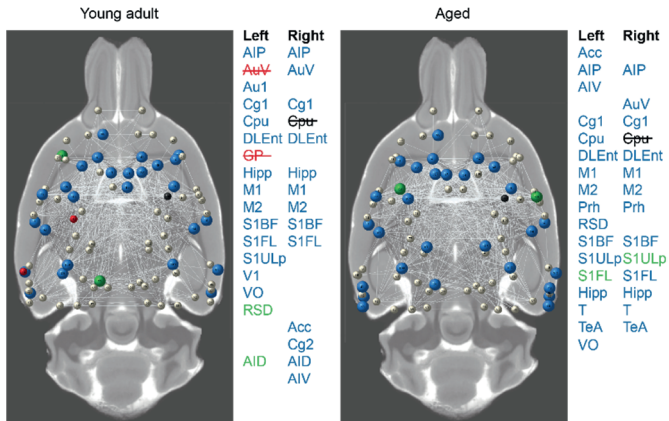
Figure 5: Hub shifts in structural whole-brain networks after unilateral stroke lesion simulations in young adult and aged rat brain. Hub shifts are displayed after unilateral (right-sided) stroke lesion simulation in (A) a small cortical area, (B) a subcortical area, and (C) a large cortical and subcortical area. Hub nodes, overlaid on an axial structural MR image of a rat brain slice, are displayed in the 3D network as large nodes, whereas other (non-hub) regions are represented as small (white) nodes. Regions with maintained hub station after stroke lesion simulation are shown as large blue nodes, whereas regions that acquired a hub status are presented as large green nodes. Regions that lost hub status are presented as small red nodes. Lesioned nodes are presented in dark-grey color. Networks are shown for young adult (left) and aged rats (right). Hub regions are listed right from the maps. Regions with acquired hub status are shown in green, and regions with lost hub status are crossed-out in red or black (lesioned nodes).

Figure 6: Hub shifts in functional whole-brain networks after unilateral stroke lesion simulations in young adult and aged rat brain. Hub shifts are displayed after unilateral (right-sided) stroke lesion simulation in (A) a small cortical area, (B) a subcortical area and (C) a large cortical and subcortical area. Hub nodes, overlaid on an axial structural MR image of a rat brain slice, are displayed in the 3D network as large nodes, whereas other (non-hub) regions are represented as small (white) nodes. Regions with maintained hub status after stroke lesion simulation are shown as large blue nodes, whereas regions that acquired a hub status are presented as large green nodes. Regions that lost hub status are presented as small red nodes. Lesioned nodes are presented in dark-grey color. Networks are shown for young adult (left) and aged rats (right). Hub regions are listed right from the maps. Regions with acquired hub status are shown in green, and regions with lost hub status are crossed-out in red or black (lesioned nodes).

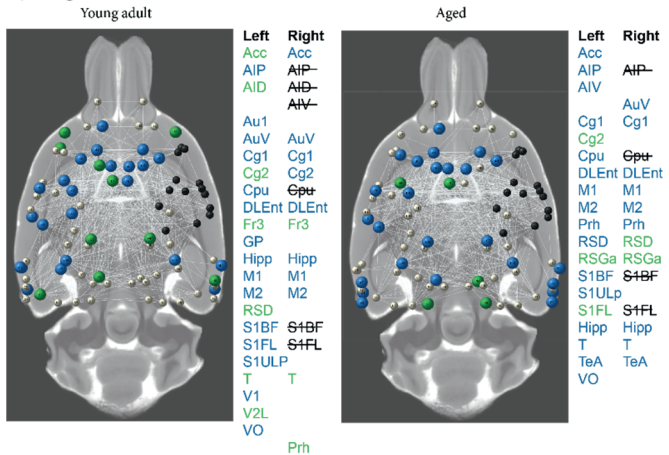
A) Small cortical lesion



B) Subcortical lesion



C) Large cortical and subcortical lesion



Discussion

In this study, we investigated whether the effects of simulated lesions – representing topographical profiles of different rodent stroke models – on structural and functional network organization in rat brain differed between young adulthood and old age. Overall, global network features were largely comparable, however, local differences in structural and functional networks were observed between young adult and aged rats, particularly expressed by shifts in hub regions in the brain. Unilateral stroke simulations induced global changes in whole-brain structural and functional network organization, which was most significant for the large stroke simulation, involving cortical and subcortical lesioning. Global network changes after stroke simulations were comparable between young adult and aged rats. On the other hand, lesion-induced regional changes in hub status, which were more pronounced in the structural than in the functional brain network, differed between young adult and aged rats.

Whole-brain structural and functional networks – effects of aging

The measured similarity of global network characteristics between healthy young adult and aged rats, as measured from the path length, clustering and small-worldness in the structural and functional networks, is in line with human data. Small-world topology has been demonstrated in structural brain networks of young and aged adult humans (Gong et al., 2009b; Zhu et al., 2012), and no aging effect was found for global network efficiency (Gong et al., 2009b). However, other studies reported lower global efficiency in younger individuals (Wu et al., 2012; Zhu et al., 2012). This discrepancy may be explained by the use of different age categories across studies. It has been demonstrated that global efficiency follows an inverted u-curve pattern between young and old age (Wu et al., 2012). Because the age groups in our study were at the extremities of this curve, we may have missed possible changes in global network characteristics that develop between the two time-points.

In functional networks, human resting-state fMRI studies have shown an increased minimum path length and clustering coefficient in older adults (Sala-Llonch et al., 2014). In addition, task-fMRI studies during memory encoding and recognition in healthy individuals demonstrated a similar increase in path length with aging (Wang et al., 2010). Although we did not find statistically significant aging effects on global networks, we did see a trend

towards a higher path length and lower small-worldness in the functional network of old rats, resembling the described effects of aging in humans.

While global network features were largely the same, we identified local differences in structural and functional brain networks between young adult and aged rats. Node strength increased for many regions, such as the bilateral primary and secondary motor cortices and caudate putamen, within the whole-brain structural network, which seems in contrast to reductions in structural connectivity during aging as observed in humans (Gong et al., 2009b). Loss of structural connectivity may be reflective of white matter degeneration in aging brains (Meier-Ruge et al., 1992; Salat et al., 2005). However, white matter degeneration may not be similarly prominent in aging rats. In fact, diffusion tensor imaging studies have revealed ongoing brain maturation in rats during adulthood (Mengler et al., 2014) with increasing fractional anisotropy in rodent white matter structures up to old age (Blockx et al., 2011). Furthermore, the mean diameter and volume density of myelinated fibers in the cortex are higher while the length density is lower, which may be explained by specific loss of thinner myelinated fibers, in aged as compared to younger adult rats (Zhang et al., 2009). These white matter differences can affect the diffusion-based tractography pattern and explain changes in node strengths that we observed between young adults and aged rats.

In addition to node strength differences in structural networks, we found shifts in hub regions from young adulthood to old age in structural and functional networks. Increased homotopical symmetry of hub regions in aged rats may be reflective of altered lateralization, which has also been reported for aged humans (Agcaoglu et al., 2015). Also, increasing homotopic connectivity with age, particularly between sensorimotor regions, has been found in a human resting-state fMRI study (Zuo et al., 2010). Moreover, similar to studies in human subjects, we observed a posterior shift in hub regions in the functional network, exemplified by hub status for the bilateral temporal association areas and perirhinal cortex in aged rats, although in humans this has been explained by lost hub status of frontal brain regions due to decreasing local network efficiency (Achard and Bullmore, 2007; Meunier et al., 2009).

Whole-brain structural and functional networks – effects of stroke lesion simulations

Computational lesion studies, as recently reviewed by Aerts et al. (Aerts et al., 2016), may substitute, complement or guide empirical studies in humans or animal models. Lesion

simulation studies can be applied to already existing data, and provide a simple, cheap and non-invasive alternative to complicated longitudinal *in vivo* lesion studies, thereby contributing to replacement, reduction and refinement of animal research (Balls et al., 1995).

In the current study we simulated unilateral stroke lesions, based on lesion topographies of three popular rat stroke models. Additionally, we simulated focal lesions in a single hub (i.e., right hippocampus) or non-hub region (i.e., right medial parietal association cortex) region. Significant changes in global network features were measured in whole-brain structural and functional networks. Results from our *in silico* lesion simulation study are largely in agreement with our previous *in vivo* resting-state fMRI study, in which we measured changes in the bilateral sensorimotor network after transient MCAO in young adult rats (van Meer et al., 2012). In both studies we found a longer path length and higher clustering coefficient in functional networks in response to stroke lesions in subcortical, or cortical plus subcortical tissue. The effects were considerably smaller when lesions were confined to only subcortical or cortical tissue, regardless of whether this was a hub (i.e., hippocampus or CPU) or a non-hub region (i.e., medial parietal association cortex), which reflects robustness of the functional and structural networks against relatively small focal injury. Apparently, this was not affected by age, because the results were similar in young adult and aged rats.

Our stroke lesion simulations also resulted in clear shifts of hub regions in the structural and functional networks. Network hub regions are believed to be key players in the outcome of brain disorders (Crossley et al., 2014; Stam, 2014). Hub damage may have severe consequences for network function, while hub shifts may contribute to network remodeling. In our study, the number of hub shifts was higher in structural than in functional networks, which we observed in young adult as well as old rats. We speculate that this relates to the dependency of functional connectivity on direct as well as indirect structural connections (Adachi et al., 2012; Honey et al., 2009), which may facilitate network resilience. Since we only removed nodes and their direct connections in our lesion simulations, diffusion-based structural networks, which in essence only contain direct connections, would be more severely affected.

The lesion-induced hub shifts were different between young adult and aged rats. In aged rats contralesional somatosensory areas acquired hub status after subcortical or cortical plus subcortical stroke lesion simulations, which was not observed in young adult rats. This may relate to enhanced neural activity or functional connectivity in the contralesional

hemisphere, which has been measured in stroke patients and animal models (Grefkes and Fink, 2014; van Meer et al., 2010a, 2010b). Why increased involvement of contralesional sensorimotor areas after unilateral stroke appeared more specifically in aged brain in our simulation study, and whether it may lead to worsening of functional outcome or contribute to functional recovery, remains to be elucidated. The local differences in structural and functional brain networks, including hub regions, between healthy young adult and aged rats, may have contributed to the different effects of lesion simulations between the two age groups. This underlines the critical role of age in the outcome of preclinical stroke studies in animal models, which often only involve young adult rodents, thereby limiting bench-to-bedside translation (Dirnagl, 2016).

It is important to realize that our computational simulation study only assessed direct effects of lesions on network status by elimination of nodes. Dynamic network responses, such as subsequent degeneration or regeneration, which can strongly depend on age (Betzel et al., 2014; Damoiseaux, 2017; Wang et al., 2015; Burke and Barnes, 2006; Niccoli and Partridge, 2012), were not accounted for. Another limitation is the use of anesthesia during resting-state fMRI, which is known to affect functional connectivity measurements (Paasonen et al., 2018). However, it might be argued that functional connectivity in anesthetized animals better reflects ‘resting state’ (i.e., baseline) connectivity than functional connectivity under awake conditions, which may be significantly affected by stress and motion. We used the same anesthesia protocol for all developmental stages, which enabled us to compare age effects under the same conditions. Nevertheless, future studies should look into (differences in) effects of anesthesia on network parameters across the lifespan and after stroke.

A limitation of diffusion-based tractography for structural connectivity measurement, is that white matter tracts are reconstructed from the underlying diffusion profiles, with limited power to resolve complex fiber configurations (e.g., crossing, bending, and fanning fibers). This can result in considerable amounts of false positive and false negative connections (E. Calabrese et al., 2015; Jeurissen et al., 2017; Sinke et al., 2018; Thomas et al., 2014). Nevertheless, diffusion-based tractography is currently the only method to map whole-brain structural connections *in vivo* at the macro-scale. For our study we used a state-of-the-art approach, combining CSD-based tractography – which partially accounts for crossing fibers – with whole-brain filtering of tracts, which has been shown to yield biologically accurate connectomes (Smith et al., 2015, 2013).

Future research involving longitudinal *in vivo* imaging studies and improved structural and functional connectivity reconstruction algorithms combined with advanced network analysis strategies may provide further insights in the causes and consequences of age-related differences in susceptibility and resilience to stroke injury. In the end, knowledge of the structural and functional network status of a stroke patient's brain, could guide selection of appropriate recovery-enhancing treatment strategies targeted at optimal engagement of a patient's intact neural circuitry.

In conclusion, our study showed that global structural and functional network features are largely similar in young adult and old aged rat brains and respond comparably to different types of stroke simulations. On the other hand, local network differences, particularly reflected by shifts in hub nodes, were identified between the brains of young adult and aged rats, before and after simulated stroke. These age-dependent neural network changes may play a critical role in the vulnerability and resilience to (stroke-induced) brain injury.

References

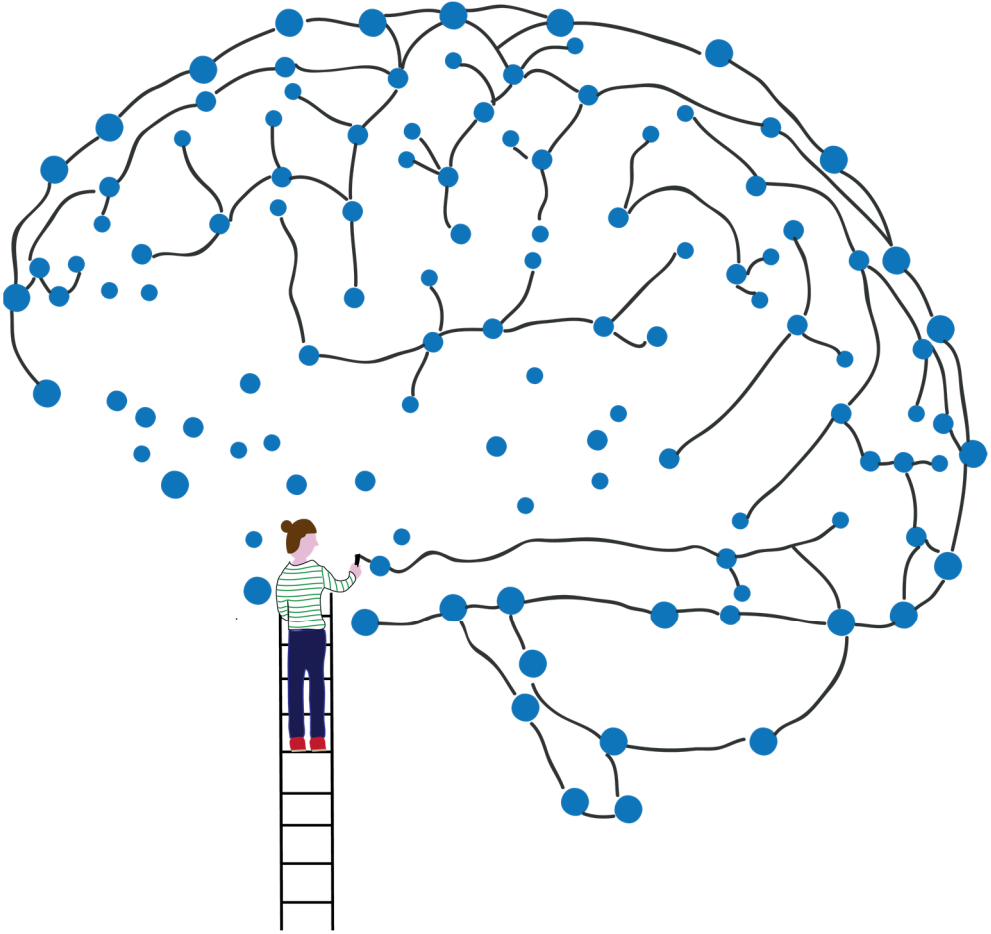
- Achard, S., Bullmore, E., 2007. Efficiency and cost of economical brain functional networks. *PLoS Comput. Biol.* 3, 0174–0183. <https://doi.org/10.1371/journal.pcbi.0030017>
- Adachi, Y., Osada, T., Sporns, O., Watanabe, T., Matsui, T., Miyamoto, K., Miyashita, Y., 2012. Functional Connectivity between Anatomically Unconnected Areas Is Shaped by Collective Network-Level Effects in the Macaque Cortex. *Cereb. Cortex* 22, 1586–1592. <https://doi.org/10.1093/cercor/bhr234>
- Aerts, H., Fias, W., Caeyenberghs, K., Marinazzo, D., 2016. Brain networks under attack: Robustness properties and the impact of lesions. *Brain* 139, 3063–3083. <https://doi.org/10.1093/brain/aww194>
- Agcaoglu, O., Miller, R., Mayer, A., Hugdahl, K., Calhoun, V., 2015. Lateralization of Resting State Networks and Relationship to Age and Gender. *Neuroimage* 104, 310–325. <https://doi.org/10.1016/j.neuroimage.2014.09.001>
- Altman, D.G., Bland, J.M., 2011. How to obtain the P value from a confidence interval. *BMJ* 343, d2304. <https://doi.org/10.1136/bmj.d2304>
- Andersson, J.L.R., Jenkinson, M., Smith, S., 2007. Non-linear registration, aka spatial normalisation. FMRIB Technical Report TR07JA2., Oxford Centre for Functional Magnetic Resonance Imaging of the Brain, Department of Clinical Neurology, Oxford University, Oxford, UK.
- Andersson, J.L.R., Sotiropoulos, S.N., 2016. An integrated approach to correction for off-resonance effects and subject movement in diffusion MR imaging. *Neuroimage* 125, 1063–1078. <https://doi.org/10.1016/j.neuroimage.2015.10.019>
- Balls, M., Goldberg, A., Fentem, J.H., Broadhead, C., Bursch, R., Festing, M., Frazier, J., Hendriksen, F., Jennings, M., van der Kamp, M., Morton, D., Rowan, A., Russell, C., Russell, W., Spielmann, H., Stephens, M., Stokes, W., Straughan, D., Yager, J., Zurlo, J., van Zuphen, B., 1995. The three Rs: the way forward. *Altern. to Lab. Anim. ATLA* 23, 838–866.
- Barrat, A., Barthélemy, M., Pastor-Satorras, R., Vespignani, A., 2004. The architecture of complex weighted networks. *Proc. Natl. Acad. Sci. U. S. A.* 101, 3747–3752. <https://doi.org/10.1073/pnas.0400087101>
- Bassett, D.S., Bullmore, E.T., 2009. Human brain networks in health and disease. *Curr. Opin. Neurology* 22, 340–347. <https://doi.org/10.1097/WCO.0b013e32832d93dd>
- Bassett, D.S., Sporns, O., 2017. Network neuroscience. *Nat. Neurosci.* 20, 353–364. <https://doi.org/10.1038/nn.4502>
- Benjamini, Y., Hochberg, Y., 1995. Controlling the false discovery rate: A practical and powerful approach to multiple testing. *J. R.*

- Stat. Soc. Ser. B 57, 289–300.
- Betzal, R.F., Byrge, L., He, Y., Goni, J., Zuo, X.N., Sporns, O., 2014. Changes in structural and functional connectivity among resting-state networks across the human lifespan. *Neuroimage* 102, 345–357. <https://doi.org/10.1016/j.neuroimage.2014.07.067>
- Biernaskie, J., Corbett, D., 2001. Enriched rehabilitative training promotes improved forelimb motor function and enhanced dendritic growth after focal ischemic injury. *J. Neurosci.* 21, 5272–5280. <https://doi.org/10.1523/JNEUROSCI.21-14-05272.2001>
- Bland, J.M., Altman, D.G., 2015. Statistics notes: Bootstrap resampling methods. *BMJ* 350, h2622. <https://doi.org/10.1136/bmj.h2622>
- Blockx, I., Van Camp, N., Verhoye, M., Boisgard, R., Dubois, A., Jegu, B., Jonckers, E., Raber, K., Siquier, K., Kuhnast, B., Dollé, F., Nguyen, H.P., Von Hörsten, S., Tavitian, B., Van der Linden, A., 2011. Genotype specific age related changes in a transgenic rat model of Huntington’s disease. *Neuroimage* 58, 1006–1016. <https://doi.org/10.1016/j.neuroimage.2011.07.007>
- Brandes, U., 2001. A Faster Algorithm for Betweenness Centrality. *J. Math. Sociol.* 25, 163–177.
- Bullmore, E., Sporns, O., 2009. Complex brain networks: Graph theoretical analysis of structural and functional systems. *Nat. Rev. Neurosci.* 10, 186–198. <https://doi.org/10.1038/nrn2575>
- Burke, S.N., Barnes, C.A., 2006. Neural plasticity in the ageing brain. *Nat. Rev. Neurosci.* 7, 30–40. <https://doi.org/10.1038/nrn1809>
- Cai, J., Ji, Q., Xin, R., Zhang, D., Na, X., Peng, R., Li, K., 2016. Contralateral cortical structural reorganization contributes to motor recovery after sub-cortical stroke: a longitudinal voxel-based morphometry study. *Front. Hum. Neurosci.* 10, 393. <https://doi.org/10.3389/fnhum.2016.00393>
- Calabrese, E., Badea, A., Cofer, G., Qi, Y., Johnson, G.A., 2015. A diffusion MRI tractography connectome of the mouse brain and comparison with neuronal tracer data. *Cereb. Cortex* 1–10. <https://doi.org/10.1093/cercor/bhv121>
- Carter, A.R., Shulman, G.L., Corbetta, M., 2012. Why use a connectivity-based approach to study stroke and recovery of function? *Neuroimage* 62, 2271–2280. <https://doi.org/10.1016/j.neuroimage.2012.02.070>
- Cox, R.W., 1996. AFNI: Software for Analysis and Visualization of Functional Magnetic Resonance Neuroimages. *Comput. Biomed Res.* 29, 162–173.
- Cramer, S.C., 2008. Repairing the human brain after stroke: I. Mechanisms of spontaneous recovery. *Ann. Neurol.* 63, 272–287. <https://doi.org/10.1002/ana.21393>
- Crofts, J.J., Higham, D.J., Bosnell, R., Jbabdi, S., Matthews, P.M., Behrens, T.E.J., Johansen-Berg, H., 2011. Network analysis detects changes in the contralateral hemisphere following stroke. *Neuroimage* 54, 161–169. <https://doi.org/10.1016/j.neuroimage.2010.08.032>
- Crossley, N.A., Mechelli, A., Scott, J., Carletti, F., Fox, P.T., McGuire, P., Bullmore, E.T., 2014. The hubs of the human connectome are generally implicated in the anatomy of brain disorders. *Brain* 137, 2382–2395. <https://doi.org/10.1093/brain/awu132>
- Dacosta-Aguayo, R., Graña, M., Fernández-Andújar, M., López-Cancio, E., Cáceres, C., Bargalló, N., Barrios, M., Clemente, I., Monserrat, P.T., Sas, M.A., Dávalos, A., Auer, T., Mataró, M., 2014. Structural integrity of the contralateral hemisphere predicts cognitive impairment in ischemic stroke at three months. *PLoS One* 9, e86119. <https://doi.org/10.1371/journal.pone.0086119>
- Damoiseaux, J.S., 2017. Effects of Aging on Functional and Structural Brain Connectivity. *Neuroimage* 160, 32–40. <https://doi.org/10.1016/j.neuroimage.2017.01.077>
- Dijkstra, E.W., 1959. A Note on Two Problems in Connexion with Graphs. *Numer. Math.* 1, 269–271. <https://doi.org/10.1007/BF01386390>
- Dirnagl, U., 2016. Thomas Willis lecture: Is translational stroke research broken, and if so, how can we fix it? *Stroke* 47, 2148–2153. <https://doi.org/10.1161/STROKEAHA.116.013244>
- Fagiolo, G., 2007. Clustering in Complex Directed Networks. *Phys. Rev. E* 76, 026107. <https://doi.org/10.1103/PhysRevE.76.026107>
- Feigin, V.L., Forouzanfar, M.H., Krishnamurthi, R., Mensah, G.A., Connor, M., Bennett, D.A., Moran, A.E., Sacco, R.L., Anderson, L., Truelsen, T., O’Donnell, M., Venketasubramanian, N., Barker-Collo, S., Lawes, C.M.M., Wang, W., Shinohara, Y., Witt, E., Ezzati, M., Naghavi, M., Murray, C., Global Burden of Diseases, Injuries, and R.F.S. 2010 (GBD 2010) and the G.S.E.G., 2014. Global and regional burden of stroke during 1990–2010: findings from the Global Burden of Disease Study 2010. *Lancet* 383, 245–54. [https://doi.org/10.1016/S0140-6736\(13\)61953-4](https://doi.org/10.1016/S0140-6736(13)61953-4)
- Fluri, F., Schuhmann, M.K., Kleinschnitz, C., 2015. Animal models of ischemic stroke and their application in clinical research. *Drug Des. Devel. Ther.* 9, 3445–3454. <https://doi.org/10.2147/DDDT.S56071>
- Freeman, L.C., 1977. A set of measures of centrality based on betweenness. *Sociometry* 40, 35–41.
- Garcia, J.H., Liu, K.-F., Ho, K.-L., 1995. Neuronal Necrosis After Middle Cerebral Artery Occlusion in Wistar Rats Progresses at Different Time Intervals in the Caudoputamen and the Cortex. *Stroke* 26, 636–643. <https://doi.org/https://doi.org/10.1161/01.STR.26.4.636>
- Gong, G., Rosa-Neto, P., Carbonell, F., Chen, Z.J., He, Y., Evans, A.C., 2009. Age- and gender-related differences in the cortical anatomical network. *J. Neurosci.* 29, 15684–15693. <https://doi.org/10.1523/JNEUROSCI.2308-09.2009>
- Granziera, C., Ay, H., Koniak, S.P., Krueger, G., Sorensen, A.G., 2012. Diffusion tensor imaging shows structural remodeling of stroke

- mirror region: Results from a pilot study. *Eur. Neurol.* 67, 370–376. <https://doi.org/10.1159/000336062>
- Gratton, C., Nomura, E.M., Pérez, F., D'Esposito, M., 2012. Focal brain lesions to critical locations cause widespread disruption of the modular organization of the brain. *J. Cogn. Neurosci.* 24, 1275–1285. https://doi.org/10.1162/jocn_a_00222
- Grefkes, C., Fink, G.R., 2014. Connectivity-based approaches in stroke and recovery of function. *Lancet Neurol.* 13, 206–216. [https://doi.org/10.1016/S1474-4422\(13\)70264-3](https://doi.org/10.1016/S1474-4422(13)70264-3)
- Grefkes, C., Fink, G.R., 2011. Reorganization of cerebral networks after stroke: New insights from neuroimaging with connectivity approaches. *Brain* 134, 1264–1276. <https://doi.org/10.1093/brain/awr033>
- Herson, P.S., Traystman, R.J., 2014. Animal models of stroke: translational potential at present and in 2050. *Future Neurol.* 9, 541–551. <https://doi.org/10.2217/fnl.14.44>
- Honey, C.J., Sporns, O., Cammoun, L., Gigandet, X., Thiran, J.P., Meuli, R., Hagmann, P., 2009. Predicting human resting-state functional connectivity from structural connectivity. *Proc. Natl. Acad. Sci. U. S. A.* 106, 2035–2040. <https://doi.org/10.1073/pnas.0811168106>
- Humphries, M.D., Gurney, K., 2008. Network ‘Small-World-Ness’: A Quantitative Method for Determining Canonical Network Equivalence. *PLoS One* 3, e0002051. <https://doi.org/10.1371/journal.pone.0002051>
- Jenkinson, M., Bannister, P., Brady, M., Smith, S., 2002. Improved optimization for the robust and accurate linear registration and motion correction of brain images. *Neuroimage* 17, 825–841. <https://doi.org/10.1006/nimg.2002.1132>
- Jenkinson, M., Beckmann, C.F., Behrens, T.E.J., Woolrich, M.W., Smith, S.M., 2012. Fsl. *Neuroimage* 62, 782–790. <https://doi.org/10.1016/j.neuroimage.2011.09.015>
- Jenkinson, M., Smith, S., 2001. A global optimisation method for robust affine registration of brain images. *Med. Image Anal.* 5, 143–156. [https://doi.org/10.1016/S1361-8415\(01\)00036-6](https://doi.org/10.1016/S1361-8415(01)00036-6)
- Jeurissen, B., Descoteaux, M., Mori, S., Leemans, A., 2017. Diffusion MRI fiber tractography of the brain. *NMR Biomed.* e3785. <https://doi.org/10.1002/nbm.3785>
- Jeurissen, B., Tournier, J.-D., Dhollander, T., Connelly, A., Sijbers, J., 2014. Multi-tissue constrained spherical deconvolution for improved analysis of multi-shell diffusion MRI data. *Neuroimage* 103, 411–426. <https://doi.org/10.1016/j.neuroimage.2014.07.061>
- Jiang, L., Xu, H., Yu, C., 2013. Brain Connectivity Plasticity in the Motor Network after Ischemic Stroke. *Neural Plast.* 2013, 1–11. <https://doi.org/10.1155/2013/924192>
- Johansen-Berg, H., Scholz, J., Stagg, C.J., 2010. Relevance of structural brain connectivity to learning and recovery from stroke. *Front. Syst. Neurosci.* 4, 146. <https://doi.org/10.3389/fnsys.2010.00146>
- Jones, T.A., 2017. Motor compensation and its effects on neural reorganization after stroke. *Nat. Rev. Neurosci.* 18, 267–280. <https://doi.org/10.1038/nrn.2017.26>
- Jones, T.A., Kleim, J.A., Greenough, W.T., 1996. Synaptogenesis and dendritic growth in the cortex opposite unilateral sensorimotor cortex damage in adult rats: A quantitative electron microscopic examination. *Brain Res.* 733, 142–148. [https://doi.org/10.1016/S0006-8993\(96\)00792-5](https://doi.org/10.1016/S0006-8993(96)00792-5)
- Li, Y., Chopp, M., Jiang, N., Zhang, Z.G., Zaloga, C., 1995. Induction of DNA fragmentation after 10 to 120 minutes of focal cerebral ischemia in rats. *Stroke* 26, 1252–1258. <https://doi.org/10.1161/01.STR.26.7.1252>
- Liang, A.C., Mandeville, E.T., Maki, T., Shindo, A., Som, A.T., Egawa, N., Itoh, K., Chuang, T.T., McNeish, J.D., Holder, J.C., Lok, J., Lo, E.H., Arai, K., 2016. Effects of aging on neural stem/progenitor cells and oligodendrocyte precursor cells after focal cerebral ischemia in spontaneously hypertensive rats. *Cell Transplant.* 25, 705–714. <https://doi.org/10.3727/096368916X690557>
- Liu, F., Yuan, R., Benashski, S.E., McCullough, L.D., 2009. Changes in experimental stroke outcome across the lifespan. *J. Cereb. Blood Flow Metab.* 29, 792–802. <https://doi.org/10.1038/jcbfm.2009.5>
- Longa, E.Z., Weinstein, P.R., Carlson, S., Cummins, R., 1989. Reversible Middle Cerebral Artery Occlusion Without Craniectomy in Rats. *Stroke* 20, 84–91. <https://doi.org/10.1161/01.STR.20.1.84>
- Majka, P., Kublik, E., Furga, G., Wójcik, D.K., 2012. Common atlas format and 3D brain atlas reconstructor: Infrastructure for constructing 3D brain atlases. *Neuroinformatics* 10, 181–197. <https://doi.org/10.1007/s12021-011-9138-6>
- Maslov, S., Sneppen, K., 2002. Specificity and Stability in Topology of Protein Networks. *Science* (80-.). 296, 910–914.
- Meier-Ruge, W., Ulrich, J., Brühlmann, M., Meier, E., 1992. Age-related white matter atrophy in the human brain. *Ann. N. Y. Acad. Sci.* 673, 260–269. <https://doi.org/10.1111/j.1749-6632.1992.tb27462.x>
- Mengler, L., Khmelinskii, A., Diedenhofen, M., Po, C., Staring, M., Lelieveldt, B.P.F., Hoehn, M., 2014. Brain maturation of the adolescent rat cortex and striatum: Changes in volume and myelination. *Neuroimage* 84, 35–44. <https://doi.org/10.1016/j.neuroimage.2013.08.034>
- Meunier, D., Achard, S., Morcom, A., Bullmore, E., 2009. Age-related changes in modular organization of human brain functional networks. *Neuroimage* 44, 715–723. <https://doi.org/10.1016/j.neuroimage.2008.09.062>
- Murphy, T.H., Corbett, D., 2009. Plasticity during stroke recovery: from synapse to behaviour. *Nat. Rev. Neurosci.* 10, 861–872.

- <https://doi.org/10.1038/nrn2735>
- Newman, M.E.J., 2003. The Structure and Function of Complex Networks. *Soc. Ind. Appl. Math. Rev.* 45, 167–256.
- Niccoli, T., Partridge, L., 2012. Ageing as a risk factor for disease. *Curr. Biol.* 22, R741–52. <https://doi.org/10.1016/j.cub.2012.07.024>
- Paasonen, J., Stenroos, P., Salo, R.A., Kiviniemi, V., Gröhn, O., 2018. Functional connectivity under six anesthesia protocols and the awake condition in rat brain. *Neuroimage* 172, 9–20. <https://doi.org/10.1016/j.neuroimage.2018.01.014>
- Paxinos, G., Watson, W., 2005. The rat brain in stereotaxic coordinates 5th edition. Elsevier Academic Press, Amsterdam.
- Rehme, A.K., Grefkes, C., 2013. Cerebral network disorders after stroke: Evidence from imaging-based connectivity analyses of active and resting brain states in humans. *J. Physiol.* 591, 17–31. <https://doi.org/10.1113/jphysiol.2012.243469>
- Sala-Llonch, R., Junqué, C., Arenaza-Urquijo, E.M., Vidal-Piñeiro, D., Valls-Pedret, C., Palacios, E.M., Domènech, S., Salvà, A., Bargalló, N., Bartrés-Faz, D., 2014. Changes in whole-brain functional networks and memory performance in aging. *Neurobiol. Aging* 35, 2193–2202. <https://doi.org/10.1016/j.neurobiolaging.2014.04.007>
- Salat, D.H., Tuch, D.S., Greve, D.N., Van Der Kouwe, A.J.W., Hevelone, N.D., Zaleta, A.K., Rosen, B.R., Fischl, B., Corkin, S., Diana Rosas, H., Dale, A.M., 2005. Age-related alterations in white matter microstructure measured by diffusion tensor imaging. *Neurobiol. Aging* 26, 1215–1227. <https://doi.org/10.1016/j.neurobiolaging.2004.09.017>
- Schaechter, J.D., Fricker, Z.P., Perdue, K.L., Helmer, K.G., Vangel, M.G., Greve, D.N., Makris, N., 2009. Microstructural status of ipsilesional and contralesional corticospinal tract correlates with motor skill in chronic stroke patients. *Hum. Brain Mapp.* 30, 3461–3474. <https://doi.org/10.1002/hbm.20770>
- Sinke, M.R.T., Otte, W.M., Christiaens, D., Schmitt, O., Leemans, A., van der Toorn, A., Sarabdjitsingh, R.A., Joëls, M., Dijkhuizen, R.M., 2018. Diffusion MRI-based cortical connectome reconstruction: dependency on tractography procedures and neuroanatomical characteristics. *Brain Struct. Funct.* 223, 2269–2285. <https://doi.org/10.1007/s00429-018-1628-y>
- Smith, R.E., Tournier, J.D., Calamante, F., Connelly, A., 2015. The effects of SIFT on the reproducibility and biological accuracy of the structural connectome. *Neuroimage* 104, 253–265. <https://doi.org/10.1016/j.neuroimage.2014.10.004>
- Smith, R.E., Tournier, J.D., Calamante, F., Connelly, A., 2013. SIFT: Spherical-deconvolution informed filtering of tractograms. *Neuroimage* 67, 298–312. <https://doi.org/10.1016/j.neuroimage.2012.11.049>
- Smith, S.M., 2002. Fast robust automated brain extraction. *Hum. Brain Mapp.* 17, 143–155. <https://doi.org/10.1002/hbm.10062>
- Sporns, O., 2010. *Networks of the Brain*. MIT Press.
- Sporns, O., Honey, C.J., Kötter, R., 2007. Identification and Classification of Hubs in Brain Networks. *PLoS One* 2, e1049. <https://doi.org/10.1371/journal.pone.0001049>
- Stam, C.J., 2014. Modern network science of neurological disorders. *Nat. Rev. Neurosci.* 15, 683–695. <https://doi.org/10.1038/nrn3801>
- Stam, C.J., Haan, W. De, Daffertshofer, A., Jones, B.F., Manshanden, I., Walsum, A.M.V.C. Van, Montez, T., Verbunt, J.P.A., Munck, J.C. De, Dijk, B.W. Van, Berendse, H.W., Scheltens, P., 2009. Graph theoretical analysis of magnetoencephalographic functional connectivity in Alzheimer’s disease. *Brain* 132, 213–224. <https://doi.org/10.1093/brain/awn262>
- Stroemer, R.P., Kent, T.A., Hulsebosch, C.E., 1995. Neocortical neural sprouting, synaptogenesis, and behavioral recovery after neocortical infarction in rats. *Stroke* 26, 2135–2144. <https://doi.org/10.1161/01.STR.26.11.2135>
- Thomas, C., Ye, F.Q., Irfanoglu, M.O., Modi, P., Saleem, K.S., Leopold, D.A., Pierpaoli, C., 2014. Anatomical accuracy of brain connections derived from diffusion MRI tractography is inherently limited. *Proc. Natl. Acad. Sci. U. S. A.* 111, 16574–16579. <https://doi.org/10.1073/pnas.1405672111>
- Tournier, J.D., Calamante, F., Connelly, A., 2012. MRtrix: Diffusion tractography in crossing fiber regions. *Int. J. Imaging Syst. Technol.* 22, 53–66. <https://doi.org/10.1002/ima.22005>
- Tournier, J.D., Calamante, F., Connelly, A., 2010. Improved probabilistic streamlines tractography by 2nd order integration over fibre orientation distributions. *Proc. Int. Soc. Magn. Reson. Med.* 1670.
- van den Heuvel, M.P., Bullmore, E.T., Sporns, O., 2016a. Comparative Connectomics. *Trends Cogn. Sci.* 20, 345–361. <https://doi.org/10.1016/j.tics.2016.03.001>
- van den Heuvel, M.P., de Reus, M.A., Feldman Barrett, L., Scholtens, L.H., Coopmans, F.M.T., Schmidt, R., Preuss, T.M., Rilling, J.K., Li, L., 2015. Comparison of Diffusion Tractography and Tract-Tracing Measures of Connectivity Strength in Rhesus Macaque Connectome. *Hum. Brain Mapp.* 36, 3064–3075. <https://doi.org/10.1002/hbm.22828>
- van den Heuvel, M.P., Mandl, R.C.W., Stam, C.J., Kahn, R.S., Hulshoff Pol, H.E., 2010. Aberrant Frontal and Temporal Complex Network Structure in Schizophrenia: A Graph Theoretical Analysis. *J. Neurosci.* 30, 15915–15926. <https://doi.org/10.1523/JNEUROSCI.2874-10.2010>
- van den Heuvel, M.P., Scholtens, L.H., de Reus, M.A., 2016b. Topological organization of connectivity strength in the rat connectome. *Brain Struct. Funct.* 221, 1719–1736. <https://doi.org/10.1007/s00429-015-0999-6>
- van Meer, M.P.A., Otte, W.M., van der Marel, K., Nijboer, C.H., Kavelaars, A., Berkelbach van der Sprenkel, J.W., Viergever, M.A., Dijkhuizen, R.M., 2012. Extent of bilateral neuronal network reorganization and functional recovery in relation to stroke severity. *J. Neurosci.* 32, 4495–4507. <https://doi.org/10.1523/JNEUROSCI.3662-11.2012>

- van Meer, M.P.A., van der Marel, K., Otte, W.M., Berkelbach van der Sprenkel, J.W., Dijkhuizen, R.M., 2010a. Correspondence between altered functional and structural connectivity in the contralesional sensorimotor cortex after unilateral stroke in rats: a combined resting-state functional MRI and manganese-enhanced MRI study. *J. Cereb. Blood Flow Metab.* 30, 1707–11. <https://doi.org/10.1038/jcbfm.2010.124>
- van Meer, M.P.A., van der Marel, K., Wang, K., Otte, W.M., el Bouazati, S., Roeling, T.A.P., Viergever, M.A., Berkelbach van der Sprenkel, J.W., Dijkhuizen, R.M., 2010b. Recovery of sensorimotor function after experimental stroke correlates with restoration of resting-state interhemispheric functional connectivity. *J. Neurosci.* 30, 3964–3972. <https://doi.org/10.1523/JNEUROSCI.5709-09.2010>
- Wang, L., Li, Y., Metzack, P., He, Y., Woodward, T.S., 2010. Age-related changes in topological patterns of large-scale brain functional networks during memory encoding and recognition. *Neuroimage* 50, 862–872. <https://doi.org/10.1016/j.neuroimage.2010.01.044>
- Wang, Z., Dai, Z., Gong, G., Zhou, C., He, Y., 2015. Understanding Structural-Functional Relationships in the Human Brain. *Neurosci.* 21, 290–305. <https://doi.org/10.1177/1073858414537560>
- Watson, B.D., Dietrich, W.D., Busto, R., Wachtel, M.S., Ginsberg, M.D., 1985. Induction of reproducible brain infarction by photochemically initiated thrombosis. *Ann. Neurol.* 17, 497–504. <https://doi.org/10.1002/ana.410170513>
- Wu, K., Taki, Y., Sato, K., Kinomura, S., Goto, R., Okada, K., Kawashima, R., He, Y., Evans, A.C., Fukuda, H., 2012. Age-related changes in topological organization of structural brain networks in healthy individuals. *Hum. Brain Mapp.* 33, 552–568. <https://doi.org/10.1002/hbm.21232>
- Yin, Y., Yasuda, K., 2006. Similarity coefficient methods applied to the cell formation problem: A taxonomy and review. *Int. J. Prod. Econ.* 101, 329–352. <https://doi.org/10.1016/j.ijpe.2005.01.014>
- Zhang, W., Yang, S., Li, C., Chen, L., Tang, Y., 2009. Stereological investigation of age-related changes of myelinated fibers in the rat cortex. *J. Neurosci. Res.* 87, 2872–2880. <https://doi.org/10.1002/jnr.22114>
- Zhu, W., Wen, W., He, Y., Xia, A., Anstey, K.J., Sachdev, P., 2012. Changing topological patterns in normal aging using large-scale structural networks. *Neurobiol. Aging* 33, 899–913. <https://doi.org/10.1016/j.neurobiolaging.2010.06.022>
- Zuo, X.-N., Kelly, C., Di Martino, A., Mennes, M., Margulies, D.S., Bangaru, S., Grzadzinski, R., Evans, A.C., Zang, Y., Castellanos, X., Milham, M.P., 2010. Growing together and growing apart: Regional and sex differences in the lifespan developmental trajectories of functional homotopy. *J. Neurosci.* 30, 15034–15043. <https://doi.org/10.1523/JNEUROSCI.2612-10.2010>



General discussion

The studies described in this thesis have provided insight into how MRI-based structural and functional connectivity are arranged and associated in the healthy and diseased brain. We assessed the relationship between structural and functional connectivity in the healthy rat brain in **Chapters 2 and 3**. In **Chapters 4, 5 and 6**, we investigated how changes in structural and functional connectivity during brain maturation and aging relate to the vulnerability to develop diseases during these specific periods of the life span. The results from this thesis demonstrate that: I) structural and functional connectivity in the brain are related, but distinct structure-function relationships exist across brain regions, hierarchical levels and non-linear components reflect the complexity of this relationship (**Chapters 2 and 3**); II) structural and functional connectivity in the rat brain change during maturation and aging (**Chapters 4 and 6**); and III) aging-related changes in structural and functional brain networks contribute to connectivity abnormalities seen in diseases that develop during maturation and aging, such as obsessive-compulsive disorder (OCD) and stroke (**Chapters 4-6**).

In the following paragraphs, I will specifically focus on the implications of these findings, possibilities for future research and methodological considerations of the used methods.

Structure-function relationship in the mammalian brain

The first aim of this thesis was to characterize the relationship between structural and functional connectivity in the rat brain. Although structural and functional connectivity are related, our results support the current view that the structure-function relationship is not one-to-one and more complex. The moderate correlation that we found between structural and functional connectivity indicates that functional connectivity is not directly explained by structural connectivity (Straathof et al., 2019) (**Chapters 2 and 3**). We showed that the moderate correlation may be due to distinct linear and non-linear structure-function relationships across the rat brain (**Chapters 2 and 3**), like in the mouse and human brain (Grandjean et al., 2017; Zimmermann et al., 2016), with high correspondence in primary unimodal somatosensory and motor regions, and low correspondence in secondary transmodal association areas (Vázquez-Rodríguez et al., 2019). This may be caused by increasing complexity from unimodal to transmodal regions, including more dynamic functional behavior and more parallel and less hierarchical processing in transmodal regions, resulting in weaker structure-function relationships.

In addition, the measured moderate linear correlation may also be explained by lack of association of weak structural connectivity with functional connectivity, which appears to correlate from a specific structural connectivity strength onwards, the structure-function tipping point, which we observed in human and rat brain (**Chapter 3**). I believe that these results indicate that simple linear whole-brain correlation analyses are not going to move the field much forward anymore. More advanced analyses methods are needed, taking higher order and non-linear interactions and indirect and polysynaptic connections between brain regions into account. One promising analysis strategy may be multi-layer networks, in which different types of connectivity data can be combined (De Domenico, 2017; Lim et al., 2019; Vaiana and Muldoon, 2018).

Since functional connectivity varies considerably across individuals (Gordon et al., 2017; Mueller et al., 2013), this may also explain part of the moderate correlation between structural and functional connectivity that we found in **Chapters 2 and 3**, in which structural and functional connectivity were not measured in the same individual. I do not believe that this individual variation fully explains the moderate correlation between structural and functional connectivity, since similar correlations have been found in studies comparing structural and functional connectivity within the same individual (Straathof et al., 2019). Nevertheless, mapping the structure-function relationship within individual brains in future studies would allow the characterization of individual differences in the structure-function relationship, which may relate to cognitive ability (Medaglia et al., 2018) and behavior.

I am intrigued by our finding that functional connectivity did not significantly correlate with gold-standard neuronal tracer-based structural connectivity, whereas it does correlate with diffusion-based structural connectivity (**Chapter 2**). Why are neuronal tracer-based structural connectivity and functional connectivity not related? Do MRI-based measures of structural and functional connectivity relate because they are both measured at the macro-scale or both dependent on a similar MRI signal? To answer these questions, more experiments are needed and ideally performed in rodents, since large online databases of neuronal tracer-based connectivity are available (Noori et al., 2017; Oh et al., 2014; Schmitt and Eipert, 2012). In our study, we focused on connections present in both diffusion-based and neuronal tracer-based structural networks. Future studies could determine where these structural networks differ and investigate the structure-function relationship in these connections specifically.

Brain maturation and aging contribute to vulnerability to disease

The second aim of thesis was to determine whether brain maturation and aging relate to the vulnerability to develop diseases during these life periods, for example OCD during maturation and stroke during aging. Our data confirmed that structural and functional connections change during brain maturation and aging in rats (**Chapters 4 and 6**). We further investigated whether the development of OCD is associated with abnormal maturation of structural and functional connections (**Chapter 4**), and whether aging-induced changes in structural and functional connections affect the impact of lesions in the brain (**Chapter 6**).

Since OCD develops during childhood and adolescence in three-quarters of the patients (Taylor, 2011), it is increasingly considered to be a neurodevelopmental disorder, caused by abnormal brain maturation (Huyser et al., 2009). Since we included a baseline measurement before the induction of compulsive behavior in our rat model, we could directly relate the development of compulsive behavior to alterations in brain maturation. Our findings confirmed the hypothesis that increased FA values in large white matter tracts in pediatric OCD reflect premature or increased brain maturation (**Chapter 4**). To further elucidate the pattern of abnormal white matter maturation in children and adolescents with OCD, additional time points in longitudinal MRI experiments would be necessary. Since a baseline measurement is not possible and longitudinal studies are difficult and costly in the human population, our introduced animal model provides a valuable alternative for future assessments.

Aging increases both the risk and the severity of stroke (Herson and Traystman, 2014; Johnson et al., 2019; Liang et al., 2016; Liu et al., 2009). However, age is an often-overlooked factor in experimental stroke studies. We showed that the aging rat brain is characterized by local changes in structural and functional networks that potentially make the brain more vulnerable to damage (**Chapter 6**). Our computational study also demonstrated that simulated lesions induce different local effects on structural and functional networks in young adult and aged rat brains. These results contribute to a growing body of literature suggesting that stroke has a different effect in young animals compared to old animals (Baltan et al., 2019; Liang et al., 2016; Liu et al., 2009). It has even been suggested that the age discrepancy between experimental stroke models (young adults) and human stroke patients (elderly population) may be one of the causes of poor bench-to-bedside translation (Dirnagl, 2016). Our findings further underline that age should be considered in experimental stroke studies.

Chapters 4-6 demonstrate the value of longitudinal MRI experiments to study normal and abnormal patterns of structural and functional connectivity during brain maturation and aging in relation to disorders. The relatively fast aging process in rats facilitates these longitudinal MRI experiments, which may cover the entire lifespan. Next to characterizing age-induced changes in structural and functional networks separately, I believe that combining those measurements and studying how the structure-function relationship changes with aging would be of added value. The structure-function coupling changes during development and correlates with cognitive performance (Baum et al., 2020; Zimmermann et al., 2018), and may potentially also relate to the vulnerability of disease. The structure-function tipping point that we introduced in **Chapter 3** may be a sensitive parameter to evaluate these relationships.

Translational value of experimental MRI studies

In this thesis, we used animal models to increase our understanding of structural and functional connectivity patterns associated with aging and disorders, which we could compare against human data obtained with similar MRI protocols. We found many similarities in structural and functional brain connectivity between humans and rats, including similar structure-function relationships (**Chapters 2 and 3**), similar changes during brain maturation (**Chapter 4**) and healthy aging (**Chapter 6**), and similar abnormalities associated with OCD (**Chapters 4 and 5**) and stroke (**Chapter 6**). Since experimental studies can be easily performed in homogeneous groups of animals with little variation in age, genetic background, and medication history, environmental or genetic biases that contribute to interindividual variation in similar studies in humans can be excluded.

To assess the translational value of animal models of mental disorders, three types of validity have been introduced (Willner, 1984): face, construct, and predictive validity. Whereas face validity describes observed similarity in, for example, symptoms between the animal model and clinical population, construct validity describes similar underlying mechanisms. Our introduced adolescent animal model of compulsive behavior demonstrated clear compulsive checking behavior and similar increases in white matter FA values as measured in children and adolescents with OCD (Gruner et al., 2012; Zarei et al., 2011), thereby showing face and construct validity (**Chapters 4 and 5**). We did not investigate its predictive validity, which we could have done by testing the effects of a treatment known to reduce compulsive behavior in children and adolescents with OCD, such as selective

serotonin reuptake inhibitors (SSRIs) (Geller et al., 2003). Instead, we evaluated a novel treatment, the anti-glutamatergic drug memantine, which has shown promising effects in adults with OCD (Ghaleiha et al., 2013; Haghghi et al., 2013). However, memantine did not reduce compulsive behavior in our adolescent rats, possibly because of pharmacological interactions with quinpirole, the agent used to induce OCD in rats (**Chapter 5**). I believe pharmacological MRI is a promising tool to study these interactions, which may help to identify subgroups of patients who do not benefit from specific treatment regimes. Furthermore, assessment of glutamate levels with magnetic resonance spectroscopy (Ramadan et al., 2013) could aid in the monitoring of anti-glutamatergic treatment.

Despite the many similarities we showed between the human and rat brain (**Chapters 2, 4 and 6**), we also detected differences in brain network organization (**Chapter 3**). More research is needed to investigate whether these differences relate to distinct brain sizes, evolutionary processes or interspecies differences in behavior and cognition (M. P. van den Heuvel et al., 2016a). Nevertheless, these differences imply that not all structural and functional connectivity measures can directly be translated between the human and rat brain.

Methodological considerations

All studies described in this thesis included resting-state fMRI measurements in rats under light isoflurane anesthesia to reduce stress and minimize motion. However, anesthesia influences functional connectivity values (Paasonen et al., 2018) and may change the relationship between structural and functional connectivity (Barttfeld et al., 2015), which may have affected the results described in this thesis. Nevertheless, anesthesia-induced changes in functional connectivity have been shown to have minimal effects on the global organization of functional networks in rodents (Liang et al., 2012), and previous studies have demonstrated reliability of comparisons of structure-function relationships between anesthetized rodents and awake humans (Díaz-Parra et al., 2017; Grandjean et al., 2017; Straathof et al., 2020b, 2019). Since we used similar anesthesia protocols for the different groups in each study, I am confident that significant group differences were detectable. In addition, I believe, especially for the studies described in **Chapters 4-6**, that motion reduction due to the use of light anesthesia is an advantage. Motion-induced fluctuations in the resting-state BOLD signal are difficult to detect and remove (Maknojia et al., 2019; Power et al., 2012; Van Dijk et al., 2012). The populations studied in these **Chapters 4-6** included children and elderly people, who are known to move more during MRI (Pardoe et al., 2016), introducing motion-induced differences in functional connectivity (Satterthwaite et al., 2012). The light

anesthesia used in our studies excluded the influence of these motion-induced changes in functional connectivity. Nevertheless, based on recently published studies, I would have chosen for a different anesthesia protocol, since isoflurane has been shown to affect functional connectivity more than other anesthetics, such as a combination of dexmedetomidine and low levels of isoflurane (Paasonen et al., 2018).

We have used rats in our experimental model for OCD in **Chapters 4 and 5**. It is important to keep in mind that animal models of psychiatric disorders only model parts of the disease or specific symptoms. While obsessions are difficult to assess because they rely on communication, compulsivity is often expressed behaviorally, and can therefore be modeled in experimental animals. The rats described in **Chapters 4 and 5** clearly showed altered behavior after repeated quinpirole injections. It remains difficult to assess whether rats are truly compulsive and how this compulsivity would match with compulsivity seen in patients with OCD. However, the methods used to assess compulsive behavior in the quinpirole rat model have also been successfully applied to study compulsive behavior in individuals with OCD (Eilam, 2017). Therefore, I believe that the quinpirole-induced rat model is valuable to study compulsive checking behavior both in adults and adolescents.

Lastly, in **Chapter 6** we made use of computational lesion simulations to study whether age affects the result of stroke lesions on structural and functional networks in the brain. Because these lesion simulations can be applied to already existing data, they may contribute to the replacement, reduction and refinement of animal research (Balls et al., 1995). However, it is important to realize that in our lesion simulation study we only simulated the direct effect of a lesion on the network, and we did not take secondary changes, including subsequent remodeling of networks, into account, which may happen at later time points.

Future steps

The work described in this thesis demonstrates how age-related changes in structural and functional connectivity may contribute to the vulnerability to develop diseases during these critical periods of our life. In addition, we have increased our understanding of the relationship between structural and functional connectivity in the brain and acquired more evidence of the complexity of this relationship. Although some future directions have already been suggested in the specific paragraphs above, there are a few more general future steps I would like to propose:

Future studies investigating functional brain networks may connect brain regions through novel, innovative analysis techniques, which may improve the characterization of functional networks. In most of the chapters of this thesis I used static functional connectivity analyses, a straightforward and often applied approach for resting-state fMRI data. However, it does not consider the dynamic nature of resting-state networks (Chang and Glover, 2010; Hutchison et al., 2013). We used dynamic analyses in **Chapter 3** and demonstrated fluctuations in functional connectivity in both the human and rat brain, which may provide additional information about functional network organization. Alternatively, effective connectivity approaches, which are computationally more complex, can provide information on directionality of interacting brain regions (Friston et al., 2013; Friston, 2011).

Next to investigating how structural and functional connectivity relate, I think future research should also focus on the dissimilarity between structural and functional connectivity (Lim et al., 2019). Where structural and functional connectivity are not related or even disagree, they may be complementary. In those regions and connections, acquiring both diffusion-based structural connectivity and resting-state functional connectivity may provide more information than acquiring only a single modality. For example, after corpus callosum resection structural connections may be lost, but functional connectivity remained when the anterior commissure was still intact (O'Reilly et al., 2013), showing the importance of combining structural and functional measures.

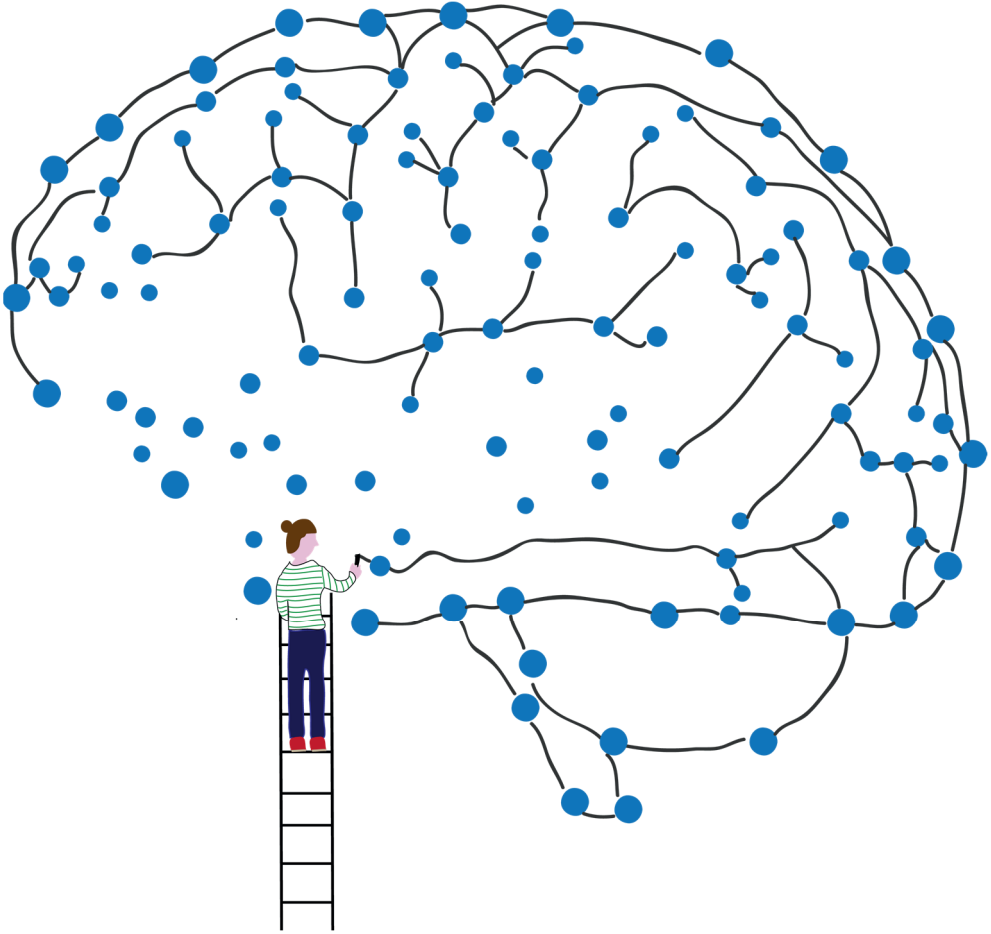
Lastly, I would like to encourage researchers to share their structural and functional connectivity datasets. Increased availability of open source structural and functional connectivity data will facilitate the intra- and inter-species comparison of network organization across the brain. Although the sharing of data is already more common in human research, the preclinical MRI community stays behind. Combining datasets acquired with different parameters, under different anesthesia protocols and on different scanners may really reveal how structural connectivity constrains, maintains, and regulates the functional network. The first multicenter fMRI studies in mice and rats have already been initiated (Grandjean et al., 2020).

References

- Balls, M., Goldberg, A., Fentem, J.H., Broadhead, C., Bursch, R., Festing, M., Frazier, J., Hendriksen, F., Jennings, M., van der Kamp, M., Morton, D., Rowan, A., Russell, C., Russell, W., Spielmann, H., Stephens, M., Stokes, W., Straughan, D., Yager, J., Zurlo, J., van Zuphen, B., 1995. The three Rs: the way forward. *Altern. to Lab. Anim. ATLA* 23, 838–866.
- Baltan, S., Shi, Y., Keep, R.F., Chen, J., 2019. The effect of aging on brain injury and recovery after stroke. *Neurobiol. Dis.* 126, 1–2. <https://doi.org/10.1016/j.nbd.2019.04.001>
- Barttfeld, P., Uhrig, L., Sitt, J.D., Sigman, M., Jarraya, B., Dehaene, S., 2015. Signature of consciousness in the dynamics of resting-state brain activity. *Proc. Natl. Acad. Sci. U. S. A.* 112, 887–892. <https://doi.org/10.1073/pnas.1515029112>
- Baum, G.L., Cui, Z., Roalf, D.R., Ciric, R., Betzel, R.F., Larsen, B., Cieslak, M., Cook, P.A., Xia, C.H., Moore, T.M., Ruparel, K., Oathes, D.J., Alexander-Bloch, A.F., Shinohara, R.T., Raznahan, A., Gur, R.E., Gur, R.C., Bassett, D.S., Satterthwaite, T.D., 2020. Development of structure–function coupling in human brain networks during youth. *Proc. Natl. Acad. Sci. U. S. A.* 117, 771–778. <https://doi.org/10.1073/pnas.1912034117>
- Chang, C., Glover, G.H., 2010. Time-frequency dynamics of resting-state brain connectivity measured with fMRI. *Neuroimage* 50, 81–98. <https://doi.org/10.1016/j.neuroimage.2009.12.011>
- De Domenico, M., 2017. Multilayer modeling and analysis of human brain networks. *Gigascience* 6, 1–8. <https://doi.org/10.1093/gigascience/gix004>
- Díaz-Parra, A., Osborn, Z., Canals, S., Moratal, D., Sporns, O., 2017. Structural and functional, empirical and modeled connectivity in the cerebral cortex of the rat. *Neuroimage* 159, 170–184. <https://doi.org/10.1016/j.neuroimage.2017.07.046>
- Dirnagl, U., 2016. Thomas Willis lecture: Is translational stroke research broken, and if so, how can we fix it? *Stroke* 47, 2148–2153. <https://doi.org/10.1161/STROKEAHA.116.013244>
- Eilam, D., 2017. From an animal model to human patients: An example of a translational study on obsessive compulsive disorder (OCD). *Neurosci. Biobehav. Rev.* 76, 67–76. <https://doi.org/10.1016/j.neubiorev.2016.12.034>
- Friston, K., Moran, R., Seth, A.K., 2013. Analysing connectivity with Granger causality and dynamic causal modelling. *Curr. Opin. Neurobiol.* 23, 172–178. <https://doi.org/10.1016/j.conb.2012.11.010>
- Friston, K.J., 2011. Functional and Effective Connectivity: A Review. *Brain Connect.* 1, 13–36. <https://doi.org/10.1089/brain.2011.0008>
- Geller, D.A., Biederman, J., Stewart, S.E., Mullin, B., Martin, A., Spencer, T., Faraone, S. V., 2003. Which SSRI? A Meta-Analysis of Pharmacotherapy Trials in Pediatric Obsessive-Compulsive Disorder. *Am. J. Psychiatry* 160, 1919–1928.
- Ghaleiha, A., Entezari, N., Modabbernia, A., Najand, B., Askari, N., Tabrizi, M., Ashrafi, M., Hajiaghvae, R., Akhondzadeh, S., 2013. Memantine add-on in moderate to severe obsessive-compulsive disorder: Randomized double-blind placebo-controlled study. *J. Psychiatr. Res.* 47, 175–180. <https://doi.org/10.1016/j.jpsychires.2012.09.015>
- Gordon, E.M., Laumann, T.O., Gilmore, A.W., Newbold, D.J., Greene, D.J., Berg, J.J., Ortega, M., Hoyt-Drazen, C., Gratton, C., Sun, H., Hampton, J.M., Coalson, R.S., Nguyen, A.L., McDermott, K.B., Shimony, J.S., Snyder, A.Z., Schlaggar, B.L., Petersen, S.E., Nelson, S.M., Dosenbach, N.U.F., 2017. Precision Functional Mapping of Individual Human Brains. *Neuron* 95, 791–807. <https://doi.org/10.1016/j.neuron.2017.07.011>
- Grandjean, J., Canella, C., Anckaerts, C., Ayrançi, G., Bougacha, S., Bienert, T., Buehlmann, D., Coletta, L., Gallino, D., Gass, N., Garin, C.M., Nadkarni, N.A., Hübner, N.S., Karatas, M., Komaki, Y., Kreitz, S., Mandino, F., Mechling, A.E., Sato, C., Sauer, K., Shah, D., Strobel, S., Takata, N., Wank, I., Wu, T., Yahata, N., Yeow, L.Y., Yee, Y., Aoki, I., Chakravarty, M.M., Chang, W.T., Dhenain, M., von Elverfeldt, D., Harsan, L.A., Hess, A., Jiang, T., Keliris, G.A., Lerch, J.P., Meyer-Lindenberg, A., Okano, H., Rudin, M., Sartorius, A., Van der Linden, A., Verhoye, M., Weber-Fahr, W., Wenderoth, N., Zerbi, V., Gozzi, A., 2020. Common functional networks in the mouse brain revealed by multi-centre resting-state fMRI analysis. *Neuroimage* 205. <https://doi.org/10.1016/j.neuroimage.2019.116278>
- Grandjean, J., Zerbi, V., Balsters, J.H., Wenderoth, N., Rudin, M., 2017. Structural basis of large-scale functional connectivity in the mouse. *J. Neurosci.* 37, 8092–8101. <https://doi.org/10.1523/JNEUROSCI.0438-17.2017>
- Gruner, P., Vo, A., Ikuta, T., Mahon, K., Peters, B.D., Malhotra, A.K., Uluğ, A.M., Szeszko, P.R., 2012. White matter abnormalities in pediatric obsessive-compulsive disorder. *Neuropsychopharmacology* 37, 2730–2739. <https://doi.org/10.1038/npp.2012.138>
- Haghighi, M., Jahangard, L., Mohammad-Beigi, H., Bajoghli, H., Hafezian, H., Rahimi, A., Afshar, H., Holsboer-Trachsler, E., Brand, S., 2013. In a double-blind, randomized and placebo-controlled trial, adjuvant memantine improved symptoms in inpatients suffering from refractory obsessive-compulsive disorders (OCD). *Psychopharmacology (Berl)*. 228, 633–640. <https://doi.org/10.1007/s00213-013-3067-z>
- Herson, P.S., Traystman, R.J., 2014. Animal models of stroke: translational potential at present and in 2050. *Future Neurol.* 9, 541–551. <https://doi.org/10.2217/fnl.14.44>
- Hutchison, R.M., Womelsdorf, T., Allen, E.A., Bandettini, P.A., Calhoun, V.D., Corbetta, M., Della Penna, S., Duyn, J.H., Glover,

- G.H., Gonzalez-Castillo, J., Handwerker, D.A., Keilholz, S., Kiviniemi, V., Leopold, D.A., de Pasquale, F., Sporns, O., Walter, M., Chang, C., 2013. Dynamic functional connectivity: Promise, issues, and interpretations. *Neuroimage* 80, 360–78. <https://doi.org/10.1016/j.neuroimage.2013.05.079>
- Huysler, C., Veltman, D.J., de Haan, E., Boer, F., 2009. Paediatric obsessive-compulsive disorder, a neurodevelopmental disorder? Evidence from neuroimaging. *Neurosci. Biobehav. Rev.* 33, 818–830. <https://doi.org/10.1016/j.neubiorev.2009.01.003>
- Johnson, C.O., Nguyen, M., Roth, G.A., Nichols, E., Alam, T., Abate, D., Abd-Allah, F., Abdelalim, A., Abraha, H.N., Abu-Rmeileh, N.M., Adebayo, O.M., Adeoye, A.M., Agarwal, G., Agrawal, S., Aichour, A.N., Aichour, I., Aichour, M.T.E., Alahdab, F., Ali, R., Alvis-Guzman, N., Anber, N.H., Anjomshoa, M., Arabloo, J., Arauz, A., Ärnlöv, J., Arora, A., Awasthi, A., Banach, M., Barboza, M.A., Barker-Collo, S.L., Bärnighausen, T.W., Basu, S., Belachew, A.B., Belayneh, Y.M., Bennett, D.A., Bensenor, I.M., Bhattacharyya, K., Biadgo, B., Bijani, A., Bikbov, B., Bin Sayeed, M.S., Butt, Z.A., Cahuana-Hurtado, L., Carrero, J.J., Carvalho, F., Castañeda-Orjuela, C.A., Castro, F., Catalá-López, F., Chaiah, Y., Chiang, P.P.C., Choi, J.Y.J., Christensen, H., Chu, D.T., Cortinovis, M., Damasceno, A.A.M., Dandona, L., Dandona, R., Daryani, A., Davletov, K., De Courten, B., De la Cruz-Góngora, V., Degfe, M.G., Dharmaratne, S.D., Diaz, D., Dubey, M., Duken, E.E., Edessa, D., Endres, M., Faraon, E.J.A., Farzadfar, F., Fernandes, E., Fischer, F., Flor, L.S., Ganji, M., Gebre, A.K., Gebremichael, T.G., Geta, B., Gezae, K.E., Gill, P.S., Gnedovskaya, E. V., Gómez-Dantés, H., Goulart, A.C., Grosso, G., Guo, Y., Gupta, R., Haj-Mirzaian, Arvin, Haj-Mirzaian, Arya, Hamidi, S., Hankey, G.J., Hassen, H.Y., Hay, S.I., Hegazy, M.I., Heidari, B., Herial, N.A., Hossaini, M.A., Hostiuc, S., Irvani, S.S.N., Islam, S.M.S., Jahanmeh, N., Javanbakht, M., Jha, R.P., Jonas, J.B., Józwiak, J.J., Jürisson, M., Kahsay, A., Kalani, R., Kalkonde, Y., Kamil, T.A., Kanchan, T., Karch, A., Karimi, N., Karimi-Sari, H., Kasacian, A., Kassa, T.D., Kazemini, H., Kefale, A.T., Khader, Y.S., Khalil, I.A., Khan, E.A., Khang, Y.H., Khubchandani, J., Kim, D., Kim, Y.J., Kisa, A., Kivimäki, M., Koyanagi, A., Krishnamurthi, R.K., Anil Kumar, G., Lafranconi, A., Lewington, S., Li, S., Lo, W.D., Lopez, A.D., Lorkowski, S., Lotufo, P.A., Mackay, M.T., Majdan, M., Majdzadeh, R., Majeed, A., Malekzadeh, R., Manafi, N., Mansournia, M.A., Mehndiratta, M.M., Mehta, V., Mengistu, G., Meretoja, A., Meretoja, T.J., Miazgowski, B., Miazgowski, T., Miller, T.R., Mirakhorimov, E.M., Mohajer, B., Mohammad, Y., Mohammadoo-Khorasani, M., Mohammed, S., Mohebi, F., Mokdad, A.H., Mokhayeri, Y., Moradi, G., Morawska, L., Moreno Velásquez, I., Mousavi, S.M., Muhammed, O.S.S., Muruet, W., Naderi, M., Naghavi, M., Naik, G., Nascimento, B.R., Negoi, R.I., Nguyen, C.T., Nguyen, L.H., Nirayo, Y.L., Norrving, B., Noubiap, J.J., Ofori-Asenso, R., Ogbo, F.A., Olagunju, A.T., Olagunju, T.O., Owolabi, M.O., Pandian, J.D., Patel, S., Perico, N., Piradov, M.A., Polinder, S., Postma, M.J., Poustchi, H., Prakash, V., Qorbani, M., Rafiei, A., Rahim, F., Rahimi, K., Rahimi-Movaghar, V., Rahman, M., Rahman, M.A., Reis, C., Remuzzi, G., Renzaho, A.M.N., Ricci, S., Roberts, N.L.S., Robinson, S.R., Roeber, L., Roshandel, G., Sabbagh, P., Safari, H., Safari, S., Safiri, S., Sahebkar, A., Salehi Zahabi, S., Samy, A.M., Santalucia, P., Santos, I.S., Santos, J.V., Santric Milicevic, M.M., Sartorius, B., Sawant, A.R., Schutte, A.E., Sepanlou, S.G., Shafieesabet, A., Shaikh, M.A., Shams-Beyranvand, M., Sheikh, A., Sheth, K.N., Shibuya, K., Shigematsu, M., Shin, M.J., Shiu, I., Siabani, S., Sobaih, B.H., Sposato, L.A., Sutradhar, I., Sylaja, P.A., Szoek, C.E.L., Te Ao, B.J., Temsah, M.H., Temsah, O., Thrift, A.G., Tonelli, M., Topor-Madry, R., Tran, B.X., Tran, K.B., Truelsen, T.C., Tsadik, A.G., Ullah, I., Uthman, O.A., Vaduganathan, M., Valdez, P.R., Vasankari, T.J., Vasanathan, R., Venketasubramanian, N., Vosoughi, K., Vu, G.T., Waheed, Y., Weiderpass, E., Wedelgwegs, K.G., Westerman, R., Wolfe, C.D.A., Wondafraash, D.Z., Xu, G., Yadollahpour, A., Yamada, T., Yatsuya, H., Yimer, E.M., Yonemoto, N., Yousefifard, M., Yu, C., Zaidi, Z., Zamani, M., Zarghi, A., Zhang, Y., Zodpey, S., Feigin, V.L., Vos, T., Murray, C.J.L., 2019. Global, regional, and national burden of stroke, 1990–2016: a systematic analysis for the Global Burden of Disease Study 2016. *Lancet Neurol.* 18, 439–458. [https://doi.org/10.1016/S1474-4422\(19\)30034-1](https://doi.org/10.1016/S1474-4422(19)30034-1)
- Liang, A.C., Mandeville, E.T., Maki, T., Shindo, A., Som, A.T., Egawa, N., Itoh, K., Chuang, T.T., McNeish, J.D., Holder, J.C., Lok, J., Lo, E.H., Arai, K., 2016. Effects of aging on neural stem/progenitor cells and oligodendrocyte precursor cells after focal cerebral ischemia in spontaneously hypertensive rats. *Cell Transplant.* 25, 705–714. <https://doi.org/10.3727/096368916X690557>
- Liang, Z., King, J., Zhang, N., 2012. Intrinsic organization of the anesthetized brain. *J. Neurosci.* 32, 10183–10191. <https://doi.org/10.1523/JNEUROSCI.1020-12.2012>
- Lim, S., Radicchi, F., van den Heuvel, M.P., Sporns, O., 2019. Discordant attributes of structural and functional brain connectivity in a two-layer multiplex network. *Sci. Rep.* 9, 1–13. <https://doi.org/10.1038/s41598-019-39243-w>
- Liu, F., Yuan, R., Benashski, S.E., McCullough, L.D., 2009. Changes in experimental stroke outcome across the lifespan. *J. Cereb. Blood Flow Metab.* 29, 792–802. <https://doi.org/10.1038/jcbfm.2009.5>
- Maknojia, S., Churchill, N.W., Schweizer, T.A., Graham, S.J., 2019. Resting state fMRI: Going through the motions. *Front. Neurosci.* 13, 1–13. <https://doi.org/10.3389/fnins.2019.00825>
- Medaglia, J.D., Huang, W., Karuza, E.A., Kelkar, A., Thompson-Schill, S.L., Ribeiro, A., Bassett, D.S., 2018. Functional alignment with anatomical networks is associated with cognitive flexibility. *Nat. Hum. Behav.* 2, 156–164. <https://doi.org/10.1038/s41562-017-0260-9>
- Mueller, S., Wang, D., Fox, M.D., Yeo, T.B.T., Sepulcre, J., Sabuncu, M.R., Shafee, R., Lu, J., Liu, H., 2013. Individual Variability in Functional Connectivity Architecture of the Human Brain. *Neuron* 77, 586–595.

- <https://doi.org/10.1016/j.neuron.2012.12.028>
- Noori, H.R., Schöttler, J., Ercsey-Ravasz, M., Cosa-linan, A., Varga, M., Toroczka, Z., Spanagel, R., 2017. A multiscale cerebral neurochemical connectome of the rat brain. *PLoS Biol.* 15, e2002612. <https://doi.org/https://doi.org/10.1371/journal.pbio.2002612>
- O'Reilly, J.X., Croxson, P.L., Jbabdi, S., Sallet, J., Noonan, M.P., Mars, R.B., Browning, P.G.F., Wilson, C.R.E., Mitchell, A.S., Miller, K.L., Rushworth, M.F.S., Baxter, M.G., 2013. Causal effect of disconnection lesions on interhemispheric functional connectivity in rhesus monkeys. *Proc. Natl. Acad. Sci. U. S. A.* 110, 13982–13987. <https://doi.org/10.1073/pnas.1305062110>
- Oh, S.W., Harris, J.A., Ng, L., Winslow, B., Cain, N., Mihalas, S., Wang, Q., Lau, C., Kuan, L., Henry, A.M., Mortrud, M.T., Ouellette, B., Nguyen, T.N., Sorensen, S.A., Slaughterbeck, C.R., Wakeman, W., Li, Y., Feng, D., Ho, A., Nicolas, E., Hirokawa, K.E., Bohn, P., Joines, K.M., Peng, H., Hawrylycz, M.J., Phillips, J.W., Hohmann, J.G., Wahnoutka, P., Gerfen, C.R., Koch, C., Bernard, A., Dang, C., Jones, A.R., Zeng, H., 2014. A mesoscale connectome of the mouse brain. *Nature* 508, 207–214. <https://doi.org/10.1038/nature13186>
- Paasonen, J., Stenroos, P., Salo, R.A., Kiviniemi, V., Gröhn, O., 2018. Functional connectivity under six anesthesia protocols and the awake condition in rat brain. *Neuroimage* 172, 9–20. <https://doi.org/10.1016/j.neuroimage.2018.01.014>
- Pardoe, H.R., Kucharsky Hiess, R., Kuzniecky, R., 2016. Motion and morphometry in clinical and nonclinical populations. *Neuroimage* 135, 177–185. <https://doi.org/10.1016/j.neuroimage.2016.05.005>
- Power, J.D., Barnes, K.A., Snyder, A.Z., Schlaggar, B.L., Petersen, S.E., 2012. Spurious but systematic correlations in functional connectivity MRI networks arise from subject motion. *Neuroimage* 59, 2142–2154. <https://doi.org/10.1016/j.neuroimage.2011.10.018>
- Ramadan, S., Lin, A., Stanwell, P., 2013. Glutamate and glutamine: A review of in vivo MRS in the human brain. *NMR Biomed.* 26, 1630–1646. <https://doi.org/10.1002/nbm.3045>
- Satterthwaite, T.D., Wolf, D.H., Loughhead, J., Ruparel, K., Elliot, M.A., Hakon, H., Gur, R.C., Gur, R.E., 2012. Impact of In-Scanner Head Motion on Multiple Measures of Functional Connectivity: Relevance for Studies of Neurodevelopment in Youth. *Neuroimage* 60, 623–632. <https://doi.org/10.1016/j.neuroimage.2011.12.063>
- Schmitt, O., Eipert, P., 2012. neuroVIISAS: Approaching multiscale simulation of the rat connectome. *Neuroinformatics* 10, 243–267. <https://doi.org/10.1007/s12021-012-9141-6>
- Straathof, M., Sinke, M.R., Dijkhuizen, R.M., Otte, W.M., on behalf of the TACTICS consortium, 2019. A systematic review on the quantitative relationship between structural and functional network connectivity strength in mammalian brains. *J. Cereb. Blood Flow Metab.* 39, 189–209. <https://doi.org/10.1177/0271678X18809547>
- Straathof, M., Sinke, M.R.T., Roelofs, T.J.M., Bleszer, E.L.A., Sarabdjitsingh, R.A., van der Toorn, A., Schmitt, O., Otte, W.M., Dijkhuizen, R.M., 2020. Distinct structure-function relationships across cortical regions and connectivity scales in the rat brain. *Sci. Rep.* 10, 56. <https://doi.org/10.1038/s41598-019-56834-9>
- Taylor, S., 2011. Early versus late onset obsessive-compulsive disorder: evidence for distinct subtypes. *Clin. Psychol. Rev.* 31, 1083–1100. <https://doi.org/10.1016/j.cpr.2011.06.007>
- Vaiana, M., Muldoon, S.F., 2018. Multilayer Brain Networks. *J. Nonlinear Sci.* 1–23. <https://doi.org/10.1007/s00332-017-9436-8>
- van den Heuvel, M.P., Bullmore, E.T., Sporns, O., 2016. Comparative Connectomics. *Trends Cogn. Sci.* 20, 345–361. <https://doi.org/10.1016/j.tics.2016.03.001>
- Van Dijk, K.R.A., Sabuncu, M.R., Buckner, R.L., 2012. The Influence of Head Motion on Intrinsic Functional Connectivity MRI. *Neuroimage* 59, 431–438. <https://doi.org/10.1016/j.neuroimage.2011.07.044>
- Vázquez-Rodríguez, B., Suárez, L.E., Markello, R.D., Shafiei, G., Paquola, C., Hagmann, P., van den Heuvel, M.P., Bernhardt, B.C., Spreng, R.N., Misisic, B., 2019. Gradients of structure – function tethering across neocortex. *Proc. Natl. Acad. Sci. U. S. A.* 116, 21219–21227. <https://doi.org/10.1073/pnas.1903403116>
- Willner, P., 1984. The validity of animal models of depression. *Psychopharmacology (Berl.)* 83, 1–16. <https://doi.org/10.1007/BF00427414>
- Zarei, M., Mataix-Cols, D., Heyman, I., Hough, M., Doherty, J., Burge, L., Winmill, L., Nijhawan, S., Matthews, P.M., James, A., 2011. Changes in gray matter volume and white matter microstructure in adolescents with obsessive-compulsive disorder. *Biol. Psychiatry* 70, 1083–1090. <https://doi.org/10.1016/j.biopsych.2011.06.032>
- Zimmermann, J., Griffiths, J.D., McIntosh, A.R., 2018. Unique mapping of structural and functional connectivity on cognition. *J. Neurosci.* 38, 9658–9667. <https://doi.org/10.1523/JNEUROSCI.0900-18.2018>
- Zimmermann, J., Ritter, P., Shen, K., Rothmeier, S., Schirner, M., McIntosh, A.R., 2016. Structural architecture supports functional organization in the human aging brain at a regionwise and network Level. *Hum. Brain Mapp.* 37, 2645–2661. <https://doi.org/10.1002/hbm.23200>





Summary

Samenvatting

Summary

The brain is a complex system composed of regions that are interacting at the micro-, meso- and macrolevel. The communication between those regions is essential for all our daily life functions, including reading this thesis. Understanding the organization and functioning of the brain has been one of the fundamental goals in neuroscience, forming the basis of this thesis. To fully understand the organization of the brain, we have to consider the connections and interactions between individual brain regions. To that aim, within network neuroscience, the brain is conceptually divided into brain regions (represented by nodes or dots) and connections (represented by edges or lines). One can look at these connections in two ways. First, there are functional connections between brain regions, which are assumed to reflect information transfer between regions (i.e., signals sent from one brain region to another). Second, there are structural connections, which are the physical connections between brain regions. The network organization of structural and functional brain connections is ideally studied non-invasively *in vivo*, which is feasible with magnetic resonance imaging (MRI).

In this thesis, I aimed to “connect the dots”. First, we connected dots in images of the brain, by assessing connectivity between different brain regions, represented by dots. In addition, we connected dots in a more figurative way, by identifying how biological or pathological phenomena, like aging across the lifespan or disease processes, affect brain network organization. The first part of this thesis describes how the structural network constrains and restricts the functional network, by characterizing the relationship between structural and functional connectivity in the rat and human brain. Identifying how structural and functional connectivity relate will help to understand how brain networks are organized, and why functional abnormalities in brain disorders are related to characteristic patterns of disconnection or reorganization. The exact relationship between structural and functional connectivity may vary across brain regions, different levels of connectivity and species. Therefore, in this thesis, we characterized the relationship between structural and functional connectivity across different scales in the rat and human brain.

The second part of this thesis shows how aging across the lifespan affects brain network organization and may relate to the vulnerability to diseases. Structural and functional connectivity changes during maturation may contribute to developmental disorders like obsessive-compulsive disorder (OCD), whereas changes during aging may contribute to the higher risk of neurodegenerative and cerebrovascular diseases, like stroke.

Therefore, in this thesis, we studied structural and functional brain networks during healthy brain maturation and aging in rats, and assessed how abnormal development or aging may relate to OCD or stroke pathology, respectively.

Chapter 1 provides an overview of this thesis. We describe the applied MRI techniques and analysis methods to measure structural and functional connectivity. Besides, changes in structural and functional connectivity associated with development and aging, with OCD and stroke, are described.

Structure-function mapping in the healthy adult brain

The aim of **Chapter 2** was to identify to what extent structural and functional connectivity strengths are linearly correlated across the rat brain. We measured functional connectivity with resting-state fMRI, and structural connectivity with diffusion-weighted MRI and neuronal tract tracers. We found a moderate linear correlation between whole-brain functional connectivity and MRI-based macro-scale structural connectivity in the rat brain. However, we did not find a significant correlation between functional connectivity and meso-scale structural connectivity measured with neuronal tract tracing. In addition, we showed distinct structure-function relationships across brain regions in the rat brain. We found strong functional connectivity in robust resting-state networks, like the sensorimotor and default mode networks. Strong functional connectivity within these networks coincided with strong short-range intrahemispheric structural connectivity, but with weak heterotopic interhemispheric and long-range intrahemispheric structural connectivity. This study indicates the importance of combining measures of connectivity at distinct hierarchical levels to accurately determine connectivity across networks in the healthy and diseased brain.

Although linear correlation approaches offer a clear and easily interpretable way to characterize structure-function relationships in the brain, they may not completely cover the complex nature of this relationship. Therefore, in **Chapter 3**, we mapped the structure-function relationship in the rat brain by taking non-linear components of this relationship into account. These analyses showed that weak structural connectivity was not significantly associated with functional connectivity, but structural and functional connectivity correlated from a specific structural connectivity strength onwards: the structure-function tipping point. We showed that from this tipping-point onwards, whole-brain structural and functional connectivities become significantly positively associated. We speculate that this structure-function tipping point may relate to the small-world organization of brain networks. These networks are characterized by strong structural connections within

specialized functional modules, which may strongly associate with functional connectivity, and sparse weak structural connections between those functional modules, which are less strongly associated with functional connectivity.

We directly compared the non-linear structure-function relationship and corresponding structure-function tipping point between the rat and human brain in **Chapter 3**. Whereas both the human and rat brain showed non-linear structure-function relationships, the tipping point occurred at a higher structural connectivity value in the rat compared to the human brain. In the human brain we found a non-linear structure-function relationship in primary unimodal sensory and motor regions as well as in secondary multimodal integration areas, with similar structure-function tipping points. In comparison, in the rat brain, the structure-function relationship showed stronger non-linear behavior in primary compared to secondary brain regions. Whether these differences between the human and rat brain are simply due to differences in brain size, differences in the degree of small-world organization, or due to species differences in the development of specific brain regions remains to be investigated. Our non-linear correlation analyses can aid in the elucidation of the complex interaction between functional and structural connectivity in neural networks, and may offer unique markers of brain development, aging and dysfunction.

Maturation of the brain in relation to obsessive-compulsive disorder

To be able to study the association between brain maturation and OCD during childhood and adolescence, we modified the established adult rat model of quinpirole-induced compulsive checking behavior towards an adolescent model in **Chapter 4**. In the adult model, repeated injections with the dopamine D2/D3 receptor agonist quinpirole in adult rats, in combination with placement of the rat on an open field table, results in compulsive checking behavior. By starting quinpirole injections during childhood, we showed that the rats developed compulsive checking behavior before the age of 10 weeks, which is around young adulthood in rats. We applied serial MRI measurements of structural and functional connectivity before and after the repetitive quinpirole injections to assess (ab)normal brain maturation and its association with compulsive behavior. Rat brain development was characterized by increases in diffusion fractional anisotropy (FA) values along large white matter fiber bundles. The developmental rise in FA in the internal capsule and forceps minor was larger in compulsive rats compared to controls. This study underlines the involvement of white matter structural integrity disturbances in disease processes of OCD in children and adolescents.

Because animal models provide a well-controlled setting with little interindividual variation, they are well suited to test the efficacy of novel therapeutic treatments. Therefore, the aim of **Chapter 5** was to test the therapeutic efficacy of the NMDA receptor antagonist memantine in reducing compulsive behavior in the above-described adolescent rat model of OCD. In addition, we aimed to identify the therapeutic mode of action of memantine, by studying its effect on structural and functional connectivities as well as functional activation in the frontostriatal circuitry. Memantine did not reduce compulsive behavior in the adolescent rat model, and correspondingly also did not influence structural and functional connectivities. Pharmacological MRI executed during a single memantine injection showed activation of widespread areas in the brain of control rats, which was not observed after repeated or single quinpirole injections. This points towards an interaction between the pharmacologically induced OCD model (quinpirole: dopamine system) and therapeutic treatment (memantine: glutamatergic system). This finding may suggest that the NMDA receptor antagonist memantine might not be effective in individuals with a disrupted dopamine system.

Brain aging and vulnerability to stroke-induced brain damage

In **Chapter 6**, we investigated whether age-related changes in structural and functional networks affect the impact of stroke lesions on the brain. We used graph analyses to determine local and global network properties of diffusion MRI-based structural and resting-state fMRI-based functional connectivity in the young adult and aged rat brain. We did not find differences in global network measures, including path length, clustering and small-worldness, between young adult and aged rats. However, we did find local network differences between young adult and aged rats, characterized by a shift in hub regions in both structural and functional networks.

We simulated three different lesion types, based on the lesion topology in popular experimental stroke models. Although the effects of these stroke lesions on global network measures were similar for young adult and aged rats, we found differences in lesion-induced hub shifts between young adult and aged rats. These different lesion-induced hub shifts across age may be due to the distinct local organization of structural and functional brain networks in young adult and aged rats. These results suggest that structural and functional networks change with aging, and that especially local changes like hub shifts contribute to stroke induced damage. Hereby, this chapter underscores the importance of considering age in experimental stroke studies.

In **Chapter 7**, we discuss the implications of our findings, methodological considerations of the used methods and possibilities for future research.

Samenvatting

Onze hersenen bestaan uit verschillende gebieden die met elkaar communiceren op micro-, meso- en macro-niveau. Deze communicatie tussen hersengebieden is essentieel voor ons dagelijks functioneren, zoals het lezen van dit proefschrift. Een van de fundamentele doelen in de neurowetenschappen is het begrijpen van de organisatie en het functioneren van onze hersenen. Dit vormt ook de basis van dit proefschrift. Om de hersenen goed te kunnen begrijpen, moeten we rekening houden met zowel de verbindingen als de communicatie tussen de verschillende hersengebieden. Daarom worden de hersenen binnen “netwerk-neurowetenschappen” onderverdeeld in gebieden en hun connecties (verbindingen). Je kunt op twee manieren naar de connecties kijken. Functionele connecties vertellen iets over de communicatie en informatie-uitwisseling tussen hersengebieden (bijvoorbeeld signalen die van het ene naar het andere gebied worden gezonden). Daarnaast zijn er structurele connecties. Dit zijn de fysieke verbindingen tussen hersengebieden. Het concept van structurele en functionele connecties is overal in het dagelijks leven te vinden, zoals bijvoorbeeld in het treinnetwerk. In dit voorbeeld vormen de treinrails tussen twee stations de structurele verbinding, en is het aantal treinen dat over deze rails rijdt de functionele verbinding. Met magnetische resonantie imaging (MRI) technieken kunnen de organisatie en het functioneren van de hersenen en de structurele en functionele connecties tussen hersengebieden bestudeerd worden.

In dit proefschrift, heb ik geprobeerd om “punten te verbinden”. Als eerste, hebben we punten verbonden aan de hand van MRI-scans van de hersenen. Hersengebieden kunnen worden weergegeven als knooppunten. De connecties tussen verschillende hersengebieden worden weergegeven door verbinding van deze punten. Daarnaast hebben we meer figuurlijk “punten verbonden”, of verbanden gelegd. We hebben onderzocht hoe biologische of pathologische fenomenen, zoals ouder worden of ziekteprocessen, invloed hebben op de structurele en functionele verbindingen in de hersenen.

Het eerste deel van dit proefschrift beschrijft hoe de structurele verbindingen de functionele verbindingen in de hersenen beïnvloeden en beperken. Daarvoor hebben we de onderlinge relatie tussen structurele en functionele connectiviteit bepaald. Meer inzicht in de relatie tussen structurele en functionele connectiviteit helpt om de organisatie van de hersenen beter te begrijpen. Daarnaast zou op basis van deze relatie verklaard kunnen worden hoe functionele problemen in hersenziektes gekarakteriseerd worden door specifieke patronen van disconnecties. De precieze relatie tussen structurele en functionele

verbindingen kan variëren over de verschillende gebieden in de hersenen, over verschillende niveaus van connectiviteit en tussen species. Daarom hebben we in dit proefschrift de relatie tussen verschillende niveaus van structurele en functionele connectiviteit gemeten in verschillende delen van de hersenen van ratten en mensen.

In het tweede deel van dit proefschrift hebben we onderzocht hoe ouder worden de organisatie van de hersenen beïnvloedt en hoe dit bijdraagt aan de kwetsbaarheid om hersenziektes te ontwikkelen. Veranderingen in structurele en functionele verbindingen tijdens de ontwikkeling van kind naar puber dragen mogelijk bij aan het ontstaan van ontwikkelingsstoornissen zoals obsessieve-compulsieve stoornis (OCD). Tijdens het verouderingsproces kunnen structurele en functionele hersenveranderingen bijdragen aan het hogere risico op neurodegeneratieve en cerebrovasculaire ziektes, zoals een beroerte. In dit proefschrift hebben we de gezonde ontwikkeling van structurele en functionele verbindingen in de hersenen van ratten bestudeerd, en onderzocht of OCD in jongeren en hersenbloedingen in ouderen gerelateerd zijn aan abnormale ontwikkeling van deze verbindingen.

Hoofdstuk 1 geeft een overzicht van de indeling van dit proefschrift. We beschrijven de gebruikte MRI-technieken en analysemethoden waarmee we structurele en functionele hersenconnectiviteit gemeten hebben. Daarnaast beschrijven we de veranderingen in structurele en functionele connecties die geassocieerd zijn met ouder worden, OCD en beroerte.

De relatie tussen structurele en functionele verbindingen in de gezonde volwassen hersenen

Het doel van **Hoofdstuk 2** was om vast te stellen hoe structurele en functionele connecties lineair gecorreleerd zijn in de hersenen van ratten. We hebben functionele connectiviteit gemeten met resting-state functionele MRI, en structurele connectiviteit met diffusie-gewogen MRI en neuronale tract tracers. We maten een matige lineaire correlatie tussen functionele connectiviteit en MRI-gebaseerde structurele connectiviteit op macro-niveau in de hersenen van de rat. Dit betekent, hoe sterker de structurele verbinding tussen hersengebieden, hoe sterker ook de functionele verbinding. Echter, we vonden geen correlatie tussen functionele connectiviteit en structurele connectiviteit op meso-niveau gemeten met neuronale tract tracers. Daarnaast zagen we dat de structuur-functie relatie in de hersenen verschillend is in verschillende gebieden. We vonden hoge functionele connectiviteit in

bekende resting-state netwerken, zoals het sensorimotorische en het default mode netwerk. Sterke functionele connectiviteit in deze netwerken ging gepaard met sterke korte intrahemisferische structurele connectiviteit, maar met zwakke heterotopie interhemisferische en lange intrahemisferische structurele verbindingen. Deze studie benadrukt het belang van het combineren van connectiviteitsmetingen op verschillende niveaus om nauwkeurig de connectiviteit tussen gebieden te bepalen in gezonde en zieke hersenen.

Hoewel lineaire correlatie methoden een duidelijke en gemakkelijk te interpreteren manier zijn om structuur-functie relaties in de hersenen te bepalen, dekken ze niet volledig de complexiteit van deze relaties. Daarom hebben we in **Hoofdstuk 3** de non-lineaire componenten van de structuur-functie relatie in de hersenen van ratten bepaald. Deze analyses laten zien dat zwakke structurele connectiviteit niet significant geassocieerd is met functionele connectiviteit, maar dat structurele en functionele connectiviteit pas significant gecorreleerd zijn vanaf een specifieke structurele connectiviteitswaarde, het zogenaamde structuur-functie kantelpunt. Vanaf dit kantelpunt zijn structurele en functionele verbindingen significant geassocieerd. We denken dat dit structuur-functie kantelpunt gerelateerd is aan de small-world organisatie van de hersenen. Small-world netwerken bestaan uit sterke structurele connecties binnen gespecialiseerde functionele modules, die sterk correleren met functionele connectiviteit, en zwakke structurele connecties tussen deze modules, die minder sterk associëren met functionele connectiviteit.

We hebben de non-lineaire structuur-functie relatie en kantelpunten direct vergeleken tussen de hersenen van ratten en mensen in **Hoofdstuk 3**. Zowel de hersenen van ratten en mensen laten non-lineaire structuur-functie relaties zien, maar het structuur-functie kantelpunt ligt bij een hogere structurele connectiviteit in de hersenen van ratten dan die van mensen. In de hersenen van mensen vonden we vergelijkbare non-lineaire structuur-functie relaties in de primaire sensorische gebieden en secundaire hogere orde integratie gebieden. Echter, in de hersenen van ratten vertoonde de structuur-functie relatie meer non-lineariteit in primaire dan in secundaire hersengebieden. Of de verschillen tussen de hersenen van ratten en mensen komen door een verschil in hersengrootte, verschillen in small-world organisatie of door species verschillen in de ontwikkeling van specifieke hersenregio's moet nog worden uitgezocht. Non-lineaire structuur-functie analyse kan helpen om de complexe interactie tussen structurele en functionele connectiviteit in neuronale netwerken verder te onderzoeken en biedt mogelijke markers voor hersenontwikkeling, hersenveroudering en ziekte.

Ontwikkeling van de hersenen in relatie tot obsessieve-compulsieve stoornis (OCD)

Om de link te kunnen leggen tussen hersenontwikkeling en OCD in kinderen en adolescenten hebben we een bestaand volwassen rat model van quinpirole-geïnduceerd compulsief checkgedrag aangepast naar een adolescent model in **Hoofdstuk 4**. In het volwassen model leiden herhaalde injecties met de dopamine D2/D3 receptor agonist quinpirole, tot compulsief checkgedrag bij het plaatsen van het dier op een open veld. Door de injecties al tijdens de kindertijd te geven, hebben we in dit hoofdstuk laten zien dat ratten compulsief checkgedrag vertonen voordat ze 10 weken oud zijn, wat rond adolescentie is in ratten. We hebben MRI metingen van structurele en functionele connectiviteit gedaan, voor en na de herhaalde quinpirole injecties, om (ab)normale hersenontwikkeling en de relatie daarvan met compulsief gedrag te onderzoeken. Hersenontwikkeling in ratten werd gekenmerkt door een toename in de diffusie fractionele anisotropie (FA) in grote structurele verbindingen. Deze ontwikkelingstoename in FA in de capsula interna en forceps minor was groter in compulsieve ratten dan in gezonde controles. Hiermee onderstreept deze studie de betrokkenheid van (veranderingen in) structurele connectiviteit bij OCD in kinderen en adolescenten.

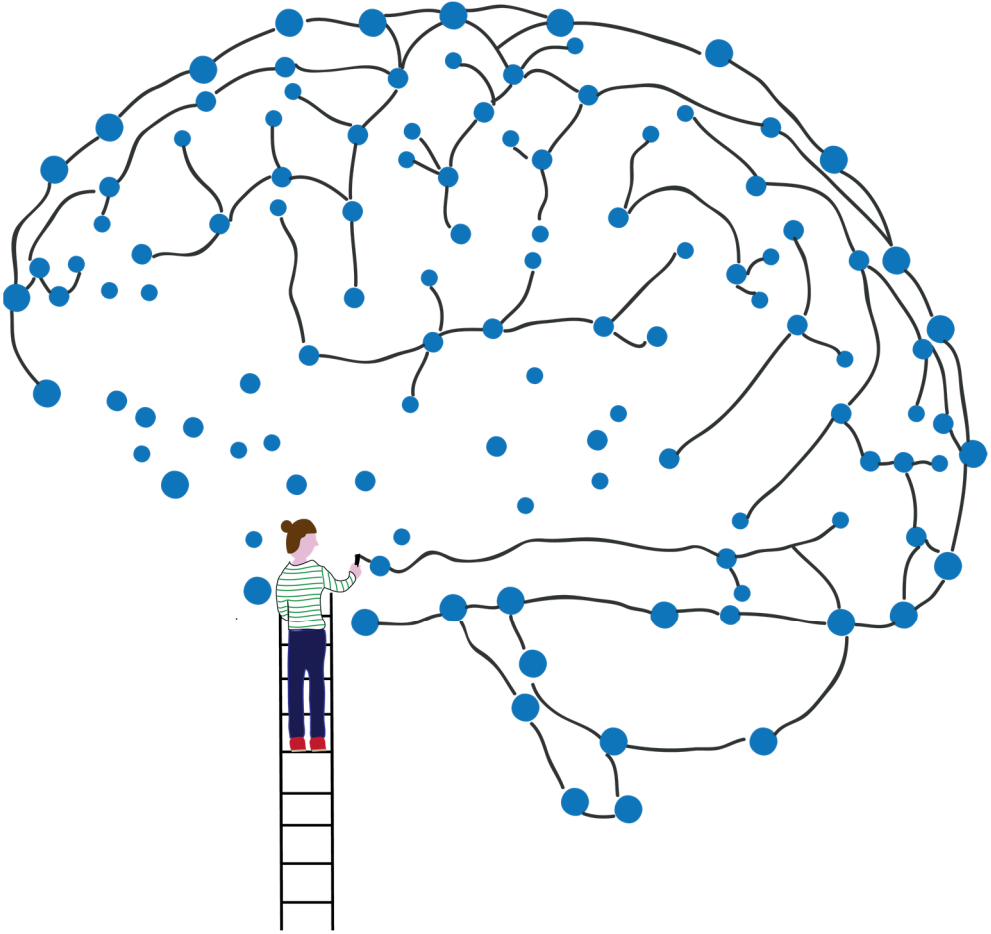
Omdat diermodellen een gecontroleerde onderzoekssetting bieden met beperkte variatie, zijn ze bijzonder geschikt om nieuwe behandelmethoden te testen. In **Hoofdstuk 5** was het doel om de potentie van de NMDA receptor antagonist memantine om compulsief gedrag te verminderen te testen in het hierboven beschreven adolescente rat model. Daarnaast wilden we het mechanisme van de therapeutische werking van memantine ophelderen, waarvoor we het effect op structurele en functionele verbindingen, en functionele activatie, in het frontostriatale systeem in de hersenen hebben gemeten. Memantine verminderde niet het compulsieve checkgedrag in het adolescente quinpirole rat model, en beïnvloedde in lijn hiermee ook niet de structurele en functionele verbindingen. Farmacologische MRI, uitgevoerd tijdens een memantine injectie, toonde activatie van wijdverspreide hersengebieden in controle ratten aan, wat niet waarneembaar was na herhaaldelijke of een enkele quinpirole injectie. Dit wijst op een interactie tussen ons farmacologisch geïnduceerde OCD model (quinpirole: dopamine systeem) en de behandeling (memantine: glutamaterg systeem). Deze bevinding kan suggereren dat memantine mogelijk niet effectief is tegen compulsief gedrag in individuen met een verstoord dopamine systeem.

Veroudering van de hersenen en gevoeligheid voor hersenschade door een beroerte

In **Hoofdstuk 6** hebben we onderzocht of veranderingen in structurele en functionele verbindingen door veroudering invloed hebben op de impact van beroertes. We hebben graafanalyses gebruikt om lokale en globale kenmerken te bepalen in structurele en functionele netwerken, gemeten met respectievelijk diffusie MRI en resting-state fMRI, in het jongvolwassen en oude rattenbrein. We vonden geen verschillen in globale netwerkmaten, zoals padlengte, clustering en small-worldness, tussen jongvolwassen en oude ratten. We vonden echter wel lokale netwerkverschillen tussen jongvolwassen en oude ratten, gekenmerkt door een verplaatsing in hub regio's in structurele en functionele netwerken.

We hebben verschillende typen laesies gesimuleerd, gebaseerd op de laesies in populaire experimentele beroerte diermodellen. Hoewel de globale netwerkeffecten van deze laesies vergelijkbaar waren in jongvolwassen en oude ratten, vonden we verschillen in laesie-geïnduceerde hubverplaatsingen tussen jongvolwassen en oude ratten. Deze leeftijdsafhankelijke laesie-geïnduceerde hubverplaatsing worden mogelijk veroorzaakt door verschillen in lokale structurele en functionele netwerkorganisatie in jongvolwassen en oude ratten. Onze resultaten suggereren dat structurele en functionele netwerken veranderen tijdens veroudering, en dat lokale veranderingen zoals hubverplaatsing bij kunnen dragen aan schade door beroertes. Hierbij onderstreept dit hoofdstuk het belang om leeftijd als factor mee te nemen in experimentele onderzoeken naar beroertes.

In **Hoofdstuk 7** bediscussiëren we de implicaties van onze bevindingen, methodologische overwegingen over de gebruikte methoden, en mogelijkheden voor vervolgonderzoek.





Dankwoord

Zo'n proefschrift schrijf je zeker niet alleen. Ik wil hierbij graag iedereen bedanken die tijdens mijn promotietijd bij het onderzoek betrokken is geweest, geholpen heeft, interesse heeft gehad of mij ontspanning heeft gegeven.

Prof. Dr. Dijkhuizen, beste Rick, dank dat je mij deze promotieplaats aangeboden hebt. Ondanks mijn twijfel in het begin ben ik blij dat ik in jouw lab gepromoveerd ben. Dank voor je interesse, vertrouwen en steun, zeker ook toen het niet zo goed ging. Jouw uitgebreide feedback op geschreven stukken en presentaties heb ik altijd erg gewaardeerd en hebben mijn schrijfkwaliteiten sterk verbeterd. Al was het soms slikken om een rood gemarkeerd document terug te krijgen. Ik bewonder het dat je, mits af en toe met een kleine herinnering, zo goed op de hoogte bent van alle verschillende projecten die in jouw groep draaien. Bedankt dat je mij zo vrij gelaten hebt, en zelf mijn richting hebt laten kiezen, al was dat niet altijd de eenvoudigste weg. Ik zal onze tafeltennis en airhockey wedstrijdes op Fuerteventura niet snel vergeten. Ondanks dat ik nu de overstap terug naar "the dark side" in Amsterdam maak, hoop ik dat we elkaar nog tegen zullen komen!

Dr. Otte, beste Wim, wat heb ik een hoop van jou geleerd! Al je kennis over programmeren, MRI data analyses en statistiek, maar met name ook van jouw kwaliteit om een goede balans te vinden tussen werk en privé. Ik bewonder je vele interesses, en je vermogen om zoveel zaken met elkaar te combineren. Dank voor de mega snelle feedback, vele rustgevende woorden in stressvolle momenten en de boekentips! Succes met je volgende stap, en wie weet zien we elkaar nog eens in Amsterdam?

De leden van de beoordelingscommissie, Prof. Dr. Sarah Durston, Prof. Dr. Jeroen Pasterkamp, Dr. Natalia Petridou, Prof. Dr. Nick Ramsey en Prof. Dr. Liesbeth Reneman, wil ik bedanken voor het lezen en beoordelen van mijn proefschrift.

Graag wil ik alle co-auteurs op de artikelen in dit proefschrift bedanken voor de samenwerking, input en constructieve feedback. I would like to thank all the co-authors for their contribution and collaborations to this thesis.

Geralda, ondanks dat we officieel niet aan elkaar gelinkt zijn was het fijn om bij jou altijd een luisterend oor te vinden. Heel veel dank voor al je stimulerende woorden, het sparren over analyses en de lekkere kopjes koffie binnen en buiten het lab. Onze gezamenlijke interesse en frustraties over (resting-state) fMRI hebben ons (soms iets te) veel hoofdbreken gegeven.

Zebra- en bijenpatronen zullen altijd aan me blijven plakken.. Hopelijk kunnen we samen blijven wandelen en skeeleren, en wie weet tot in Houten? ;-)

Gerard, Annette & Caroline, hartelijk dank voor al jullie ondersteunende en soms onzichtbare hulp, zonder jullie was dit proefschrift er niet geweest! Gerard, bedankt voor het bouwen van die mooie deuterium spoelen, ook al zijn de DMI experimenten uiteindelijk niet in dit proefschrift beland. Ik zal mijn laatste scan dag klussend met jou aan de gradient power supply niet snel vergeten.. Ik hoop dat je me snel beter kunt leren zeilen! Annette, die zebrapatronen en resting-state fMRI waren niet jouw favoriete onderwerpen om over te sparren, maar we zijn er zeker door vooruit gekomen. Dank ook voor je hulp bij de spectroscopie experimenten. Caroline, ik herinner mijn eerste momenten beneden bij de ratten nog goed; jij hebt mij met bibberende handen geleerd ratten op te pakken en te injecteren. Dank voor je hulp bij het uitvoeren van alle MRI experimenten, ook degene die niet in dit proefschrift staan.

Erwin, jij was degene met wie het allemaal begon, met de overname van het TACTICS project. Bedankt dat je mij hebt leren scannen! Dear TACTICS Consortium, and especially Jan & Jeffrey, thanks for the very sociable meetings at different beautiful and sunny islands, the fanatic table tennis games and successful collaborations and papers.

Prof. Dr. De Graaf en Dr. De Feyter, beste Robin en Henk, ondanks dat de DMI experimenten uiteindelijk toch niet in mijn proefschrift beland zijn, wil ik jullie bedanken voor de begeleiding van mijn tijd in Yale. Het waren leerzame maanden, die mijn interesse voor spectroscopie en metabolisme gewekt hebben!

Heel veel dank ook aan alle ondersteunende hulp, de medewerkers en diervverzorgers van het GDL en Maria, Jacqueline en Marjan voor de ondersteuning.

Julia, onze samenwerking begon met het schrijven van een gezamenlijke CCD aanvraag voor nieuwe experimenten, waar steeds maar weer nieuwe en meer experimenten bij kwamen, wat een klus was dat! Wat volgde waren veel overlegmomenten op werk, maar ook gezellige etentjes, wijntjes en een Zuid-Afrikaanse braai (zonder vlees ;-)) in Breukelen. Bedankt voor alle gezelligheid, en hopelijk blijven we elkaar zien! Op naar regelmatig nieuwe thee-/wijnkransjes samen met Tessa.

Anu, ik had me geen fijnere labbuurvrouw kunnen wensen! Dank voor de vele wandelingen met of zonder hond, yogalessen met kopjes koffie, de etentjes, jouw support en interesse in

de DMI experimenten, onze gezamenlijke scandagen met oliebollen en ons weekend in New York. Fijn om goed en slecht nieuws met elkaar te kunnen delen. Onze “ventileer momenten” hebben mij er zeker in de wat moeilijkere periodes doorheen geholpen! Heel veel plezier in Finland, wie weet kunnen we daar nog eens een wandeling maken?!

Bart, Eline, Esther, Jord, Karlijn, Maik, Michel, Romain, Tessa, Trude en Vera, wat een fijne collega’s waren jullie in korte of langere periodes van mijn promotie traject. Naast veel samenwerkingen en overleg, hebben we ook een hoop gelachen, geklaagd, getafeltennist, hotelkamers gedeeld, geborreld en gegeten. Dank voor alle hulp tijdens experimenten en de gezelligheid! Bart, Vera en Anu, onze korte reis in Japan, in Tokio en bij Mount Fuji, zal ik niet snel vergeten. Zoveel sushi, noedels, bento boxen, matcha en groene thee dat we daar na een week wel weer klaar mee waren. Esther, dank voor de ontspanning in onze veelvuldige skeelerrondjes, op naar een rondje op de ijsbaan binnenkort! Tessa en Michel, zonnen in de sneeuw tijdens een congres in de Franse Alpen met 4-gangen lunches en avondeten, sleeën en wandelen, dank voor de gezelligheid.

Rachelle, lieve Ra, wat ben ik blij met een vriendin zoals jij! Samen begonnen bij Spaarnestad dames 1 in Haarlem, en elkaar nooit meer uit het oog verloren, ondanks het wonen in veel verschillende landen en steden. Je staat altijd klaar met een luisterend oor en veel interesse, ik ben blij dat jij naast me staat als mijn paranimf. Wat hebben we gelachen tijdens jouw bezoek in Yale, wat hebben we een hoop aan elkaar gehad toen we het allebei moeilijk hadden, daarvoor duizendmaal dank! Jij hebt die donkere periode toch een stukje lichter gemaakt. Dank voor je interesse en alle ontspanning die je mij tijdens dit traject hebt gegeven, de vele wandelingen, biertjes, wijntjes, de natte kanotocht, etentjes & museumuitjes, hopelijk nog veel meer in de toekomst!

Mirthe, Svenja, Annemiek & Silvie, lieve meiden van Psychobiologie, samen is de liefde voor de hersenen geboren 10 jaar geleden op het Science Park in Amsterdam. Ondanks alle kortere en langere periodes in het buitenland, zijn we elkaar toch blijven zien. De afgelopen jaren zaten we allemaal in hetzelfde schuitje met een promotieonderzoek, fijn om samen lief en leed daarover te kunnen delen tijdens onze etentjes! Lieve Miek & Sil, ons afscheidelijke duo, we zien elkaar wat minder, maar het is altijd fijn samen. Sil, jij was als eerste helemaal klaar, heel veel succes in Zwitserland! Miek, voor jou nu ook de laatste loodjes, ik kijk uit naar jouw verdediging! Lieve Mirthe, al vanaf de 1e dag in de introductieweek hebben wij elkaar gevonden. Super knap dat jij het promoveren combineert met je opleiding tot neuroloog. Wat heerlijk dat je zo dichtbij woont in Utrecht, dank voor de vele kopjes koffie, de etentjes, het

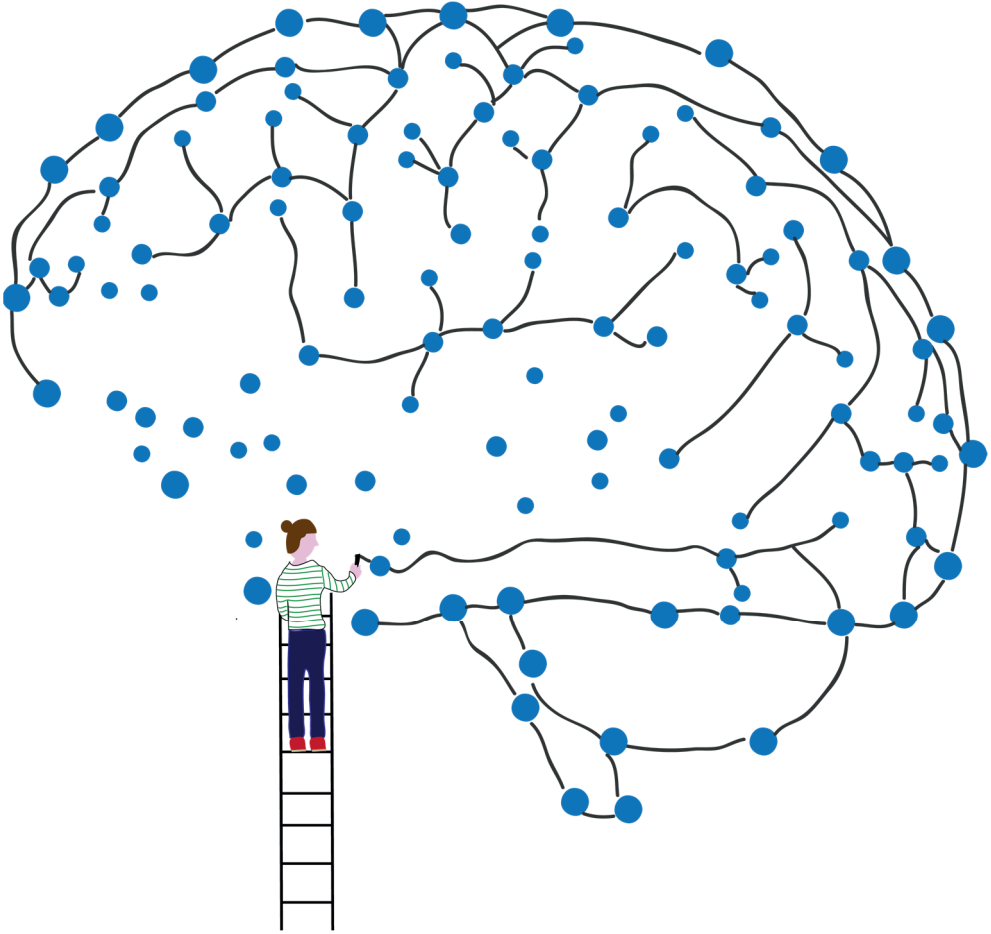
schilderen van muren, de creatieve middagjes en je steun de laatste tijd! Lieve Sven, wat een doorzetter ben jij, nu weer als student geneeskunde! Ik bewonder jouw enorme enthousiasme waarmee je steeds weer aan iets nieuws begint. Hopelijk kunnen we regelmatig lunchen nu we allebei in het AMC zijn.

Wietske, Rob, Piet & Susan, fijn om jullie als schoonfamilie te hebben! Dank voor jullie interesse, en de ontspannende momenten tijdens etentjes & weekendjes weg in Groningen, Oss en Zeeland.

Roel, lieve dokter Oellie, grote broer. Wat is het fijn om te weten dat je altijd achter me staat, en er bent als het wat minder gaat. Allebei veel interesse in de hersenen en de neurologie, is dat toeval of toch onze genen? Ik bewonder jouw vermogen om goed te weten wat je wil, en daar ook naar te handelen. Bedankt dat jij naast mij wilt staan als paranimf, jouw rust en relaxte houding zal me zeker helpen! Hierna zijn we allebei dokter! Lieve Ilse, al is het nog maar kort, fijn dat jij samen met Roel hier bent. Die sup tocht gaan we volgende zomer plannen. Dank voor je interesse in mijn onderzoek.

Papa en mama, lieve papa en mama, wat een tijd is dit geweest. Het is een fijn gevoel om te weten dat jullie er altijd zijn, zeker als het niet zo goed gaat. Zonder jullie onvoorwaardelijke steun en liefde had ik hier nu niet gestaan. Dank dat jullie altijd in me (zijn blijven) geloven, en me er altijd aan herinneren dat er ook nog een leven is buiten werk. Ondanks dat jullie helemaal niet in hetzelfde veld zitten, hebben jullie altijd geprobeerd om te begrijpen waar ik nu weer mee bezig was. Al was het af en toe voor jullie choquerend om te horen wat ik nu weer met die ratjes deed.. Nu is het tijd voor meer dagjes weg, wandelen, fietsen, vogels spotten en creatief bezig zijn!

Jelle, lieve Jelle, eindelijk is hij af! Dit was me niet gelukt zonder jouw steun, rustgevende woorden, liefde & humor. Heerlijk om iemand thuis te hebben die altijd rustig blijft en me steeds weer van mijn donder-stress wolk af kan halen. Dank dat jij, wanneer ik vroeg op moest voor experimenten, altijd samen met mij opstond, om rond 7 uur in de vrieskou hard te lopen. Jij herinnert me er altijd aan dat het “maar” werk is, dat ik er vaak op dat moment weinig aan kon doen en er nog veel meer in het leven is. Dank voor alle heerlijke gerechten die jij klaarmaakte als ik weer eens langer op werk bleef en de vele ontspannende wandelingen, vakanties en weekendjes weg. Het was een fijn einde van mijn promotietijd in Utrecht om samen met jou onze eerste huttentocht in de bergen te wandelen. Ik hou van je, op naar nog veel mooie momenten samen!





About the author

Curriculum Vitae

Milou Straathof was born on May the 18th 1992 in Haarlem, the Netherlands. In 2010 she finished secondary school at Hageveld in Heemstede (VWO, cum laude). Thereafter, she studied Psychobiology at the University of Amsterdam (cum laude). She obtained her Master's degree (cum laude) in Neuroscience at the University of Utrecht. During her master, she performed an internship at the ALS Center in the UMC Utrecht, where she investigated MRI characteristics of genetic subgroups of ALS patients. In addition, she visited the Oxford Center for functional MRI (FMRIB) at the University of Oxford to investigate the possibilities of post-mortem tractography in brains of ALS patients.



In February 2016 she started as a PhD student at the UMC Utrecht under the supervision of prof. dr. R.M. Dijkhuizen and dr. W.M. Otte, which has resulted in this thesis. During her PhD project she spend 4 months at Yale University as a visiting research fellow to study the brain using Deuterium Metabolic Imaging (DMI). From August 2021 Milou has worked as a junior researcher in the research group of prof. dr. R.M. Dijkhuizen. In October 2021 Milou will has started a postdoc position at the Amsterdam Medical Center with dr. E. Hoekzema, investigating brain changes during pregnancy.

List of publications

Westeneng, H.J., Walhout, R., **Straathof, M.**, Schmidt, R., Hendrikse, J., Veldink, J.H., van den Heuvel, M.P. & van den Berg, L.H. (2016). Widespread structural brain involvement in ALS is not limited to the C9orf72 repeat expansion. *Journal of Neurology, Neurosurgery and Psychiatry*, 87 (12), 1354-1360.

Straathof, M.*, Sinke, M.R.T.*, van der Toorn, A., Weerheim, P.L., Otte, W.M. & Dijkhuizen, R.M. (2019). Differences in structural and functional networks between young adult and aged rat brains before and after stroke lesion simulations. *Neurobiology of Disease*, 126, 23-35.

Straathof, M., Sinke, M.R.T., Dijkhuizen, R.M. & Otte, W.M. (2019). A systematic review on the quantitative relationship between structural and functional network connectivity strength in mammalian brains. *Journal of Cerebral Blood Flow and Metabolism*, 39 (2), 189-209.

Roelofs, T.J.M., **Straathof, M.**, van der Toorn A., Otte, W.M., Adan, R.A.H & Dijkhuizen, R.M. (2019) Diet as connecting factor: Functional brain connectivity in relation to food intake and sucrose tasting, assessed with resting-state functional MRI in rats. *Journal of Neuroscience Research*, [online ahead of print].

Mandino, F., Cerri, D., Garin, C.M., **Straathof, M.**, van Tilborg, G.A.F., Chakravarty, M.M., Dhenain, M., Dijkhuizen, R.M., Gonzi, A., Hess, A., Keilholz, S.D., Lerch, J.P., Ian Shih, Y-Y., Grandjean, J. (2020) Animal functional magnetic resonance imaging: Trends and path toward standardization. *Frontiers in Neuroinformatics*, 13, 78.

Straathof, M., Sinke, M.R.T., Roelofs, T.J.M., Blezer, E.L.A., Sarabdjitsingh, R.A., van der Toorn, A., Schmitt, O., Otte, W.M. & Dijkhuizen, R.M. (2020) Distinct structure-function relationships across brain regions and connectivity scales in the rat brain. *Scientific Reports*, 10(1), 56.

Straathof, M., Blezer, E.L.A., van Heijningen, C., Smeele, C.E., van der Toorn, A., TACTICS Consortium, Buitelaar, J.K., Glennon, J.C., Otte, W.M. & Dijkhuizen, R.M. (2020) Structural and functional MRI of abnormal brain development in a novel adolescent rat model of quinpirole-induced compulsive checking behavior. *European Neuropsychopharmacology*, 33, 58-70.

Boonzaier, J. *, **Straathof, M. ***, Ardesch, D.J. *, Otte, W.M., van der Toorn, A., van Vliet, G., van Heijningen, C., Neggers, S.F.W. & Dijkhuizen, R.M. (2021) Acute BOLD response and subsequent changes in functional connectivity in rat cortex after bilateral transcranial direct current stimulation. *Journal of Neuroscience*, 99(5), 1377-1389.

Straathof, M. *, Meerwaldt, A.E. *, De Feyter, H.M., de Graaf, R.A. & Dijkhuizen, R.M. (2021) Deuterium metabolic imaging of the healthy and diseased brain. *Neuroscience*, [online ahead of print].

Sinke, M.R.T., van Tilborg, G.A.F., Meerwaldt, A.E., van Heijningen, C.L., van der Toorn, A., **Straathof, M.**, Rakib, F., Ali, M.H.M., Al-Saad, K., Otte, W.M. & Dijkhuizen, R.M. (2021) Remote corticospinal tract degeneration after cortical stroke in rats may not preclude spontaneous sensorimotor recovery. *Neurorehabilitation and Neural Repair*, [online ahead of print].

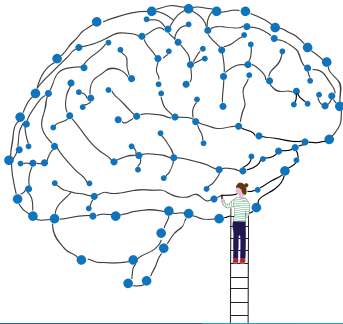
Straathof, M., Otte, W.M. & Dijkhuizen R.M. Non-linear relationships between structural and functional connectivity in the human and rat cerebral cortex. *Submitted*.

Straathof, M., Blezer, E.L.A., Smeele, C.E., van Heijningen, C., van der Toorn, A., TACTICS Consortium, Buitelaar, J.K., Glennon, J.C., Otte, W.M., Dijkhuizen, R.M. Memantine treatment does not affect compulsive behavior or frontostriatal connectivity in an adolescent rat model for quinpirole-induced compulsive checking behavior. *Submitted*.

A.E. Meerwaldt, **Straathof, M.**, van Heijningen, C., van Vliet, G., van der Toorn, A., De Feyter, H.M., de Graaf, R.M., Dijkhuizen, R.M. Changes in poststroke active glucose metabolism are dependent on lesion severity as revealed by complementary metabolic imaging techniques. *In preparation*.

Straathof, M., van Heijningen, C., van Vliet, G.M., de Feyter, H.M., van der Toorn, A., Otte, W.M., de Graaf, R.A. & Dijkhuizen, R.M. Aerobic glucose metabolism does not completely restore with reperfusion after ischemic stroke. *In preparation*.

* These authors contributed equally.



UMC Utrecht



Universiteit Utrecht

ISBN 978-94-6423-484-8